Production of heavy Higgs bosons and decay into top quarks at the LHC

Von der Fakultät für Mathematik, Informatik und Naturwissenschaften der RWTH Aachen University zur Erlangung des akademischen Grades eines Doktors der Naturwissenschaften genehmigte Dissertation

vorgelegt von

Diplom-Physiker
Clemens Mellein
aus Malsch (Baden-Württemberg)

Berichter:	Universitätsprofessor Dr. W. Bernreuther
	Universitätsprofessor Dr. M. Krämer
Tag der mündlichen Prüfung:	20. Oktober 2015

Production of heavy Higgs bosons and decay into top quarks at the LHC

Clemens Mellein

Abstract

Even in the light of the recent discovery of a neutral spin-0 boson at the LHC, the details of the Higgs sector as the favored mechanism of electroweak symmetry breaking in the SM are far from clarified. Several extensions of the minimal version are under discussion and they commonly predict additional Higgs bosons in the physical particle spectrum. The main aspect of this thesis is the investigation of the effects of heavy, neutral spin-0 bosons with a mass larger than twice the top-quark mass and non-suppressed Yukawa couplings to the top quark in $t\bar{t}$ production at the LHC. As a model with rather generic features we use the type-II 2HDM with softly broken Z_2 symmetry which predicts three neutral Higgs bosons, one of which can easily be aligned to the recent experimental findings. It further provides scenarios where the other two neutral Higgs bosons are heavy and with dominant coupling to the top quark. The inclusive cross section as well as several distributions, most notebaly the $M_{t\bar{t}}$ spectrum, are computed at next-to-leading order in the strong coupling. The NLO QCD corrections are computed in the large m_t limit where the Higgs-gluon coupling is described by an effective Lagrangian. In the last part, some spin and polarization observables computed on the level of dilepton final states will be studied as well.

Zusammenfassung

Trotz der Entdeckung eines neutralen Spin-0 Bosons am LHC bleiben viele Fragen über die Details des Higgsmechanismus offen. Verschiedene mögliche Erweiterungen des Higgssektors im Standard Modell werden untersucht, allen gemein ist die Vorhersage von zusätzlichen Higgsbosonen im Teilchenspektrum. In dieser Arbeit werden die Effekte von schweren, neutralen Spin-0 Bosonen, welche vorwiegend an das Top-Quark koppeln, in der $t\bar{t}$ Produktion am LHC untersucht. Beispielhaft wird hier die Klasse der Typ-II 2HDM mit schwach gebrochener Z_2 Symmetrie untersucht, welche drei neutrale Higgsbosonen vorhersagen. Innerhalb dieses 2HDM lassen sich leicht Szenarien finden, in denen eines der neutralen Higgsbosonen mit dem neu entdeckten Teilchen identifiziert werden kann und die anderen beiden wesentlich schwereren Higgsbosonen die gewünschten Kopplungen an das Top-Quark aufweisen. In dieser Arbeit werden sowohl der inklusive Wirkungsquerschnitt als auch verschiedene differenzielle Verteilungen in nächst-führender Ordnung der starken Kopplung berechnet. Für die Berechnung der Strahlungskorrekturen wird die Kopplung der Higgsbosonen an Gluonen im Limes $m_t \to \infty$ beschrieben. Im letzten Teil dieser Arbeit werden einige Spin- und Polarisationsobservablen für dileptonische Endzustände berechnet und die Effekte der schweren Higgsbosonen untersucht.

Contents

1. Introduction

The Standard Model of particle physics (SM) is the current theoretical framework that describes all known elementary particles and their interactions. Using this framework one can make quantitative predictions which so far have proven very successful when confronted with experimental data.

The SM Lagrangian is constructed to be invariant under Lorentz transformations and local gauge transformations described by the symmetry group $G_{\mathrm{SM}} = SU(3)_C \times SU(2)_L \times U(1)_Y$. The gauge group of Quantum Chromodynamics (QCD) $SU(3)_C$ requires 8 self-interacting, massless gluons and allows that each quark appears in 3 color states, as observed experimentally. The electroweak sector is defined by the chiral $SU(2)_L \times U(1)_Y$ gauge group, which implies two charged and two neutral gauge bosons, namely the $W^{\pm}$ and Z bosons and the photon γ. The left-handed and right-handed components of quark and lepton fields are then organized in doublets and singlets under $SU(2)_L$, respectively. In this way their interactions with the $W^{\pm}$ and Z bosons can be formulated such that they exhibit the observed violation of parity and charge conjugation, whereas the interactions with the photon conserve these symmetries.

A major issue of the SM is the implementation of massive gauge bosons and fermions since the requirement of invariance under the chiral part $SU(2)_L \times U(1)_Y$ of the gauge group G_{SM} forbids the direct inclusion of mass terms. On first sight this poses a major problem since the $W^{\pm}$ and Z bosons as well as the quarks and leptons are experimentally confirmed to be massive. But, as shown by Brout, Englert and Higgs in the 1960's [1],[2], the masses of gauge bosons and fermions can be generated dynamically by spontaneous symmetry breaking while the full gauge symmetry is retained in the initial Lagrangian. The minimal version of this mechanism requires one $SU(2)_L$ doublet of self-interacting scalar fields, which acquires a vacuum expectation value (VEV). Below the energy scale set by this VEV, the electroweak $SU(2)_L \times U(1)_Y$ gauge symmetry is broken down to $U(1)_{\mathrm{em}}$, the gauge symmetry associated with electromagnetism. The electromagnetic $U(1)_{\mathrm{em}}$ as well as color $SU(3)_C$ gauge transformations remain exact symmetries of the SM, implying that the photon as well as the gluons stay massless. The most important phenomenological implication of the minimal Higgs mechanism is the existence of a single, electrically neutral spin-0 boson in the physical particle spectrum.

In 2012 the two LHC experiments ATLAS and CMS discovered a neutral spin-0 boson [3, 4] with a measured mass of 126 ± 0.8 GeV [5], respectively 125.3 ± 0.9 GeV [6]. According to the present experimental status [5, 6] this particle is a Higgs boson and its properties are compatible with the hypothesis that it is the Higgs boson of the SM. This discovery strongly supports the Higgs mechanism of electroweak symmetry breaking (EWSB). Though, it remains to be shown with increased precision that this newly found boson has indeed all the properties that are predicted by the SM Higgs mechanism.

The discovery also rises the question if this is the only Higgs boson or if there exists an extended scalar sector in nature. From the theoretical side several viable extensions are conceivable and under discussion. The class of two-Higgs doublet models (2HDM) is the simplest extension of the minimal Higgs sector, but nethertheless introduces many new phenomenological aspects, most notably it implies 5 Higgs bosons in the physical particle spectrum and provides a new source of CP violation [7] beyond the CKM mechanism of the SM. Supersymmetry is a very popular extension of the standard model as a whole, adding bosonic partners to each chiral fermion and vice versa. In the minimal supersymmetric standard model (MSSM) the Higgs sector resembles a 2HDM but with additional constraints on the parameters [8, 9].

The top quark plays a major role in all Higgs studies, since as the heaviest of all elementary particles with a mass of $m_t = 173.34$ GeV [10] it is expected to be very sensitive to the Higgs-sector. The total top-quark decay width has been calculated up to next-to-next-to-leading order (NNLO) QCD [11], its value of $\Gamma_t(m_t = 173.34 \text{ GeV}) = 1.338$ GeV[1] corresponds to a mean lifetime of approximately $\tau_t \sim 5 \cdot 10^{-25}$ s. This is about one order of magnitude lower than the mean hadronization time $\tau_{\text{had.}} \propto \Lambda_{\text{QCD}}^{-1}$, which is given by the QCD scale $\Lambda_{\text{QCD}} \sim \mathcal{O}(200\,\text{MeV})$. This means that hadronization effects can be mostly neglected and a perturbative description of processes involving the top quark is reliable. Within the SM the main decay mode of the top quark is $t \to bW^+$ with a branching ratio of roughly 99.8%, whereas the decays to s- and d-quarks are strongly suppressed by the CKM mechanism [12]. The decays of the top quark are then further classified by the decay products of the intermediate W^+ boson. Especially the leptonic decay mode $W^+ \to l^+ + \nu_l$ with $l \in \{e, \mu, \tau\}$ provides a very clean signature and is therefore often used in the analyses of experimental data, though it is suppressed with respect to the hadronic decay modes $W^+ \to u + \bar{d}$ and $W^+ \to c + \bar{s}$ due to lower multiplicity. The fact that the top quark decays almost exclusicely via a W^+ boson implies that the lepton (or down-quark) direction of flight is nearly 100% correlated with the spin direction of the decaying top-quark. Thus the top-quark spin can be regarded as a good observable which is accessible via angular distributions of the top-quark decay products. This allows for example to study the spin and CP properties of the underlying production mechanisms in more detail.

In the search for additional Higgs bosons at the LHC, the $t\bar{t}$ invariant mass spectrum is of central importance, because any new resonance with mass above the $t\bar{t}$ threshold is expected to leave a measurable imprint on this observable, particularly in scenarios where the coupling to the top quark is dominant [13, 14]. During the last run with a center-of-mass energy of $\sqrt{s} = 8$ TeV, the LHC delivered a luminosity of roughly 20 fb^{-1} corresponding to $5 \cdot 10^7$ $t\bar{t}$ pairs. Although this is a large number compared to previous experiments, statistics still limit the significance of observables like the $t\bar{t}$ invariant mass spectrum and spin observables. In fact, both the CMS and the ATLAS experiment have searched in the $t\bar{t}$ invariant mass distribution for heavy resonances which decay to $t\bar{t}$ pairs [15, 16, 17, 18]. So far, the searches were unsuccessful. The CMS experiment [15] has put bounds on the production cross section $\sigma_{pp\to\phi\to t\bar{t}}$ at $\sqrt{s} = 8$ TeV of a heavy

[1] The b-quark mass is neglected in the calculation, the relevant input parameters to obtain this value are: $G_F = 1.16637 \cdot 10^{-5}$ GeV^{-2}, $m_W = 80.385$ GeV, $\alpha_s(m_t) = 0.1076$.

spin-0 resonance ϕ for an assumed mass of $m_\phi = 500$ GeV and 750 GeV, respectively. However, these bounds are of limited significance because it was assumed that ϕ is a narrow resonance and that interference with the QCD background for $t\bar{t}$ production is negligible.

The new run at the LHC, starting in 2015 with increased luminosity and a center-of-mass energy of $\sqrt{s} = 13$ TeV, provides the next chance to find new physics in form of additional heavy particles or to exclude them up to scales of several TeV. Regarding searches for additional Higgs bosons in $t\bar{t}$ production, the large irreducible QCD background poses a major challenge. The QCD cross-section for $pp \to t\bar{t}$ has been calculated up to NNLO in the strong coupling including next-to-next-to-leading logarithm (NNLL) resummation, at a proton-proton center-of-mass energy of $\sqrt{s} = 13$ TeV the result is $\sigma_{pp\to t\bar{t}}(14\text{TeV}) = 953.6$ pb [19]. The cross-section for $t\bar{t}$ production via heavy spin-0 resonances does not amount to more than a few percent of that value in most scenarios. But, as known from the total SM Higgs production cross section, which is dominated by Higgs production via gluon fusion, higher order QCD corrections are large [20, 21, 22, 23, 24, 25, 26, 27]. Thus it is very important to have an estimate of the radiative corrections also for prediction of $t\bar{t}$ production via heavy spin-0 resonances.

The aim of this thesis is to investigate the resonant production of heavy, neutral Higgs bosons ϕ_i with masses $m_i > 2m_t$ and their decay into $t\bar{t}$ pairs at the LHC at next-to-leading order (NLO) QCD. The main ϕ_i production mode is gluon fusion,

$$gg \to \phi_i \to t\bar{t} + X,$$

but also production by $q\bar{q}$ annihilation and qg fusion must be taken into account when dealing with the radiative corrections. We are concerned with the case that the resonances ϕ_i are not narrow and in particular we take into account the interference of the ϕ_i production amplitudes with the respective non-resonant QCD $t\bar{t}$ production amplitudes at leading order (LO) and NLO in the QCD coupling. At NLO, the $gg\phi_i$ coupling is treated in the limit of an infinitely heavy top-quark, whereas b-quark effects are neglected. We compute a number of distributions, in particular the $t\bar{t}$ invariant mass distribution, and investigate the effects of ϕ_i production in the resonance regions of these distributions. We consider also the subsequent decay of the $t\bar{t}$ pair to dileptonic and lepton plus jets final states, taking into account the $t\bar{t}$ spin correlations at NLO in the gauge couplings. We investigate the effect of heavy Higgs resonances on a set of dilepton angular correlations and top-quark polarization observables. In particular, we analyze the possibility of neutral Higgs sector CP violation, i.e. the possibility that the heavy Higgs bosons ϕ_i have CP-violating Yukawa couplings to top quarks. These effects can be traced with CP-odd angular correlations in dileptonic and lepton plus jets final states. This NLO analysis is, to a large extent, model-independent and can be applied to SM extensions which contain heavy ϕ_i bosons in their particle spectrum. However, consistent computations which are in accordance with the constraints due to unitarity should be done within a concrete SM extension. The computations and predictions below were made within the class of type-II two-Higgs doublet extensions. Within this class we identify the lightest neutral Higgs boson with the 125 GeV Higgs resonance with SM-like couplings to quarks, leptons and weak gauge bosons. For definiteness, we consider three different scenarios, two CP-conserving and one CP-violating Higgs scenario, such that the two heavy neutral Higgs bosons, ϕ_2 and ϕ_3, are heavier than $2m_t$ and that their Yukawa couplings to top-quarks are unsuppressed compared to the SM values.

This thesis is organized as follows. First, the minimal Higgs mechanism, as implemented in the SM, is reviewed in Sec. 1.1 as a preparation for the introduction of the class of two-Higgs doublet models in Sec. 1.2. A certain subset of these models, the type-II 2HDM with softly broken Z_2 symmetry, is of major importance for this project since it provides viable physical scenarios to which the following computations can be applied. We give a detailed account of these models, both without and with CP violation in the Higgs sector, and address briefly present experimental constraints on the parameters of type-II 2HDM. In Sec. 1.2.5 we will discuss the possible decay modes of the neutral Higgs bosons. The results of the computation of the total widths for the three specific scenarios within the type-II 2HDM including QCD corrections are summarized in Sec. 3.7.1. Sec. 1.3 concludes the introduction to the Higgs sector of the SM and the 2HDM with a short discussion of the Higgs sector of the MSSM. In Sec. 2 the results for the total production cross section of a neutral spin-0 boson in proton-proton collisions including the QCD radiative corrections obtained in the large m_t limit are presented. These are compared to the most precise results available in the literature to see how well the large m_t approximation works over a wide mass range. This is of relevance since the approximation is also applied in Sec. 3, where the NLO QCD corrections to $t\bar{t}$ production in proton-proton collisions are computed including the effects of two neutral heavy Higgs bosons. In Sec. 3.7 the numerical results of our computation are presented. We compute the input parameters, the Higgs masses, widths and Yukawa couplings, within three different type-II 2HDM scenarios, as summarized in Sec. 3.7.1. Besides the total $t\bar{t}$ production cross section, the $M_{t\bar{t}}$ spectrum, where the heavy Higgs resonances show up in form of a distinct peak-dip structure, is of major importance. We will further investigate the effects of the heavy Higgs resonances on the transverse momentum and rapidity distributions of top and antitop quark. In the last part we compute the inclusive values of some spin and polarization observables as well as their $M_{t\bar{t}}$ distributions and discuss the results.

1.1. The Standard Model Higgs sector

In this section we will briefly review the Higgs mechanism which generates the masses of fermions and the weak vector bosons in the SM. Only the most relevant pieces will be presented here, for a comprehensive review on the SM Lagrangian and the resulting Feynman rules see for example [28]. A thorough review of the SM Higgs mechanism and its phenomenology is also provided in [29].

The minimal version of the Higgs mechanism comprises one scalar complex $SU(2)$ doublet with hypercharge $Y = +1$

$$\Phi = \left(\varphi^{+}, \varphi^{(0)}\right)^{T}, \tag{1.1}$$

where φ^{+} denotes a field with electric charge $+1$ and $\varphi^{(0)}$ an electrically neutral field. Its couplings to the electroweak gauge bosons and self-interactions are described by the Lagrangian

$$\mathcal{L}_{\text{Higgs}} = \left(D_{\mu}\Phi\right)^{\dagger}\left(D^{\mu}\Phi\right) - V\left(|\Phi|^{2}\right), \tag{1.2}$$

where D^{μ} denotes the covariant derivative

$$D^{\mu} = \partial^{\mu} - ig'\frac{Y}{2}B^{\mu} - ig\frac{\sigma_i}{2}W_i^{\mu}. \tag{1.3}$$

The most general hermitian and renormalizable potential for a single doublet is

$$V\left(|\Phi|^{2}\right) = -\mu^{2}|\Phi|^{2} + \lambda|\Phi|^{4}, \tag{1.4}$$

with real parameters μ and λ. The Lagrangian (1.2) is invariant under local transformations of the symmetry group $SU(2)_L \times U(1)_Y$. The real numbers g and g' are the $SU(2)_L$ and $U(1)_Y$ gauge couplings, respectively, $\frac{Y}{2}$ and $\frac{\sigma_i}{2}$ the corresponding group generators. The physical fields corresponding to the $W^{\pm}$, Z bosons and the photon A are given as linear combinations of the fundamental fields B^{μ} and W_i^{μ}

$$\begin{aligned} W^{\pm\,\mu} &= \frac{1}{\sqrt{2}}\left(W_1^{\mu} \mp iW_2^{\mu}\right), \\ Z^{\mu} &= \cos\theta_W W_3^{\mu} - \sin\theta_W B^{\mu}, \\ A^{\mu} &= \sin\theta_W W_3^{\mu} + \cos\theta_W B^{\mu} \\ &. \end{aligned} \tag{1.5}$$

The weak mixing angle θ_W can be expressed through the gauge couplings as $\cos\theta_W = \frac{g}{\sqrt{g'^2+g^2}}$.

If one chooses $\mu > 0$ and $\lambda > 0$ in (1.4) the potential has a stable ground sate $|0\rangle$ with non-zero expectation value $\langle 0|\Phi|0\rangle$, which is found by minimizing (1.4) with respect to $|\Phi|$. One finds

$$|\Phi|_0 = \frac{\mu}{\sqrt{2\lambda}} \equiv \frac{v}{\sqrt{2}}.$$

Without loss of generality[2] the ground state expectation value can be written as

$$\langle 0|\Phi|0\rangle = \langle\Phi\rangle = \left(0, \frac{v}{\sqrt{2}}\right)^T, \tag{1.6}$$

which corresponds to the tree-level approximation of the vacuum expectation value (VEV) of the quantum field Φ. This state is obviously not invariant under general $SU(2)_L \times U(1)_Y$ transformations, only the invariance under $U(1)_{\text{em}}$ remains. In the following it is useful to rewrite the doublet (1.1) as

$$\Phi = \left(\phi^+, \frac{1}{\sqrt{2}}(v + h + i\chi)\right)^T, \tag{1.7}$$

where h and χ denote two real fields, of which h is CP-even and χ CP-odd. All component fields now have vanishing VEVs, i.e. $\langle\phi^+\rangle = \langle h\rangle = \langle\chi\rangle = 0$. Plugging (1.7) into (1.2) one can express $\mathcal{L}_{\text{Higgs}}$ in terms of the fields ϕ^+, h and χ, which describe the fluctuations around the ground state (1.6). From the kinetic term in (1.2) the mass terms for the electroweak gauge bosons arise as well as the trilinear and quartic couplings with the Higgs boson

$$\begin{aligned}(D_\mu\Phi)^\dagger(D^\mu\Phi) &= \frac{1}{2}(\partial_\mu h)(\partial^\mu h) + \left(\frac{gv}{2}\right)^2 W^+_\mu W^{-\mu} + \frac{1}{2}\left(\frac{gv}{2\cos\theta_W}\right)^2 Z_\mu Z^\mu \\ &+ \frac{g^2 v}{4\cos^2\theta_W} hZ^\mu Z_\mu + \frac{g^2 v}{2} hW^{+\mu}W^-_\mu \\ &+ \frac{g^2}{8\cos^2\theta_W} h^2 Z^\mu Z_\mu + \frac{g^2}{4} h^2 W^{+\mu}W^-_\mu \\ &+ \text{terms involving } \phi^+, \chi.\end{aligned} \tag{1.8}$$

The pseudo-Goldstone fields ϕ^+ and χ still present in the full expressions of (1.11) do not constitute physical degrees of freedoms, instead they can be removed completely from

[2] Different choices of $\langle\Phi\rangle$ can be rotated by a global $SU(2)_L$ transformation into this form.

the Lagrangian (1.2) by applying a local gauge transformation described by a matrix $U(x) \in SU(2)_L \times U(1)_Y$, such that

$$\Phi(x) \quad \to \quad U(x)\,\Phi(x) = \left(0, \frac{1}{\sqrt{2}}\,(v + h(x))\right)^T . \tag{1.9}$$

The two degrees of freedom corresponding to ϕ^+ and χ are transferred to the - now massive - gauge bosons $W^\pm$ and Z, which in this procedure acquired each a longitudinal polarization state. The unitary gauge (1.9) is useful as long as no radiative corrections in the electroweak gauge couplings are considered. Since we only deal with QCD corrections here, we will in the following make use of this gauge to obtain simpler results.

From (1.8) one can deduce the tree-level relations of the gauge boson masses m_W, m_Z and the electroweak parameters g, $\cos\theta_W$ and v:

$$\begin{aligned} m_W &= \frac{gv}{2}, \\ m_Z &= \frac{gv}{2\cos\theta_W}. \end{aligned} \tag{1.10}$$

The photon γ, described by the field A^μ in (1.5), remains massless. The values $g = \frac{e}{\sin\theta_W} \simeq 0.652$, $\sin^2\theta_W = 0.2313$, as well as the pole masses $m_W \simeq 80.385$ GeV and $m_Z \simeq 91.188$ GeV are known from experiment [12]. To be consistent one has to set $v \simeq 246$ GeV in (1.10).

Plugging (1.9) into the Higgs potential (1.4) one finds a mass term for the field h as well as triple and quartic self-couplings:

$$V\left(|\Phi|^2\right) = \frac{m_h^2}{2}h^2 + \frac{g_{3h}}{3!}h^3 + \frac{g_{4h}}{4!}h^4, \tag{1.11}$$

where $g_{4h} = 3\frac{m_h^2}{v^2}$ and $g_{3h} = 3\frac{m_h^2}{v}$. The Higgs mass $m_h^2 = 2\lambda v^2$ is directly connected to the self-coupling parameter λ. Thus with v fixed by the conditions (1.10) there is only one free parameter in the SM Higgs sector. If one interprets the recent discovery of a boson with mass near 125 GeV as the SM Higgs boson, one gets a direct prediction for the strength of the Higgs self-interactions, which has to be verified experimentally to support the Higgs mechanism in this form.

The masses of the fermions are generated by introducing the $SU(2)_L \times U(1)_Y$ invariant Yukawa interaction terms

$$\mathcal{L}_{\mathrm{Y}}^{(\mathrm{SM})} = -y_i^{(l)}\,\overline{L_{L,i}}\Phi\, l_{R,i} - \hat{y}_{ij}^{(d)}\,\overline{Q'_{L,i}}\Phi\, d'_{R,j} - \hat{y}_{ij}^{(u)}\,\overline{Q'_{L,i}}\left(i\sigma_2\Phi^*\right)\, u'_{R,j} + \text{h.c.}, \tag{1.12}$$

where the doublets $L_{L,i} = \left(\nu_{L,i}, l_{L,i}\right)^T$ contain the left-chiral (LC) components of the neutrinos and charged leptons, $Q'_{L,i} = \left(u'_{L,i}, d'_{L,i}\right)^T$ contain the LC components of up-and down-type quarks in the basis of weak eigenstates. Analogously, $l_{R,i}$, $d'_{R,i}$, $u'_{R,i}$ denote the respective right-chiral (RC) fields. The indices $i, j \in \{1, 2, 3\}$ label the respective fermion generation. The doublet

$$(i\sigma_2\Phi^*) \;=\; \left(\frac{1}{\sqrt{2}}\,(v+h)\,, 0\right)^T \tag{1.13}$$

is the $Y = -1$ counterpart to (1.9) and is used to generate the masses of the up-type quarks. Although it is known from neutrino oscillations that at least two neutrinos must have a mass, the question remains whether they are Dirac or Majorana fermions. In any case, the SM has to be extended by $SU(2)_L \times U(1)_Y$ singlet neutrino fields, but since we are not concerned with neutrinos here we neglect their masses in (1.12). We will further ignore the possible mixing in the lepton sector and therefore assume only three real coupling parameters $y_i^{(l)}$ in (1.12).

The complex quark Yukawa matrices $\hat{y}_{ij}^{(u)}$ and $\hat{y}_{ij}^{(d)}$ can be diagonalized by transforming the LC and RC up- and down-type quark fields independently to their mass basis (the kinetic terms of chiral quark and lepton fields are invariant under such basis changes). The basis change is expressed in terms of 4 unitary 3×3 matrices $U_{L,R}^{(u,d)}$ acting on the generation indices of the fermions:

$$u'_{L,\,i} = U_{L,\,ij}^{(u)\,\dagger}\,u_{L,\,j}\;,\quad u'_{R,\,i} = U_{R,\,ij}^{(u)\,\dagger}\,u_{R,\,j}\;,\quad d'_{L,\,i} = U_{L,\,ij}^{(d)\,\dagger}\,d_{L,\,j}\;,\quad d'_{R,\,i} = U_{R,\,ij}^{(d)\,\dagger}\,d_{R,\,j}\quad. \tag{1.14}$$

Note that in the unitary gauge the flavour-nondiagonal interaction terms with the charged pseudo-Goldstone boson G^+ in (1.12) disappear. We can then choose the matrices $U_{L,R}^{(u,d)}$ such that the couplings of the quarks and the neutral Higgs boson become diagonal:

$$y_i^{(u)}\,\delta_{ij} = U_{L,\,ik}^{(u)}\,\hat{y}_{kl}^{(u)}\,U_{R,\,lj}^{(u)\,\dagger}\;,\quad y_i^{(d)}\,\delta_{ij} = U_{L,\,ik}^{(d)}\,\hat{y}_{kl}^{(d)}\,U_{R,\,lj}^{(d)\,\dagger}\quad, \tag{1.15}$$

with real $y_i^{(u,d)}$. Now we can rewrite (1.12) as

$$\begin{aligned}\mathcal{L}_{\mathrm{Y}}^{(\mathrm{SM})} \;=\; & \sum_{i=e,\mu,\tau}\frac{y_i^{(l)}}{\sqrt{2}}\left[v\,\overline{l}_i l_i + \overline{l}_i l_i\,h\right] + \sum_{i=d,s,b}\frac{y_i^{(d)}}{\sqrt{2}}\left[v\,\overline{d}_i d_i + \overline{d}_i d_i\,h\right]\\ & + \sum_{i=u,c,t}\frac{y_i^{(u)}}{\sqrt{2}}\left[v\,\overline{u}_i u_i + \overline{u}_i u_i\,h\right],\end{aligned} \tag{1.16}$$

so that one can immediately identify the tree-level masses of the fermions:

$$m_i^{(l)} = \frac{v}{\sqrt{2}}\, y_i^{(l)} \ , \quad m_i^{(d)} = \frac{v}{\sqrt{2}}\, y_i^{(d)} \ , \quad m_i^{(u)} = \frac{v}{\sqrt{2}}\, y_j^{(u)} .$$

Note that for the top quark these relations imply a very large Yukawa coupling $y_t = \mathcal{O}(1)$. Therefore it plays a central role in all processes involving Higgs bosons, for example the total Higgs boson production cross section and the quantum corrections to the Higgs boson mass.

In the SM, the single physical Higgs boson h is a purely CP-even state, thus it couples only to the scalar fermion currents. In the extended Higgs models discussed in the following section, the neutral Higgs bosons can be CP-mixtures so that they also couple to the pseudoscalar fermion currents $\bar{f} i \gamma_5 f$. The interference of amplitudes with scalar and pseudoscalar exchange can lead to observable CP-violation in these scattering processes [30], [31], [32], [33].

1.2. The two-Higgs doublet extension

In this class of models the Higgs sector of the SM is extended by a second complex scalar $SU(2)_L$ doublet with hypercharge $Y = +1$. Adopting the notation from the previous section we write them as

$$\Phi_1 = \left(\varphi_1^+, \varphi_1^{(0)}\right)^T \quad , \quad \Phi_2 = \left(\varphi_2^+, \varphi_2^{(0)}\right)^T . \tag{1.17}$$

In principle both fields can take part in EWSB by acquiring each a nonzero VEV, denoted by v_1 and v_2 in the following. Although this extension seems very straightforward, a detailed treatment of these models can get very extensive. The book [34] and the review [35] for example provide thorough introductions. The possible ground states and masses of the physical Higgs bosons are determined by the potential. The most general hermitian, gauge invariant and renormalizable two-Higgs potential [35] reads

$$\begin{aligned} V\left(\Phi_1,\Phi_2\right) \;=\;& -\mu_1^2|\Phi_1|^2 - \mu_2^2|\Phi_2|^2 - \left(\mu_3^2\Phi_1^\dagger\Phi_2 + \text{h.c.}\right) \\ & + \frac{\lambda_1}{2}|\Phi_1|^4 + \frac{\lambda_2}{2}|\Phi_2|^4 + \lambda_3|\Phi_1|^2|\Phi_2|^2 + \lambda_4|\Phi_1^\dagger\Phi_2|^2 \\ & + \left[\frac{\lambda_5}{2}\left(\Phi_1^\dagger\Phi_2\right)^2 + \lambda_6\left(\Phi_1^\dagger\Phi_1\right)\left(\Phi_1^\dagger\Phi_2\right) + \lambda_7\left(\Phi_2^\dagger\Phi_2\right)\left(\Phi_1^\dagger\Phi_2\right) + \text{h.c.}\right], \end{aligned} \tag{1.18}$$

with real numbers μ_1^2, μ_2^2, $\lambda_{1,2,3,4}$ and complex numbers μ_3^2, $\lambda_{5,6,7}$, adding up to 14 free parameters. Note that the actual number of free parameters is smaller, as will be discussed below. For the potential (1.18) to have a stable ground state it is necessary that it is bounded from below, i.e. it should tend to $+\infty$ for all directions in (Φ_1,Φ_2) space. It is shown in [35] that the conditions

$$\begin{aligned} \lambda_1 \geq 0 \quad &, \quad \lambda_2 \geq 0, \\ \lambda_3 \geq -\sqrt{\lambda_1\lambda_2} \quad &, \quad \lambda_3 + \lambda_4 - |\lambda_5| \geq -\sqrt{\lambda_1\lambda_2} \end{aligned} \tag{1.19}$$

are necessary for a bounded potential. In the following we will be concerned with the case

$$\lambda_6 = \lambda_7 = 0,$$

where the conditions (1.19) are even sufficient. Note that these are tree-level relations. To be more precise one must compute the quantum corrections to V, in particular one has to take the running of parameters into account and investigate at which energy scales the conditions (1.19) are still fullfilled.

The coupling of the two doublets (1.17) to the SM gauge sector as well as their self-interactions are described by the Lagrangian

$$\mathcal{L}_{\text{Higgs}} = \sum_{i=1,2} (D_\mu \Phi_i)^\dagger (D^\mu \Phi_i) - V(\Phi_1, \Phi_2), \tag{1.20}$$

with D^μ defined as in (1.3). In the 2HDM both doublets can contribute to the generation of the gauge boson masses with terms proportional to their VEVs $|v_i|$. However, the squared sum has to be fixed to the value derived from (1.10) in the last section

$$v = \sqrt{|v_1|^2 + |v_2|^2} = 246\,\text{GeV}.$$

One important and widely used parameter in all 2HDMs is the ratio of the two VEVs:

$$\tan\beta = \frac{|v_2|}{|v_1|}. \tag{1.21}$$

The two doublets (1.17) themselves can not be regarded as physical quantities. The kinetic term in (1.20) is invariant under basis changes

$$\Phi_i' = \sum_{j=1,2} U_{ij} \Phi_j, \tag{1.22}$$

where U_{ij} is a unitary 2×2 matrix. This allows one to eliminate 3 of the 14 parameters in the potential (1.18), leaving only 11 free parameters in the most general case[3]. Further this implies that all physically meaningful quantities must be expressed in terms of invariants under (1.22). These are, for example, the mass eigenstates and eigenvalues of the potential that describe the physical Higgs bosons, [36].

Still, there is a high number of free parameters left which allows for a broad range of phenomenological outcomes. One often further reduces this number of parameters in a systematic way by enforcing additional symmetries on the Lagrangian (1.20). For example, imposing the Z_2 symmetry

$$\Phi_1, \Phi_2 \to \Phi_1, -\Phi_2 \tag{1.23}$$

eliminates the terms proportional to μ_3^2, λ_6 and λ_7 in (1.18). This symmetry, if extended appropriately to the Yukawa interactions, also suppresses flavour changing neutral currents (FCNCs) at tree-level in the interactions with fermions, as will be seen later. In

[3] The overall phase of the unitary matrix U has no effect on the parameters of the potential, therefore one can assume that $U \in SU(2)$. Thus with (1.22) one can eliminate at most one phase and two real parameters [35].

the following we will focus on scenarios where CP parity is broken by the potential (1.18) at tree-level. In this case one has to retain the μ_3^2 term that breaks the symmetry (1.23) only softly, meaning that it is restored at high energy scales where dimension two operators become unimportant[4]. Otherwise the complex phase of the parameter λ_5 alone could be eliminated by rephasing the Φ_i and CP would be conserved, see [35] for details. Thus, it is the relative phase of the complex parameters μ_3 and λ_5 that determines if CP is broken in the 2HDM. The requirement of tree-level CP violation is often formulated in terms of the condition

$$\mathrm{Im}\left(\frac{\lambda_5}{\mu_3^2}\right) \neq 0.$$

To determine the condition for EWSB in the potential (1.18) one has to evaluate its first derivatives and find the non-trivial solution of

$$\frac{\partial V}{\partial \varphi_i^\pm} = 0 \quad , \quad \frac{\partial V}{\partial \varphi_i^{(0)}} = 0. \tag{1.24}$$

We will use the freedom to rephase the two Φ_i independently and assume that

$$\langle \Phi_1 \rangle = \left(0, \frac{v_1}{\sqrt{2}}\right) \quad , \quad \langle \Phi_2 \rangle = \left(0, \frac{v_2}{\sqrt{2}}\right), \tag{1.25}$$

with real numbers v_i, is a solution of (1.24) and that it is the global minimum of (1.18)[5]. The conditions (1.24) can then be used to relate the parameters $\mu_{1,2}^2$ to the VEVs $v_{1,2}$. Again it is useful at this point to rewrite (1.17) as

$$\Phi_1 = \left(\varphi_1^+, \frac{1}{\sqrt{2}}\left(v_1 + \varphi_1 + i\chi_1\right)\right)^T \quad , \quad \Phi_2 = \left(\varphi_2^+, \frac{1}{\sqrt{2}}\left(v_2 + \varphi_2 + i\chi_2\right)\right)^T. \tag{1.26}$$

Similarly to the minimal model described in Sec. 1.1, the φ_i^+ are complex fields and φ_i, χ_i are real fields, the first CP-even and the latter CP-odd. The linear combinations of these field that describe the physical Higgs bosons are identified by diagonalizing the matrices of second derivatives of the potential

$$\begin{aligned} \mathcal{M}_{ij}^{\pm\,2} &= \left.\frac{\partial^2 V}{\partial \varphi_i^+ \partial \varphi_j^-}\right|_{\langle\Phi_1\rangle,\,\langle\Phi_2\rangle}, \\ \mathcal{M}_{ij}^{2} &= \left.\frac{1}{2}\frac{\partial^2 V}{\partial N_i \partial N_j}\right|_{\langle\Phi_1\rangle,\,\langle\Phi_2\rangle}, \qquad N^T = \left(\varphi_1, \varphi_2, \chi_1, \chi_2\right), \end{aligned} \tag{1.27}$$

[4] As to loop corrections, the UV structure is the same as in the theory with exact Z_2 symmetry.

[5] We exclude a possible charge breaking minimum from the discussion and neglect also the issue of multiple minima, for details on this see [35].

and determining their eigenstates and eigenvalues. In (1.27) it is already assumed that the derivatives $\left.\frac{\partial^2 V}{\partial\varphi_i^+ \partial N_j}\right|_{\langle\Phi_1\rangle, \langle\Phi_2\rangle} = 0$ vanish, i.e. that the charged and neutral states decouple. Note that both matrices contain a zero eigenvalue corresponding to the charged and neutral pseudo-Goldstone bosons that appear after EWSB as the longitudinal degrees of freedom of the weak gauge bosons. Non-zero off-diagonal entries $\mathcal{M}_{13}^2$, $\mathcal{M}_{23}^2$ in the neutral mass matrix indicate mixing of the CP-eigenstates φ_i and χ_i into physical states with undefined CP parity.

In the next two subsections the couplings of the physical Higgs bosons to the gauge bosons and fermions will be derived. This is crucial because they determine the production mechanisms and decay signatures of the Higgs bosons.

1.2.1. Higgs basis and mass basis

A basis transformation of the type (1.22) also redistributes the VEVs among the two doublets (1.26). The transformation

$$\begin{pmatrix} \Phi_1' \\ \Phi_2' \end{pmatrix} = \begin{pmatrix} \cos\beta & \sin\beta \\ -\sin\beta & \cos\beta \end{pmatrix} \begin{pmatrix} \Phi_1 \\ \Phi_2 \end{pmatrix} \tag{1.28}$$

shifts the VEV completely to the first doublet. In this basis (the 'Higgs-basis') the ground state of the potential has the form

$$\langle\Phi_1'\rangle = \left(0, \frac{v}{\sqrt{2}}\right)^T \quad , \quad \langle\Phi_2'\rangle = (0,0)^T ,$$

and we can parametrize the two doublets as

$$\Phi_1' = \left(G^+, \frac{1}{\sqrt{2}}\left(v + H_1 + iG_0\right)\right)^T \quad , \quad \Phi_2' = \left(H^+, \frac{1}{\sqrt{2}}\left(H_2 + iA\right)\right)^T . \tag{1.29}$$

The CP properties of the component fields remain unchanged, i.e. H_1 and H_2 are CP-even whereas A and G_0 are CP-odd. Transforming the mass matrices (1.27) to the Higgs basis one can identify the two states corresponding to the eigenvalue 0 in the charged and neutral Higgs mass matrices,

$$\begin{aligned} G^+ &= \cos\beta\,\varphi_1^+ + \sin\beta\,\varphi_2^+, \\ G_0 &= \cos\beta\,\chi_1 + \sin\beta\,\chi_2, \end{aligned} \tag{1.30}$$

as the pseudo-Goldstone bosons which get absorbed by the $W^\pm$ and Z. For further details see appendix B. The linear combination orthogonal to G^+,

$$H^+ \;=\; -\sin\beta\,\varphi_1^+ + \cos\beta\,\varphi_2^+,$$

describes the physical charged Higgs boson with mass

$$m_\pm^2 \;=\; \frac{v^2}{2}\left(2\nu - \lambda_4 - \mathrm{Re}\left(\lambda_5\right)\right). \tag{1.31}$$

The dimensionless parameter ν is defined by

$$\nu \;=\; \frac{\mathrm{Re}\left(\mu_3^2\right)}{v^2\,\cos\beta\sin\beta}. \tag{1.32}$$

It is often used instead of μ_3^2 to control the soft breaking of the symmetry (1.23) in the model. The relation of the neutral mass eigenstates $\phi_{1,2,3}$ to the CP eigenstates $\varphi_{1,2}$ and A is given by an orthogonal matrix R,

$$\begin{pmatrix}\phi_1\\ \phi_2\\ \phi_3\end{pmatrix} \;=\; \underbrace{\begin{pmatrix} c_1c_2 & c_2s_1 & s_2\\ -c_1s_2s_3 - c_3s_1 & c_1c_3 - s_1s_2s_3 & c_2s_3\\ -c_1s_2c_3 + s_3s_1 & -c_1s_3 - s_1s_2c_3 & c_2c_3\end{pmatrix}}_{=R}\begin{pmatrix}\varphi_1\\ \varphi_2\\ A\end{pmatrix}, \tag{1.33}$$

which is conventionally parametrized in terms of three angles $\alpha_{1,2,3}$. We defined $c_i = \cos\alpha_i$ and $s_i = \sin\alpha_i$. Due to the symmetries of the mixing matrix R one can restrict the range of the angles to $-\frac{\pi}{2} < \alpha_i < \frac{\pi}{2}$ [37]. Note that in this convention the relation of the Higgs basis to the mass eigenstates reads

$$\begin{pmatrix}\phi_1\\ \phi_2\\ \phi_3\end{pmatrix} \;=\; R\underbrace{\begin{pmatrix} c_\beta & -s_\beta & 0\\ s_\beta & c_\beta & 0\\ 0 & 0 & 1\end{pmatrix}}_{=B'}\begin{pmatrix}H_1\\ H_2\\ A\end{pmatrix}, \tag{1.34}$$

where the abbreviations $\sin\beta = s_\beta$ and $\cos\beta = c_\beta$ were used. For further studies within this model it is useful to express the 10 parameters

$$\mathcal{P}_0 \;=\; \{\mu_{1,2}^2,\ \mathrm{Re}\left(\mu_3^2\right),\ \mathrm{Im}\left(\mu_3^2\right),\lambda_{1,2,3,4},\ \mathrm{Re}\left(\lambda_5\right),\ \mathrm{Im}\left(\lambda_5\right)\} \tag{1.35}$$

of the potential (1.18) in terms of the more physical parameters

$$\mathcal{P} \;=\; \{v,\, \tan\beta, m_{1,2}, m_{\pm}, \nu, \alpha_{1,2,3}\,\}. \tag{1.36}$$

The details of the transition from (1.35) to (1.36) are given in appendix B. Since $v = 246$ GeV is fixed there are in total 8 free parameters left in the 2HDM with softly broken Z_2 symmetry. One of the CP conserving scenarios is obtained by setting $\alpha_3 = \alpha_2 = 0$. In this case $\phi_{1,2}$ are CP-even and ϕ_3 is CP-odd and only the angle α_1 is left as a free parameter, describing the mixing of the two CP-even components $\phi_{1,2}$. This scenario is realized for example in the minimal supersymmetric extension of the SM, described in section 1.3.

1.2.2. Couplings to the gauge bosons and self-interactions

Expanding the kinetic term in (1.20) with the doublets in the Higgs-basis (1.29) one can identify the various tree-level vertices involving Higgs and gauge bosons. In [38] this is done for a general model with an arbitrary number of $SU(2)_L$ doublets and singlets and can easily be adjusted to this 2HDM. Using the unitary gauge (1.9) to eliminate the pseudo-Goldstone bosons G^+ and G_0, one obtains

$$\begin{aligned}
(D_\mu \Phi'_i)^\dagger\,(D^\mu \Phi'_i) \;=\; & \frac{1}{2}\,(\partial_\mu H_1)\,(\partial^\mu H_1) + \frac{1}{2}\,(\partial_\mu H_2)\,(\partial^\mu H_2) + \frac{1}{2}\,(\partial_\mu A)\,(\partial^\mu A) + \left(\partial_\mu H^+\right)\left(\partial^\mu H^-\right) \\
& + m_W^2 W^{+\mu} W^-_\mu + \frac{m_Z^2}{2} Z^\mu Z_\mu \\
& + i\left(eA_\mu + \frac{g(2s_W^2-1)}{2c_W} Z_\mu\right)\left(H^+\partial^\mu H^- - H^-\partial^\mu H^+\right) \\
& + \frac{g}{2c_W} Z_\mu\,(H_2 \partial^\mu A - A\,\partial^\mu H_2) \\
& + i\frac{g}{2} W^+_\mu \left(H^-\partial^\mu H_2 - H_2\partial^\mu H^- + iH^-\partial^\mu A - iA\,\partial^\mu H^-\right) + \text{h.c.} \\
& + g\left(m_W W^{+\mu} W^-_\mu + \frac{m_Z}{2c_W} Z^\mu Z_\mu\right) H_1 \\
& + \text{quartic terms.}
\end{aligned} \tag{1.37}$$

Here one can see that the neutral CP-even field H_1 (coming from the doublet with the non-zero VEV in the Higgs basis) exhibits the same interactions with the gauge bosons as h in the SM, but note that H_1 does not describe a physical Higgs boson in general. Using (B.5) and (1.33) to express the CP-eigenstates in the Higgs basis in terms of the mass eigenstates one can identify the following trilinear interaction terms:

$$H^\pm H^\mp \gamma\,,\; H^\pm H^\mp Z\,,\; \phi_i \phi_j Z\,,\; \phi_i H^\pm W^\mp\,,\; \phi_i VV. \tag{1.38}$$

The Feynman rules for the $\phi_i\phi_j Z$ and $\phi_i VV$ interactions will be used later and are therefore written down in (A.11) and (A.12). Note that the orthogonality of R implies the following sum rule for the $\phi_i VV$ couplings:

$$\left(2\frac{m_V^2}{v}\right)^2 \sum_{j=1}^{3} (\cos\beta R_{j1} + \sin\beta R_{j2})^2 \quad = \quad g^2 m_V^2 \ , \quad V = \{W^\pm, Z\}. \tag{1.39}$$

This guarantees the cancellation of growing energy terms in $W_L W_L/Z_L Z_L \to W_L W_L/Z_L Z_L$ scattering amplitudes so that the interactions of electroweak gauge bosons remain perturbative as long as the Higgs bosons are not too heavy. To guarantee unitarity also in $f\bar{f} \to VV$ scattering amplitudes, similar sum rules must hold for the Higgs-fermion couplings. See [39] for details.

In the full expression of (1.37), c.f. [38] or the appendix of [35], one can also find the following quartic interactions:

$$\begin{aligned} \phi_j H^\pm W^\mp Z \quad &, \quad \phi_j H^\pm W^\mp \gamma, \\ \phi_j^2 VV \quad &, \quad H^\pm H^\mp W^\pm W^\mp, \\ H^\pm H^\mp \gamma\gamma \quad &, \quad H^\pm H^\mp ZZ, \\ H^\pm H^\mp \gamma Z \quad &. \end{aligned} \tag{1.40}$$

The self-interactions of the physical Higgs bosons can be derived from the potential (1.18) if the relation (1.33) is substituted. The resulting expression is rather large and the following self-coupling structures can be identified:

$$\begin{aligned} \phi_i H^+ H^- \quad &, \quad H^+ H^- H^+ H^-, \\ \phi_i \phi_j \phi_k \quad &, \quad \phi_i \phi_j H^+ H^-, \\ & \quad\ \ \phi_i \phi_j \phi_k \phi_l. \end{aligned} \tag{1.41}$$

The Feynman rule for the $\phi_i\phi_j\phi_k$ vertex is derived in (A.13) for later use, for the Feynman rules corresponding to the other interaction terms c.f. the appendix of [40]. Note that in the CP-conserving scenario with $\alpha_3 = \alpha_2 = 0$ one finds that the tree-level $\phi_1 VV$ coupling given in (A.11) vanishes. Thus analyzing the decay channels $\phi_1 \to ZZ, W^+W^-$ can help to distinguish between CP-even and CP-odd Higgs bosons.

In the following we want to identify one of the 3 neutral Higgs bosons with the boson that was recently discovered at the LHC. The measurement of the couplings to gauge boson pairs and third generation fermion pairs point to the SM value, c.f. table (1.1) and [6], [41]. Though, it should be noted that the uncertainties of 10-30% are still rather large and that these particular results (1.1) were obtained assuming a purely CP-even boson. It is still possible that this boson contains a sizeable CP-odd component. Choosing $\phi_1 = h$ as the candidate, we have to set $m_1 \simeq 125$ GeV and align the reduced $\phi_1 VV$ coupling with the SM value, i.e. $\cos\beta R_{11} + \sin\beta R_{12} \simeq 1$ in (A.11). The sum rule (1.39) then implies that the couplings $\phi_{2,3}VV$ of the other two neutral Higgs bosons to gauge boson pairs are suppressed. This is an interesting case for us, because it allows for scenarios where the total widths of the other two neutral Higgs bosons $\phi_{2,3}$ are dominated by the decay $\phi_{2,3} \to t\bar{t}$, given that their masses are above the threshold $m_{2,3} > 2m_t$.

Table 1.1. – *CMS measurement of the reduced Higgs boson couplings with 68% confidence intervals [6]. Assuming that the* 125 *GeV resonance is a purely CP-even boson, the hVV and $hf\bar{f}$ couplings have the form $\kappa_V \frac{2m_V^2}{v}$ and $\kappa_f \frac{m_f}{v}$ with $v = 246.22$ GeV, respectively.*

κ_W	$0.95^{+0.14}_{-0.13}$
κ_Z	$1.05^{+0.16}_{-0.16}$
κ_t	$0.81^{+0.19}_{-0.15}$
κ_b	$0.74^{+0.33}_{-0.29}$
κ_τ	$0.84^{+0.19}_{-0.18}$
κ_μ	< 1.87

1.2.3. Yukawa couplings in the type-II 2HDM

The 2HDM are further classified by the couplings of the Higgs doublets to the fermions. In the following we will focus on the type-II two-Higgs doublet models. They are defined as follows:

- Φ_1 is coupled only to right chiral (RC) down-type quarks $d_{R,j}$ and RC leptons $l_{R,j}$,
- Φ_2 is coupled only to RC up-type quark $u_{R,j}$.

This setup avoids tree-level flavor changing neutral currents (FCNC) which are highly constrained by experimental data. As already mentioned, these couplings can be enforced by extending the Z_2 symmetry (1.23) to the fermion sector:

$$\begin{aligned} \Phi_1 &\rightarrow \Phi_1, \\ d_{R,j} &\rightarrow d_{R,j}, \\ \Phi_2 &\rightarrow -\Phi_2, \\ u_{R,j} &\rightarrow -u_{R,j}. \end{aligned} \tag{1.42}$$

The Z_2 and $SU(2)_L \times U(1)_Y$ invariant Yukawa couplings are given by

$$\mathcal{L}_{\mathrm{Y}}^{(2\mathrm{HDM})} = -y_i^{(l)} \overline{L_{L,i}} \Phi_1 \, l_{R,i} - \hat{y}_{ij}^{(d)} \overline{Q'_{L,i}} \Phi_1 \, d'_{R,j} - \hat{y}_{ij}^{(u)} \overline{Q'_{L,i}} \left(i\sigma_2 \Phi_2^*\right) u'_{R,j} + \text{h.c.}, \tag{1.43}$$

where $L_{L,i} = (\nu_{L,i}, l_{L,i})^T$ and $Q'_{L,i} = \left(u'_{L,i}, d'_{L,i}\right)^T$ denote again the left chiral (LC) components of the leptons and quarks in the weak basis, respectively, and $l_{R,i}$, $d'_{R,j}$, $u'_{R,j}$ denote the RC components. The indices $i, j \in \{1, 2, 3\}$ label the fermion generation. The Yukawa couplings of quarks and the neutral components $\varphi_{1,2}^{(0)}$ in (1.43) are diagonalized analogously to (1.15) by transforming the LC and RC quark fields to the mass eigenstates $u_{L,R}$, $d_{L,R}$, c.f. (1.14). The Yukawa couplings of quarks and the charged components $\varphi_{1,2}^{\pm}$ however can not be diagonalized simultaneously, but the quark mixing in these interaction terms can be expressed in terms of a single unitary matrix $V_{\mathrm{CKM}} = U_L^{(d)} U_L^{(u)\,\dagger}$. Suppressing the generation indices one can write

$$\begin{aligned} \mathcal{L}_{\mathrm{Y},\pm}^{(2\mathrm{HDM})} &= -\overline{u'_L}\, \hat{y}^{(d)}\, d'_R\, \varphi_1^+ + \overline{d'_L}\, \hat{y}^{(u)}\, u'_R\, \varphi_2^- + \text{h.c.} \\ &\overset{(1.14)}{\rightarrow} -\overline{u_L} \left(V_{\mathrm{CKM}}\, y^{(d)}\right) d_R\, \varphi_1^+ + \overline{d_L} \left(V_{\mathrm{CKM}}^\dagger\, y^{(u)}\right) u_R\, \varphi_2^- + \text{h.c.}, \end{aligned} \tag{1.44}$$

where $y^{(u)}$ and $y^{(d)}$ are the diagonal up- and down-type quark Yukawa coupling matrices, defined analogously to (1.15). Note that $i\sigma_2 \Phi_2^* = \left(\varphi^{(0)\,*},\ -\varphi^-\right)^T$ in (1.43). In the unitary gauge, where we set $G^+ = 0$ in (1.30), one can substitute

$$\begin{aligned}\varphi_1^\pm &= -\sin\beta\, H^\pm ,\\ \varphi_2^\pm &= \cos\beta\, H^\pm ,\end{aligned}$$

and rewrite (1.44) as

$$\mathcal{L}^{(\mathrm{2HDM})}_{\mathrm{Y},\pm} = \overline{u_L}\left(V_{\mathrm{CKM}}\, y^{(d)}\right) d_R\, \sin\beta\, H^+ + \overline{d_L}\left(V^\dagger_{\mathrm{CKM}}\, y^{(u)}\right) u_R\, \cos\beta\, H^- + \text{h.c.}. \tag{1.45}$$

For the sake of completeness the resulting Feynman rule is written down in (A.8). More important for our investigations in the following sections are the Yukawa interaction terms of quarks and leptons with the neutral component of the Higgs doublets. For example, the Yukawa interaction term of the up-type quarks with $i\sigma_2\Phi_2^*$ in (1.43) can be simplified as follows:

$$-\overline{u_L}\, y^{(u)}\, u_R\, \frac{v_2 + \varphi_2 - i\chi_2}{\sqrt{2}} + \text{h.c.} = -\frac{1}{\sqrt{2}}\left[\overline{u}\, y^{(u)}\, u\, \left(v_2 + \varphi_2\right) - \overline{u}\,\gamma_5 y^{(u)}\, u\, i\chi_2\right],$$

and analogously for down-type quarks and leptons. Using the relations (1.33) and

$$\begin{aligned}\chi_1 &= -\sin\beta\, A,\\ \chi_2 &= \cos\beta\, A,\end{aligned}$$

where we assumed $G_0 = 0$ in the unitary gauge, we can bring (1.43) into the form

$$\begin{aligned}\mathcal{L}^{(\mathrm{2HDM})}_{\mathrm{Y}} &= -\sum_{j=1,2,3}\sum_f \left[m_f \overline{f} f + \frac{m_f}{v}\left(a_{f,j}\,\overline{f} f - i b_{f,j}\,\overline{f}\gamma_5 f\right)\phi_j\right]\\ &\quad + \mathcal{L}^{(\mathrm{2HDM})}_{\mathrm{Y},\pm}.\end{aligned} \tag{1.46}$$

In this expression, the letter f denotes the Dirac field of the respective quark or charged lepton and m_f its mass.

$$m_i^{(l)} = \frac{v_1}{\sqrt{2}}\, y_i^{(l)}\ ,\quad m_i^{(d)} = \frac{v_1}{\sqrt{2}}\, y_i^{(d)}\ ,\quad m_i^{(u)} = \frac{v_2}{\sqrt{2}}\, y_j^{(u)}.$$

The Feynman rule for neutral scalar interactions with fermions derived from the Lagrangian (1.46) is written down in (A.7) in the appendix. Computing physical observables, the exchange of each neutral Higgs boson generates interferences of scalar and pseudoscalar amplitudes with a CP-odd phase proportional to

$$\gamma^{(f)}_{\mathrm{CP,j}} \;=\; a_{f,j}\, b_{f,j} = \begin{cases} \frac{\cos\beta}{\sin^2\beta} R_{j2}R_{j3}\ , & f = u\ , \\ \frac{\sin\beta}{\cos^2\beta} R_{j1}R_{j3}\ , & f = d/l\ , \end{cases} \tag{1.47}$$

which quantifies to which amount CP is violated in the Yukawa sector, c.f. [30], [31], [32], [33]. The second equality in (1.47) is only valid for the type-II 2HDM where the reduced Yukawa couplings in (1.46) have the form

$$\begin{aligned} a_{u,j} &= \frac{R_{j2}}{\sin\beta} \quad , \quad b_{u,j} = R_{j3}\cot\beta, \\ a_{d/l,j} &= \frac{R_{j1}}{\cos\beta} \quad , \quad b_{d/l,j} = R_{j3}\tan\beta. \end{aligned} \tag{1.48}$$

In the alignment limit where ϕ_1 corresponds to a SM-like Higgs boson with mass of 125 GeV, one has to tune $\tan\beta$ and the mixing angles α_i such that the reduced couplings (1.48) correspond to the SM values, i.e.

$$\begin{aligned} a_{u,1} &= \frac{R_{12}}{\sin\beta} \approx 1 \quad , \quad b_{u,1} = R_{13}\cot\beta \approx 0, \\ a_{d/l,1} &= \frac{R_{11}}{\cos\beta} \approx 1 \quad , \quad b_{d/l,1} = R_{13}\tan\beta \approx 0. \end{aligned} \tag{1.49}$$

This strongly constrains two of the three angles in R to values $\alpha_1 \approx \beta$ and $\alpha_2 \approx 0$, corresponding to $R_{12} \approx \sin\beta$, $R_{11} \approx \cos\beta$ and $R_{13} \approx 0$. Thus

$$R^{\text{align.}} \;\approx\; \begin{pmatrix} c_\beta & s_\beta & 0 \\ -c_3 s_\beta & c_\beta c_3 & s_3 \\ s_3 s_\beta & -c_\beta s_3 & c_3 \end{pmatrix} \tag{1.50}$$

with $c_\beta = \cos\beta$ and $s_\beta = \sin\beta$. I.e. in this case ϕ_1 is a mixture of the two CP-even fields φ_1 and φ_2 only. The remaining free parameter α_3 controls the size of the CP-odd component A in the mass eigenstates $\phi_{2,3}$. The reduced Yukawa couplings of fermions and $\phi_{2,3}$ are

$$\begin{aligned} a_{u,2} &= \frac{R_{22}}{\sin\beta} \approx \cot\beta\cos\alpha_3 \quad , \quad b_{u,2} = R_{23}\cot\beta \approx \sin\alpha_3\cot\beta, \\ a_{d/l,2} &= \frac{R_{21}}{\cos\beta} \approx -\tan\beta\cos\alpha_3 \quad , \quad b_{d/l,2} = R_{23}\tan\beta \approx \sin\alpha_3\tan\beta, \end{aligned} \tag{1.51}$$

and

$$\begin{aligned} a_{u,3} &= \frac{R_{32}}{\sin\beta} \approx -\cot\beta\sin\alpha_3 \quad , \quad b_{u,3} = R_{33}\cot\beta \approx \cos\alpha_3\cot\beta, \\ a_{d/l,3} &= \frac{R_{31}}{\cos\beta} \approx -\tan\beta\sin\alpha_3 \quad , \quad b_{d/l,3} = R_{33}\tan\beta \approx \cos\alpha_3\tan\beta. \end{aligned} \tag{1.52}$$

Because the SM top-quark Yukawa coupling $\frac{m_t}{v}$ is $\mathcal{O}(1)$, small values of $\tan\beta$ in the reduced coupling (1.48) quickly lead to an enhancement above the naive perturbativity bound which requires $y_t < 4\pi$. For a comprehensive survey of the theoretical limits on the 2HDM parameters arising from the requirements of perturbativity and vacuum stability see for example [42]. Large values of $\tan\beta$ on the other hand simultaneously enhance the reduced bottom-quark Yukawa coupling and suppress the reduced top-quark Yukawa coupling in (1.48) until y_t and y_b are of comparable size. We want to avoid this scenario in the following. Setting $\tan\beta \sim 1$ the top-Yukawa coupling y_t is dominant and y_b, y_τ are small enough so that the resulting rates for the decays of the $\phi_{2,3}$ to $b\bar{b}$ and $\tau^+\tau^-$ are very small if $m_{2,3} > 2m_t$, c.f. Sec. 1.2.5.

Also here the LHC measurements of the reduced Yukawa couplings of the 125 GeV resonance to the third generation fermions point to the SM values $a_{f,i} = 1$ and $b_{f,i} = 0$ but the uncertainties of 20% - 30% are still rather large, c.f. table (1.1) and [41], [43]. Therefore this can not be regarded as a stringent restriction at the moment, specifically the values of the mixing angles $\alpha_{1,2}$ are allowed to deviate from the alignment values $\alpha_1 = \beta$ and $\alpha_2 = 0$.

1.2.4. Note on experimental constraints on the 2HDM parameters

Besides the constraints derived from theoretical considerations, notably that of vacuum stability and perturbativity, which were briefly mentioned in the previous sections, there are constraints on the physical parameters (1.36) coming from various experiments. Most important are the results from B-physics, electric dipole moments (EDMs) of leptons and nucleons and the recent LHC data for the light Higgs boson which point - within errors of 10-30% - to the SM values, see Tab. (1.1).

The non-observation of deviations from the SM predictions in B-physics data places limits on the parameters $\tan\beta$ and $m_\pm$. These parameters control the effect of charged Higgs bosons on loop induced observables like rare decays $B \to X_s + \gamma$ (X_s denotes hadrons with total strangeness $s = -1$) and neutral $B_d^0 - \bar{B}_d^0$ mixing. In general the loop-effects of charged Higgs bosons decrease with increasing mass $m_\pm$ and vice versa. In the type-II 2HDM the coupling of the charged Higgs to the top-quark yields a factor $m_t\cot\beta$, c.f. the Feynman rule (A.8). Thus, small values of $\tan\beta$ need to be compensated by larger $m_\pm$ to be consistent with experimental data [44].

The non-observation of electric dipole moments (EDM) of the electron and the neutron puts limits on the CP violating phases such as (1.47). Although these limits are highly model dependent, in particular the measurement of the electron EDM excludes a large pseudoscalar coupling of the light Higgs boson to the third quark generation [45]. Working in the alignment limit (1.50) ensures that one is consistent with the EDM data.

The electroweak parameter $\rho = \frac{m_W^2}{\cos^2\theta_W\, m_Z^2} = 1.00040 \pm 0.00024$ [12] is very sensitive to new physics that affect the gauge boson self-energies. The tree-level value is fixed to $\rho = 1$ in the SM and also in all extensions of the Higgs sector as long as only $SU(2)_L \times U(1)_Y$ doublets with $Y = \pm 1$ or singlets with $Y = 0$ are considered. Additional neutral and charged Higgs bosons affect the gauge boson self-energies through loop corrections [38]. These effects must be small since the experimental value of ρ matches the SM prediction very precisely. The constraints from electroweak precision measuremtnts are satisfied within 2HDM scenarios where the masses of the additional Higgs bosons are large and the mixing angles are such that the couplings to the gauge bosons are suppressed with respect to the SM couplings.

1.2.5. Neutral Higgs boson decay widths

The total decay widths of the neutral physical Higgs bosons $\phi_{1,2,3}$ enter as parameters in the computation of the process $pp \to \phi_i \to t\bar{t}$ which constitutes the main part of this thesis. Therefore the relevant leading order decay widths are collected and discussed in this section. We are interested in scenarios where one of the neutral Higgs bosons, say ϕ_1, is light with mass close to 125 GeV and with couplings within a 10% - 30% range of the SM values. The other two neutral bosons ϕ_2 and ϕ_3 shall be heavy, with masses in the range $2m_t < m_2, m_3 < 800$ GeV, so that their decay to top quarks is kinematically allowed. Regarding the charged Higgs boson $H^\pm$, we will assume in the following that it is sufficiently heavy, so that the decays $\phi_{2,3} \to H^+H^-$ are not allowed. In this setup the following two-body decay modes of the two heavy neutral Higgs bosons $\phi_{2,3}$ are most relevant:

$$\phi_{2,3} \quad \to \quad W^+W^-,\, ZZ,\, t\bar{t},\, b\bar{b},\, \tau^+\tau^-,\, Z\phi_1,\, \phi_1\phi_1,\, gg\,.$$

The three-body decays induced by the quartic couplings (1.40) are suppressed due to the reduced phase space and will be omitted in the following discussion.

The decay to fermion pairs $\phi_{2,3} \to f\bar{f}$

The tree-level decay width is given by

$$\Gamma(\phi_j \to f\bar{f}) \;=\; \frac{N_c}{8\pi}\frac{m_f^2}{v^2}\, m_j\, \left(a_{f,j}^2\beta_f^3 + b_{f,j}^2\beta_f\right)\,, \quad j \in \{2,3\}\,, \tag{1.53}$$

with $\beta_f^2 = 1 - \frac{4m_f^2}{m_j^2}$. We have to set $N_c = 3$ for the decay to quarks and $N_c = 1$ for the decay to charged leptons. Note that at the production threshold the decay of a CP-even boson is suppressed by a factor β_f^2 with respect to that of a CP-odd boson. The reason is that the parity of the $f\bar{f}$ state is $P = (-1)^{l+1}$ if the total angular momentum quantum number is l. Thus, near threshold, a CP-odd boson will produce the $f\bar{f}$ pair in a ${}^1S_0$ state whereas a CP-even boson produces the fermions in a ${}^3P_0$ state.

As already mentioned, we will set $\tan\beta \sim 1$, so that the Yukawa couplings of the down type quarks and leptons are much smaller than the SM Yukawa couplings, c.f. (1.51) and (1.52). Then, for $\phi_{2,3}$, only the decays $\phi_{2,3} \to t\bar{t}$ will be relevant in this category.

The decay to gauge boson pairs $\phi_{2,3} \to W^+W^-$, ZZ

The tree-level decay width is given by

$$\Gamma(\phi_j \to VV) = N \frac{f_{jVV}^2}{16\pi v^2} m_j^3 \beta_V \left(1 - 4\frac{m_V^2}{m_j^2} + 12\frac{m_V^4}{m_j^4}\right) , \quad j \in \{2,3\} , \tag{1.54}$$

with $\beta_V = \sqrt{1 - \frac{4m_V^2}{m_j^2}}$ and $V = W^\pm$ or $V = Z$. The tree-level coupling is given by

$$f_{jVV} = (\cos\beta R_{j1} + \sin\beta R_{j2}) , \quad j \in \{2,3\}.$$

We have to adjust the symmetry factor $N = 1$ for the decay to W^+W^- and $N = \frac{1}{2}$ for the decay to ZZ. Note again that there are two disctinct ways in which this decay can be suppressed: either the decaying heavy Higgs boson ϕ_j has only a small CP-even component, so that R_{j1} and R_{j2} are both small, or the couplings of the light Higgs boson ϕ_1 to gauge boson pairs are very close to the SM values. In that case the suppression of the $\phi_{2,3}VV$ couplings follows from the sum rule (1.39).

If the decays to gauge bosons are not suppressed then the total widths $\Gamma_{2,3}$ will increase, which leads to a reduced branching fraction $\mathrm{Br}(\phi_{2,3} \to t\bar{t})$. Signals in top observables, for instance the $t\bar{t}$ mass spectrum, will then be diminished considerably.

The decay $\phi_{2,3} \to \phi_1 Z$

The tree-level width for the decay of a heavy Higgs boson to a light Higgs ϕ_1 and a Z boson is given by

$$\Gamma(\phi_j \to \phi_1 Z) = \frac{f_{j1Z}^2}{16\pi v^2} \frac{\lambda(m_j^2,m_1^2,m_Z^2)^{\frac{3}{2}}}{m_j^3} , \quad j \in \{2,3\} , \tag{1.55}$$

with the tree-level coupling

$$f_{j1Z} \;=\; (-\sin\beta R_{11} + \cos\beta R_{12})\, R_{j3} \;-\, (j \leftrightarrow 1) \;\;, \quad j \in \{2,3\}.$$

The function $\lambda(x,y,z)$ is defined as

$$\lambda(x,y,z) \;=\; x^2 + y^2 + z^2 - 2xz - 2xy - 2yz.$$

In the CP-conserving scenario where we set $\alpha_2 = \alpha_3 = 0$ in (1.33), the neutral boson ϕ_2 will be purely CP-even and ϕ_3 CP-odd. Since $R_{23} = 0$ in this case, we find

$$\Gamma(\phi_2 \to \phi_1 Z) \stackrel{\text{CP}}{=} 0.$$

The decay $\phi_{2,3} \to \phi_1\phi_1$

The decay to a pair of light scalars $\phi_j \to \phi_1\phi_1$ is possible if $m_j > 2m_1$. The tree-level decay width is

$$\Gamma(\phi_j \to \phi_1\phi_1) \;=\; \frac{f_{j11}^2}{32\pi}\frac{\beta_1}{m_j} \;, \quad j \in \{2,3\}. \tag{1.56}$$

The trilinear neutral Higgs coupling f_{j11} takes a quite complicated form in the general type-II 2HDM and is derived in (A.13).

The decay $\phi_{2,3} \to gg$

This decay is induced at leading order by a top-quark loop. The contribution of the bottom quark is rather small in the case $\tan\beta \simeq 1$ which is considered here. The leading order decay width is given by the squared matrix element (3.41) for the process $gg \to \phi$, only the spin average factor and the $\phi \to t\bar{t}$ decay part have to be removed. Adding appropriate flux and phase space factors one obtains

$$\Gamma(\phi_j \to gg) \;=\; \frac{1}{2m_j}\frac{C_F C_A}{16\pi}\left(\frac{\alpha_s}{\pi}\right)^2 \left(|\mathcal{F}_s|^2 + |\mathcal{F}_p|^2\right), \tag{1.57}$$

where the form factors $\mathcal{F}_{s,p}$ will be defined in (2.10). The colour factors are $C_A = N_c$ and $C_F = \frac{N_c^2-1}{2N_c}$, where $N_c = 3$.

The decays $\phi_{2,3} \to \gamma\gamma$ and $\phi_{2,3} \to Z\gamma$

The loop-mediated decay $\phi_1 \to \gamma\gamma$ provided the signal for the discovery of the 125 GeV boson at the LHC, although the branching fraction is several orders of magnitude smaller than those of $\phi_i \to W^+W^-, ZZ$ and $\phi_i \to b\bar{b}$ [34]. One reason for that suppression is the destructive interference of fermion and gauge boson loops that contribute to the leading order decay amplitude. For large Higgs masses m_i the leading order decay width decreases as $\Gamma(\phi_i \to \gamma\gamma) \sim m_i^{-1}$. The same applies for $\phi_i \to Z\gamma$ so that both channels can be safely neglected in the computation of the decay widths of heavy neutral Higgs bosons.

Radiative corrections

The C++ code 2HDMC [46] can be used to compute decay widths within the general CP-conserving 2HDM. The program includes all the above mentioned two-body decays as well as the three-body decays $\phi_i \to V^*V \to f\bar{f}V$ for one off-shell gauge boson. It can also be used to check the tree-level stability, perturbativity and unitarity relations for a given set of parameters. Additionally, the NNLO QCD corrections to the processes $\phi_i \to f\bar{f}$ and $\phi_i \to gg$ in the large m_t limit are included.

Since we also consider CP-violating scenarios, the 2HDMC results can not be used directly. But as can be seen from (1.53), which can be put in the form

$$\Gamma(\phi_j \to f\bar{f}) \quad = \quad a_{f,j}^2\, \tilde{\Gamma}(H_j \to f\bar{f}) + b_{f,j}^2\, \tilde{\Gamma}(A_j \to f\bar{f}),$$

the interference of CP-even and CP-odd components, H_j and A_j respectively, of the Higgs boson ϕ_j do not contribute to the total decay width. Further, the QCD corrections to the total widths can be expressed as a global factor [46]. Thus one can add the corresponding partial widths obtained with 2HDMC and reweight them with the reduced Higgs-fermion couplings in the following way:

$$\Gamma\left(\phi_i \to f\bar{f}\right) \quad = \quad \frac{a_{f,i}^2}{\tilde{a}_f^2}\,\Gamma^{\text{2HDMC}}\left(H \to f\bar{f}\right) + \frac{b_{f,i}^2}{\tilde{b}_f^2}\,\Gamma^{\text{2HDMC}}\left(A \to f\bar{f}\right).$$

In this equation, $\tilde{a}_f$ and $\tilde{b}_f$ are the reduced Yukawa coupling for mass degenerate CP-even and CP-odd Higgs bosons used in 2HDMC[6], whereas $a_{f,i}$ and $b_{f,i}$ are the reduced Yukawa couplings of the Higgs boson ϕ_i obtained via (1.48). One can proceed similarly to calculate the NNLO QCD width for $\phi_i \to gg$ for the general CP violating 2HDM.

[6] In 2HDMC, a tree-level CP conserving 2HDM potential is assumed, i.e. the Yukawa couplings depend only on $\tan\beta$ and the parameter $\sin(\alpha - \beta)$. The latter is related to the parameter α_1 in our convention by $\alpha = \alpha_1 + \frac{\pi}{2}$.

1.3. The Higgs sector in the MSSM

In this section we want to discuss briefly the Higgs sector in the minimal supersymmetric standard model (MSSM). This is interesting for our discussion because the MSSM Higgs sector resembles a type-II 2HDM where the parameters of the Higgs potential are fixed in terms of the gauge coupling parameters g and g'. Thorough reviews on supersymmetry in general and the MSSM can be found in [9] and [8]. The phenomenology of the MSSM Higgs sector is also covered in the book [34]. The MSSM Higgs sector comprises two complex $SU(2)_L$ doublets which we will denote as

$$H_1 = \left(\varphi_1^+, \frac{1}{\sqrt{2}}\left(v_1 + \varphi_1 + i\chi_1\right)\right)^T \quad , \quad H_2 = \left(\frac{1}{\sqrt{2}}\left(v_2 + \varphi_2 + i\chi_2\right), \varphi_2^-\right)^T . \tag{1.58}$$

The assignment (1.58) allows to generate masses of up- and down-type quarks simultaneously without the introduction of a charge-conjugate doublet like (1.13), the appearance of which would violate supersymmetry. Further, to avoid chiral anomalies it is necessary that the hypercharges of the fermionic superpartners – introduced together with the scalar doublets – obey $\sum_i Y_i = 0$. For these reasons (1.58) is the minimal Higgs multiplet structure for an anomaly-free supersymmetric theory with massive up- and down-type quarks. The Higgs potential can be written as

$$\begin{aligned} V\left(H_1,H_2\right) \;=\;& \left(\mu^2 - m_1^2\right)|H_1|^2 + \left(\mu^2 - m_2^2\right)|H_2|^2 - \left[m_3^2\, H_1^T\left(i\sigma_2 H_2\right) + \text{c.c.}\right] \\ & + \frac{\lambda_1}{2}|H_1|^4 + \frac{\lambda_2}{2}|H_2|^4 + \lambda_3|H_1|^2|H_2|^2 + \lambda_4|H_1^\dagger H_2|^2 . \end{aligned} \tag{1.59}$$

The terms proportional to μ^2 and λ_i derive from the superpotential, whereas the terms proportional to m_i^2 were introduced together with a minimal set of softly supersymmetry-breaking terms. The phase of m_3^2 can be eliminated by a redefinition of the H_i, thus we can assume that all parameters are real. The quartic couplings in (1.59) are related to the electroweak gauge couplings g and g' as follows:

$$\lambda_1 = \lambda_2 = \lambda_3 = \frac{g^2 + g'^2}{4} \; , \quad \lambda_4 = \frac{g^2}{2} . \tag{1.60}$$

After EWSB one finds the same physical Higgs spectrum as in the non-supersymmetric, CP-conserving 2HDM, namely one charged Higgs boson and its antiparticle $H^\pm$ and three neutral ones, two CP-even, denoted as h and H, and one CP-odd, denoted as A. It turns out that the terms proportional to m_i^2 in (1.59) are necessary to have a $SU(2)_L \times U(1)_Y$ breaking ground state, meaning that EWSB is triggered automatically by the mechanism that also leads to SUSY breaking[7].

[7] However one has to adjust parameters such that the ground state does not break $SU(3)_\mathrm{c}$ or $U(1)_\mathrm{em}$.

In the MSSM Higgs sector there remain only 2 free parameters after EWSB. For example one could choose the mass of the pseudoscalar m_A and $\tan\beta$. At tree level, the Higgs masses and the angle α, describing the mixing of the two CP-even Higgs bosons, are related via

$$
\begin{aligned}
m_\pm^2 &= m_A^2 + m_W^2, \\
m_{h,H}^2 &= \frac{1}{2}\left[m_A^2 + m_Z^2 \mp \sqrt{\left(m_A^2 + m_Z^2\right)^2 - 4m_A^2 m_Z^2 \cos^2 2\beta}\right], \\
\alpha &= \frac{1}{2}\arctan\left(\frac{m_A^2 + m_Z^2}{m_A^2 - m_Z^2}\tan(2\beta)\right).
\end{aligned}
\tag{1.61}
$$

One important implication of (1.61) is that the tree-level mass m_h is bounded from above

$$
m_h \leq m_Z \cos 2\beta. \tag{1.62}
$$

The radiative corrections to the light Higgs boson mass m_h are dominated by top and stop loops. Due to SUSY breaking the cancellation of these graphs is incomplete, leading to a considerable positive shift

$$
\Delta(m_h) = \frac{3}{4\pi}\frac{\cos^2\alpha}{v^2\sin^2\beta}\log\frac{m_{\tilde{t}_1}m_{\tilde{t}_2}}{m_t^2}.
$$

Indentifying h with the recently discovered boson $m_h \approx 125$ GeV this translates (together with experimental limits on the stop masses) into limits on $\tan\beta$. Global fits to data typically yield $\tan\beta > 5$ within the constrained MSSM [47, 12].

The couplings to the gauge bosons and fermions are the same as in a CP-conserving type-II 2HDM with $\alpha_2 = \alpha_3 = 0$ and $\alpha_1 = \alpha$ in (1.33) and the identification $\phi_1 = h$, $\phi_2 = H$ and $\phi_3 = A$. The constraint on $\tan\beta$ implies that the reduced top-quark Yukawa coupling is suppressed and the bottom- and τ couplings are enhanced. Thus within the MSSM one would choose the $b\bar{b}$ and $\tau\bar{\tau}$ decay modes to search for additional neutral Higgs bosons.

Although the MSSM Higgs potential conserves CP at the tree-level, it should be noted that a sizeable mixing of the CP eigenstates can be induced by loop-corrections involving trilinear interactions of the Higgs bosons and third generation squarks [48], [49].

2. Inclusive Higgs production in proton-proton collisions

For the theoretical description of hard scattering reactions in high energy proton-proton collisions one usually takes the simplified viewpoint of the so-called parton model, where protons are modelled as being composed of massless partons, a collective term for quarks, antiquarks and gluons, each carrying a momentum fraction x_i and having negligible transverse momentum with respect to the proton direction of flight. In a high energy collision one parton from each proton enters the hard scattering process with momentum $p_1 = x_1 P_1$ and $p_2 = x_2 P_2$, respectively, where the proton momenta are denoted by P_1 and P_2. The hadronic and partonic center-of-mass energies, s_{had} and s respectively, are then related by $s = x_1 x_2 s_{\text{had}}$. The partonic cross-section $\hat{\sigma}_{ij\to X}\left(s, \mu_F, \mu_R, \alpha_s(\mu_R)\right)$, where μ_F and μ_R are the factorization and renormalization scale, can be computed in perturbation theory[1], whereas the information about the parton content of the proton must be extracted from experimental data. This information is encoded in the parton distribution functions (PDF) of the proton, labelled as $f_{i,p}(x_i,\mu_F^2)$ in the following. The PDFs $f_{i,p}(x_i,\mu_F^2)$ are the probability distribution functions for finding a parton of type i with momentum fraction x_i inside a proton when it is probed in a hard scattering reaction at an energy scale μ_F. The x_i dependence of these functions has to be measured at a fixed energy scale $\mu_F = \mu_0$, then the dependence on μ_F can be computed in perturbative QCD. The hadronic cross section $\sigma_{pp\to X}(s_{\text{had}}, \mu_F, \mu_R)$ can then be written as the incoherent sum over all possible parton configurations weighted with the PDF $f_{i,p}(x_i,\mu_F^2)$ times the corresponding partonic cross section. To be more specific, for the inclusive production of a neutral Higgs boson ϕ in proton-proton collisions,

$$p(P_1)\, p(P_2) \quad \to \quad \phi + X,$$

the relevant parton processes are

$$g(p_1)\, g(p_2) \to \phi + X \quad , \tag{2.1}$$

$$g(p_1)\, q(p_2) \to \phi + X \quad , \qquad q = \{u, d, s, c, b\}, \tag{2.2}$$

$$g(p_1)\, \bar{q}(p_2) \to \phi + X \quad , \qquad \bar{q} = \{\bar{u}, \bar{d}, \bar{s}, \bar{c}, \bar{b}\}, \tag{2.3}$$

$$q(p_1)\, \bar{q}(p_2) \to \phi + X \quad , \tag{2.4}$$

where X denotes generically all possible additional final state particles. In the SM and in the application to 2HDM with $\tan\beta \sim 1$, (2.1) gives the dominant contribution [50],

[1] We will consider at this point only the perturbation expansion in the strong coupling α_s.

whereas in the type-II 2HDM with large $\tan\beta$ the Higgs Yukawa couplings to down-type quarks are enhanced and the production process (2.4) with $q = b$ becomes also important. Summing over these sub-processes and all possible values of x_1 and x_2 one obtains the total hadronic cross-section for inclusive Higgs production

$$\begin{aligned}\sigma_{pp\to\phi+X}(s_{\text{had}}) \;&=\; \int_0^1 dx_1 \int_0^1 dx_2 \sum_{i,j} f_{i,p}(x_1,\mu_F^2) f_{j,p}(x_2,\mu_F^2) \\ &\quad \times \hat{\sigma}_{ij\to\phi+X}\left(s, \mu_F, \mu_R, \alpha_S(\mu_R)\right) \;+\; \mathcal{O}\left(\frac{\Lambda_{QCD}}{\mu_F^2}\right). \end{aligned} \tag{2.5}$$

As indicated, the factorization of the whole reaction into soft processes, encoded in the PDFs $f_{i,p}$, and hard scattering, encoded in $\hat{\sigma}_{ij\to X}$, only holds up to corrections of order $\frac{\Lambda_{\text{QCD}}}{\mu_F^2}$ [51]. In high energy reactions with characteristic scales $\mu_F \gg \Lambda_{QCD} \simeq \mathcal{O}(200)$ MeV this can be regarded a good approximation. If (2.5) could be computed exactly, the hadronic production cross section would be independent of the arbitrary scales μ_F and μ_R. However, in practice, a dependence on μ_F and μ_R remains since the perturbation series of $\hat{\sigma}_{ij\to X}\left(s, \mu_R^2, \alpha_S(\mu_R^2)\right)$ is truncated at a certain order in α_s. Usually one identifies the two scales $\mu_F = \mu_R = \mu$ in (2.5) and sets μ to the characteristic energy scale of the process, in this case the mass of the Higgs boson $\mu = \mu_0 \simeq m_\phi$. The remaining dependence on μ is used to asses the theoretical uncertainty of the obtained results by varying μ around the characteristic scale, usually one varies within the interval given by $\frac{\mu_0}{2}$ and $2\mu_0$.

The leading order term in the squared scattering amplitude corresponding to the process (2.1) can be computed from the one-loop Feynman graph in Fig. 2.1 and is of $\mathcal{O}(\alpha_s^2)$. The leading terms corresponding to the parton processes (2.2) - (2.4) on the other hand are of $\mathcal{O}(\alpha_s^3)$. As already mentioned, in the particular case of (2.4) with $q = b$ this is only true for $\tan\beta \sim 1$ in the 2HDM. In the SM and 2HDM with $\tan\beta \sim 1$, the main contribution in (2.1) comes from a top-quark loop, only at lower values of m_ϕ the effect of the bottom quark is sizeable. In the intermediate mass range $2m_b < m_\phi < 2m_t$ the two amplitudes interfere destructively[2], therefore the bottom contribution reduces the total cross-section up to 10% in case of the SM Higgs boson [52]. For the mass range $m_\phi > 2m_t$ that is most relevant for this project the contribution of the bottom-quark loop is negligible in the SM and in our 2HDM scenarios.

[2] Note the relative signs of the one-loop form factors given in Eq (2.10).

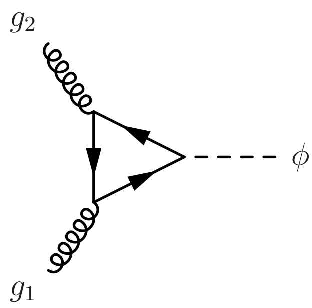

Figure 2.1. – *Leading order diagram for the production of a neutral scalar boson ϕ via gluon fusion $gg \to \phi$. In principle all quarks are present in the loop, in practice only the heavy quarks are relevant because the $q\bar{q}\phi$ Yukawa couplings are proportional to their masses, $y_i \propto \frac{m_i}{v}$.*
.

Since the SM Higgs Yukawa couplings to the fermions are proportional to the fermion masses $y_i = \frac{m_i}{v}$ the one-loop amplitude corresponding to (2.1) exhibits the following behaviour in the small and large quark mass limits [34]:

$$\mathcal{M}_{gg\to\phi} \to \begin{cases} 0, & \frac{2m_q}{m_\phi} \ll 1, \\ \text{const} \times \frac{m_\phi^2}{v}, & \frac{2m_q}{m_\phi} \gg 1, \end{cases} \tag{2.6}$$

This lead to the idea to neglect the lighter quarks completely and write down an effective vertex for the coupling of the Higgs to gluons, which is strictly valid only in the limit $\frac{2m_t}{m_\phi} \to \infty$. This simplifies significantly the calculation of the QCD radiative corrections to the process (2.1), which turn out to be very important, increasing the rate by up to 100% at the LHC at NLO and further by up to 25% at NNLO [27]. Already some time ago the NLO corrections have been calculated exactly [22],[21], meaning that the full top- and bottom-quark mass dependence is included. More recent calculations include the NNLO corrections in the large m_t limit [23],[24] as well as some electroweak corrections [26],[53]. Comparing exact NLO results with the effective approximation [20] shows that the latter works very well for lighter Higgs bosons. In the following section the leading order effective gluon-Higgs couplings will be derived. Subsequently the validity of the effective approach will be tested numerically for the case of heavy neutral Higgs bosons which is most relevant for main part of this thesis.

2.1. Higgs-gluon coupling in the large m_t limit

Applying the Feynman rules in App. A to the diagram in Fig. 2.1 one obtains the leading order amplitude for the production of a single Higgs boson ϕ with undefined CP via gluon fusion,

$$\mathcal{M}_{gg\to\phi} \quad = \quad -i\frac{\alpha_s}{2\pi}\delta^{a_1a_2}\left[\mathcal{F}_S\left(\frac{2p_1^{\rho_2}p_2^{\rho_1}}{s} - g^{\rho_1\rho_2}\right) + \mathcal{F}_P\,\epsilon^{\mu\nu\rho_1\rho_2}\frac{2p_1^{\mu}p_2^{\nu}}{s}\right], \tag{2.7}$$

where p_1 and p_2 are the momenta of the incoming gluons, μ_1, μ_2 and a_1, a_2 the corresponding Lorentz and colour indices, and $s = (p_1+p_2)^2 = m_\phi^2$ the partonic center-of-mass energy. The model-dependent scalar and pseudoscalar form factors are given within the SM with 3 quark generations by[3]

$$\begin{aligned}\mathcal{F}_S \quad &= \quad \sum_{q=t,b}\frac{m_q^2}{v}\,a_q\left((s-4m_q^2)\,C_0[s,0,0;m_q^2,m_q^2,m_q^2]-2\right),\\ \mathcal{F}_P \quad &= \quad \sum_{q=t,b}\frac{m_q^2}{v}\,b_q\,s\,C_0[s,0,0;m_q^2,m_q^2,m_q^2],\end{aligned} \tag{2.8}$$

where the contributions of the first and second generation quarks have been neglected in the sums. a_q and b_q are the reduced scalar and pseudoscalar couplings of the heavy quarks to the Higgs boson ϕ, c.f. (1.48). The scalar 3-point function $C_0[s,0,0;m_q^2,m_q^2,m_q^2]$ is finite as long as $m_q > 0$ and can be expressed in the compact form

$$C_0[s,0,0;m_q^2,m_q^2,m_q^2] = \begin{cases} -\frac{2}{s}\left[\arcsin\left(\frac{\sqrt{s}}{2m_q}\right)\right]^2, & 0 < s < 4m_q^2,\\ \frac{1}{2s}\left[\ln\left(\frac{1+\beta_q}{1-\beta_q}\right) - i\pi\right]^2, & 4m_q^2 < s,\end{cases} \tag{2.9}$$

where $\beta_q^2 = 1-\frac{4m_q^2}{s}$. In the limit $m_t \to \infty$, where all other quarks are considered massless, only the top-quark loop contributes in (2.8) and one can expand (2.9) in $\frac{s}{m_t^2} \ll 1$, which yields

$$\arcsin^2\left(\frac{\sqrt{s}}{2m_t}\right) = \frac{s}{4m_t^2} + \frac{s^2}{48m_t^4} + \mathcal{O}\left(\frac{s^3}{m_t^6}\right).$$

For $m_t \gg \frac{\sqrt{s}}{2}$ in (2.9) the leading term of the expansion of the form factors (2.8) has the form

[3] In the MSSM also squark contributions must be taken into account.

$$\begin{aligned}\mathcal{F}_S &\overset{m_t\to\infty}{=} -\frac{a_t}{v}\frac{s}{3}+\mathcal{O}\left(m_t^{-2}\right),\\ \mathcal{F}_P &\overset{m_t\to\infty}{=} -\frac{b_t}{v}\frac{s}{2}+\mathcal{O}\left(m_t^{-2}\right).\end{aligned} \tag{2.10}$$

Thus the leading order Higgs-gluon coupling in the large m_t limit can be written as

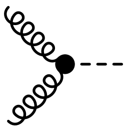

$$= \quad 4i\frac{\alpha_s}{\pi}\delta^{a_1a_2}\left[f_H^{(0)}\left(p_1^{\rho_2}p_2^{\rho_1}-g^{\rho_1,\rho_2}\,p_1.p_2\right)-2f_A^{(0)}\,\epsilon^{p_1p_2\rho_1\rho_2}\right],$$

with

$$\begin{aligned}f_H^{(0)} &= \frac{a_t}{12v},\\ f_A^{(0)} &= -\frac{b_t}{16v}.\end{aligned} \tag{2.11}$$

In general, this result as well as the Feynman rule (A.10) can be derived from the Lagrangian

$$\mathcal{L}_{\text{eff.}} \quad = \quad f_H\,G_a^{\mu\nu}G^a_{\mu\nu}\,\phi+f_A\,\epsilon^{\mu\nu\rho\sigma}G^a_{\mu\nu}G^a_{\rho\sigma}\,\phi,$$

which encodes the effective scalar and pseudoscalar couplings of the physical Higgs boson ϕ to the gluon field strength tensor $G_a^{\mu\nu}$. The effective coupling constants

$$f_{H/A} \quad = \quad \frac{\alpha_s}{\pi}f_{H/A}^{(0)}+\left(\frac{\alpha_s}{\pi}\right)^2 f_{H/A}^{(1)}+\cdots$$

are then obtained by matching the effective theory order by order in α_s to the exact result. The next-to-leading order effective Higgs-gluon couplings (in the $\overline{MS}$ scheme) were derived in [23] and [54]:

$$\begin{aligned}f_H^{(1)} &= \frac{(4\pi)^\epsilon}{\Gamma(\epsilon)}\frac{a_t}{12v}\left(\frac{11}{4}-\frac{\beta_0}{\epsilon}\right),\\ f_A^{(1)} &= \frac{(4\pi)^\epsilon}{\Gamma(\epsilon)}\frac{b_t}{16v}\frac{\beta_0}{\epsilon},\end{aligned} \tag{2.12}$$

where $\beta_0=\frac{1}{4}\left(11-\frac{2}{3}N_f\right)$ and $\epsilon=\frac{4-d}{2}$. This effective approach can easily be generalized to models with more than one neutral Higgs boson and will be applied also in the main part of this thesis.

2.2. Numerical results and comparison

In this section the numerical results for the inclusive production of a Higgs boson $\phi = H$ with SM couplings,

$$a_t = 1\,,\; b_t = 0\,,\; a_b = 1\,,\; b_b = 0\,,$$

will be presented. The radiative QCD corrections through next-to-leading order in α_s obtained in the large m_t limit are included. The results are compared to the best perturbative predictions available in the literature in a wide mass range from $m_H = 100$ GeV to 1 TeV. This serves as a benchmark for the validity of the large m_t approximation for Higgs masses above the $t\bar{t}$ threshold $m_H > 350$ GeV. In the following, the Higgs-gluon vertex with full top-quark and bottom-quark dependence will be denoted with a shaded circle

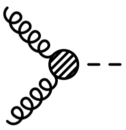
$= \sum_{t,b}$
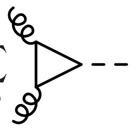
, (2.13)

whereas the effective Higgs-gluon vertex will be denoted with a big dot

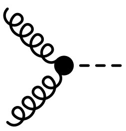
.

The latter will be used for the computation of the virtual and real corrections. The partonic cross-section for the gluon fusion process is obtained by adding all these contributions, schematically

$\sigma_{gg\to HX} \propto \Big|$
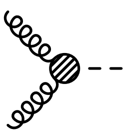
$\Big|^2 + 2\mathrm{Re}\Big[$
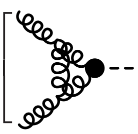
$\Big|$
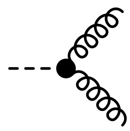
$\Big] + \Big|$
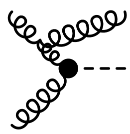
$\Big|^2$. (2.14)

Although not mentioned explicitly, the corrections from the processes $qg \to Hg$ and $q\bar{q} \to Hq$ are included in the computation. In the following this standard setup will be compared numerically to the cross-section obtained when the radiative corrections are rescaled by a global K-factor, schematically

$$\sigma^{K}_{gg\to HX} \quad \propto$$

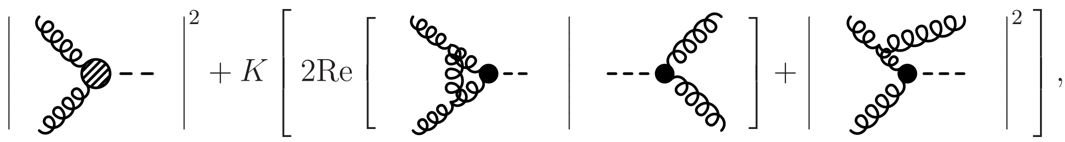

(2.15)

which is given by the ratio of the full leading-order Higgs-gluon vertex and the effective vertex,

$$K^2(m_H, m_t, m_b, a_t, a_b) \quad =$$

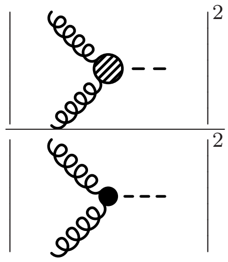

$$= \frac{|\mathcal{F}_S|^2 + |\mathcal{F}_P|^2}{16 m_H^4 \left(\left| f_H^{(0)} \right|^2 + 4 \left| f_A^{(0)} \right|^2 \right)}. \quad (2.16)$$

This approximation method was proposed and tested first in [55]. The contributions $\sigma_{qg\to Hq}$ and $\sigma_{q\bar{q}\to Hg}$ are treated similarly. The complex one-loop form factors $\mathcal{F}_S$ and $\mathcal{F}_p$ were already given in (2.8). For on-shell Higgs production, the factor K^2 does not depend on the phase-space, only on the masses and couplings of the involved particles.

To summarize, the following setup is used for the computation of the total inclusive Higgs production cross section:

- The renormalization and factorization scale are set to $\mu_R = \mu_F = \frac{m_H}{2}$ following the approach in [53] to emulate soft gluon resummation [25].
- The strong coupling $\alpha_s^{(5)}(\mu)$ runs with 5 active flavours from $\alpha_s^{(5)}(m_Z) = 0.118001$ ($m_Z = 91.1876$ GeV) to the respective scale $\mu = \frac{m_H}{2}$.
- The top-quark mass is set to the most recent world average $m_t = 173.34$ GeV [10]. This value is taken to be the top mass in the on-shell scheme.
- For the bottom-quark the $\overline{\text{MS}}$ running mass is used with the reference value $\overline{m}_b(\overline{m}_b) =$ 4.213 GeV

$$\overline{m}_b(\mu) \quad = \quad \overline{m}_b(\overline{m}_b) \left(\frac{\alpha_s^{(5)}(\mu)}{\alpha_s^{(5)}(\overline{m}_b)} \right)^{\frac{12}{33-2n_f}} \quad , \quad n_f = 5.$$

- Only the top-quark contributes to the effective Higgs-gluon coupling, the SM values $a_t = 1$ and $b_t = 0$ are used .
- The CT10 NLO PDF set [56] is used to obtain the total hadronic cross sections at $\sqrt{s_{\text{had}}} = 7$ TeV and $\sqrt{s_{\text{had}}} = 14$ TeV.

The computation of Anastasiou, et. al. (ABPS) [53], to which the results will be compared, uses the following setup:

- QCD effects through NLO are computed exactly, including the full dependence on top and bottom quark.
- The NNLO QCD corrections are obtained in the large m_t limit.
- Some mixed electroweak/QCD corrections (using an effective Lagrangian valid for $m_H < m_W$) are included, see [53] for details.
- Renormalization and factorization scale are set to $\mu_R = \mu_F = \frac{m_H}{2}$.
- The top-quark mass is set to $m_t = 170.9$ GeV .
- For the bottom-quark the $\overline{\mathrm{MS}}$ running mass is used with the reference value

$$\overline{m}_b(10\,\mathrm{GeV}) = 3.609\,\mathrm{GeV}. \tag{2.17}$$

- The MSTW2008 NNLO PDFs [57] are used to obtain the total hadronic cross section.

In [26] one can find another set of NNLO predictions for inclusive Higgs production. It turns out that the results are very similar to the ABPS computation, see [27] for an overview. In tables (2.1) and (2.2) one can find the numerical results of my computation for inclusive Higgs production at NLO for $\sqrt{s_{\text{had}}} = 7$ TeV and $\sqrt{s_{\text{had}}} = 14$ TeV, respectively, using the approximation described above. These are compared to the ABPS results, showing that the rescaling with the effective K-factor (2.16) leads to an agreement of my results and the NNLO computation to better than 10% for 450 GeV $\leq m_H < 1$ TeV at $\sqrt{s_{\text{had}}} = 7$ TeV and $\sqrt{s_{\text{had}}} = 14$ TeV, c.f. also the plot (2.2) for the latter case. The scale dependence of the ABPS computation is not sown explicitly. It is below 10%, see [53] and [27] for details. In Figs. 2.3 and 2.4 the individual parton level contributions (for $\sqrt{s_{\text{had.}}} = 14$ TeV) to my complete NLO result are shown without and with the effective K-factor, respectively. It can be expected that my computation is also compatible with the 'exact' NNLO computation whithin the 2HDM with $\tan\beta \sim 1$ where the top-quark loops, too, are by far the dominant contributions to the effective gluon Higgs couplings.

In [58] a study was made for distributions of the parton process $gg \to \phi ggg$ computed both in the effective Lagrangain approximation and exactly (at LO), within 2HDM. The conclusion was that in the small $\tan\beta$ region the effective Lagrangain approximation gives accurate results for invariant mass distributions as well as P_T^{jet} distributions if $P_T^{\text{jet}} < 200$ GeV. We shall apply the effective K-factor approximation in the following sections to type-II 2HDM with $\tan\beta \sim 1$, where – according to the studies above – the K-factor method should provide a reasonably accurate approximation. We emphasize that we are primarily interested in the contributions to distributions of heavy Higgs bosons with masses below 1 TeV relative to the NLO SM distributions in the resonance region.

Table 2.1. – *Inclusive Higgs production cross section* $pp \to H + X$ *for* $\sqrt{s_{\text{had}}} = 7$ *TeV and* $\mu_R = \mu_F = \mu = \frac{m_H}{2}$.

m_H [GeV]	σ_{tot} [pb]	σ^{K}_{tot} [pb]	$\sigma^{\text{ABPS}}_{\text{tot}}$ [pb]
100	19.26	18.63	24.81
125	12.31	12.24	15.74
150	8.36	8.52	10.79
200	4.40	4.73	5.36
250	2.63	3.02	3.37
300	1.76	2.20	2.45
320	1.56	2.03	2.28
340	1.44	1.98	2.25
360	1.43	2.14	2.44
380	1.34	2.08	2.31
400	1.19	1.87	2.05
450	0.814	1.28	1.35
500	0.533	0.810	0.844
550	0.348	0.509	0.522
600	0.230	0.321	0.325
700	0.105	0.132	0.131
800	0.0518	0.0576	0.0850
900	0.0271	0.0265	0.0253
1000	0.0149	0.0127	0.0119

Table 2.2. – *Inclusive Higgs production cross section* $pp \to H + X$ *for* $\sqrt{s_{\text{had}}} = 14$ *TeV and* $\mu_R = \mu_F = \mu = \frac{m_H}{2}$.

m_H [GeV]	σ_{tot} [pb]	σ_{tot}^{K} [pb]	$\sigma_{\text{tot}}^{\text{ABPS}}$ [pb]
100	56.09	54.19	76.07
125	38.60	38.34	51.47
150	27.92	28.45	37.43
200	16.45	17.70	20.64
250	10.91	12.47	14.23
300	8.00	9.92	11.28
320	7.32	9.51	10.81
340	6.96	9.58	11.00
360	7.20	10.70	12.30
380	6.95	10.73	12.01
400	6.39	9.99	10.98
450	4.70	7.31	7.81
500	3.31	5.01	5.24
550	2.31	3.38	3.48
600	1.63	2.28	2.32
700	0.855	1.07	1.07
800	0.477	0.530	0.525
900	0.282	0.276	0.270
1000	0.175	0.150	0.146

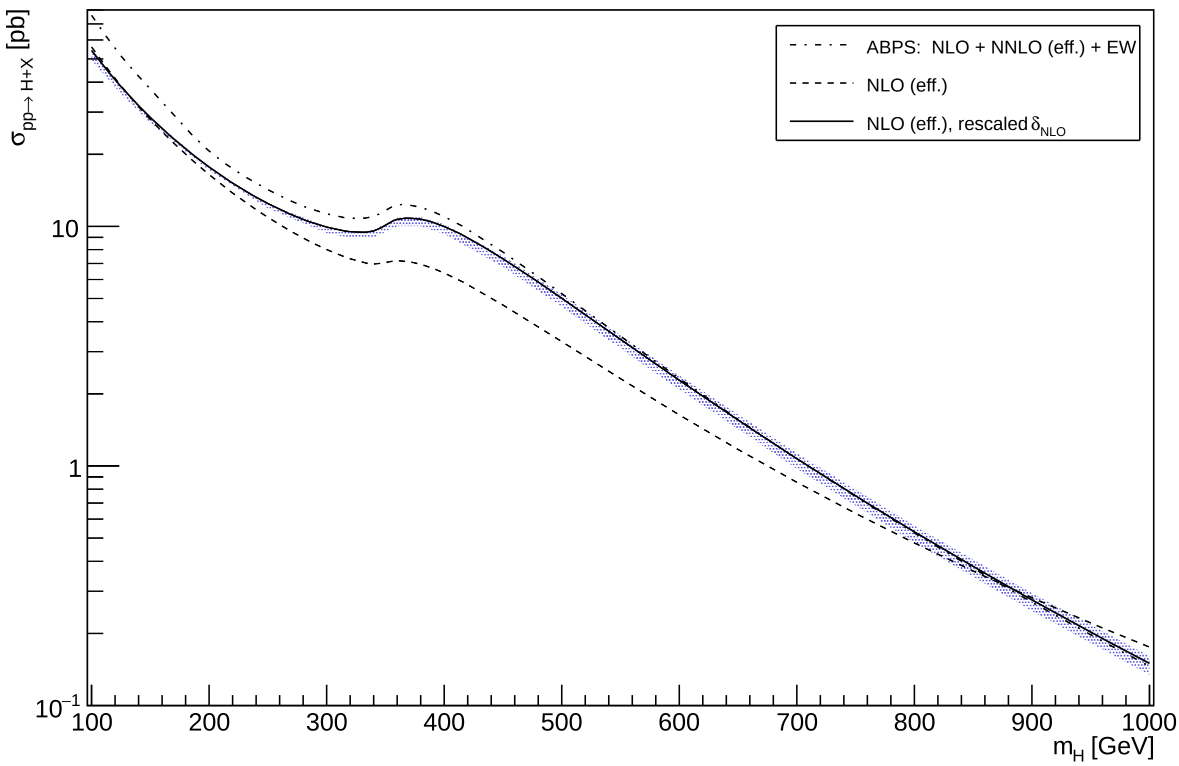

Figure 2.2. – *Comparison of the two NLO (effectve) calculations with NNLO results from [53] for* $\sqrt{s_{\text{had}}} = 14$ *TeV and* $\mu_R = \mu_F = \mu = \frac{m_H}{2}$. *The effect of scale variation between* $\frac{m_H}{4} < \mu < m_H$ *is indicated by the shaded band.*

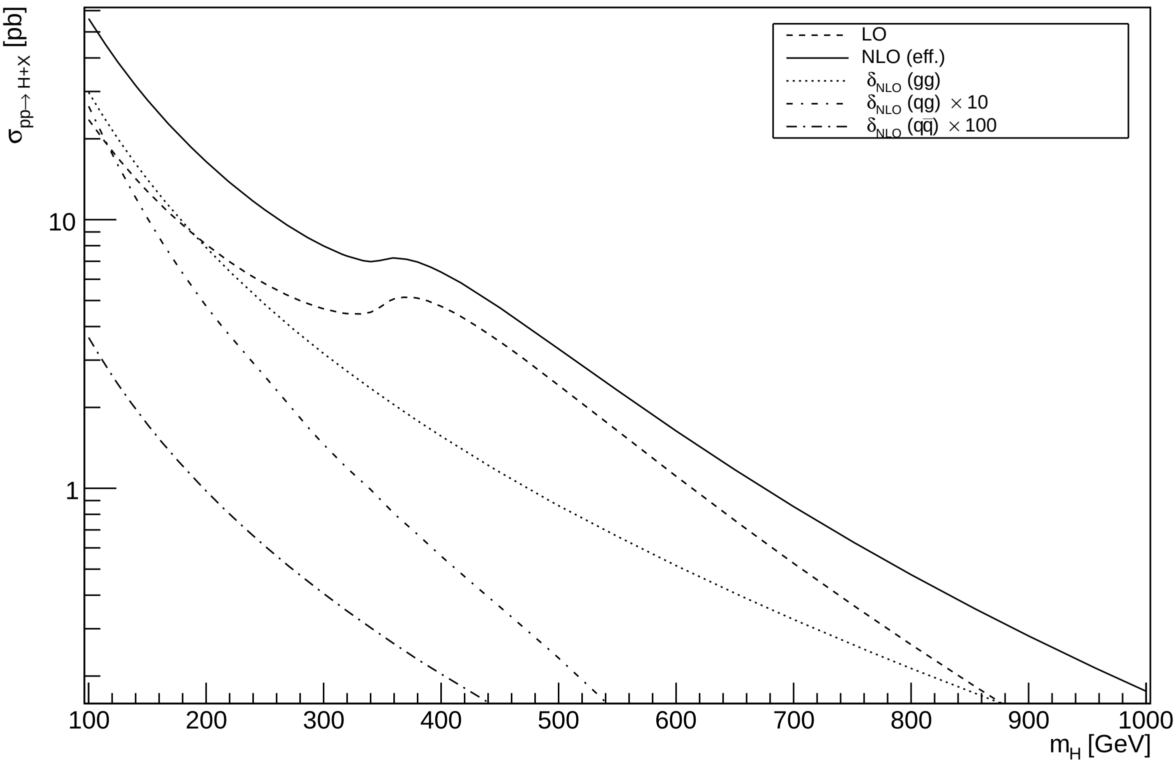

Figure 2.3. – *NLO (effective) total Higgs production cross-section obtained via (2.14) for* $\sqrt{s_{\text{had}}} = 14$ *TeV and* $\mu_R = \mu_F = \mu = \frac{m_H}{2}$. *The three parton subprocesses contributing with* $\delta_{NLO}(ij)$ *to the total cross-section are depicted separately* $(\sigma_{\text{NLO}} = \sigma_{LO} + \sum \delta_{NLO}(ij))$.

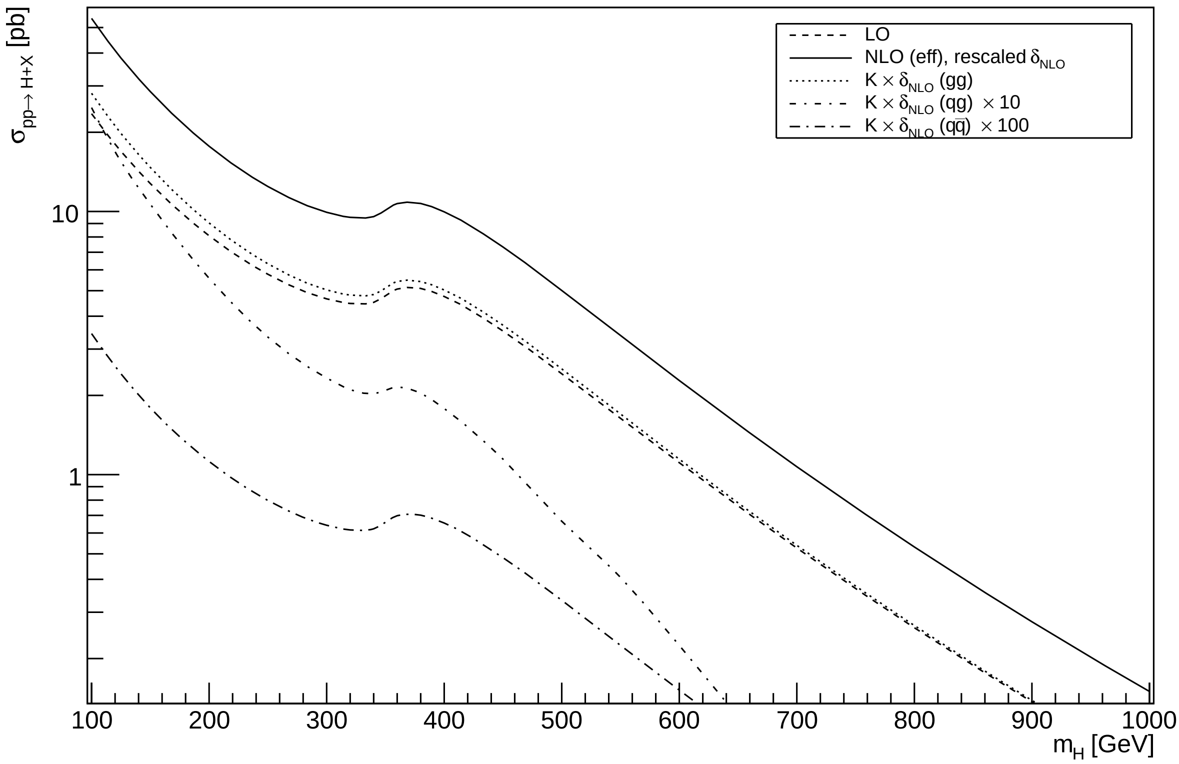

Figure 2.4. – *NLO (effective) total Higgs production cross-section obtained via (2.15) for $\sqrt{s_{\text{had}}} = 14$ TeV and $\mu_R = \mu_F = \mu = \frac{m_H}{2}$. The three NLO contributions $K\,\delta_{NLO}(ij)$ have been rescaled with the factor (2.16).*

3. Top-quark pair production in proton-proton collisions

In this chapter we will study the inclusive production of top-quark pairs in proton proton collisions and their decay to two leptons and b-jets

$$pp \;\to\; t\,\bar{t} + X \;\to\; l^+\nu_l b + l'^-\bar{\nu}_{l'}\bar{b} + X, \tag{3.1}$$

or one lepton and jets

$$pp \;\to\; t\,\bar{t} + X \;\to\; l^+\nu_l b + q\bar{q}'\bar{b} + X, \tag{3.2}$$

including effects of heavy, neutral Higgs bosons with undefined CP in the s-channel. In (3.1) and (3.2), the letter X denotes generically all additional final state particles. Since the top-quark width is much smaller than the mass, $\frac{\Gamma_t}{m_t} \sim \mathcal{O}(1\%)$, it is reasonable to work in the narrow width approximation and split the whole process into the production of $t\bar{t}$ pairs in an arbitrary spin configuration and their subsequent decay. This is achieved by the replacement

$$\frac{1}{\left(q^2 - m_t^2\right)^2 + \Gamma_t^2 m_t^2} \;\to\; \frac{\pi}{\Gamma_t m_t}\,\delta\left(q^2 - m_t^2\right),$$

in the full, squared matrix element. It was shown in [59] that non-factorizable corrections connecting production and decay phase are of $\mathcal{O}\left(\frac{\Gamma_t}{m_t}\right)$ and can thus be neglected. Since the top-quark spin can be analyzed via its decay products we will keep the full top-spin dependence in the calculation of the cross-section for the process

$$p\,p \;\to\; t\,(k_1,s_1)\;\bar{t}\,(k_2,s_2) + X, \tag{3.3}$$

where k_1, k_2 denote the top and antitop quark 4-momenta, and s_1, s_2 the top and antitop quark spin 4-vectors which obey $s_i^2 = -1$ and $s_i.k_i = 0$.

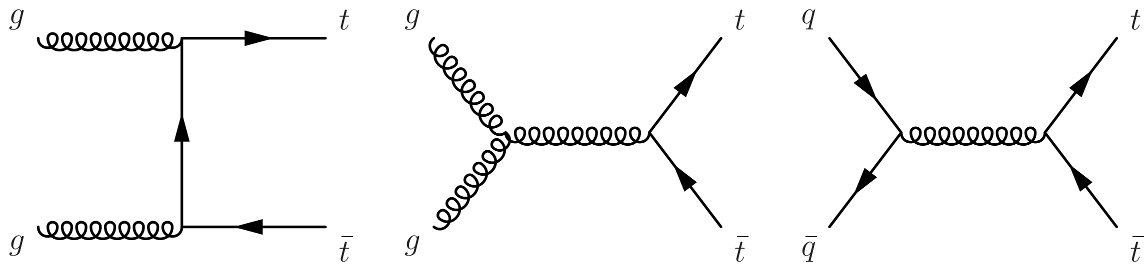

Figure 3.1. – *Leading order QCD Feynman diagrams for $t\bar{t}$ production in hadron-hadron collisions.*

Analogously to (2.5), the hadronic cross section can be written as the incoherent sum over all underlying parton cross sections $\hat{\sigma}_{ij\to t\bar{t}+X}$:

$$\begin{aligned}\sigma_{pp\to t\bar{t}+X}(s_{\text{had}}) &= \int_0^1 dx_1 \int_0^1 dx_2 \sum_{i,j} f_{i,p}(x_1,\mu^2) f_{j,p}(x_2,\mu^2)\, \hat{\sigma}_{ij\to t\bar{t}+X}\left(s,\mu^2,\alpha_S(\mu^2)\right) \\ &\quad +\mathcal{O}\left(\frac{\Lambda_{QCD}}{\mu^2}\right). \end{aligned} \tag{3.4}$$

In (3.4) we set $\mu_R = \mu_F = \mu$. The usual choice for $t\bar{t}$ production would be $\mu = m_t$ but in this project we will tie the scale to the masses of the considered Higgs resonances $\mu = \frac{m_\phi}{2}$. The factor $\frac{1}{2}$ is motivated by results from inclusive Higgs production, where it reproduces the resummation of soft gluon contributions, c.f. Sec. 2. The parton processes contributing to the reaction (3.3) are

$$g(p_1)\; g(p_2) \to t\,(k_1,s_1)\; \bar{t}\,(k_2,s_2) + X \quad , \tag{3.5}$$
$$g(p_1)\; q(p_2) \to t\,(k_1,s_1)\; \bar{t}\,(k_2,s_2) + X \quad , \qquad q \in \{u,d,s,c,b\}, \tag{3.6}$$
$$g(p_1)\; \bar{q}(p_2) \to t\,(k_1,s_1)\; \bar{t}\,(k_2,s_2) + X \quad , \qquad \bar{q} \in \{\bar{u},\bar{d},\bar{s},\bar{c},\bar{b}\}, \tag{3.7}$$
$$q(p_1)\; \bar{q}(p_2) \to t\,(k_1,s_1)\; \bar{t}\,(k_2,s_2) + X \quad , \tag{3.8}$$

At proton-proton colliders like the LHC, the dominant parton process is the gluon fusion (3.9). The two Feynman diagrams contributing at $\mathcal{O}(\alpha_s^2)$ to the partonic cross section are depicted in Fig. 3.1 in the left and center pane. The quark-antiquark annihilation process (3.12) also contributes at $\mathcal{O}(\alpha_s^2)$ with the Feynman graph depicted in the right pane of Fig. 3.1. However, in the case of proton-proton collisions this latter process receives a suppression from the (anti-) quark PDF which becomes stronger with higher hadronic center-of-mass energy. During the $\sqrt{s_{\text{had}}} = 8$ TeV run at the LHC nearly 90% of all top-quark pairs were produced via gluon fusion (3.9), whereas quark-antiquark annihilation (3.12) amounted to only 10%, [12]. The remaining parton processes, (3.10) and (3.11), contribute at $\mathcal{O}(\alpha_s^3)$ to the cross section and will be taken into account as part of the real QCD corrections to the process $pp \to t\bar{t} + X$ in Sec. 3.5.

To summarize, the perturbation expansion of the parton scattering amplitudes through next-to-leading order QCD involves the tree-level ($\mathcal{O}\left(\alpha_s^1\right)$) and one-loop ($\mathcal{O}\left(\alpha_s^2\right)$) graphs corresponding to the parton processes

$$\begin{aligned}
g(p_1)\, g(p_2) &\to t\,(k_1,s_1)\, \bar{t}\,(k_2,s_2) \quad , \\
q(p_1)\, \bar{q}(p_2) &\to t\,(k_1,s_1)\, \bar{t}\,(k_2,s_2) \quad ,
\end{aligned}$$

and the tree-level ($\mathcal{O}\left(g_s^3\right)$) graphs corresponding to the reactions

$$g(p_1)\, g(p_2) \to t\,(k_1,s_1)\, \bar{t}\,(k_2,s_2) + g(p_3) \quad , \tag{3.9}$$

$$q(p_1)\, g(p_2) \to t\,(k_1,s_1)\, \bar{t}\,(k_2,s_2) + q(p_3) \quad , \qquad q \in \{u,d,s,c,b\}, \tag{3.10}$$

$$\bar{q}(p_1)\, g(p_2) \to t\,(k_1,s_1)\, \bar{t}\,(k_2,s_2) + \bar{q}(p_3) \quad , \qquad \bar{q} \in \{\bar{u},\bar{d},\bar{s},\bar{c},\bar{b}\}, \tag{3.11}$$

$$q(p_1)\, \bar{q}(p_2) \to t\,(k_1,s_1)\, \bar{t}\,(k_2,s_2) + g(p_3) \quad . \tag{3.12}$$

In the following we will assume that the SM particle spectrum is extended by one or more heavy, neutral, colourless spin-0 bosons, generically denoted as ϕ_i, which couple preferably to the top-quark. Their masses m_i lie above the $t\bar{t}$ threshold, so that on top of the QCD processes discussed above, resonant production of $t\bar{t}$ pairs is possible:

$$pp \;\to\; \phi_i \;\to\; t\,\bar{t} + X. \tag{3.13}$$

The CP properties of ϕ_i are not fixed so that both couplings to the scalar and pseudoscalar top-antitop current have to be taken into account, c.f. (1.46). We will further assume that its decays to gauge bosons $\phi_i \to W^+W^-, ZZ$ and to the third generation down-type fermions $\phi_i \to b\bar{b}, \tau\bar{\tau}$ are suppressed, so that the total width is given to a good approximation by

$$\Gamma_i^{\text{tot}} \approx \Gamma_i(\phi \to t\bar{t}).$$

Only under these conditions a signal of the resonances could be visible in observables like the $t\bar{t}$ invariant mass spectrum on top of the large irreducible QCD background. Up to these specifications, the setup of the computation is kept generic, only the reduced Yukawa couplings $a_{t,i}$, $b_{t,i}$ as well as the masses m_i and widths Γ_i of each neutral Higgs boson have to be specified. Thus, the computation can in principle be applied to all physical models that provide scenarios which are compatible with the requirements stated above. For the purpose of this project we will compute the widths $\Gamma_i^{\text{tot.}}$ and couplings in Sec. 3.7.1 for the type-II 2HDM, which has been discussed in Sec. 1.2.

The couplings of the Higgs bosons ϕ_i to gluons, denoted with the shaded circle in the left pane of (3.2), are induced at leading order by top- and bottom-quark loops as discussed in Sec. 2. Regarding the radiative QCD corrections to the process (3.13), we will content ourselves with the large m_t approximation which has been discussed in Sec. 2.1 and applied in the computation of inclusive SM Higgs production in Sec. 2.2. There we could show that the large m_t approximation yields reasonable results also for heavy Higgs bosons with masses above the $t\bar{t}$ threshold, so that it can be assumed that it gives a good estimate of the size of the radiative QCD corrections in this computation.

The parton scattering amplitudes receive several new contributions from resonant heavy Higgs production. We have to consider

$$
\begin{aligned}
&g(p_1)\, g(p_2) && \to\ \phi_i\ \to && t\,(k_1,s_1)\,\bar{t}\,(k_2,s_2) + g(p_3), && && (3.14)\\
&g(p_1)\, q(p_2) && \to \phi_i + q(p_3) \to && t\,(k_1,s_1)\,\bar{t}\,(k_2,s_2) + q(p_3)\ , && q \in \{u,d,s,c,b\}, && (3.15)\\
&g(p_1)\, \bar{q}(p_2) && \to \phi_i + \bar{q}(p_3) \to && t\,(k_1,s_1)\,\bar{t}\,(k_2,s_2) + \bar{q}(p_3)\ , && \bar{q} \in \{\bar{u},\bar{d},\bar{s},\bar{c},\bar{b}\}, && (3.16)\\
&q(p_1)\, \bar{q}(p_2) && \to\ \phi_i\ \to && t\,(k_1,s_1)\,\bar{t}\,(k_2,s_2) + g(p_3)\ , && && (3.17)\\
&q(p_1)\, \bar{q}(p_2) && \to \phi_i + g(p_3) \to && t\,(k_1,s_1)\,\bar{t}\,(k_2,s_2) + g(p_3)\ . && && (3.18)
\end{aligned}
$$

As mentioned above, we consider scenarios where the couplings of the heavy neutral Higgs bosons to the gauge bosons are suppressed. Thus, the electroweak production mechanisms do not play an important role in this setup. Otherwise, in particular the vector boson fusion would become very important for the production of heavy, CP-even Higgs bosons [12]. The contributions from gluon fusion and quark-antiquark annihilation to the parton scattering amplitude enter the computation at leading order whereas the processes (3.14) – (3.18) contribute initially to the next-to-leading order real radiation corrections. The leading order contribution to the quark-antiquark annihilation process (3.18) and (3.17) is depicted in Fig. 3.2 in the right pane. These diagrams, however, are suppressed by a factor $\frac{m_q}{v}$ so that they can be neglected in the calculation. The same applies for all one-loop graphs featuring a $q\bar{q}\phi_i$ vertex. The interferences of resonant ϕ_i production (3.13) and the QCD processes (3.3) are crucial in the calculation. These interference terms cause a distinct peak-dip structure in the $t\bar{t}$ invariant mass spectrum and other observables [13, 14].

3.1. QCD parton cross sections at next-to-leading order

For the computation of the NLO QCD corrections to the processes discussed above we will apply the dipole subtraction method described in [60, 61] to handle the infrared and collinear (IR) singularities appearing in the real and virtual corrections. A set of counter terms will be constructed to render the real corrections integrable over the full $2 \to 3$ phase space. The d-dimensional, integrated version of these counter terms will be added back to the virtual corrections to cancel all remaining IR divergences, which appear as poles in the parameter $\epsilon = \frac{4-d}{2}$ in dimensional regularization. Schematically the NLO contribution to the partonic cross sections can be written as

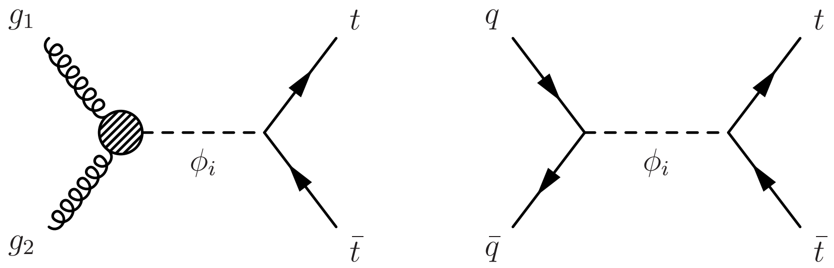

Figure 3.2. – *Leading order contributions to top-pair production with intermediate scalar ϕ boson. Since the ϕ_i couplings to fermions are proportional to the fermion masses, the contribution from the annihilation of light quark-antiquark pairs depicted in the right pane is negligible in the SM or in models with* $\tan\beta \simeq 1$.

$$\begin{aligned}\delta\sigma^{ab}_{NLO} &= \int d\Phi_{2\to2}\left[\frac{d\sigma^{ab}_V}{d\Phi_{2\to2}} + \sum \frac{d\sigma^{ab}_B}{d\Phi_{2\to2}} \otimes \mathbf{I}\right]_{\epsilon=0} \\ &+ \int dx \int d\Phi^{(x)}_{2\to2} \sum \frac{d\sigma^{ab}_B}{d\Phi^{(x)}_{2\to2}} \otimes \left[\mathbf{P}(x) + \mathbf{K}(x)\right]_{\epsilon=0} \\ &+ \int d\Phi_{2\to3}\left[\frac{d\sigma^{ab}_R}{d\Phi_{2\to3}} - \sum \frac{d\sigma^{ab}_B}{d\Phi_{2\to2}} \otimes \mathcal{V}_{\mathrm{dip}}\right], \end{aligned} \tag{3.19}$$

where the phase spaces for $2 \to 2$ and $2 \to 3$ reactions are defined as

$$\begin{aligned} d\Phi_{2\to2} &= \prod_{i=1,2} \frac{d^3\vec{k}_i}{(2\pi)^3 2E_i}(2\pi)^4\delta^{(4)}\left(p_1+p_2-k_1-k_2\right) \\ &= \frac{1}{16\pi}\beta_t dy, \end{aligned} \tag{3.20}$$

and

$$\begin{aligned} d\Phi_{2\to3} &= \prod_{i=1,2} \frac{d^3\vec{k}_i}{(2\pi)^3 2E_i}\frac{d^3\vec{p}_3}{(2\pi)^3 2E_3}(2\pi)^4\delta^{(4)}\left(p_1+p_2-k_1-k_2-p_3\right) \\ &= \frac{1}{2\sqrt{s}}\frac{1}{(2\pi)^5}\frac{|\vec{p}_3|}{2}\,d\Omega_3\,dm_{12}\,\frac{|\vec{k}^*_1|}{2}\,d\Omega^*_1, \end{aligned} \tag{3.21}$$

respectively. In (3.20) we used $s = (p_1+p_2)^2$, $\beta_t = \sqrt{1-\frac{4m_t^2}{s}}$ and $y = \cos\theta_t$ denotes the cosine of the top-quark scattering angle defined in the initial parton zero-momentum frame with respect to the z-axis which is aligned to the beam direction. In (3.21) we used

$$m_{12} = \sqrt{s_{12}} = \sqrt{(k_1+k_2)^2},$$

and Ω_3 denotes the solid angle of the parton with momentum p_3, the gluon in this case, defined in the initial parton zero-momentum frame. The quantities $\vec{k}_1^*$ and $d\Omega_1^*$ denote the 3-momentum and solid angle of the top-quark defined in the $t\bar{t}$ zero-momentum frame.

The set of integrated counter terms in (3.19) is already decomposed into terms constructed from the universal **I**, **P** and **K** operators. The first contains the part of the IR divergencies which is cancelled against the virtual corrections, whereas **P** and **K** constitute the finite remainder of the initial state collinear counter terms. The divergent part of the latter is absorbed in a redefinition of the PDFs. The integrated and unintegrated dipoles will be addressed again in the following sections where real and virtual corrections are discussed.

3.2. Top-quark decay modes

The top- and anti-top quarks can not be detected directly in experiments, thus their decays have to be taken into account to construct realistic observables or apply kinematical cuts. Here we will consider the dominant decay modes. Within the SM almost 100% of the top and antitop quarks decay via

$$\begin{aligned} t(k_1,s_1) &\to W^+ + b, \\ \bar{t}(k_2,s_2) &\to W^- + \bar{b}. \end{aligned} \tag{3.22}$$

The intermediate $W^{\pm}$ bosons subsequently decay either leptonically or hadronically

$$W^{\pm} \;\to\; l^{\pm}\nu_l\,,\, q\bar{q}'\,, \qquad q,q' \in \{u,d,s,c\}.$$

Since the decay $W^+ \to t\bar{b}$ is kinematically not allowed one counts in total 9 possible final states for the decay of either top or anti-top quark. A $t\bar{t}$ pair can thus decay into 81 different final states. In the following we will refer to the decays

$$\begin{aligned} t\bar{t} &\to l^+\nu_l + \bar{u}d/\bar{c}s + b\bar{b}, \\ t\bar{t} &\to l^-\bar{\nu}_l + u\bar{d}/c\bar{s} + b\bar{b}, \end{aligned}$$

with $l = \{e,\mu\}$ as the single-lepton channels. The decays $W^{\pm} \to \tau^{\pm}\nu_\tau$ are not considered here since the detection of the τ lepton is rather difficult. The branching ratio is to a good approximation $\mathrm{Br}(t\bar{t} \to 1l) = \frac{24}{81} \approx 30\%$. The double-lepton channels involve the decays

$$t\bar{t} \;\to\; l^+\nu_l + l'^-\bar{\nu}_{l'} + b\bar{b},$$

with $l, l' = \{e, \mu\}$, the branching ratio is $\mathrm{Br}(t\bar{t} \to 2l) = \frac{4}{81} \approx 5\%$. Thus, as long as only spin-independent observables at the $t\bar{t}$ level are considered, the decays of top and anti-top are taken into account by multiplying with the respective branching fractions for either single-lepton or the double-lepton channel. Below we take these branching ratios at NLO QCD into account.

In the following we will consider type-II 2HDM extensions of the SM, where flavour changing neutral Higgs interactions are absent at tree-level. Thus the decays

$$t \;\; \to \;\; \phi_i + q \; , \quad q \in \{u, d\}$$

for $m_i < m_t$ are loop-induced and thereby highly suppressed. Further, we will analyze scenarios of the type-II 2HDM where the mass of the charged Higgs is much larger than the top-mass, $m_\pm \gg m_t$, so that the contribution

$$t \;\; \xrightarrow{H^+} \;\; f\bar{f}' + b \; ,$$

to semileptonic and non-leptonic top-quark decays is negligible. As a result, the SM description of top-quark decays is sufficient, also within the 2HDM scenarios that are considered in the following.

3.2.1. Decay of polarized top-quarks

The one-particle inclusive decay density matrices for top or antitop quarks decaying to charged fermions are given by

$$\Gamma^\pm \;\; = \;\; \frac{\Gamma_{f^\pm}}{2} \left[\mathbb{1} \pm \kappa_{f^\pm} \; (\hat{q}_{f^\pm} \cdot \vec{\sigma}\,) \right] , \tag{3.23}$$

where σ_i are the Pauli matrices and $\hat{q}_{f^\pm}$ is the momentum direction of the charged final state fermion $f^\pm$, defined in the top or antitop restframe, respectively. For $f^\pm = l^\pm$ we have $\kappa_{l^\pm} = 0.998$ and $\kappa_b = -0.37$ for b-jets at NLO QCD [62, 63].

If $R^{ab\to t\bar{t}X}$ denotes the $t\bar{t}$ production density matrix for the parton reaction $ab \to t\bar{t} + X$, then the parton cross section in the on-shell approximation for the intermediate top and antitop quark can be written as

$$d\sigma \;\; = \;\; \frac{1}{2s}\, d\Phi \; \mathrm{Tr}\left[\Gamma^+ R^{ab\to t\bar{t}X}\, \Gamma^- \right] ,$$

where $d\Phi$ denotes the measure of the respective phase space.

3.3. Description of Higgs resonances

The unstable particles which are involved in the reactions considered in this thesis are the top quark, the weak gauge bosons, and the three neutral Higgs bosons of the 2HDM extension of the SM. The charged Higgs boson does not play any role here – see the 2HDM scenarios considered in Sec. 3.7.1. While we take higher order QCD corrections to $ab \to t\bar{t} + X$ for $ab \in \{gg, qg, \bar{q}g, gq, g\bar{q}, q\bar{q}\}$ as well as the t and $\bar{t}$ decay into account, we emphasize that we incorporate the electroweak gauge boson and Yukawa interactions only to leading order. This is important to keep in mind for the following discussion.

As argued above, the top quark can be treated in the narrow width approximation. The Z boson appears in $t\bar{t} + X$ production as s-channel resonance only far off-shell, $Z^* \to t\bar{t} + X$. Hence its width can be safely neglected. The same statement applies to the light Higgs boson ϕ_1 with $m_1 = 125$ GeV[1]. The $W^\pm$ boson is resonantly produced in t and $\bar{t}$ decay, respectively. As we work to lowest order in the weak gauge couplings this can be taken into account by using the width Γ_W in the W-boson propagator.

In the resonant production of the heavy Higgs bosons, $ab \to \phi_{2,3} \to t\bar{t}+X$, the finite width effects must be taken into account. The adequate method which respects gauge invariance also with respect to higher-order electroweak corrections is the so-called complex mass scheme [64, 65, 66]. Let us illustrate this method for the case at hand, using only one ϕ. We consider the amplitude for the process $ab \to \phi \to t\bar{t} + X$, taking only factorizable QCD corrections into account. The non-factorizable QCD corrections are analyzed in Sec. 3.6.3. In the complex mass scheme the amplitude is of the form

$$\mathcal{M}_{ij} = S_{ij}\left(q^2, \cdots\right) iP(q^2)\, S_f\left(q^2, \cdots\right) + \mathcal{N}\,, \qquad P(q^2) = \frac{1}{q^2 - \mu_\phi^2}\,, \tag{3.24}$$

where the complex mass parameter μ_ϕ^2 is the pole of the full ϕ propagator, i.e. the point in the complex q^2 plane where the renormalized Higgs-boson self-energy $\Pi(s)$ vanishes:

$$\Pi(\mu_\phi^2) = 0\,. \tag{3.25}$$

The symbol $\mathcal{N}$ in Eq. (3.24) denotes the non-resonant contribution to the scattering matrix element. The complex mass parameter must be used wherever the ϕ mass squared occurs in the scattering amplitude. However, as we compute (3.24) only to lowest order in the electroweak and Yukawa interactions, μ_ϕ^2 does not appear in the loops contributing to S_{ij} and S_f, but only in $P(s)$. We parameterize

$$\mu_\phi^2 = m^2 - im\Gamma\,. \tag{3.26}$$

Let us now determine the meaning of m and Γ. The relation between the renormalized and bare Higgs-boson self-energy is to one-loop order in the electroweak and Yukawa coulings:

[1] We note in addition that the total width of ϕ_1 is SM-like, i.e. very small in the 2HDM scenarios considered below, $\Gamma_1 \sim 4$ MeV.

$$\Pi(q^2) = \Pi_0(q^2) - \delta\mu_\phi^2 + (q^2 - \mu_\phi^2)\,\delta\mathcal{Z}_\phi\,, \tag{3.27}$$

where $\mathcal{Z}_\phi = 1 + \delta\mathcal{Z}_\phi$ is the complex Higgs wave-function renormalization constant and $\delta\mu_\phi^2$ is the complex mass counterterm. The relation between the *real* bare Higgs mass squared, m_0^2, and the complex renormalized mass squared μ_ϕ^2 is

$$m_0^2 = \mu_\phi^2 + \delta\mu_\phi^2\,. \tag{3.28}$$

The condition (3.25) is the complex-mass-scheme generalization of the usual on-shell renormalization condition. Using (3.27) it implies that

$$\delta\mu_\phi^2 = \Pi_0(\mu_\phi^2)\,.$$

Now we use the parameterization (3.26) and the relation (3.28), i.e. $\delta\mu_\phi^2 = m_0^2 - \mu_\phi^2$. Taking the real part of this relation shows that m can be interpreted as the on-shell mass of ϕ. Taking the imaginary part gives the equation

$$m\Gamma = \text{ Im}\left[\Pi_0(m^2 - im\Gamma)\right]\,, \tag{3.29}$$

which in general can be solved iteratively for Γ. Expanding this relation around m, one gets to one-loop order in the electroweak and Yukawa couplings [65]:

$$m\Gamma = \text{ Im}\left[\Pi_0(m^2)\right] - m\Gamma\ \text{Re}\left[\Pi_0'(m^2)\right]\,, \tag{3.30}$$

where the prime denotes the derivative with respect to q^2. Again, this equation may be solved iteratively for Γ. Because we work to lowest order in the electroweak and Yukawa couplings we can neglect the second term in (3.30). Then Γ is the total ϕ-boson width in the usual on-shell scheme.

In summary we use (3.24) where μ_ϕ^2 is determined by the on-shell mass and total width of the respective Higgs boson ϕ_2, ϕ_3.

3.4. Leading order matrix elements

At leading order in the strong coupling α_s, the parton processes

$$\begin{aligned} g(p_1)\, g(p_2) &\to t\,(k_1,s_1)\, \bar{t}\,(k_2,s_2) \quad , && && (3.31)\\ q(p_1)\, \bar{q}(p_2) &\to t\,(k_1,s_1)\, \bar{t}\,(k_2,s_2) \quad , && q \in \{u,d,s,c,b\}, && (3.32) \end{aligned}$$

and

$$\begin{aligned} g(p_1)\, g(p_2) &\to \phi_i \to \quad t\,(k_1,s_1)\, \bar{t}\,(k_2,s_2)\,, && && (3.33)\\ q(p_1)\, \bar{q}(p_2) &\to \phi_i \to \quad t\,(k_1,s_1)\, \bar{t}\,(k_2,s_2)\,, && q \in \{u,d,s,c,b\}, && (3.34) \end{aligned}$$

contribute to the reaction (3.3). The resepective amplitudes are labelled as

$$\begin{aligned} \mathcal{M}_B^{gg} &= \mathcal{M}_{B,QCD}^{gg} + \sum_{i=1,2} \mathcal{M}_{B,\phi_i}^{gg},\\ \mathcal{M}_B^{q\bar{q}} &= \mathcal{M}_{B,QCD}^{q\bar{q}} + \sum_{i=1,2} \mathcal{M}_{B,\phi_i}^{q\bar{q}}. \end{aligned} \tag{3.35}$$

The contributions from resonant $t\bar{t}$ production via quark-antiquark annihilation in (3.35) contain a factor $\frac{m_q}{v} \ll 1$ and can be neglected. In the case $q = b$ this is only valid as long as one avoids scenarios where one of the ϕ_i has an enhanced coupling to the b-quark. The squared gluon fusion matrix element contains the following terms:

$$\begin{aligned} |\mathcal{M}_B^{gg}|^2 &= \left|\mathcal{M}_{B,QCD}^{gg}\right|^2 && (3.36)\\ &\quad + \sum_{i=1,2} 2\,\mathrm{Re}\left(\mathcal{M}_{B,QCD}^{gg}\mathcal{M}_{B,\phi_i}^{gg\,*}\right) && (3.37)\\ &\quad + \left|\sum_{i=1,2} \mathcal{M}_{B,\phi_i}^{gg}\right|^2 . && (3.38) \end{aligned}$$

The computation of the non-resonant QCD contribution (3.36) as well as $|\mathcal{M}_{B,QCD}^{q\bar{q}}|^2$ for $q \in \{u,d,s,c,b\}$ including the next-to-leading order corrections have already been accomplished [67, 68] and the results can be used for this project. Here we will be concerned only with the interference terms of resonant $t\bar{t}$ production amplitudes with the non-resonant QCD background (3.37) and the purely resonant contribution (3.38). Note that due to the presence of two heavy neutral Higgs bosons in our 2HDM scenarios, the sum (3.38) contains additional interference terms.

3.4.1. The parton process $gg \to t\bar{t}$

Interference of non-resonant and resonant LO amplitudes

The interference of resonant $t\bar{t}$ production amplitudes with the non-resonant background (3.37) is given at leading order by the first two Feynman diagrams in Fig. 3.1 and the first one in Fig. 3.2. Applying the Feynman rules in Appendix A one gets the result

$$\begin{aligned}
\sum{}' 2\,\mathrm{Re}\left(\mathcal{M}^{gg}_{B,QCD}\mathcal{M}^{gg\,*}_{B,\phi_i}\right) \quad = \quad & \frac{2}{N_c^2-1}\frac{\alpha_s^2}{(1-\beta_t^2y^2)}\frac{m_t^2}{v}\times\Bigg\{ \\
& \left(a_{t,i}\beta_t^2\,\mathrm{Re}(\tilde{\mathcal{F}}_{S,i}) + \,\mathrm{Re}(\tilde{\mathcal{F}}_{P,i})\,b_{t,i}\right) \\
+ \quad & (k_1\cdot s_2 + k_2\cdot s_1)\,\frac{2m_t}{s}\left(a_{t,i}\;\mathrm{Im}(\tilde{\mathcal{F}}_{P,i}) \;-b_{t,i}\,\mathrm{Im}(\tilde{\mathcal{F}}_{S,i})\right) \\
- \quad & (s_1\cdot s_2)\left(a_{t,i}\beta_t^2\,\mathrm{Re}(\tilde{\mathcal{F}}_{S,i}) - b_{t,i}\,\mathrm{Re}(\tilde{\mathcal{F}}_{P,i})\right) \\
+ \quad & \epsilon^{k_1k_2s_1s_2}\,\frac{2}{s}\left(a_{t,i}\,\mathrm{Re}(\tilde{\mathcal{F}}_{P,i}) + b_{t,i}\,\mathrm{Re}(\tilde{\mathcal{F}}_{S,i})\right) \\
+ \quad & (k_1\cdot s_2)(k_2\cdot s_1)\frac{2}{s}\left(a_{t,i}\,\mathrm{Re}(\tilde{\mathcal{F}}_{S,i}) - b_{t,i}\,\mathrm{Re}(\tilde{\mathcal{F}}_{P,i})\,\right)\Bigg\}.
\end{aligned} \tag{3.39}$$

Here we summed and averaged over initial spin and colour states, which is indicated by the symbol $\sum'$. To simplify the notation, the complex form factors $\mathcal{F}_{S,i}$ and $\mathcal{F}_{P,i}$ defined in Sec. 2.1 have been combined with the Higgs propagator,

$$P_i(s) \quad = \quad \frac{1}{s-m_i^2+i\Gamma_i m_i}, \tag{3.40}$$

in the following way:

$$\begin{aligned}
\tilde{\mathcal{F}}_{S,i} \quad &= \quad P_i(s)\,\mathcal{F}_{S,i}(s), \\
\tilde{\mathcal{F}}_{P,i} \quad &= \quad P_i(s)\,\mathcal{F}_{P,i}(s).
\end{aligned}$$

The quantities s, β_t and y are defined as in Eq. (3.20). In (3.39) the shorthand notation $\epsilon^{k_1k_2s_1s_2} = \epsilon_{\mu\nu\rho\sigma}k_1^\mu k_2^\nu s_1^\rho s_2^\sigma$ was used. In the following we will always use the convention $\epsilon^{0123} = +1$.

Summing over all $t\bar{t}$ spin configurations only the first term in (3.39) remains with a factor 4:

$$\sum_{s_1 s_2} \sum{}' \, 2\,\mathrm{Re}\left(\mathcal{M}^{gg}_{B,QCD}\mathcal{M}^{gg\,*}_{B,\phi_i}\right) \;=\; \frac{2}{N_c^2-1}\frac{\alpha_s^2}{(1-\beta_t^2 y^2)}\frac{m_t^2}{v} \times \Bigg\{ 4\left(a_{t,i}\beta_t^2\,\mathrm{Re}(\tilde{\mathcal{F}}_{S,i}) + \mathrm{Re}(\tilde{\mathcal{F}}_{P,i})\,b_{t,i}\right)\Bigg\}.$$

Squared resonant LO amplitudes

The squared resonant $t\bar{t}$ production amplitude for a single boson is computed by applying the Feynman rules given in Appendix A to the first graph in Fig. 3.2. The result can be written in the following form:

$$\sum{}' \left|\mathcal{M}^{gg}_{B,\phi_i}\right|^2 \;=\; \frac{1}{8\,(N_c^2-1)}\left(\frac{\alpha_s}{\pi}\right)^2 \left(|\mathcal{F}_{S,i}(s)|^2 + |\mathcal{F}_{P,i}(s)|^2\right)|P_i(s)|^2 K_i\left(k_1,k_2,s_1,s_2\right). \tag{3.41}$$

The function $K_i\left(k_1,k_2,s_1,s_2\right)$ describes the decay $\phi_i \to t\bar{t}$ at tree-level and is given by

$$\begin{aligned} K_i\left(k_1,k_2,s_1,s_2\right) \;=\; & \frac{N_c}{2}\left(\frac{m_t}{v}\right)^2 \{s(a_{t,i}^2\beta_t^2 + b_{t,i}^2) + s(b_{t,i}^2 - a_{t,i}^2\beta_t^2)(s_1\cdot s_2) \\ & +2(a_{t,i}^2 - b_{t,i}^2)(k_1\cdot s_2)(k_2\cdot s_1) + 4a_{t,i}b_{t,i}\epsilon^{k_1,k_2,s_1,s_2}\}. \end{aligned} \tag{3.42}$$

If one sums over the final $t\bar{t}$ spin states this reduces to

$$\sum_{s_1 s_2} K_i\left(k_1,k_2,s_1,s_2\right) \;=\; \frac{N_c}{2}\left(\frac{m_t}{v}\right)^2 \{4s\,(a_{t,i}^2\beta_t^2 + b_{t,i}^2)\}.$$

Additionally, the interference of two neutral Higgs bosons has to be computed:

$$\begin{aligned} \sum{}' \, 2\,\mathrm{Re}\left(\mathcal{M}^{gg}_{B,\phi_i}\mathcal{M}^{gg\,*}_{B,\phi_j}\right) \;=\; & \frac{1}{4\,(N_c^2-1)}\left(\frac{\alpha_s}{\pi}\right)^2 \\ & \times \mathrm{Re}\left[\left(\mathcal{F}_{S,i}\mathcal{F}^*_{S,j} + \mathcal{F}_{P,i}\mathcal{F}^*_{P,j}\right)P_{ij}(s)K_{ij}\left(k_1,k_2,s_1,s_2\right)\right]. \end{aligned} \tag{3.43}$$

Here the abbreviation $P_{ij}(s) = P_i(s)\,P_j^*(s)$ was used. Note, that we do not encounter interference terms proportional to $\mathcal{F}_{S,i}\mathcal{F}^*_{P,j}$. This is due to the fact that the two Lorentz structures in the full as well as the effective $gg\phi_i$ vertices are orthogonal, c.f. (A.9). If only the top-quark coupling is taken into account in the one-loop $gg\phi_i$ vertices, one has $\mathcal{F}_{S,i} = a_{t,i}\hat{\mathcal{F}}_S$ and $\mathcal{F}_{P,i} = b_{t,i}\hat{\mathcal{F}}_P$ so that

$$\begin{aligned} \mathcal{F}_{S,i}\mathcal{F}^*_{S,j} &= a_{t,i}a_{t,j}\left|\hat{\mathcal{F}}_S\right|^2 , \\ \mathcal{F}_{P,i}\mathcal{F}^*_{P,j} &= b_{t,i}b_{t,j}\left|\hat{\mathcal{F}}_P\right|^2 . \end{aligned}$$

Eq. (3.43) then simplifies:

$$\begin{aligned} \sum{}' 2\,\mathrm{Re}\left(\mathcal{M}^{gg}_{B,\phi_i}\mathcal{M}^{gg\,*}_{B,\phi_j}\right) &= \frac{1}{4\,(N_c^2-1)}\left(\frac{\alpha_s}{\pi}\right)^2\left[a_{t,i}a_{t,j}\left|\hat{\mathcal{F}}_S\right|^2 + b_{t,i}b_{t,j}\left|\hat{\mathcal{F}}_P\right|^2\right] \\ &\quad \times \mathrm{Re}\left[P_{ij}(s)K_{ij}\left(k_1,k_2,s_1,s_2\right)\right] . \end{aligned} \tag{3.44}$$

The complex function $K_{ij}\left(k_1,k_2,s_1,s_2\right)$ in (3.43) and (3.44) describes the interference of the two decays $\phi_{i,j} \to t\bar{t}$ at tree-level and is given by

$$\begin{aligned} K_{ij}\left(k_1,k_2,s_1,s_2\right) &= \frac{N_c}{2}\left(\frac{m_t}{v}\right)^2\Big\{s\left(a_{t,i}a_{t,j}\beta_t^2 + b_{t,i}b_{t,j}\right) \\ &\quad -s\left(a_{t,i}a_{t,j}\beta_t^2 - b_{t,i}b_{t,j}\right)(s_1\cdot s_2) \\ &\quad +2(a_{t,i}a_{t,j} - b_{t,i}b_{t,j})(k_1\cdot s_2)(k_2\cdot s_1) \\ &\quad +2(a_{t,i}b_{t,j} + a_{t,j}b_{t,i})\,\epsilon^{k_1,k_2,s_1,s_2} \\ &\quad -2i\ m_t(a_{t,i}b_{t,j} - a_{t,j}b_{t,i})(k_1\cdot s_2 + k_2\cdot s_1)\Big\} . \end{aligned} \tag{3.45}$$

If one sums over top and anti-top spins this reduces to

$$\sum_{s_1 s_2} K_{ij}\left(k_1,k_2,s_1,s_2\right) = \frac{N_c}{2}\left(\frac{m_t}{v}\right)^2\left\{4s(a_{t,i}a_{t,j}\beta_t^2 + b_{t,i}b_{t,j})\right\} .$$

Note that the first 4 terms in (3.45) have the same structure as in (3.42) and can be obtained by simple substitutions: $a^2_{t,i}, b^2_{t,i} \to a_{t,i}a_{t,j}, b_{t,i}b_{t,j}$ and $2a_{t,i}b_{t,i} \to (a_{t,i}b_{t,j}+a_{t,j}b_{t,i})$. Only the imaginary part in (3.45) is new.

3.5. Real radiation corrections

The next-to-leading order real radiation corrections to the reaction (3.3) consist of the squared tree-level matrix elements corresponding to the resonant parton processes (3.14) – (3.18) and the interferences with the tree-level matrix elements corresponding to the non-resonant processes (3.9) – (3.12). Of these, the processes with initial gg and qg require special attention since the corresponding amplitudes exhibit divergences in the phase space regions where the parton momentum p_3 becomes soft or collinear with the initial state parton momenta p_1 and p_2. The Feynman graphs that represent the corresponding amplitudes are:

$$\begin{aligned}
\mathcal{M}^{gg}_{R,QCD} &= \mathcal{M}^{gg}_{R,QCD,ISR}\,[\text{Figs. } 3.3] + \mathcal{M}^{gg}_{R,QCD,INT}\,[\text{Figs. } 3.5] \\
&\quad + \mathcal{M}^{gg}_{R,QCD,FSR}\,[\text{Figs. } 3.4]\,, \\
\mathcal{M}^{qg}_{R,QCD} &= [\text{Figs. } 3.9]\,, \\
\mathcal{M}^{q\bar{q}}_{R,QCD} &= [\text{Figs. } 3.11, 3.12]\,, \\
\mathcal{M}^{gg}_{R,\phi_i} &= \mathcal{M}^{gg}_{R,\phi_i,ISR}\,[\text{Figs. } 3.6] + \mathcal{M}^{gg}_{R,\phi_i,INT}\,[\text{Figs. } 3.7] \\
&\quad + \mathcal{M}^{gg}_{R,\phi_i,FSR}\,[\text{Figs. } 3.8]\,, \\
\mathcal{M}^{qg}_{R,\phi_i} &= [\text{Fig. } 3.10(a)]\,, \\
\mathcal{M}^{q\bar{q}}_{R,\phi_i} &= [\text{Fig. } 3.10(b)]\,.
\end{aligned} \tag{3.46}$$

Again, we will focus here on the ocmputation of the squared resonant $\phi_i \to t\bar{t}$ production matrix elements and their interferences with the non-resonant QCD background, i.e. we are concerned with the last two terms of

$$\left|\mathcal{M}^{ab}_{R}\right|^2 = \left[\left|\mathcal{M}^{ab}_{R,QCD}\right|^2 + \sum_{i=1,2} 2\,\mathrm{Re}\left(\mathcal{M}^{ab}_{R,QCD}\mathcal{M}^{ab\,*}_{R,\phi_i}\right) + \left|\sum_{i=1,2}\mathcal{M}^{ab}_{R,\phi_i}\right|^2\right], \tag{3.47}$$

where $ab \in \{gg, qg, \bar{q}g, gq, g\bar{q}, q\bar{q}\}$. The first term in (3.47) is part of the computation described in [67, 68].

Interference of non-resonant QCD background and resonant real emission

The interference terms $\sum_{i=1,2} 2\,\mathrm{Re}\left(\mathcal{M}^{ab}_{R,QCD}\mathcal{M}^{ab\,*}_{R,\phi_i}\right)$ with $ab \in \{gg, qg, \bar{q}g, gq, g\bar{q}, q\bar{q}\}$ can not be expressed in compact form, therefore no analytic expressions will be given here. Nevertheless, to simplify the computation it is useful to discuss which interferences vanish due to colour algebra. Therefore one should classify the relevant Feynman graphs due to the colour state of the initial gg or $q\bar{q}$ and final $t\bar{t}$ pair, i.e. if either of them is in a pure colour singlet or octet state. Interferences of pure singlet and octet states can then directly be dropped from the computation. Table 3.1 gives an overview.

Table 3.1. – *Characterization of real amplitudes according to the colour state of the initial gg or final $t\bar{t}$ pair.*

$\mathcal{M}^{gg}_{R,\phi_i}$	
ISR, INT: Figs. 3.6, 3.7	$t\bar{t}$ singlet
FSR: Figs. 3.8	gg singlet $t\bar{t}$ octet

$\mathcal{M}^{gg}_{R,QCD}$	
ISR: Figs. 3.3(c), 3.3(d)	$t\bar{t}$ octet
ISR: Figs. 3.4(c), 3.4(d), 3.5(b)	gg octet
INT: Figs. 3.5(b), 3.5(c)	$t\bar{t}$ octet
FSR: Figs. 3.4(c), 3.4(d)	gg octet

$\mathcal{M}^{qg}_{R,\phi_i}$	
Fig. 3.10(a)	$t\bar{t}$ singlet

$\mathcal{M}^{qg}_{R,QCD}$	
Fig. 3.9(a)	$t\bar{t}$ octet

$\mathcal{M}^{q\bar{q}}_{R,\phi_i}$	
Fig. 3.10(b)	$t\bar{t}$ singlet

$\mathcal{M}^{q\bar{q}}_{R,QCD}$	
ISR, Figs. 3.11(a), 3.11(b)	$t\bar{t}$ octet
INT, Fig. 3.11(c)	$t\bar{t}$ octet

Similar arguments hold for the other parton processes, for example the non-resonant QCD diagram 3.9(a) does not contribute to the interference $\sum_{i=1,2} 2\,\mathrm{Re}\left(\mathcal{M}^{qg}_{R,QCD}\mathcal{M}^{qg\,*}_{R,\phi_i}\right)$ because the $t\bar{t}$ pair is in a colour octet state, whereas in the resonant diagram 3.10(a) it is in a colour singlet.

3.5.1. Higgs production in gluon-fusion

Real emission from the initial state

The squared resonant $t\bar{t}$ production amplitudes can be expressed in a rather compact form. The analytic expressions will be presented here to emphasize again the additional interference terms that occur in the computation with two or more neutral Higgs bosons. The squared amplitude given by the Feynman graphs in Figs. 3.6 and 3.7 can be written as

$$\sum{}' \,|\mathcal{M}^{gg}_{R,\phi_i,ISR} + \mathcal{M}^{gg}_{R,\phi_i,INT}|^2 = |\mathcal{M}_{gg\to\phi_i g}|^2 |P_i(s_{12})|^2\, K_i(k_1,k_2,s_1,s_2)\,, \tag{3.48}$$

where the first factor, which describes gluon radiation from the initial state, is given by

$$|\mathcal{M}_{gg\to\phi_i g}|^2 = \frac{16\pi^2 C_A}{N_c^2-1}\left(\frac{\alpha_s}{\pi}\right)^3 \left(|f^{(0)}_{H,i}|^2 + 4|f^{(0)}_{A,i}|^2\right) \frac{[(s+t+u)^4 + s^4 + t^4 + u^4]}{s\,t\,u}\,. \tag{3.49}$$

Summation and averaging over initial spin and colour is indicated by $\sum'$ in (3.48). The functions $P_i(s)$ and $K_i(k_1,k_2,s_1,s_2)$ that describe the propagation and decay of the Higgs boson ϕ_i into a $t\bar{t}$ pair at tree-level were defined in Sec. 3.4. Note that here we consider $2 \to 3$ scattering so that $s_{12} = (k_1+k_2)^2 \neq s = (p_1+p_2)^2$ and one has to use $\beta_t^2 = 1 - \frac{4m_t^2}{s_{12}}$ in $K_i(k_1,k_2,s_1,s_2)$, c.f. (3.42). Further, the definitions

$$t = (k_3 - p_1)^2, \quad u = (k_3 - p_2)^2, \tag{3.50}$$

were used in (3.49). The soft ($E_3 \to 0$) and collinear ($y_3 \to \pm 1$) divergences in (3.48) become apparent if one expresses the denominator in (3.49) in terms of energies and scattering angles:

$$\frac{1}{s\,t\,u} = \frac{4}{E_3^2(1-y_3)(1+y_3)s^2}.$$

In this equation, E_3 denotes the outgoing gluon energy and $y_3 = \cos\theta_3$ the gluon scattering angle in the initial parton zero-momentum frame with respect to the z-axis, which is defined by the direction of p_1.

Real emission from the final state

In the squared final gluon radiation amplitude

$$\sum' |\mathcal{M}^{gg}_{R,\phi_i,FSR}|^2 = |\mathcal{M}_{gg\to\phi_i}|^2 |P_i(s)|^2 K_{i,FSR}(k_1,k_2,p_3,s_1,s_2)\,, \tag{3.51}$$

the Higgs to $t\bar{t}$ decay form factor contains additional correlations of the top and anti-top spins s_1 and s_2 with the gluon momentum p_3,

$$\begin{aligned} K_{i,FSR}(k_1,k_2,p_3,s_1,s_2) \;=\; & \mathcal{N}[A_i + c_{0,i}(k_1\cdot s_2)(k_2\cdot s_1) + c_{1,i}(s_1\cdot s_2) - c_{2,i}\epsilon(k_1,k_2,s_1,s_2) \\ & + c_{3,i}(k_1\cdot s_2)(k_3\cdot s_1) + c_{4,i}(k_2\cdot s_1)(k_3\cdot s_2) + c_{5,i}(k_3\cdot s_1)(k_3\cdot s_2) \\ & - c_{7,i}\epsilon(k_1,k_3,s_1,s_2) - c_{8,i}\epsilon(k_2,k_3,s_1,s_2)]\,. \end{aligned} \tag{3.52}$$

The squared, leading order matrix element for Higgs production via gluon fusion,

$$|\mathcal{M}_{gg\to\phi_i}|^2 = \frac{2}{N_c^2-1}\left(\frac{\alpha_s}{\pi}\right)^2 s^2 \left(|f^{(0)}_{H,i}|^2 + 4|f^{(0)}_{A,i}|^2\right) \tag{3.53}$$

can be extracted from (3.41) and the propagator $|P_i(s)|^2$ has already been defined in (3.40). The normalization factor in (3.52) is

$$\mathcal{N} = 4\pi\alpha_s(N_c^2-1)\left(\frac{m_t^2}{v^2}\right)\frac{1}{s_{13}'^2 s_{23}'^2}. \tag{3.54}$$

Here the abbreviations

$$\begin{aligned} s &= (k_1+k_2+k_3)^2 = (p_1+p_2)^2\,, \\ s_{13}' &= s_{13}-m_t^2 = (k_1+k_3)^3 - m_t^2 = 2k_1\cdot k_3\,, \\ s_{23}' &= s_{23}-m_t^2 = (k_2+k_3)^3 - m_t^2 = 2k_2\cdot k_3\,, \end{aligned}$$

were used. The soft singularity in (3.51) becomes apparent if one expresses the denominator of (3.54) in terms of the gluon energies and scattering angles:

$$\frac{1}{s_{13}'^2 s_{23}'^2} = \frac{1}{\left(E_3^2 E_1 E_2 (1-\frac{|\vec{k}_1|}{E_1}z_{13})(1-\frac{|\vec{k}_2|}{E_2}z_{23})\right)^2}.$$

Here E_1 and E_2 denote the top and anti-top energies and $z_{13} = \cos\theta_{13}$, $z_{23} = \cos\theta_{23}$ are the angles between gluon and top or anti-top directions of flight in the initial parton zero-momentum frame. One factor E_3^{-1} will be compensated by the phase space integral, but one can easily see that divergent terms remain.

The spin independent part in (3.52) is given by

$$\begin{aligned} A_i = \frac{1}{4}\Big\{ & s_{13}'s_{23}'[s_{23}'[(2s_{23}'-4s)(a_{t,i}^2+b_{t,i}^2)+16m_t^2a_{t,i}^2]+4(2m_t^2-s)[4a_{t,i}^2m_t^2-s(a_{t,i}^2+b_{t,i}^2)]] \\ & +2s_{13}'^2[s_{23}'[(2s_{23}'-2s)(a_{t,i}^2+b_{t,i}^2)+8a_{t,i}^2m_t^2]-2m_t^2s(a_{t,i}^2+b_{t,i}^2)+8a_{t,i}^2m_t^4] \\ & +2s_{23}'s_{13}'^3(a_{t,i}^2+b_{t,i}^2)+4m_t^2s_{23}'^2[4a_{t,i}^2m_t^2-s(a_{t,i}^2+b_{t,i}^2)]\Big\}\,, \end{aligned} \tag{3.55}$$

and the coefficients of the different spin structures are

$$\begin{aligned} c_{0,i} &= -2(a_{t,i}^2-b_{t,i}^2)\left[m_t^2(s_{13}'+s_{23}')^2 - ss_{13}'s_{23}'\right]\,, \\ c_{1,i} &= -[a_{t,i}^2(4m_t^2-s)+b_{t,i}^2s][m_t^2(s_{13}'+s_{23}')^2+s_{13}'s_{23}'(s_{13}'+s_{23}'-s)]\,, \\ c_{2,i} &= 4a_{t,i}b_{t,i}\left[m_t^2(s_{13}'+s_{23}')^2 - ss_{13}'s_{23}'\right]\,, \\ c_{3,i} &= 2m_t^2(s_{13}'+s_{23}')\left[-a_{t,i}^2(s_{13}'-s_{23}')+b_{t,i}^2(s_{13}'+s_{23}')\right]\,, \\ c_{4,i} &= 2m_t^2(s_{13}'+s_{23}')\left[a_{t,i}^2(s_{13}'-s_{23}')+b_{t,i}^2(s_{13}'+s_{23}')\right]\,, \\ c_{5,i} &= 2m_t^2(a_{t,i}^2+b_{t,i}^2)(s_{13}'+s_{23}')^2\,, \\ c_{7,i} &= 4m_t^2a_{t,i}b_{t,i}s_{13}'(s_{13}'+s_{23}')\,, \\ c_{8,i} &= -4m_t^2a_{t,i}b_{t,i}s_{23}'(s_{13}'+s_{23}')\,. \end{aligned} \tag{3.56}$$

Note that there are no interference terms $\mathcal{M}^{gg}_{\phi_i,ISR/INT}\mathcal{M}^{gg\,*}_{\phi_i,FSR}$ because the $t\bar{t}$ pair is produced in a colour singlet state in $\mathcal{M}^{gg}_{\phi_i,ISR/INT}$ and in a colour octet state in $\mathcal{M}^{gg}_{\phi_i,FSR}$, c.f. (3.1).

Higgs interference terms

The Higgs-gluon couplings in the effective approximation are real, thus

$$\mathrm{Im}\left(\mathcal{M}_{gg\to\phi_i g}\mathcal{M}^*_{gg\to\phi_j g}\right) = 0,$$

and the ϕ_i, ϕ_j interference of initial and intermediate radiation diagrams reduces to

$$\begin{aligned}\sum{}' 2\,\mathrm{Re}\left(\mathcal{M}^{gg}_{R,\phi_i,ISR+INT}\mathcal{M}^{gg\,*}_{R,\phi_j,ISR+INT}\right) &= 2\,\mathrm{Re}\left(\mathcal{M}_{gg\to\phi_i g}\mathcal{M}^*_{gg\to\phi_j g}\right)\\ &\quad\times \mathrm{Re}\left[P_{ij}(k_1+k_2)^2 K_{ij}(k_1,k_2,s_1,s_2)\right]\,,\end{aligned} \tag{3.57}$$

where

$$\begin{aligned}\mathrm{Re}\left(\mathcal{M}_{gg\to\phi_i g}\mathcal{M}^*_{gg\to\phi_j g}\right) &= \frac{16\pi^2 C_A}{N_c^2-1}\left(\frac{\alpha_s}{\pi}\right)^3\left(f^{(0)}_{H,i}f^{(0)}_{H,j}+4f^{(0)}_{A,i}f^{(0)}_{A,j}\right)\\ &\quad\times\frac{[(s+t+u)^4+s^4+t^4+u^4]}{s\,t\,u}.\end{aligned}$$

The complex functions $P_{ij}(s_{12})$ and $K_{ij}(k_1,k_2,s_1,s_2)$ were already defined in Sec. 3.4. In the case of the final state radiation ϕ_i, ϕ_j interference terms,

$$\begin{aligned}\sum{}' 2\,\mathrm{Re}\left(\mathcal{M}^{gg}_{R,\phi_i,FSR}\mathcal{M}^{gg\,*}_{R,\phi_j,FSR}\right) &= 2\,\mathrm{Re}\left(\mathcal{M}_{gg\to\phi_i}\mathcal{M}^*_{gg\to\phi_j}\right)\\ &\quad\times \mathrm{Re}\left[P_{ij}(k_1+k_2)^2 K_{ij,FSR}(k_1,k_2,p_3,s_1,s_2)\right]\,,\end{aligned} \tag{3.58}$$

where

$$2\,\mathrm{Re}\left(\mathcal{M}_{gg\to\phi_i}\mathcal{M}^*_{gg\to\phi_j}\right) = \frac{2}{N_c^2-1}\left(\frac{\alpha_s}{\pi}\right)^2 s^2\left(f^{(0)}_{H,i}f^{(0)}_{H,j}+4f^{(0)}_{A,i}f^{(0)}_{A,j}\right)\,,$$

we have to compute in addition the imaginary part of the interference of the decays $\phi_i,\phi_j\to t\bar{t}$ which now has the structure

$$\begin{aligned}
K_{ij,FSR}(k_1,k_2,p_3,s_1,s_2) &= \mathcal{N}[A_{ij} + c_{0,ij}(k_1 \cdot s_2)(k_2 \cdot s_1) + c_{1,ij}(s_1 \cdot s_2) - c_{2,ij}\epsilon^{k_1,k_2,s_1,s_2} \\
&\quad + c_{3,ij}(k_1 \cdot s_2)(k_3 \cdot s_1) + c_{4,ij}(k_2 \cdot s_1)(k_3 \cdot s_2) \\
&\quad + c_{5,ij}(k_3 \cdot s_1)(k_3 \cdot s_2) - c_{7,ij}\epsilon^{k_1,k_3,s_1,s_2} - c_{8,ij}\epsilon^{k_2,k_3,s_1,s_2}] \\
&\quad + i\left(c_{9,ij}(k_1 \cdot s_2 + k_2 \cdot s_1) + c_{10,ij}(p_3 \cdot s_1) + c_{11,ij}(p_3 \cdot s_2)\right) .
\end{aligned} \tag{3.59}$$

The coefficients of the spin structures that were already present in (3.52), i.e. the real part, can be obtained from (3.55) and (3.56) by simple substitutions:

$$\begin{aligned}
A_{ij} &= A_i\left[a_{t,i}^2 \to a_{t,i}a_{t,j}\,,\, b_{t,i}^2 \to b_{t,i}b_{t,j}\right], \\
c_{0,ij} &= c_{0,i}\left[a_{t,i}^2 \to a_{t,i}a_{t,j}\,,\, b_{t,i}^2 \to b_{t,i}b_{t,j}\right], \\
c_{1,ij} &= c_{1,i}\left[a_{t,i}^2 \to a_{t,i}a_{t,j}\,,\, b_{t,i}^2 \to b_{t,i}b_{t,j}\right], \\
c_{2,ij} &= c_{2,i}\left[2a_{t,i}b_{t,i} \to a_{t,i}b_{t,j} + a_{t,j}b_{t,i}\right], \\
c_{3,ij} &= c_{3,i}\left[a_{t,i}^2 \to a_{t,i}a_{t,j}\,,\, b_{t,i}^2 \to b_{t,i}b_{t,j}\right], \\
c_{4,ij} &= c_{4,i}\left[a_{t,i}^2 \to a_{t,i}a_{t,j}\,,\, b_{t,i}^2 \to b_{t,i}b_{t,j}\right], \\
c_{5,ij} &= c_{5,i}\left[a_{t,i}^2 \to a_{t,i}a_{t,j}\,,\, b_{t,i}^2 \to b_{t,i}b_{t,j}\right], \\
c_{7,ij} &= c_{7,i}\left[2a_{t,i}b_{t,i} \to a_{t,i}b_{t,j} + a_{t,j}b_{t,i}\right], \\
c_{8,ij} &= c_{8,i}\left[2a_{t,i}b_{t,i} \to a_{t,i}b_{t,j} + a_{t,j}b_{t,i}\right].
\end{aligned}$$

The imaginary part in (3.52) is given by

$$\begin{aligned}
c_{9,ij} &= (a_{3t}b_{2t} - a_{2t}b_{3t})m_t[(4m_t^2 - s + s'_{13} + s'_{23})s'_{13}s'_{23} + 2m_t^2(s'^2_{13} + s'^2_{23})]\,, \\
c_{10,ij} &= (a_{3t}b_{2t} - a_{2t}b_{3t})m_t[2m_t^2(s'^2_{13} + s'^2_{23}) + (4m_t^2 - s)s'_{13}s'_{23} - s\ s'^2_{23}]\,, \\
c_{11,ij} &= (a_{3t}b_{2t} - a_{2t}b_{3t})m_t[2m_t^2(s'^2_{13} + s'^2_{23}) + (4m_t^2 - s)s'_{13}s'_{23} - s\ s'^2_{13}]\,.
\end{aligned}$$

3.5.2. Higgs production in quark-gluon-fusion

The computation of the interference terms $\sum_{i=1,2} 2\,\mathrm{Re}\left(\mathcal{M}^{qg}_{R,QCD}\mathcal{M}^{qg\,*}_{R,\phi_i}\right)$ involves the non-resonant Feynnman graphs depicted in Figs. 3.9(b) and 3.9(c) as well as the resonant graph depicted in Fig. 3.10(a) and leads again to a rather long expression.

The squared amplitude corresponding to the process (3.15) for a single Higgs boson can be written as

$$\sum{}' \left|\mathcal{M}^{qg}_{R,\phi_i}\right|^2 = |\mathcal{M}_{qg\to\phi_i q}|^2 |P_j(s_{12})|^2\, K_i(k_1,k_2,s_1,s_2). \tag{3.60}$$

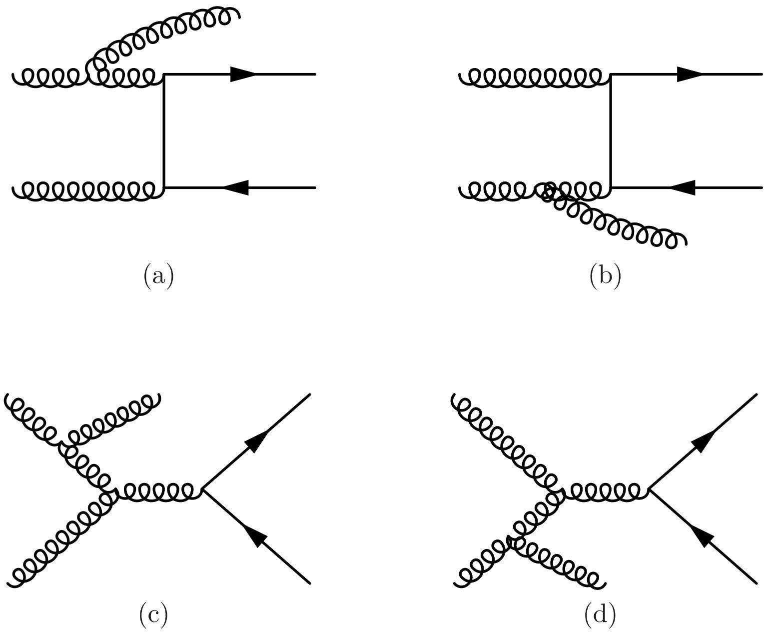

Figure 3.3. – *Tree-level Feynman graphs for the real radiation process $gg \to t\bar{t} + g$ with gluon radiation from the initial state. The corresponding amplitudes give rise to soft and collinear divergences.*

Note that the spin and colour averaging factor for a qg initial state, $(4N_c(N_c^2) - 1)^{-1}$, is different from that of the gg initial state, $((2(N_c^2 - 1))^2)^{-1}$. The correct factor is always implicitly assumed in the notation $\sum'$. Only one Feynman graph, depicted in Fig. 3.10(a), contributes to this amplitude. The squared matrix element describing the production process $qg \to \phi_i q$ is given by

$$|\mathcal{M}_{qg\to\phi_i q}|^2 = \frac{8\pi^2}{N_c}\left(\frac{\alpha_s}{\pi}\right)^3 \left(\left(f_{H,i}^{(0)}\right)^2 + 4\left(f_{A,i}^{(0)}\right)^2\right)\frac{s^2+u^2}{(-t)}.$$

The interference terms of two Higgs bosons have the form

$$\begin{aligned}\sum{}' 2\,\mathrm{Re}\left(\mathcal{M}_{R,\phi_i}^{qg}\mathcal{M}_{R,\phi_j}^{qg\,*}\right) &= 2\,\mathrm{Re}\left(\mathcal{M}_{qg\to\phi_i g}\mathcal{M}_{qg\to\phi_i q}^{*}\right)\\ &\quad\times \mathrm{Re}\left[P_{ij}(s_{12})K_{ij}(k_1,k_2,s_1,s_2)\right],\end{aligned} \tag{3.61}$$

with

$$\mathrm{Re}\left(\mathcal{M}_{qg\to\phi_i g}\mathcal{M}_{qg\to\phi_i q}^{*}\right) = \frac{8\pi^2}{N_c}\left(\frac{\alpha_s}{\pi}\right)^3\left(f_{H,i}^{(0)}f_{H,j}^{(0)} + 4f_{A,i}^{(0)}f_{A,j}^{(0)}\right)\frac{s^2+u^2}{(-t)}. \tag{3.62}$$

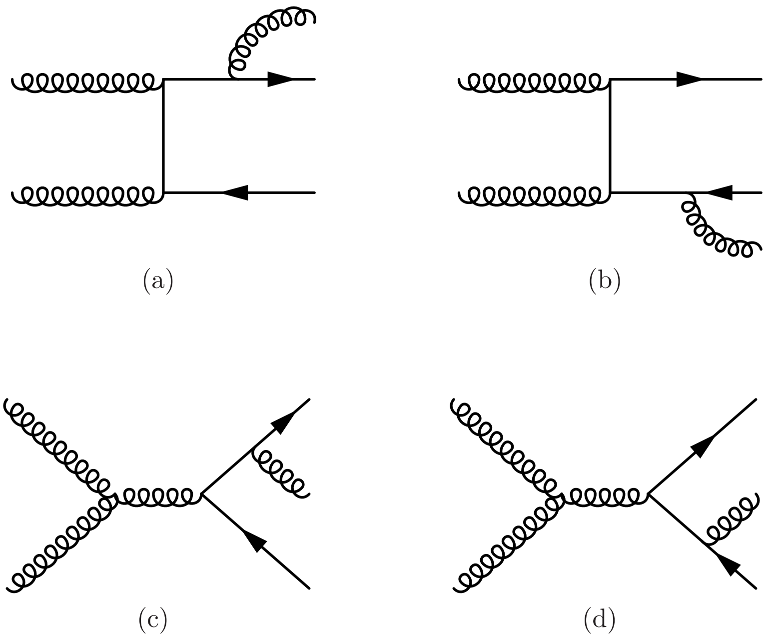

Figure 3.4. – *Tree-level Feynman graphs for the real radiation process $gg \to t\bar{t}+g$ with gluon radiation from the final state. The corresponding amplitudes give rise only to soft divergences.*

The functions $P_{ij}(s_{12})$ and $K_{ij}(k_1,k_2,s_1,s_2)$ are known from Sec. 3.4.

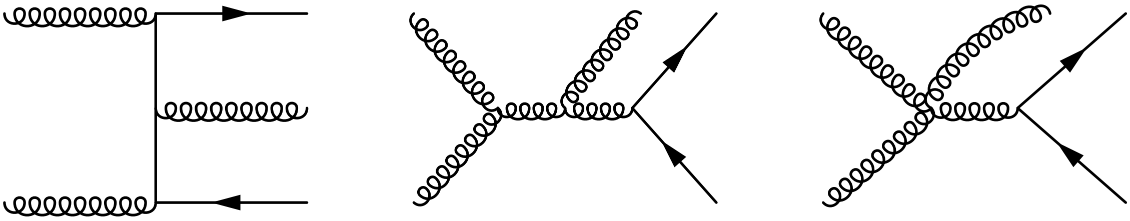

(a) (b) (c)

Figure 3.5. – *Tree-level Feynman graphs for the real radiation process $gg \to t\bar{t} + g$ with gluon radiation from internal lines or vertices. The corresponding amplitudes are IR finite.*

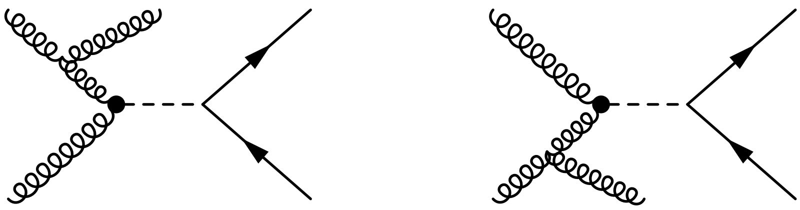

(a) (b)

Figure 3.6. – *Tree-level Feynman graphs for the real radiation process $gg \to \phi_i + g \to t\bar{t} + g$ with gluon radiation from the initial state. The corresponding amplitudes contain soft and collinear divergences.*

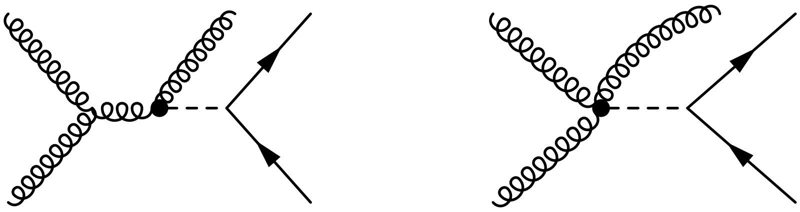

(a) (b)

Figure 3.7. – *Tree-level Feynman graphs for the real radiation process $gg \to \phi_i + g \to t\bar{t} + g$ with gluon radiation from an internal line or a ϕ_i vertex. The corresponding amplitudes are IR finite.*

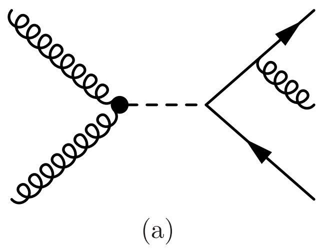

Figure 3.8. – *Tree-level Feynman graphs for the real radiation process $gg \to \phi_i \to t\bar{t} + g$. Gluon radiation from the final state. The corresponding amplitudes give rise to soft divergences.*

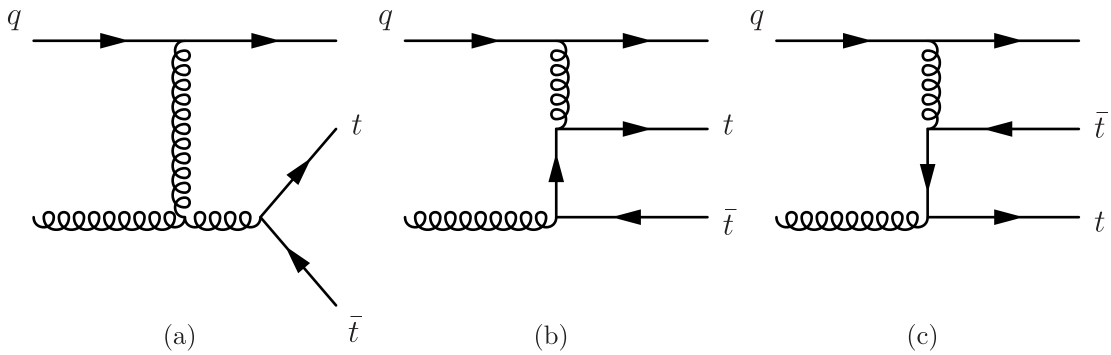

Figure 3.9. – *Tree-level Feynman graphs for the real radiation process $qg \to t\bar{t} + q$. The corresponding amplitudes are divergent in the phase space region where the outgoing light quark is collinear with the initial state quark.*

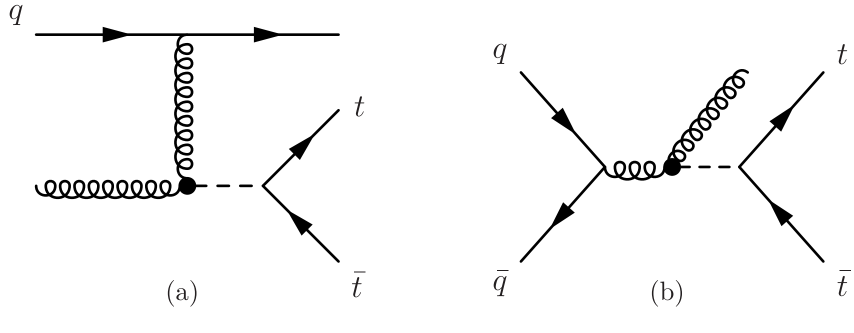

Figure 3.10. – *Tree-level Feynman graphs for the real radiation processs $qg \to \phi_i + q \to t\bar{t} + q$ and $q\bar{q} \to \phi_i + g \to t\bar{t} + g$. The amplitude corresponding to 3.10(a) is divergent in the phase space region where the outgoing light quark is collinear with the initial state quark, whereas the amplitude corresponding to 3.10(b) is IR finite.*

3.5.3. Higgs production in quark-antiquark annihilation

In this category all Feynman graphs with tree-level $q\bar{q}\phi_i$ coupling are neglected. In the case $q = b$ this is only permissible as long as one does not consider an extended Higgs sector with enhanced coupling to the b-quark. As long as $\tan\beta \simeq 1$ within the type-II 2HDM, we need to consider only the resonant diagram 3.10(b) in the interference terms $\sum_{i=1,2} 2\,\mathrm{Re}\left(\mathcal{M}^{q\bar{q}}_{R,QCD}\mathcal{M}^{q\bar{q}\,*}_{R,\phi_i}\right)$. The computation simplifies further since due to the colour structure only the non-resonant diagrams depicted in Figs. 3.12(a) and 3.12(b) contribute.

The squared amplitude corresponding to the processes (3.17) and (3.18) is again split into production, propagation and decay of the Higgs bosons:

$$\sum{}' \left|\mathcal{M}^{q\bar{q}}_{R,\phi_i}\right|^2 \;=\; |\mathcal{M}_{q\bar{q}\to\phi_i g}|^2 |P_j(s_{12})|^2\, K_i(k_1,k_2,s_1,s_2). \tag{3.63}$$

The spin and colour averaging factor for a $q\bar{q}$ initial state is $(4N_c^2)^{-1}$. Only one Feynman graph, depicted in Fig. 3.10(b), contributes to the amplitude. The squared matrix element describing the production process, $q\bar{q} \to \phi_i g$, is given by

$$|\mathcal{M}_{q\bar{q}\to\phi_i g}|^2 \;=\; 16\pi^2 \left(\frac{\alpha_s}{\pi}\right)^3 \frac{C_F}{N_c} \left(\left(f^{(0)}_{H,i}\right)^2 + 4\left(f^{(0)}_{A,i}\right)^2\right) \frac{t^2+u^2}{s},$$

the other parts are known from the previous sections. The Higgs interference terms have the form

$$\begin{aligned}\sum{}' 2\,\mathrm{Re}\left(\mathcal{M}^{q\bar{q}}_{R,\phi_i}\mathcal{M}^{q\bar{q}\,*}_{R,\phi_j}\right) \;&=\; 2\,\mathrm{Re}\left(\mathcal{M}_{q\bar{q}\to\phi_i g}\mathcal{M}^{*}_{q\bar{q}\to\phi_j g}\right) \\ &\quad \times \mathrm{Re}\left[P_{ij}(s_{12})K_{ij}(k_1,k_2,s_1,s_2)\right]\,,\end{aligned}$$

with

$$\mathrm{Re}\left(\mathcal{M}_{q\bar{q}\to\phi_i g}\mathcal{M}^{*}_{q\bar{q}\to\phi_j g}\right) \;=\; 16\pi^2 \left(\frac{\alpha_s}{\pi}\right)^3 \frac{C_F}{N_c} \left(\left(f^{(0)}_{H,i}\right)^2 + 4\left(f^{(0)}_{A,i}\right)^2\right) \frac{t^2+u^2}{s}.$$

The functions $P_{ij}(s_{12})$ and $K_{ij}(k_1,k_2,s_1,s_2)$ are known from Sec. 3.4.

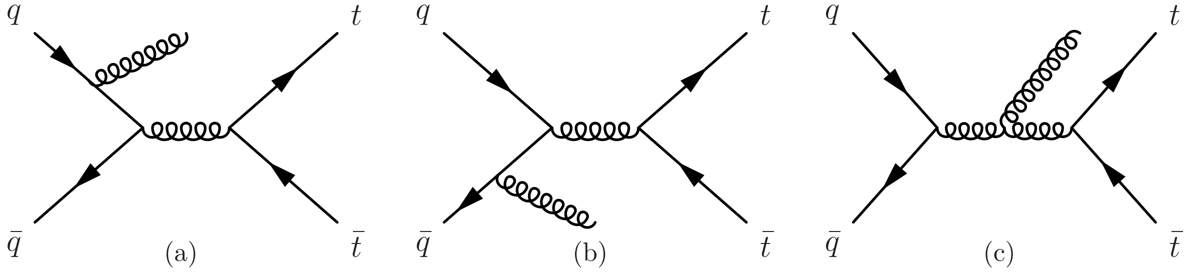

Figure 3.11. – *Tree-level Feynman graphs for the real radiation process $q\bar{q} \to t\bar{t} + g$ with gluon radiation from the light initial state quarks and internal line. The amplitudes corresponding to 3.11(a) and 3.11(b) are IR divergent, whereas 3.11(c) is finite. The divergences of the former do not concern us here since the interference with the Higgs production amplitude 3.10(b) vanishes.*

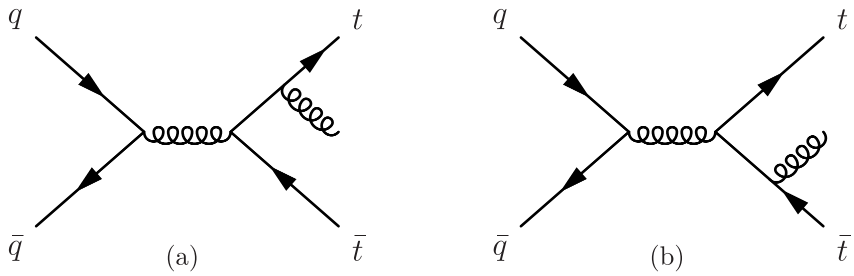

Figure 3.12. – *Tree-level Feynman graphs for the real radiation process $q\bar{q} \to t\bar{t} + g$ with gluon radiation from the final state top-quarks. The corresponding amplitudes contain soft divergences.*

3.5.4. The unintegrated dipole counter terms

As discussed in the last section, the squared matrix elements corresponding to the resonant processes (3.14), (3.15) and (3.16) as well the interference terms with the non-resonant background are IR divergent. The following section gives an overview over the dipole counter terms neccessary to subtract these divergences so that the result can be integrated over the full $2 \to 3$ phase space (3.21).

Counter terms for the reaction $g_1 g_2 \to t\bar{t} + g_3$

The real matrix elements corresponding to this parton process exhibit IR divergencies in the phase space regions where the momentum of final state gluon $g_3 = g(p_3)$ becomes soft or collinear with the momenta of the initial state gluons $g_1 = g(p_1)$ or $g_2 = g(p_2)$. According to the method described in [60, 61] a dipole subtraction term has to be constructed for each possible emitter/spectator assignment to the Born level partons $\{g(p_1), g(p_2); t(k_1), \bar{t}(k_2)\}$. The dipoles are further divided into subgroups depending on whether emitter or spectator are initial (superscript) or final state (subscript) partons. In the first category, initial state emitter and initial state spectator we have to construct two dipole terms:

$$\text{initial} - \text{initial}: \qquad \mathcal{D}^{g_1 \to g_1' g_3,\, g_2}\,, \mathcal{D}^{g_2 \to g_2' g_3,\, g_1}. \tag{3.64}$$

Further there are 4 dipoles each in the categories initial state emitter, final state spectator and vice versa,

$$\begin{aligned} \text{initial} - \text{final}: &\quad \mathcal{D}_t^{g_1 \to g_1' g_3}\,, \mathcal{D}_{\bar{t}}^{g_1 \to g_1' g_3}\,, \mathcal{D}_t^{g_2 \to g_2' g_3}\,, \mathcal{D}_{\bar{t}}^{g_2 \to g_2' g_3}, && (3.65)\\ \text{final} - \text{initial}: &\quad \mathcal{D}_{t' \to t g_3}^{g_1}\,, \mathcal{D}_{\bar{t}' \to \bar{t} g_3}^{g_1}\,, \mathcal{D}_{t' \to t g_3}^{g_2}\,, \mathcal{D}_{\bar{t}' \to \bar{t} g_3}^{g_2}. && (3.66) \end{aligned}$$

Finally, there are two final state emitter, final state spectator dipoles to be constructed,

$$\text{final} - \text{final}: \qquad \mathcal{D}_{t' \to t g_3,\, \bar{t}}\,, \mathcal{D}_{\bar{t}' \to \bar{t} g_3, t}. \tag{3.67}$$

For their construction we need the universal splitting kernels $V^{g_i \to g_i' g_3}$ and $V_{Q' \to Q\, g_3}$ with $Q \in \{t, \bar{t}\}$ for the initial state splitting $g_i' \to g_i\, g_3$, Eq. (5.148) in [60], and the final state splitting $t' \to t\, g_3$, $\bar{t}' \to \bar{t}\, g_3$, Eq. (5.7) in [61]. The respective splitting kernel and a pair of colour charge operators, depending on the emitter and spectator parton, are inserted instead of the respective sums over polarization/color states into the Born matrix elements to obtain the dipoles. To describe the procedure it is useful to emphasize the colour indices of the initial gluons $g_1(a_1)$, $g_2(a_2)$ and the final state top $t(m_1)$ and anti-top $\bar{t}(m_2)$ by introducing the notation

$$\begin{aligned}
\mathcal{M}^{gg}_{B,QCD} &= |a_1, a_2;\, m_1, m_2\rangle_{QCD}, \\
\mathcal{M}^{gg}_{B,\phi_i} &= |a_1, a_2;\, m_1, m_2\rangle_{\phi_i}, \\
\mathcal{M}^{gg}_{B,QCD} + \mathcal{M}^{gg}_{B,\phi_i} &= |a_1, a_2;\, m_1, m_2\rangle.
\end{aligned}$$

Labelling the emitter parton with a prime and the spectator parton as $S \in \{t, \bar{t}, g_1, g_2\}$, the initial state emitter dipoles are constructed as follows:

$$\mathcal{D}^{g_i \to g_i' g_3}_{S}, \mathcal{D}^{g_i \to g_i' g_3, S} \propto \langle a_1, a_2;\, m_1, m_2|\left(T_{g_i'} \cdot T_S\right) V^{g_i \to g_i' g_3}\, |a_1', a_2';\, m_1', m_2'\rangle, \tag{3.68}$$

and similarly the dipoles with final state emitter:

$$\mathcal{D}_{Q' \to Q g_3, S}, \mathcal{D}^{S}_{Q' \to Q g_3} \propto \langle a_1, a_2;\, m_1, m_2|\, (T_{Q'} \cdot T_S)\, V_{Q' \to Q g_3}\, |a_1', a_2';\, m_1', m_2'\rangle. \tag{3.69}$$

The colour charge operators associated with the emission of a gluon from the emitter or spectator parton are

$$\begin{aligned}
T_{t'} &= +t^b_{m_1, m_1'}, \\
T_{\bar{t}'} &= -t^b_{m_2, m_2'}, \\
T_{g_i'} &= i f^{a_i b a_i'}.
\end{aligned}$$

In case of the initial–initial dipoles (3.64) both emitter and spectator are gluons and we get the following colour correlations

$$\begin{aligned}
&\langle a_1, a_2;\, m_1, m_2|\left(i f_{a_1 b a_1'}\, i f_{a_2 b a_2'}\right) V^{g_1 \to g_1' g_3}\, |a_1', a_2';\, m_1, m_2\rangle \\
= \quad & -C_A \langle a_1, a_2;\, m_1, m_2|\, V^{g_1 \to g_1' g_3}\, |a_1, a_2;\, m_1, m_2\rangle,
\end{aligned}$$

and the same for $g_1 \leftrightarrow g_2$. In case of the initial–final dipoles (3.71) we get

$$\begin{aligned}
&\langle a_1, a_2;\, m_1, m_2|\left(i f_{a_1 b a_1'}\, t^b_{m_1 m_1'}\right) V^{g_1 \to g_1' g_3}\, |a_1', a_2;\, m_1', m_2\rangle \\
= \quad & -C_A \tfrac{\beta y}{2} \left[\, {}_{\phi_i}\langle a_1, a_2;\, m_1, m_2|\, V^{g_1 \to g_1' g_3}\, |a_1, a_2;\, m_1, m_2\rangle_{QCD} + \text{c.c.}\right] \quad .
\end{aligned}$$

The final–initial dipoles, where the splitting kernel $V_{Q \to Qg}$ has to be inserted, involve the same color correlations. Note that the squared resonant Higgs contribution for the final-initial and initial-final correlations vanishes and that we do not consider here the squared non-resonant QCD contribution. Looking at the Feynman diagram in Fig. 3.2 it becomes clear that an insertion of a single colour operator in the initial gluon lines or the final top or antitop lines yields zero in the squared amplitude. In case of the final–final dipoles (3.67) we find

$$\begin{aligned} & \langle a_1, a_2;\, m_1, m_2|\left(-t^b_{m_1,m_1'}t^b_{m_2,m_2'}\right) V_{t'\to tg_3}\, |a_1, a_2;\, m_1', m_2'\rangle \\ = \quad & -C_F\, \langle a_1, a_2;\, m_1, m_2|\, V_{t'\to tg_3}\, |a_1, a_2;\, m_1, m_2\rangle \qquad . \end{aligned}$$

Counter terms for the reaction $q_1\, g_2 \to t\bar{t} + q_3$

In this case, the emission of a light quark $q_3 = q(p_3)$ from the light initial state quark $q_1 = q(p_1)$ causes the collinear divergence in the real matrix element. Thus one dipole with initial state emitter, initial state spectator configuration has to be constructed:

$$\text{initial} - \text{initial} : \qquad \mathcal{D}^{q_1\to g_1' q_3,\, g_2}. \tag{3.70}$$

The splitting kernel $V^{q_1\to g_i' q_3}$, describing the initial state splitting $q_1 \to g_i'\, q_3$, can be found in Eq. (5.147) in [60]. Further, there are two dipoles in the category initial state emitter and final state spectator:

$$\text{initial} - \text{final} : \qquad \mathcal{D}_t^{q_1\to g_1' q_3}\,,\, \mathcal{D}_{\bar{t}}^{q_1\to g_1' q_3}. \tag{3.71}$$

In the formalism described in [60, 61], the colour charge operators applied to the Born matrix element refer to the emitter and spectator partons which are also identified on Born level (g_1' and g_2 in this case). Thus we have to insert the color operator $\left(if^{a_1 b a_1'}\right)\left(if^{a_2 b a_2'}\right)$, which is somewhat unintuitive. This is compensated in the end by applying the colour/spin sum and average of the Born level initial state (gg in this case).

The collinear limit for the momenta $p_3 \to p_1$

For later considerations it is useful to investigate in more detail the pattern of how the different dipole terms cancel the IR divergences in the squared real emission amplitudes. We will do this here for the squared amplitudes corresponding to the process $gg \to t\bar{t}+g$. The divergent part is found by applying the parametrization

$$p_3^\mu \;=\; (1-x)p_1^\mu + k_T^\mu - \frac{k_T^2\, n^\mu}{2(1-x)\, p_1\cdot n} \tag{3.72}$$

and expanding in k_T, the momentum component orthogonal to p_1. The vector n is an auxiliary light like vector, i.e. $n^2 = -1$. They obey $p_1 \cdot k_T = n \cdot k_T = 0$, c.f. (4.2) in [61]. Doing this one finds the following asymptotic behaviour:

$$
\begin{aligned}
2\mathrm{Re}\left[\mathcal{M}^{gg}_{R,QCD,ISR}\mathcal{M}^{gg\,*}_{R,\phi_i,ISR}\right] &\rightarrow \mathcal{O}\left(k_T^{-2}\right), &(3.73)\\
2\mathrm{Re}\left[\mathcal{M}^{gg}_{R,QCD,ISR}\mathcal{M}^{gg\,*}_{R,\phi_i,FSR}\right] &\rightarrow \mathcal{O}\left(k_T^{0}\right), &(3.74)\\
2\mathrm{Re}\left[\mathcal{M}^{gg}_{R,QCD,FSR}\mathcal{M}^{gg\,*}_{R,\phi_i,ISR}\right] &\rightarrow \mathcal{O}\left(k_T^{0}\right), &(3.75)\\
2\mathrm{Re}\left[\mathcal{M}^{gg}_{R,QCD,FSR}\mathcal{M}^{gg\,*}_{R,\phi_i,FSR}\right] &\rightarrow \mathcal{O}\left(k_T^{0}\right). &(3.76)
\end{aligned}
$$

Similar patterns arise in the squared Higgs amplitudes

$$
\begin{aligned}
\left|\sum_{i=1,2}\mathcal{M}^{gg}_{R,\phi_i,ISR}\right|^2 &\rightarrow \mathcal{O}\left(k_T^{-2}\right), &(3.77)\\
\left|\sum_{i=1,2}\mathcal{M}^{gg}_{R,\phi_i,FSR}\right|^2 &\rightarrow \mathcal{O}\left(k_T^{0}\right), &(3.78)
\end{aligned}
$$

i.e. only the initial state radiation contribution is divergent in the collinear limit. The unintegrated dipoles (3.64) – (3.67) reproduce this behaviour,

$$
\begin{aligned}
\mathcal{D}^{g_1\rightarrow g_1' g_3,\, g_2} &\rightarrow \mathcal{O}\left(k_T^{-2}\right),\\
\mathcal{D}^{g_2\rightarrow g_2' g_3,\, g_1} &\rightarrow \mathcal{O}\left(k_T^{0}\right),\\
\mathcal{D}_t^{g_1\rightarrow g_1' g_3} + \mathcal{D}_{\bar t}^{g_1\rightarrow g_1' g_3} &\rightarrow \mathcal{O}\left(k_T^{0}\right),\\
\mathcal{D}_t^{g_1\rightarrow g_1' g_3}, \mathcal{D}_t^{g_2\rightarrow g_2' g_3} &\rightarrow \mathcal{O}\left(k_T^{0}\right),\\
\mathcal{D}^{g_i}_{t'\rightarrow t g_3}, \mathcal{D}^{g_i}_{\bar t'\rightarrow \bar t g_3} &\rightarrow \mathcal{O}\left(k_T^{0}\right),\\
\mathcal{D}_{t'\rightarrow t g_3,\,\bar t}, \mathcal{D}_{\bar t'\rightarrow \bar t g_3,t} &\rightarrow \mathcal{O}\left(k_T^{0}\right),
\end{aligned}
$$

so that the initial–initial dipoles cancel the most divergent part in the the squared matrix elements:

$$
\left|\sum_{i=1,2}\mathcal{M}^{gg}_{R,\phi_i}\right|^2 + \sum_{i=1,2} 2\mathrm{Re}\left[\mathcal{M}^{gg}_{R,QCD}\mathcal{M}^{gg\,*}_{R,\phi_i}\right] - \sum_{i\neq j\in\{1,2\}} \mathcal{D}^{g_i\rightarrow g_i' g_3,\, g_j} \rightarrow \mathcal{O}\left(k_T^{-1}\right).
$$

This is integrable over the $2\rightarrow 3$ phase space (3.21) since the phase space density yields another factor k_T. Similar results are obtained in the limit where p_3 becomes collinear with p_2. To obtain the parametrization one has to substitute $p_1 \leftrightarrow p_2$ in (3.72).

The soft limit $p_3 \rightarrow 0$

To extract the soft divergences in the real corrections and unintegrated dipoles it is most convenient to apply the parametrization

$$p_3^\mu = x \cdot p^\mu, \tag{3.79}$$

and expand in x. The following contributions to the squared real matrix element are divergent in this limit,

$$2\mathrm{Re}\left[\mathcal{M}^{gg}_{R,QCD,ISR}\mathcal{M}^{gg\,*}_{R,\phi_i,ISR}\right] \;\to\; \mathcal{O}\left(x^{-2}\right), \tag{3.80}$$
$$2\mathrm{Re}\left[\mathcal{M}^{gg}_{R,QCD,ISR}\mathcal{M}^{gg\,*}_{R,\phi_i,FSR}\right] \;\to\; \mathcal{O}\left(x^{-2}\right), \tag{3.81}$$
$$2\mathrm{Re}\left[\mathcal{M}^{gg}_{R,QCD,FSR}\mathcal{M}^{gg\,*}_{R,\phi_i,ISR}\right] \;\to\; \mathcal{O}\left(x^{-2}\right), \tag{3.82}$$
$$2\mathrm{Re}\left[\mathcal{M}^{gg}_{R,QCD,FSR}\mathcal{M}^{gg\,*}_{R,\phi_i,FSR}\right] \;\to\; \mathcal{O}\left(x^{-2}\right), \tag{3.83}$$

and similarly for the squared Higgs amplitudes,

$$\left|\sum_{i=1,2}\mathcal{M}^{gg}_{R,\phi_i,ISR}\right|^2 \;\to\; \mathcal{O}\left(x^{-2}\right), \tag{3.84}$$
$$\left|\sum_{i=1,2}\mathcal{M}^{gg}_{R,\phi_i,FSR}\right|^2 \;\to\; \mathcal{O}\left(x^{-2}\right). \tag{3.85}$$

The unintegrated dipoles (3.64) – (3.67) show the same limiting behaviour, so that the differences

$$\left|\sum_{i=1,2}\mathcal{M}^{gg}_{R,\phi_i,ISR}\right|^2 + \sum_{i=1,2} 2\mathrm{Re}\left[\mathcal{M}^{gg}_{R,QCD,ISR}\mathcal{M}^{gg\,*}_{R,\phi_i,ISR}\right] - \sum_{i\neq j\in\{1,2\}} \mathcal{D}^{g_i\to g_i' g_3,\, g_j} \;\to\; \mathcal{O}\left(x^0\right),$$

$$\left|\sum_{i=1,2}\mathcal{M}^{gg}_{R,\phi_i,FSR}\right|^2 + \sum_{i=1,2} 2\mathrm{Re}\left[\mathcal{M}^{gg}_{R,QCD,FSR}\mathcal{M}^{gg\,*}_{R,\phi_i,FSR}\right] - \sum_{Q=t,\bar{t}} \mathcal{D}_{Q'\to t g_3,\, \overline{Q}} \;\to\; \mathcal{O}\left(x^0\right),$$

$$\begin{aligned}&\sum_{i=1,2} 2\mathrm{Re}\left[\mathcal{M}^{gg}_{R,QCD,ISR}\mathcal{M}^{gg\,*}_{R,\phi_i,FSR}\right]\\ &-\frac{1}{2}\left[\sum_{i=1,2}\sum_{Q=t,\bar{t}} \mathcal{D}^{g_i\to g_i' g_3}_{Q} + \sum_{i=1,2}\sum_{Q=t,\bar{t}} \mathcal{D}^{g_i}_{Q'\to Q g_3}\right] \;\to\; \mathcal{O}\left(x^0\right),\end{aligned} \tag{3.86}$$

and

$$\sum_{i=1,2} 2\mathrm{Re}\left[\mathcal{M}^{gg}_{QCD,FSR}\mathcal{M}^{gg\,*}_{\phi_i,ISR}\right]$$
$$-\frac{1}{2}\left[\sum_{i=1,2\;Q=t,\bar{t}} \mathcal{D}_Q^{g_i\to g_i' g_3} + \sum_{i=1,2\;Q=t,\bar{t}} \mathcal{D}^{g_i}_{Q'\to Q g_3}\right] \;\to\; \mathcal{O}\left(x^0\right), \tag{3.87}$$

are seperately finite.

Thus, the integral over the $2 \to 3$ phase space (3.21) can be conducted and one obtains finite results in 4 space time dimensions:

$$\begin{aligned}\tilde{\sigma}^{gg}_R \;=\;& \frac{1}{2s}\int d\Phi_{2\to 3} \sum_{gg}{}' \Bigg[\sum_{i=1,2} 2\,\mathrm{Re}\left(\mathcal{M}^{gg}_{R,QCD}\mathcal{M}^{gg\,*}_{R,\phi_i}\right) + \Bigg|\sum_{i=1,2}\mathcal{M}^{gg}_{R,\phi_i}\Bigg|^2 \\ & - \sum_{i\neq j\in\{1,2\}} \mathcal{D}^{g_i\to g_i' g_3,\, g_j} - \sum_{Q=t,\bar{t}} \mathcal{D}_{Q'\to Q g_3,\,\overline{Q}} - \sum_{i=1,2\;Q=t,\bar{t}} \left[\mathcal{D}_Q^{g_i\to g_i' g_3} + \mathcal{D}^{g_i}_{Q'\to Q g_3}\right]\Bigg] \\ & < \infty, \end{aligned} \tag{3.88}$$

and

$$\begin{aligned}\tilde{\sigma}^{qg}_R = \tilde{\sigma}^{\bar{q}g}_R \;=\;& \frac{1}{2s}\int d\Phi_{2\to 3} \left[\sum_{qg}{}' \left(\sum_{i=1,2} 2\,\mathrm{Re}\left(\mathcal{M}^{qg}_{R,QCD}\mathcal{M}^{qg\,*}_{R,\phi_i}\right) + \Bigg|\sum_{i=1,2}\mathcal{M}^{qg}_{R,\phi_i}\Bigg|^2\right)\right. \\ & \left. -\sum_{qg}{}' \left(\mathcal{D}^{q_1\to q_3 g_1',\, g_2} + \sum_{Q=t,\bar{t}} \mathcal{D}_Q^{q_1\to q_3 g_1'}\right)\right] < \infty. \end{aligned} \tag{3.89}$$

Note the different spin/colour sums and averages, $\sum'_{gg}$ for the gg initial state and $\sum'_{qg}$ for the qg initial state in the last equation. The contributions $\tilde{\sigma}^{gq}_R$ and $\tilde{\sigma}^{g\bar{q}}_R$ to the partonic cross sections are obtained by the exchange $p_1 \leftrightarrow p_2$ in the respective matrix elements and dipoles.

3.6. Virtual corrections

In this section we will discuss the virtual corrections to the reaction (3.3) at next-to-leading order in the strong coupling α_s. Since we neglect all contributions of $\mathcal{O}\left(\frac{m_q}{v}\right)$ for $q \in \{u, d, s, c, b\}$, only the one-loop Feynman diagrams for the gluon fusion processes

$$\begin{aligned} g(p_1)\, g(p_2) &\quad\rightarrow\quad t(k_1)\, \bar{t}(k_2), & (3.90)\\ g(p_1)\, g(p_2) &\;\rightarrow \phi_i \rightarrow\; t(k_1)\, \bar{t}(k_2), & (3.91)\end{aligned}$$

have to be taken into account. This is not directly obvious but a closer inspection of the remaining next-to-leading order contributions to the squared amplitudes corresponding to the parton reactions $qg \to t\bar{t}$ and $q\bar{q} \to t\bar{t}$ shows that they all vanish due to colour algebra.

The one-loop amplitudes are generally divergent in $d = 4$ space-time dimensions and can be regularized by assuming $d = 4 - 2\varepsilon$ and $\varepsilon \neq 0$. The divergences originating from UV and IR regions then appear as poles in the parameter ε. Continuing the expansion of the squared matrix element corresponding to (3.90) and (3.91) one finds the next-to-leading order contributions

$$\begin{aligned} |\mathcal{M}^{gg}|^2 \;=\; & |\mathcal{M}_B^{gg}|^2 \\ & + \sum_{i=1,2} 2\,\mathrm{Re}\left(\mathcal{M}^{gg}_{B,QCD}\mathcal{M}^{gg\,*}_{V,\phi_i}\right) & (3.92)\\ & + \sum_{i=1,2} 2\,\mathrm{Re}\left(\mathcal{M}^{gg}_{V,QCD}\mathcal{M}^{gg\,*}_{B_{\mathrm{eff},0},\phi_i}\right) & (3.93)\\ & + \sum_{i,j=1,2} 2\,\mathrm{Re}\left(\mathcal{M}^{gg}_{B_{\mathrm{eff},0},\phi_i}\mathcal{M}^{gg\,*}_{V,\phi_j}\right). & (3.94)\\ & +\mathcal{O}(\alpha_s^3), \end{aligned}$$

with $|\mathcal{M}_B^{gg}|^2$ given in Eqns. (3.36)-(3.38). The various one-loop amplitudes (subscript V) appearing in (3.92)-(3.94) are given by the following Feynman graphs:

$$\begin{aligned} \mathcal{M}^{gg}_{V,QCD} &= \mathcal{M}^{0\,gg}_{V,QCD}\,[\text{Fig. } 3.15] + \mathcal{M}^{gg}_{CT,QCD}\,[\text{Figs. } 3.13(a) - 3.13(c)]\,, & (3.95)\\ \mathcal{M}^{gg}_{V,\phi_i} &= \mathcal{M}^{gg}_{V_1,\phi_i}\,[\text{Figs. } 3.14(a) - 3.14(c)] + \mathcal{M}^{gg}_{V_2,\phi_i}\,[\text{Fig. } 3.14(d)] \\ &\quad +\mathcal{M}^{gg}_{B_{\mathrm{eff},1},\phi_i}\,[\text{Fig. } 3.13(d)]\,. & (3.96)\end{aligned}$$

Note that the renormalization counter terms are already included in the definition of the one-loop amplitudes $\mathcal{M}^{gg}_{V,QCD}$ and $\mathcal{M}^{gg}_{V,\phi_i}$. Thus, these amplitudes are UV finite and the remaining divergences originate from a soft and collinear gluon in the loop. These IR divergences are cancelled by the integrated counter parts of the dipole subtraction terms discussed in Sec. 3.5.4. Then the limit $d \to 4$ can be taken to integrate over the $2 \to 2$ phase space (3.20) as indicated in (3.19).

3.6.1. Regularization scheme

For the computation we will take the Lorentz indices of the external gluons in $d = 4$ dimension and all internal Lorentz indices in $d = 4 - 2\varepsilon$. Here we will substitute for the sum over physical gluon polarization states

$$\sum_{\text{phys.}} \epsilon(p_i)^\mu \epsilon(p_i)^\nu = -g^{(4)\,\mu\nu} + \frac{p_i^\mu \bar{p}_i^\nu + p_i^\mu \bar{p}_i^\nu}{p_i \cdot \bar{p}_i},\ i \in \{1,2\}, \tag{3.97}$$

with $g^{(4)\,\mu}_{\ \ \ \ \mu} = 4$ and $\bar{p} = (p_0, -\vec{p})^T$. Further, one needs a prescription for the treatment of γ_5 in traces with d-dimensional Lorentz indices. Will will use an anticommuting γ_5,

$$\{\gamma_5, \gamma^\mu\} \;=\; 0,$$

with $\gamma_5^2 = \mathbb{1}$ and substitute

$$\gamma_5 \;=\; \frac{-i}{4!}\epsilon_{\rho_1,\rho_2,\rho_3,\rho_4}\gamma^{\rho_1}\gamma^{\rho_2}\gamma^{\rho_3}\gamma^{\rho_4},$$

if necessary. This subsitution is sufficient since no ambiguities due to axial vector anomalies arise in this computation [69]. As already mentioned, the convention for the Levi-Civita symbol is $\epsilon^{0123} = +1$. Also the contraction of multiple occurences of ϵ-tensors is done in $d = 4$.

3.6.2. Renormalization

The one-loop amplitudes will be computed in renormalized perturbation theory where the renormalized strong coupling $\alpha_s = \frac{g_s}{4\pi}$ serves as expansion parameter. The renormalization constants which relate bare and renormalized quantities,

$$\begin{aligned}
\psi_{j,0} &= Z_{2j,R}^{1/2}\psi_j, \\
m_{t,0} &= Z_{m_t,R}m_t, \\
A_0^\mu &= Z_{3,R}^{1/2}A^\mu, \\
g_{s,0} &= Z_{g,R}\, g_s,
\end{aligned} \tag{3.98}$$

are defined through the following renormalization scheme:

- quark mass and wavefunction renormalized in the on-shell scheme and
- the strong coupling g_s in the $\overline{MS}$ scheme.

In (3.98), $\psi_{j,0}$, $m_{t,0}$ denote the bare quark field and mass for a quark of flavour j, and A_0^μ, $g_{s,0}$ the bare gluon field and the strong coupling, respectively. The renormalized quantities are labelled without the subscript 0. The one-loop renormalization constant for the strong coupling in the $\overline{MS}$ scheme is

$$\delta Z_{g,\overline{MS}} \;=\; -\frac{\alpha_s}{4\pi}\frac{C(\epsilon)}{2\epsilon}\left(\frac{11}{3}C_A - \frac{4}{3}T_F(N_f+1)\right) + \mathcal{O}(\alpha_s^2).$$

where the abbreviation $\delta Z = Z - 1$ was used. Further, we have used $C(\epsilon) = \frac{(4\pi)^\epsilon}{\Gamma(1-\epsilon)} = (4\pi)^\epsilon\,\Gamma(1+\epsilon) + \mathcal{O}(\epsilon^2)$, $C_F = \frac{N_c^2-1}{2N_c}$, $C_A = N_c$ and $T_F = \frac{1}{2}$. The number of massless flavours is $N_f = 5$. The wavefunction and mass renormalization constants for the massive top quark in the on-shell scheme are equal at one-loop order:

$$\delta Z_{2t,os} = \delta Z_{m_t,os} \;=\; \frac{\alpha_s}{4\pi}C_F\frac{C(\epsilon)}{\epsilon}\frac{2\epsilon-3}{1-2\epsilon}\left(\frac{\mu_R^2}{m_t^2}\right)^\epsilon + \mathcal{O}(\alpha_s^2).$$

For massless quarks we have $\delta Z_{m_j,os} = 0$ and also $\delta Z_{2j,os} = 0$ at one-loop order. The symbol μ_R denotes the renormalization scale. The on-shell wavefunction renormalization constant for the gluon is

$$\delta Z_{3,os} \;=\; -\frac{\alpha_s}{4\pi}T_F\frac{C(\epsilon)}{\epsilon}\frac{4}{3} + \mathcal{O}(\alpha_s^2),$$

assuming 5 active light quark flavours. The renormalization constant for the quark-gluon vertex is given in terms of $Z_{g,\overline{MS}}$, $Z_{2,os}$ and $Z_{3,os}$ as

$$\begin{aligned}
Z_1 &= Z_{g,\overline{MS}} Z_{2,os} Z_{3,os}^{1/2} \\
&= 1 + \left(\delta Z_{g,\overline{MS}} + \delta Z_{2,os} + \frac{\delta Z_{3,os}}{2}\right) + \mathcal{O}(\alpha_s^2) \\
&= 1 - \frac{\alpha_s}{4\pi}\frac{C(\epsilon)}{2\epsilon}\left(\frac{11}{3}C_A - \frac{4}{3}T_F N_f - \frac{4\epsilon-6}{1-2\epsilon}\left(\frac{\mu_R^2}{m_t^2}\right)^\epsilon\right).
\end{aligned}$$

Besides the non-resonant counter term diagrams in Fig. 3.13(a)-3.13(c) one also has to take the resonant Higgs production diagram with second order effective $gg\phi$ couplings in Fig. 3.13(d) into account to cancel the UV divergences arising from the one-loop contributions.

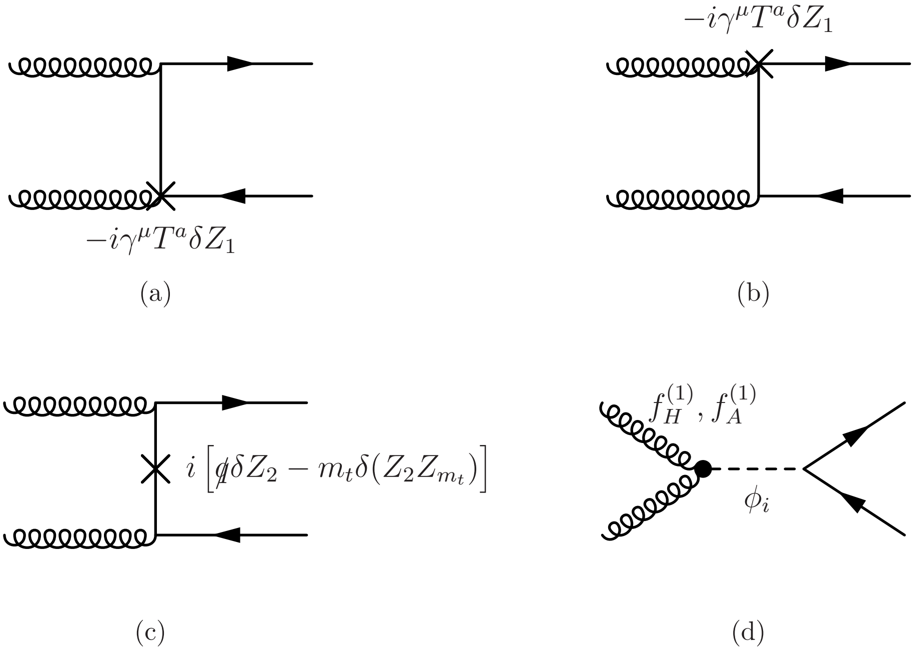

Figure 3.13. – *Figs. 3.13(a)-3.13(c): One-loop renormalization counter terms for the QCD amplitudes $gg \to t\bar{t}$. Fig. 3.13(d): Born level ϕ_i exchange diagram with next-to-leading order effective $gg\phi_i$ coupling (2.12).*

3.6.3. Non-factorizable and non-resonant one-loop Higgs exchange amplitudes

So far only the factorizable, resonant one-loop amplitudes depicted in Fig. 3.14 have been discussed. These have the structure

$$\mathcal{M}^{gg}_{V,\phi_i} \quad = \quad \mathcal{M}_{gg\to\phi_i}\, iP_i(q^2)\, \mathcal{M}_{\phi_i\to t\bar{t}}, \tag{3.99}$$

i.e. the Higgs boson propagator $P_i(q^2)$ defined in Eq. (3.40) is not included in the production or decay loop. In addition one encounters the non-factorizable diagrams depicted in Fig. 3.16 as well as non-resonant Higgs exchange diagrams which do not obey the decomposition (3.99). It was shown in [32] that the latter are negligible compared to the resonant contribution. The non-factorizable diagrams on the other hand can not be neglected because they contribute to the resonant part if the loop momentum is soft. Thus, applying the soft gluon approximation (SGA) to the loop integrand to extract the resonant part in the virtual corrections of the form $2\,\mathrm{Re}\left(\mathcal{M}_{V,\phi_i,\mathrm{NF}}\mathcal{M}^*_{B,\phi_j}\right)$ will give a reasonable approximation for observables in the vicinity if the Higgs resonances. We further assume that away from the resonances the next-to-leading order corrections are small so that the errors introduces by this procedure can be neglected.

The SGA is obtained by taking the limit $l \to 0$ in the loop integrand. As an example,

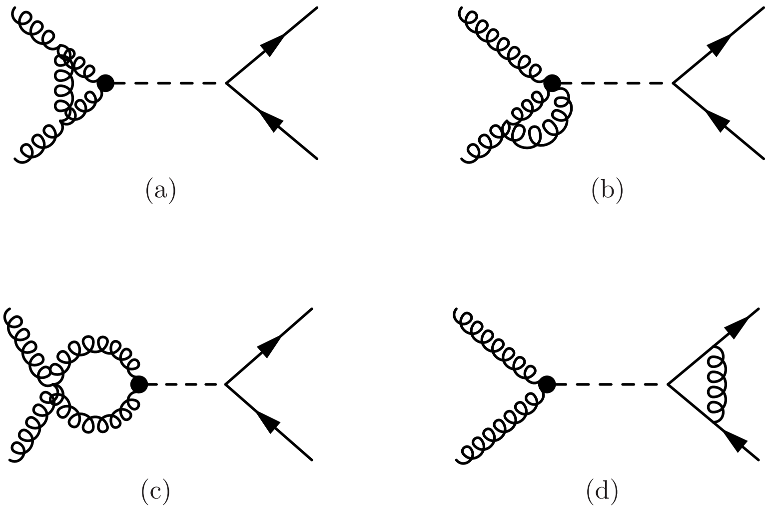

Figure 3.14. – *Feynman graphs corresponding to the factorizable, resonant one-loop amplitudes for the process $gg \to \phi + g \to t\bar{t}$.*

the amplitude corresponding to the diagram in Fig. 3.16(a) plus the crossed diagram has the following structure:

$$\begin{aligned}\mathcal{M}^{gg}_{V,\phi_i,\mathrm{NF}(a)} \propto & \int_{-\infty}^{\infty} \frac{d^d l}{(2\pi)^d} \frac{1}{(l^2+i\eta)\left[(k_1+k_2+l)^2 - m_i^2 + i\Gamma_i m_i\right]} \\ & \times \left[\frac{\not{k}_1 + \not{l} + m_t}{(k_1+l)^2 - m_t^2 + i\eta} - \frac{\not{k}_2 + \not{l} - m_t}{(k_2+l)^2 - m_t^2 + i\eta}\right].\end{aligned}$$

The amplitude is IR divergent and is regularized by assuming $d = 4 - 2\varepsilon$ space time dimensions. In the SGA the amplitude factorizes according to (3.99):

$$\begin{aligned}\mathcal{M}^{gg}_{V,\phi_i,\mathrm{NF}(a)} \xrightarrow{\mathrm{SGA}} & \frac{1}{(k_1+k_2)^2 - m_i^2 + i\Gamma_i m_i} \int_{-\infty}^{\infty} \frac{d^4 l}{(2\pi)^4} \frac{1}{l^2} \left[\frac{\not{k}_1 + m_t}{2k_1 \cdot l} - \frac{\not{k}_2 - m_t}{2k_2 \cdot l}\right] \\ = & \frac{-i}{(k_1+k_2)^2 - m_i^2 + i\Gamma_i m_i} \int_{-\infty}^{\infty} \frac{d^3 \vec{l}}{(2\pi)^3 2l_0} \left.\left[\frac{\not{k}_1 + m_t}{2k_1 \cdot l} - \frac{\not{k}_2 - m_t}{2k_2 \cdot l}\right]\right|_{l_0 = |\vec{l}|}.\end{aligned} \tag{3.100}$$

The other parts of the amplitude are suppressed by factors of $\frac{\Gamma_i}{m_i}$ [70]. Note that the integration range of l is unchanged. In the second equation in (3.100) the residue theorem was used to eliminate the l_0 integration. This procedure essentially cuts the loop at the gluon line and sets it on its mass shell, converting the loop integration into a phase space integral. In this way we obtain a diagram with gluon radiation from the initial state. Similarly, the SGA can be computed for the diagrams 3.16(b) and 3.16(c).

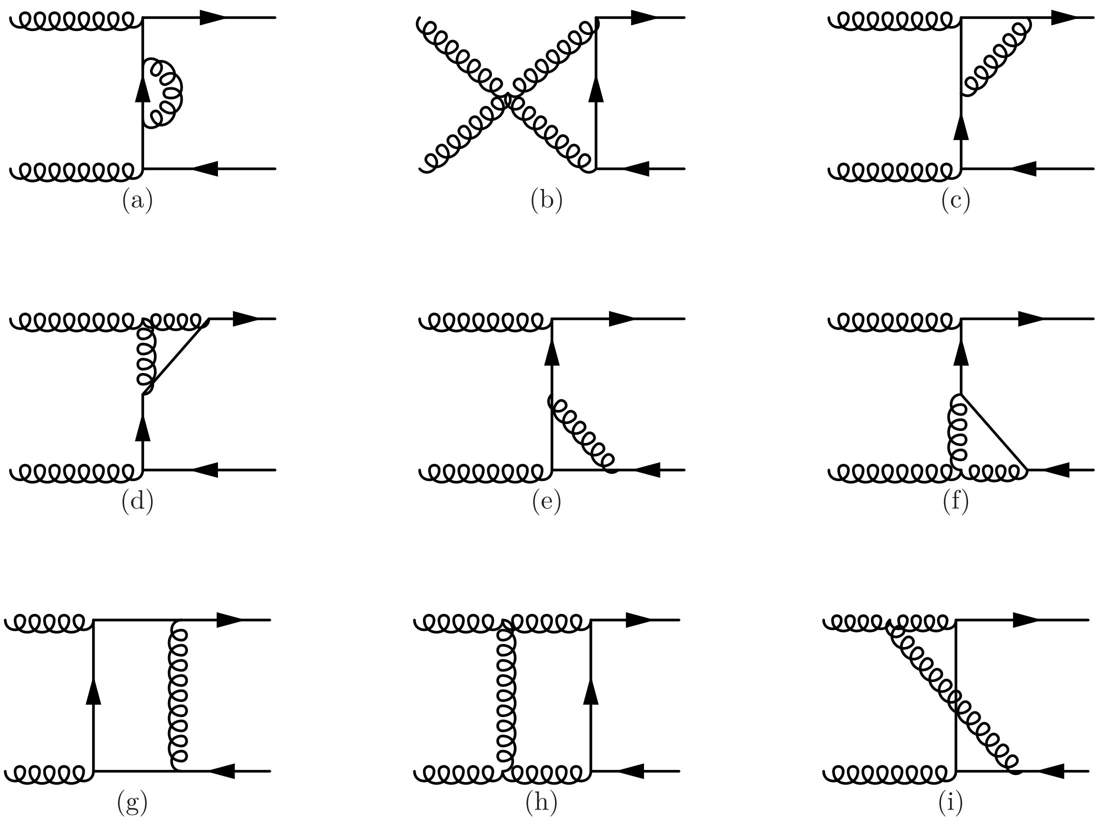

Figure 3.15. – *Set of one-loop Feynman graphs for the process $gg \to t\bar{t}$ involving only QCD partons. Crossed diagrams are implicitly included in the computation.*

Applying the same procedure to the final–initial type real corrections given by the interference of the diagrams in Figs. 3.6, 3.7 and 3.4 one can split off the phase space integration of the gluon

$$
\begin{aligned}
& \int d\Phi_{2\to 3} \,\mathrm{Re}\left(\mathcal{M}^{gg}_{\phi_i,ISR+INT}\mathcal{M}^{gg\,*}_{QCD,FSR}\right) \\
= \quad & \int \frac{d^3\vec{k}_1}{(2\pi)^3 2E_1}\frac{d^3\vec{k}_2}{(2\pi)^3 2E_2}\int_{-\infty}^{\infty}\frac{d^3\vec{p}_3}{(2\pi)^3 2p_{3,0}}\,\delta^{(4)}\left(p_1+p_2-k_1-k_2-p_3\right) \\
& \mathrm{Re}\left(\mathcal{M}^{gg}_{\phi_i,ISR+INT}\mathcal{M}^{gg\,*}_{QCD,FSR}\right) \\
\xrightarrow{\mathrm{SGA}} \quad & \int d\Phi_{2\to 2}\,\frac{d^3\vec{p}_3}{(2\pi)^3 2p_{3,0}} \;\; \mathrm{Re}\left(\mathcal{M}^{gg}_{\phi_i,ISR+INT}\mathcal{M}^{gg}_{QCD,FSR}\right)\Big|_{\mathrm{SGA}}.
\end{aligned}
$$

In this way it can be shown that in the SGA of the real corrections of the initial-final type and the non-factorizable virtual corrections cancel each other, i.e.

$$\int d\Phi_{2\to 3}\,\mathrm{Re}\left(\mathcal{M}^{gg}_{\phi_i,ISR+INT}\mathcal{M}^{gg\,*}_{QCD,FSR}\right)+\int d\Phi_{2\to 2}\,\mathrm{Re}\left(\mathcal{M}^{gg}_{V,\phi_i,\mathrm{NF}}\mathcal{M}^{gg\,*}_{B_{\mathrm{eff}},QCD}\right)\ \overset{\mathrm{SGA}}{\longrightarrow}\ 0. \tag{3.101}$$

Given this identity, which is strictly valid only in the soft-gluon approximation, we drop the non-factorizable virtual corrections from the calculation and subtract instead the term

$$\mathcal{D}^{\mathrm{SGA}}_{ISR,FSR} \;=\; 2\,\mathrm{Re}\left(\mathcal{M}^{gg}_{\phi_i,ISR+INT}\mathcal{M}^{gg\,*}_{QCD,FSR}\right)\Big|_{\mathrm{SGA}}. \tag{3.102}$$

from the real corrections. The corresponding unintegrated dipoles in Eq. (3.87) are not needed anymore, thus all the initial–final and final–initial dipoles enter the computation with a factor $\frac{1}{2}$. Eq. (3.88) has to be rewritten as

$$\begin{aligned}\tilde{\sigma}^{gg}_{R} \;=\; \frac{1}{2s}\int d\Phi_{2\to 3}\sum_{gg}{}' \Bigg[&\sum_{i=1,2} 2\,\mathrm{Re}\left(\mathcal{M}^{gg}_{R,QCD}\mathcal{M}^{gg\,*}_{R,\phi_i}\right)-\mathcal{D}^{\mathrm{SGA}}_{ISR,FSR}+\left|\sum_{i=1,2}\mathcal{M}^{gg}_{R,\phi_i}\right|^2\\ &-\sum_{i\neq j\in\{1,2\}}\mathcal{D}^{g_i\to g_i' g_3,\,g_j}-\sum_{Q=t,\bar{t}}\mathcal{D}_{Q'\to Qg_3,\,\overline{Q}}-\frac{1}{2}\sum_{i=1,2}\sum_{Q=t,\bar{t}}\left[\mathcal{D}_Q^{g_i\to g_i' g_3}+\mathcal{D}^{g_i}_{Q'\to Qg_3}\right]\Bigg]\end{aligned} \tag{3.103}$$

This must be taken into account also for the integrated dipoles which will be discussed in the next section. Note also that the term $\mathcal{D}^{\mathrm{SGA}}_{ISR,FSR}$ depends on the choice of the physical gluon polarization sum. All the following results are obtained with (3.97).

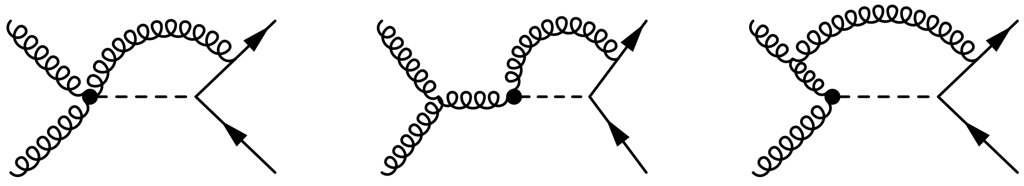

(a) (b) (c)

Figure 3.16. – *Feynman graphs corresponding to the non-factorizable one-loop amplitudes for the process $gg \to \phi + g \to t\bar{t}$. The crossed diagrams are not shown explicitly.*

3.6.4. Integrated dipoles & IR divergences

The process independent **I**, **K** and **P** insertion operators, which act on the color indices of the Born amplitudes, are given in Eqs. (6.66)–(6.68) in [61]. The dipoles constructed from the **I** operators cancel the remaining IR divergences in the virtual corrections and are thus relevant for us only in the case of the gg initial state. First we consider the integrated dipoles constructed from the interference terms of resonant Born amplitudes and the QCD background:

$$\begin{aligned}
&\sum_{i=1,2} {}_{QCD}\langle a_1, a_2;\, m_1, m_2| \left(\sum_{Q=t,\bar{t}} \mathbf{I}_{Q\overline{Q}} + \frac{1}{2} \sum_{i=1,2} \sum_{Q=t,\bar{t}} \mathbf{I}_{g_iQ} + \sum_{i\neq j \in \{1,2\}} \mathbf{I}_{g_ig_j} \right) |a_1', a_2';\, m_1', m_2'\rangle_{\phi_i} \\
&\qquad +\text{c.c.} \\
= &\ \frac{\alpha_s}{\pi} \frac{(4\pi)^\epsilon}{\Gamma(1-\epsilon)} \left\{ \frac{1}{\epsilon^2} C_A \operatorname{Re}\left[\delta\mathcal{M}_B\right] \right. \\
&+ \frac{1}{\epsilon} C_A \ln\left(\frac{t_{11}}{t_{12}}\right) \operatorname{Re}\left[\delta\tilde{\mathcal{M}}_B\right] \\
&+ \frac{1}{\epsilon} \left(C_F \left(\frac{1+\beta_t^2}{2\beta_t} \ln(x) + 1 \right) - C_A \ln\left(\frac{s}{\mu_R^2}\right) + 2\beta_0 \right) \operatorname{Re}\left[\delta\mathcal{M}_B\right] \\
&\left. + \mathcal{O}(\epsilon^0) \right\},
\end{aligned} \tag{3.104}$$

where the finite part will not be given explicitly. In (3.104) we defined $t_{1i} = 1 - \frac{(k_1-p_i)^2}{m_t^2}$, $\beta_0 = \frac{1}{4}\left(\frac{11}{3}C_A - \frac{2}{3}n_f\right)$, $x = \frac{1-\beta_t}{1+\beta_t}$ and used the abbreviations

$$\begin{aligned}
\delta\mathcal{M}_B &= \sum_{i=1,2} 2\mathcal{M}_{B,QCD}^{gg} \mathcal{M}_{B_{\text{eff},0,\phi_i}}^{gg\,*}, \\
\delta\tilde{\mathcal{M}}_B &= -\frac{\beta_t y}{2} \delta\mathcal{M}_B.
\end{aligned} \tag{3.105}$$

The latter is the Born ampltitude with final–initial color correlations which is generated by the $\mathbf{I}_{g_iQ}$ operators in (3.104). Note the factor $\frac{1}{2}$ that we have to introduce because the SGA (3.101) is used as subtraction term instead of the unintegrated dipoles (3.87). Thus also their integrated counter parts drop out of the calculation.

As a test we compute explicitly the virtual corrections including the IR poles using the Passarino-Veltman decomposition [71] to reduce the tensor loop integrals to a minimal set of scalar loop functions given in [72]. The result is

$$\begin{aligned}
\sum_{i=1,2} 2\,\mathrm{Re}\left(\mathcal{M}^{gg}_{B,QCD}\mathcal{M}^{gg\,*}_{V,\phi_i}\right) &= \frac{\alpha_s}{\pi}\frac{(4\pi)^\epsilon}{\Gamma(1-\epsilon)}\Bigg\{-\frac{1}{\epsilon^2}\frac{C_A}{2}\,\mathrm{Re}\,[\delta\mathcal{M}_B] \\
&- \frac{1}{\epsilon}\left(\tilde{C}_F\left(\frac{1+\beta_t^2}{4\beta_t}\ln(x)+\frac{1}{2}\right)-\frac{C_A}{2}\ln\left(\frac{s}{\mu_R^2}\right)+\beta_0\right)\mathrm{Re}\,[\delta\mathcal{M}_B] \\
&+ \frac{\pi}{\epsilon}\left(\tilde{C}_F\frac{1+\beta_t^2}{4\beta_t}+\frac{C_A}{2}\right)\mathrm{Im}\,[\delta\mathcal{M}_B] \\
&+ \mathcal{O}(\epsilon^0)\Bigg\},
\end{aligned} \tag{3.106}$$

where $\tilde{C}_F = \left(\frac{\mu_R^2}{m_t^2}\right)^\epsilon C_F$, and

$$\begin{aligned}
\sum_{i=1,2} 2\,\mathrm{Re}\left(\mathcal{M}^{gg}_{V,QCD}\mathcal{M}^{gg\,*}_{B_{\text{eff},0},\phi_i}\right) &= \frac{\alpha_s}{\pi}\frac{(4\pi)^\epsilon}{\Gamma(1-\epsilon)}\Bigg\{-\frac{1}{\epsilon^2}\frac{C_A}{2}\,\mathrm{Re}\,[\delta\mathcal{M}_B] \\
&- \frac{1}{\epsilon}\,C_A\,\ln\left(\frac{t_{11}}{t_{12}}\right)\mathrm{Re}\left[\delta\tilde{\mathcal{M}}_B\right] \\
&- \frac{1}{\epsilon}\left(\tilde{C}_F\left(\frac{1+\beta_t^2}{4\beta_t}\ln(x)+\frac{1}{2}\right)-\frac{C_A}{2}\ln\left(\frac{s}{\mu_R^2}\right)+\beta_0\right)\mathrm{Re}\,[\delta\mathcal{M}_B] \\
&- \frac{\pi}{\epsilon}\left(\tilde{C}_F\frac{1+\beta_t^2}{4\beta_t}+\frac{C_A}{2}\right)\mathrm{Im}\,[\delta\mathcal{M}_B] \\
&+ \mathcal{O}(\epsilon^0)\Bigg\}.
\end{aligned} \tag{3.107}$$

The sum of (3.104), (3.106) and (3.107) is finite and the limit $\epsilon \to 0$ can be taken. Next we consider the integrated dipoles constructed from the resonant Born amplitudes:

$$\begin{aligned}
&\sum_{i,j=1,2} {}_{\phi_i}\langle a_1, a_2;\, m_1, m_2|\left(\sum_{Q=t,\bar{t}}\mathbf{I}_{Q\overline{Q}}+\sum_{i=1,2}\sum_{Q=t,\bar{t}}\mathbf{I}_{g_iQ}+\sum_{i\neq j\in\{1,2\}}\mathbf{I}_{g_ig_j}\right)|a_1', a_2';\, m_1', m_2'\rangle_{\phi_j} \\
&= \sum_{i,j=1,2} {}_{\phi_i}\langle a_1, a_2;\, m_1, m_2|\left(\sum_{Q=t,\bar{t}}\mathbf{I}_{Q\overline{Q}}+\sum_{i\neq j\in\{1,2\}}\mathbf{I}_{g_ig_j}\right)|a_1', a_2';\, m_1', m_2'\rangle_{\phi_j} \\
&= \frac{\alpha_s}{\pi}\frac{(4\pi)^\epsilon}{\Gamma(1-\epsilon)}\left|\sum_{i=1,2}\mathcal{M}^{gg}_{B_{\text{eff},0},\phi_i}\right|^2\Bigg\{\frac{1}{\epsilon^2}C_A \\
&+\frac{1}{\epsilon}\,2\left(\tilde{C}_F\left(\frac{1+\beta_t^2}{4\beta_t}\ln(x)+1\right)-\frac{C_A}{2}\ln\left(\frac{s}{\mu_R^2}\right)+\beta_0\right) \\
&+\mathcal{O}(\epsilon^0)\Bigg\}.
\end{aligned} \tag{3.108}$$

The contribution of the **I** operators with final-initial correlations vanishes in (3.108) as we already observed in Sec. 3.5.4 discussing the unintegrated dipoles. The divergent part of the resonant virtual corrections (3.94) is canceled by the poles in (3.108) so that the limit $\epsilon \to 0$ can be taken as well.

The insertion operators **P** and **K** generate the finite remainder of the initial state collinear counter terms, where **P** contains the dependence on the factorization scale μ_F and **K** the factorization scheme dependent terms. The relevant **P** operators are

$$\mathbf{P}(x) \;=\; \frac{\alpha_s}{2\pi}\left(P^{gg}(x)+P^{qg}(x)\right)\left[\sum_{i\neq j\in\{1,2\}} \frac{\mathbf{T}_{g_i}\cdot\mathbf{T}_{g_j}}{C_A}\ln\frac{\mu_F^2}{x s_{ij}} + \sum_{i=1,2\;Q=t,\bar{t}} \frac{\mathbf{T}_{g_i}\cdot\mathbf{T}_Q}{C_A}\ln\frac{\mu_F^2}{s_{iQ}^{(x)}}\right],$$

where $s_{ij} = 2\,p_i{.}p_j$, $s_{iQ}^{(x)} = 2\,p_i{.}k_Q^{(x)}$ and $k_Q^{(x)}$ is the top or antitop momentum on the boosted $2 \to 2$ phase space $d\Phi_{2\to 2}^{(x)}$, c.f. (3.19) and [60, 61]. The Altarelli-Parisi splitting functions $P^{gg}(x)$ and $P^{qg}(x)$ can be found in Eqs. (5.94) and (5.89) in [61].

For the sake of clarity we split the **K** operators according to the relevant parton processes

$$\begin{aligned}
\mathbf{K}^{gg}(x) \;=\; -\frac{\alpha_s}{2\pi}\Bigg\{ &\sum_{i\neq j\in\{1,2\}} \frac{\mathbf{T}_{g_i}\cdot\mathbf{T}_{g_j}}{C_A}\Bigg\{P^{gg}_{\text{reg.}}(x)\,\ln(1-x) \\
&+C_A\left[2\left(\frac{\ln(1-x)}{1-x}\right)_+ - \frac{\pi^2}{3}\,\delta(1-x)\right]\Bigg\} \\
&+\frac{1}{2}\sum_{i=1,2\;Q=t,\bar{t}} \mathbf{T}_{g_i}\cdot\mathbf{T}_Q\left[\mathcal{F}^{gg}_Q(x,s_{iQ}^{(x)},m_t^2)+\mathcal{K}^{gg}_Q(x,s_{iQ}^{(x)},m_t^2)\right] \\
&-2\left(\overline{K}^{gg}(x)-K^{gg}_{\text{F.S.}}(x)\right)\Bigg\}
\end{aligned} \tag{3.109}$$

and

$$\begin{aligned}
\mathbf{K}^{qg}(x) \;=\; -\frac{\alpha_s}{2\pi}\Bigg\{ &\sum_{i\neq j\in\{1,2\}} \frac{\mathbf{T}_{g_i}\cdot\mathbf{T}_{g_j}}{C_A}\left\{P^{qg}_{\text{reg.}}(x)\,\ln(1-x)\right\} \\
&+\sum_{i=1,2\;Q=t,\bar{t}} \mathbf{T}_{g_i}\cdot\mathbf{T}_Q\left[\mathcal{F}^{qg}_Q(x,s_{iQ}^{(x)},m_t^2)+\mathcal{K}^{qg}_Q(x,s_{iQ}^{(x)},m_t^2)\right] \\
&-\left(\overline{K}^{qg}(x)-K^{qg}_{\text{F.S.}}(x)\right)\Bigg\}
\end{aligned} \tag{3.110}$$

For the factorization scheme dependent part we assume $K^{gg}_{\mathrm{F.S.}} = K^{qg}_{\mathrm{F.S.}} = 0$, i.e. we work in the $\overline{\mathrm{MS}}$ scheme. Note again the factor $\frac{1}{2}$ in the third line of (3.109) containing the final-initial correlations. The factor 2 in the last line of (3.109) is due to the summation over the two initial state gluons. The functions $\mathcal{F}^{gg}_{Q}$ and $\mathcal{F}^{qg}_{Q}$ are defined as follows:

$$
\begin{aligned}
\mathcal{F}^{gg}_{Q}(x,s^{(x)}_{iQ},m_t^2) &= \frac{1}{C_A}\Bigg[P^{gg}_{\mathrm{reg.}}(x)\,\ln\frac{(1-x)s^{(x)}_{iQ}}{(1-x)s^{(x)}_{iQ}+m_t^2} + \gamma_g\,\delta(1-x) \\
&\qquad \times\left(\ln\frac{s^{(x)}_{iQ}-2m_t\sqrt{s^{(x)}_{iQ}+m_t^2}+2m_t^2}{s^{(x)}_{iQ}} + \frac{2m_t}{\sqrt{s^{(x)}_{iQ}+m_t^2}+m_t^2}\right)\Bigg], \\
\mathcal{F}^{qg}_{Q}(x,s^{(x)}_{iQ},m_t^2) &= \frac{1}{C_A}\left[P^{qg}_{\mathrm{reg.}}(x)\,\ln\frac{(1-x)s^{(x)}_{iQ}}{(1-x)s^{(x)}_{iQ}+m_t^2}\right].
\end{aligned}
$$

The definitions of $\overline{K}^{gg}$, $\overline{K}^{qg}$, $\mathcal{K}^{gg}_{Q}$ and $\mathcal{K}^{qg}_{Q}$ can be found in Eqs. (6.56), (6.59) and (6.60) in [61]. These are all the neccessary ingredients to evaluate the next-to-leading order correction (3.19) to the process (3.3) numerically in a Monte-Carlo program. The results will be discussed in the next section.

3.7. Numerical results

For the analysis of the effects of heavy neutral Higgs bosons in $t\bar{t}$ production we will focus on two CP-conserving and one CP-violating scenario within the type-II 2HDM discussed in Sec. 1.2. In all scenarios the first neutral Higgs boson ϕ_1 is identified with the 125 GeV Higgs resonance discovered at the LHC, with SM like couplings to fermions and gauge bosons. Choosing $\tan\beta = 0.7$ rather small, close to the limits imposed by theoretical considerations and experiments, the effects of the two additional neutral Higgs bosons in $t\bar{t}$ production are close to maximal (within the type-II 2HDM). In the following subsections the input parameters for the computation are listed and in particular the decay widths of the two heavy Higgs bosons are given for each of the three scenarios.

3.7.1. Three type-II 2HDM scenarios

Scenario 1, CP-conserving, $\tan\beta = 0.7$

We investigate two CP-conserving scenarios where the Higgs bosons ϕ_1, ϕ_2 are CP-even and ϕ_3 is CP-odd. In this scenario, ϕ_2 and ϕ_3 are nearly mass-degenerate,

$$m_1 = 125\,\text{GeV}\ , \quad m_2 = 550\,\text{GeV}\ , \quad m_3 = 510\,\text{GeV},$$

and the charged Higgs mass is set to

$$m_\pm = 550\,\text{GeV}.$$

We will work exactly in the alignment limit, meaning that the neutral mixing angles, defined in (1.33), are set to the values

$$\alpha_1 = \beta = 0.611\ , \quad \alpha_2 = 0\ , \quad \alpha_3 = 0,$$

so that the couplings of ϕ_1 are exactly the SM values. In particular, one obtains the following values for the reduced Yukawa couplings, defined in (A.7):

$$\begin{aligned} &a_{t,1} = 1, && b_{t,1} = 0, && a_{b,1} = 1, && b_{b,1} = 0,\\ &a_{t,2} = 1.4286, && b_{t,2} = 0, && a_{b,2} = -0.700, && b_{b,2} = 0,\\ &a_{t,3} = 0, && b_{t,3} = 1.4286, && a_{b,3} = 0, && b_{b,3} = 0.700. \end{aligned} \tag{3.111}$$

The reduced couplings to gauge boson pairs, defined in (A.11), are

$$f_{1VV} = 1, \quad f_{2VV} = 0, \quad f_{3VV} = 0. \tag{3.112}$$

The decay widths obtained with the program 2HDMC are given in Tab. 3.2. The partial widths for the channels $\phi_i \to f\bar{f}$ and $\phi_i \to gg$ include the NNLO QCD corrections in

Table 3.2. – *Decay widths of the two heavy, neutral Higgs bosons ϕ_2 and ϕ_3 in the 2HDM **scenario 1**. In the cases $\phi_i \to f\bar{f}$ and $\phi_i \to gg$ the NNLO QCD corrections evaluated at $\mu = \mu_0 = \frac{m_2+m_3}{4}$ are included, c.f. [46]. For the results of $\phi_i \to t\bar{t}$ and $\phi_i \to gg$, the scale dependence introduced by the radiative corrections is indicated by a superscript ($\mu = \frac{\mu_0}{2}$) and subscript ($\mu = 2\mu_0$).*

	Γ_2 [GeV]	Γ_3 [GeV]
$\phi_i \to t\bar{t}$	$37.78^{+0.76}_{-0.61}$	$54.92^{+1.11}_{-0.89}$
$\phi_i \to b\bar{b}$	4.99×10^{-3}	4.63×10^{-3}
$\phi_i \to VV$	0	0
$\phi_i \to Z\phi_1$	0	0
$\phi_i \to \phi_1\phi_1$	0	0
$\phi_i \to gg$	$0.105^{+0.013}_{-0.011}$	$0.181^{+0.023}_{-0.020}$
tot.	$37.89^{+0.77}_{-0.62}$	$55.11^{+1.13}_{-0.91}$

the large m_t limit [46], evaluated at the scale $\mu = \mu_0 = \frac{m_2+m_3}{4}$ to be consistent with the setup described in the next section. For the computation of $\phi_i \to t\bar{t}$ and $\phi_i \to gg$, the top quark pole mass is used in the Yukawa couplings to evaluate the leading-order contributions, while in the radiative corrections the running $\overline{\text{MS}}$ mass is used. In case of the bottom-quark contributions we always use the $\overline{\text{MS}}$ mass. The decays $\phi_i \to \gamma\gamma$, $\phi_i \to \gamma Z$ and $\phi_i \to \tau^+\tau^-$ are also present but their widths are $< 10^{-3}$ and will not be considered any further.

Scenario 2, CP-conserving, $\tan\beta = 0.7$

In the second CP conserving scenario a rather large mass splitting is chosen,

$$m_1 = 125\,\text{GeV}\ , \quad m_2 = 550\,\text{GeV}\ , \quad m_3 = 700\,\text{GeV},$$

and for the charged Higgs

$$m_\pm = 700\,\text{GeV}.$$

The mixing angles and $\tan\beta$ have the same values as in scenario 1, thus also the reduced Yukawa couplings are the same as given in Eqs. (3.111) and (3.112). The decay widths obtained with the program 2HDMC are given in Tab. 3.3. Note that the decay widths for $\phi_{2,3} \to VV$, $\phi_{2,3} \to Z\phi_1$ and $\phi_{2,3} \to \phi_1\phi_1$ vanish in the CP-conserving scenarios because we work exactly in the alignment limit $\alpha_1 = \beta$, $\alpha_2 = 0$. If one drops this restriction there are substantial contributions to the total widths from the channels $\phi_2 \to VV$ and $\phi_2 \to \phi_1\phi_1$ in case of the CP-even heavy Higgs boson ϕ_2 and from $\phi_3 \to Z\phi_{1,2}$ in case of the CP-odd Higgs boson ϕ_3.

Table 3.3. – *Decay widths of the two heavy, neutral Higgs bosons ϕ_2 and ϕ_3 in the 2HDM* ***scenario 2****. In the cases $\phi_i \to f\bar{f}$ and $\phi_i \to gg$ the NNLO QCD corrections evaluated at $\mu = \mu_0 = \frac{m_2+m_3}{4}$ are included, c.f. [46]. For the results of $\phi_i \to t\bar{t}$ and $\phi_i \to gg$, the scale dependence introduced by the radiative corrections is indicated by a superscript ($\mu = \frac{\mu_0}{2}$) and subscript ($\mu = 2\mu_0$).*

	Γ_2 [GeV]	Γ_3 [GeV]
$\phi_i \to t\bar{t}$	$37.63^{+0.72}_{-0.59}$	$88.93^{+1.69}_{-1.39}$
$\phi_i \to b\bar{b}$	4.84×10^{-3}	6.16×10^{-3}
$\phi_i \to VV$	0	0
$\phi_i \to Z\phi_1$	0	0
$\phi_i \to Z\phi_2$	–	3.13
$\phi_i \to \phi_1\phi_1$	0	0
$\phi_i \to gg$	$0.103^{+0.012}_{-0.011}$	$0.196^{+0.023}_{-0.020}$
tot.	$37.74^{+0.73}_{-0.60}$	$92.26^{+1.71}_{-1.41}$

Scenario 3, CP-violating, $\tan\beta = 0.7$

In the CP-violating type-II 2HDM the three mixing angles are set to the values

$$\alpha_1 = \beta\,, \quad \alpha_2 = \frac{\pi}{15}\,, \quad \alpha_3 = \frac{\pi}{4}.$$

Since $\alpha_2 \neq 0$ this setting does not correspond to the exact alignment limit anymore, c.f. (1.50). Though, it is close enough to accomodate the recent LHC measurements for the light Higgs bosons. The mass splitting of the two heavy, neutral Higgs bosons is again chosen to be rather large. We set

$$m_1 = 125\,\text{GeV}\,, \quad m_2 = 500\,\text{GeV}\,, \quad m_3 = 800\,\text{GeV}\,,$$

and the charged Higgs mass is set to

$$m_\pm = 700\,\text{GeV}.$$

Note that these mass parameters are not subject to the condition (B.11) so that this scenario is actually not permitted within the type-II 2HDM with softly broken Z_2. Instead, the λ_6 and λ_7 terms in (1.18) have to be reintroduced to accomodate this setting. The above choice of $\tan\beta$ and the mixing angles implies the following values for the reduced Yukawa couplings defined in (A.7):

$$\begin{aligned}
a_{t,1} &= 0.9781, & b_{t,1} &= 0.2970, & a_{b,1} &= 0.9781, & b_{b,1} &= 0.1455, \\
a_{t,2} &= 0.8631, & b_{t,2} &= 0.9881, & a_{b,2} &= -0.6420, & b_{b,2} &= 0.4842, \\
a_{t,3} &= -1.1572, & b_{t,3} &= 0.9881, & a_{b,3} &= 0.3480, & b_{b,3} &= 0.4842.
\end{aligned} \tag{3.113}$$

The reduced couplings to the gauge bosons, defined in (A.11), are

$$f_{1VV} = 0.9781, \quad f_{2VV} = -0.1470, \quad f_{3VV} = -0.1470. \tag{3.114}$$

Table 3.4. – *Decay widths of the two heavy, neutral Higgs bosons ϕ_2 and ϕ_3 in the 2HDM **scenario 3**. In the cases $\phi_i \to f\bar{f}$ and $\phi_i \to gg$ the NNLO QCD corrections evaluated at $\mu = \mu_0 = \frac{m_2+m_3}{4}$ are included, c.f. [46]. For the results of $\phi_i \to t\bar{t}$ and $\phi_i \to gg$, the scale dependence introduced by the radiative corrections is indicated by a superscript ($\mu = \frac{\mu_0}{2}$) and subscript ($\mu = 2\mu_0$).*

	Γ_2 [GeV]	Γ_3 [GeV]
$\phi_i \to t\bar{t}$	$27.33^{+0.51}_{-0.42}$	$105.33^{+1.98}_{-1.64}$
$\phi_i \to b\bar{b}$	4.37×10^{-3}	6.99×10^{-3}
$\phi_i \to VV$	1.125	5.107
$\phi_i \to Z\phi_1$	0.647	3.238
$\phi_i \to Z\phi_2$	–	31.28
$\phi_i \to \phi_1\phi_1$	0.777[1]	1.453[1]
$\phi_i \to gg$	$0.115^{+0.015}_{-0.012}$	$0.192^{+0.021}_{-0.019}$
tot.	$30.00^{+0.53}_{-0.43}$	$146.61^{+2.00}_{-1.66}$

Again, the partial widths for the channels $\phi_i \to f\bar{f}$ and $\phi_i \to gg$, given in Tab. 3.4, are obtained with the program 2HDMC and include the NNLO QCD corrections in the large m_t limit, c.f. [46]. For the other channels, the tree-level formulae given in Sec. 1.2.5 are used.

Electroweak corrections

In particular for heavy Higgs bosons, the electroweak corrections to the decay processes $\phi_i \to f\bar{f}$ [73] and $\phi_i \to VV$ [74] become sizeable. A more thorough analysis would also include virtual ϕ_i exchange in the corrections to these processes. Since we consider here scenarios with suppressed $\phi_i VV$ couplings for $i = 2, 3$ the corrections to $\phi_i \to VV$ will not affect the total width very much, whereas the corrections to $\phi_i \to t\bar{t}$ can be as large as the QCD corrections.

[1] Computed with the Feynman rule (A.13) for the type-II 2HDM with $\lambda_6 = \lambda_7 = 0$. This treatment is not completely correct since, with the parameter choice given above, we disregard the constraint (B.11).

3.7.2. General Setup

As in Sec. 2.2, the CT10 NLO PDF set [56] is used to compute total cross sections and distributions at the hadron level. Renormalization and factorization scales are both set to half of the mean value of the two heavy Higgs masses:

$$\mu_0 = \mu_R = \mu_F = \frac{m_2 + m_3}{4}. \tag{3.115}$$

The additional factor $\frac{1}{2}$ is motivated by the observation that in the computation of the total inclusive Higgs production cross section the effects of soft gluon resummation are reproduced in this way [55, 24, 25]. To quantify the residual scale dependence, μ will be varied within the range $\left[\frac{\mu_0}{2}, 2\mu_0\right]$. The strong coupling $\alpha_s(\mu)$ at the respective renormalization scale is extracted from the CT10 NLO PDF set, the specific values are summarized in Tab. 3.5.

Table 3.5. – *Renormalization and factorization scales computed according to (3.115) for the three scenarios specified in Sec. 3.7.1. The value of the strong coupling $\alpha_s(\mu_0)$ is extracted from the PDFs [56] at the respective scale (5-flavour scheme).*

Scenario	μ_0 [GeV]	$\alpha_s^{(5)}(\mu_0)$
1	265.0	0.101693
2	312.5	0.099576
3	325.0	0.099085

The settings for the Higgs-specific parameters in the three 2HDM scenarios are listed in the previous section, $\tan\beta = 0.7$ is chosen for all of them. Apart from that, the setup is similar to Sec. 2.1. The radiative QCD corrections involving resonant amplitudes are computed using the Higgs-gluon in the large m_t limit, while on Born level the full top and bottom-quark dependence is taken into account. For the NLO contributions, a rescaling method similar to that described in Sec. 2.2 will be applied. The difference is that here we deal with two off-shell Higgs bosons and additionally with the interference terms with the non-resonant background. Schematically, we apply the effective K-factors in the following way:

$$\begin{aligned} \mathcal{M}_{\phi_i}\mathcal{M}^*_{\phi_j} &\longrightarrow K_i\, K_j \cdot \mathcal{M}_{\phi_i}\, \mathcal{M}^*_{\phi_j}, \\ \mathcal{M}_{QCD}\mathcal{M}^*_{\phi_i} &\longrightarrow K_i \cdot \mathcal{M}_{QCD}\mathcal{M}^*_{\phi_i}, \end{aligned}$$

with

$$K_i^2 \overset{(2.16)}{=} K^2(q^2, m_t, m_b, a_{t,i}, b_{t,i}, a_{b,i}, b_{b,i}),$$

where $q^2 > 0$ is the momentum squared carried by the Higgs bosons in the respective amplitude.

Within the SM the distributions at next-to-leading order (NLOW) were computed with the code of [68]. The acronym NLOW refers to the following corrections:

- The QCD corrections to the processes $g\,g \to t\,\bar{t}\ (g)$, $q\,\bar{q} \to t\,\bar{t}\ (g)$ and $g\,q\,(\bar{q}) \to t\,\bar{t}\,q\,(\bar{q})$ are computed to $\mathcal{O}\left(\alpha_s^3\right)$.
- The SM weak-interaction processes $q\,\bar{q} \to \gamma^*, Z^* \to t\,\bar{t}$ are included to $\mathcal{O}\left(\alpha^2\right)$.
- The mixed QCD-weak corrections to the processes $g\,g \to t\,\bar{t}$ and $q\,\bar{q} \to t\,\bar{t}\ (g)$ are included through $\mathcal{O}\left(\alpha_s^2\alpha\right)$.
- In addition to the latter, the corrections to the process $g\,q(\bar{q}) \to t\,\bar{t}\ q\,(\bar{q})$ include the $\mathcal{O}\left(\alpha_s\alpha^2\right)$ contributions.

Note that the SM weak corrections contain the contribution from the light neutral 125 GeV Higgs boson ϕ_1.

The top-quark pole mass and the combined Higgs VEV are set to values

$$\begin{aligned} m_t &= 173.34 \text{ GeV [10]}, \\ v &= 246 \text{ GeV}. \end{aligned}$$

3.7.3. Top-quark distributions

Besides the $t\bar{t}$ invariant mass spectrum, the following observables at the $t\bar{t}$ level will be investigated:

- The transverse momentum distributions of top and antitop quark, where $\vec{k}_T = (k_x, k_y)^T$ and the z-axis defines the beam direction.
- The rapidity distributions of top and antitop quark, where $y = \frac{1}{2}\log\left(\frac{E+k_z}{E-k_z}\right)$.
- The distribution of the rapidity moduli differences of top and antitop quark, $\Delta|y| = |y_t| - |y_{\bar{t}}|$.
- The transverse momentum distribution of the top/antitop system, $p_{T,t\bar{t}} = |\vec{k}_{T,t} + \vec{k}_{T,\bar{t}}|$. This observable is generated solely through the real radiation processes and the distribution should therefore be regarded as a leading-order approximation.

Although my computer program allows for the implementation of acceptance cuts at the level of dileptonic and semileptonic $t\bar{t}$ final states, no such cuts will be applied in the following.

3.7.4. LHC 8 TeV

In this section the results for $\sqrt{s_{\rm had}} = 8$ TeV proton-proton collisions are summarized. In Tab. 3.6 the total $t\bar{t}$ production cross sections at NLO QCD are listed with and without the resonant processes. As one can see the effect of the two heavy Higgs bosons on the total cross section is only around 2% in the three 2HDM scenarios under consideration. This is due to the peak-dip structure of the heavy resonances which is best visible in the $M_{t\bar{t}}$ distributions in Figs. 3.17, 3.23 and 3.29, i.e. the effects below and above the resonance region partly cancel. To estimate the expected number of signal events in the dilepton and l+jets channel due to resonant Higgs production,

$$\langle \Delta N^{2l/lj}_{\phi_2,\phi_3} \rangle \quad = \quad L \cdot \left(\sigma^{\rm NLO(W)}_{QCD+\phi_2,\phi_3} - \sigma^{\rm NLOW}_{QCD} \right) \cdot \varepsilon_{2l/lj} \cdot {\rm Br}(t\,\bar{t} \to 2l/l + {\rm jets})$$

we assume the branching fractions

$$\begin{aligned} {\rm Br}(t\,\bar{t} \to 2l) &= \frac{4}{81}, \\ {\rm Br}(t\,\bar{t} \to l + {\rm jets}) &= \frac{24}{81}, \end{aligned} \tag{3.116}$$

and an integrated luminosity and event selection efficiencies [75, 76] of

$$\begin{aligned} L &= 20\,{\rm fb}^{-1}, \\ \varepsilon_{2l} &= 0.22, \\ \varepsilon_{lj} &= 0.12. \end{aligned} \tag{3.117}$$

To get a better view of the Higgs effects we compute the NLO(W) cross sections within the $M_{t\bar{t}}$ range of $[360, 800]$ GeV below and above the resonance region and take the ratios

$$\begin{aligned} R^{(<)} &= \frac{\sigma^{\rm NLO(W)}_{QCD+\phi_2,\phi_3}\Big|_{360\ {\rm GeV}<M_{t\bar{t}}<M^*_{t\bar{t}}}}{\sigma^{\rm NLOW}_{QCD}\Big|_{360\ {\rm GeV}<M_{t\bar{t}}<M^*_{t\bar{t}}}}, \\ R^{(>)} &= \frac{\sigma^{\rm NLO(W)}_{QCD+\phi_2,\phi_3}\Big|_{800\ {\rm GeV}>M_{t\bar{t}}>M^*_{t\bar{t}}}}{\sigma^{\rm NLOW}_{QCD}\Big|_{800\ {\rm GeV}>M_{t\bar{t}}>M^*_{t\bar{t}}}}. \end{aligned} \tag{3.118}$$

Here we will define the boundary of the resonance region by the value $M^*_{t\bar{t}}$ where the ratio of the $M_{t\bar{t}}$ distributions crosses one. The results are given in Tab. 3.7 and 3.8. To estimate the significance of these deviations from the pure QCD cross sections in the light of the parameters (3.117) we first compute the p-values corresponding to the excesses and deficits given in the fourth and fifth column of Tabs. 3.7 and 3.8 with respect to the expected rates based on the QCD only hypothesis:

$$p^{2l} \;=\; 1 - F_{\chi^2}\left(2\langle N^{2l\,(<)}_{QCD}\rangle\Big|_{\mu=\mu_0}, 2N^{2l\,(<)}_{\rm obs}\right), \tag{3.119}$$

where we assume that $N^{2l\,(<)}_{\rm obs} = \langle N^{2l\,(<)}_{QCD}\rangle\Big|_{\mu=\mu_0} + \langle \Delta N^{2l}_{\phi_2,\phi_3}\rangle\Big|_{\mu=\mu_0}$ was measured experimentally. The corresponding significance is then computed as

$$S^{2l} \;=\; \Phi^{-1}\left(1 - p^{2l}\right), \tag{3.120}$$

where $F_{\chi^2}(x,y)$ denotes the cumulative χ^2 distribution and $\Phi^{-1}(x)$ the quantile of the normal distribution. We see that – assuming the statistics of the $\sqrt{s_{\rm had}} = 8$ TeV run at the LHC – excesses such as these given in Tab. 3.7 are statistically significant whereas the deficits in Tab. 3.8 are not. A similar analysis could be applied to the top-quark p_T distributions in Figs. 3.18, 3.24 and 3.30. Note that the antitop p_T distributions are not shown explicitly because – up to statistical fluctuations – they are equivalent to the top distributions. In Figs. 3.20, 3.21, 3.26, 3.27 and 3.32, 3.33 the rapidity distributions of top and antitop quark are given. The NLOW corrections to the SM processes induce a small asymmetry between these two distributions. This effect can be quantified by the charge asymmetry

$$A_C^{\Delta|y|} \;=\; \frac{N\left(\Delta|y|>0\right) - N\left(\Delta|y|<0\right)}{N\left(\Delta|y|>0\right) + N\left(\Delta|y|<0\right)}, \tag{3.121}$$

where $\Delta|y| = |y_t| - |y_{\bar t}|$ and y_i are the lab-frame rapidities. A more detailed account concerning charge asymmetries in the non-resonant QCD processes is given in [77]: The prediction for the $t\bar t$ charge asymmetry A_C at NLO QCD including electroweak corrections, for the LHC at 8 TeV, is $A_C = 1.11(4)\%$ [77]. This is in agreement with the results of the ATLAS and CMS experiment. The asymmetry is due to the fact that at NLO in the gauge couplings slightly more top-quarks than antitop quarks are produced in the forward and backward region, while it is the other way around in the central region. The size of A_C depends on the center-of-mass energy and on cuts, for instance on a cut on $M_{t\bar t}$. We want to emphasize here that through NLO QCD there is no additional contribution to the $t\bar t$ charge asymmetry A_C from the resonant Higgs processes and their interference with the non-resonant background. This can be seen in the distributions of $\Delta|y|$ shown in Figs. 3.22, 3.28 and 3.34, which are symmetric around $\Delta|y| = 0$.

In all distributions one can observe that the effect of the NLO corrections is sizeable. Also the shape of the distributions is changed significantly, note for example the shift of the one-crossing in the ratios of the $M_{t\bar t}$ spectra shown in the lower panes of Figs. 3.17, 3.23 and 3.29 or in the ratios of the top p_T distributions in the lower panes of Figs. 3.18, 3.24 and 3.30.

Table 3.6. – *Total cross-sections for $t\bar{t}$ production in proton-proton collisions at $\sqrt{s_{\rm had}} = 8$ TeV with and without effects of two heavy neutral Higgs bosons at NLO QCD. In the third and fourth column, the expected number of signal events in the dilepton and l+jets channel (l = e,μ), $\langle \Delta N^{2l}_{\phi_2,\phi_3}\rangle$ and $\langle \Delta N^{lj}_{\phi_2,\phi_3}\rangle$ respectively, due to the resonant processes is given, assuming the parameters given in* (3.117)*. The scale dependence is indicated by a superscript ($\mu = \frac{\mu_0}{2}$) and subscript ($\mu = 2\mu_0$).*

Scenario	$\sigma^{\rm NLOW}_{QCD}$ [pb]	$\sigma^{\rm NLO(W)}_{QCD+\phi_2,\phi_3}$ [pb]	$\langle \Delta N^{2l}_{\phi_2,\phi_3}\rangle$	$\langle \Delta N^{lj}_{\phi_2,\phi_3}\rangle$
1	$191.86^{+25.67}_{-25.37}$	$196.56^{+26.04}_{-25.83}$	1025^{+82}_{-101}	3355^{+269}_{-330}
2	$185.69^{+25.91}_{-24.93}$	$188.15^{+26.02}_{-25.13}$	535^{+25}_{-44}	1751^{+81}_{-145}
3	$184.22^{+25.93}_{-24.80}$	$187.68^{+26.27}_{-25.17}$	752^{+72}_{-80}	2461^{+237}_{-262}

Table 3.7. – *Ratio of total cross-sections for $t\bar{t}$ production in proton-proton collisions at $\sqrt{s_{\rm had}} = 8$ TeV with and without effects of two heavy neutral Higgs bosons at NLO QCD. The ratio of the NLO cross sections $R^{(<)}$ below the resonances is defined in Eq.* (3.118)*. In the third and fourth column the expected number of signal events, $\langle \Delta N^{2l\,(<)}_{\phi_2,\phi_3}\rangle$ and $\langle \Delta N^{lj\,(<)}_{\phi_2,\phi_3}\rangle$, in the respective $M_{t\bar{t}}$ ranges in the dilepton and l+jets channel (l = e,μ) due to the resonant processes is given, assuming the parameters in* (3.117)*. The scale dependence is indicated by a superscript ($\mu = \frac{\mu_0}{2}$) and subscript ($\mu = 2\mu_0$). See Eqs.* (3.120) *and* (3.119) *for the definition of the statistical significances $S^{2l\,(>)}$ and $S^{lj\,(>)}$.*

Sc.	$[M^{\rm min}_{t\bar{t}}, M^{*}_{t\bar{t}}]$ [GeV]	$R^{(<)}$	$\langle \Delta N^{2l\,(<)}_{\phi_2,\phi_3}\rangle$	$S^{2l\,(<)}$	$\langle \Delta N^{lj\,(<)}_{\phi_2,\phi_3}\rangle$	$S^{lj\,(<)}$
1	$[360, 540]$	$1.041^{-0.003}_{+0.002}$	1153^{+55}_{-107}	6.8	3772^{+181}_{-322}	> 16
2	$[360, 560]$	$1.020^{-0.001}_{+0.001}$	589^{+48}_{-61}	3.4	1927^{+155}_{-199}	6.2
3	$[360, 500]$	$1.036^{-0.001}_{+0.001}$	848^{+84}_{-93}	5.5	2775^{+276}_{-304}	> 16

Table 3.8. – *Ratio of total cross-sections for $t\bar{t}$ production in proton-proton collisions at $\sqrt{s_{\rm had}} = 8$ TeV with and without effects of two heavy neutral Higgs bosons at NLO QCD. The ratio of the NLO cross sections $R^{(>)}$ above the resonances is defined in Eq.* (3.118)*. In the third and fourth column the expected number of signal events, $\langle \Delta N^{2l\,(>)}_{\phi_2,\phi_3}\rangle$ and $\langle \Delta N^{lj\,(>)}_{\phi_2,\phi_3}\rangle$, in the respective $M_{t\bar{t}}$ ranges in the dilepton and l+jets channel (l = e,μ) due to the resonant processes is given, assuming the parameters in* (3.117)*. The scale dependence is indicated by a superscript ($\mu = \frac{\mu_0}{2}$) and subscript ($\mu = 2\mu_0$). See Eqs.* (3.120) *and* (3.119) *for the definition of the statistical significances $S^{2l\,(<)}$ and $S^{lj\,(<)}$.*

Sc.	$[M^{*}_{t\bar{t}}, M^{\rm max}_{t\bar{t}}]$ [GeV]	$R^{(>)}$	$\langle \Delta N^{2l\,(>)}_{\phi_2,\phi_3}\rangle$	$S^{2l\,(>)}$	$\langle \Delta N^{lj\,(>)}_{\phi_2,\phi_3}\rangle$	$S^{lj\,(>)}$
1	$[540, 800]$	$0.980^{+0.003}_{-0.002}$	-189^{+11}_{-10}	1.9	-618^{+38}_{-32}	3.5
2	$[560, 800]$	$0.991^{-0.002}_{+0.002}$	-68^{-31}_{+21}	0.8	-223^{-103}_{+69}	1.4
3	$[500, 800]$	$0.9907^{-0.0001}_{+0.0001}$	-123^{-19}_{+18}	1.1	-401^{-63}_{+60}	1.9

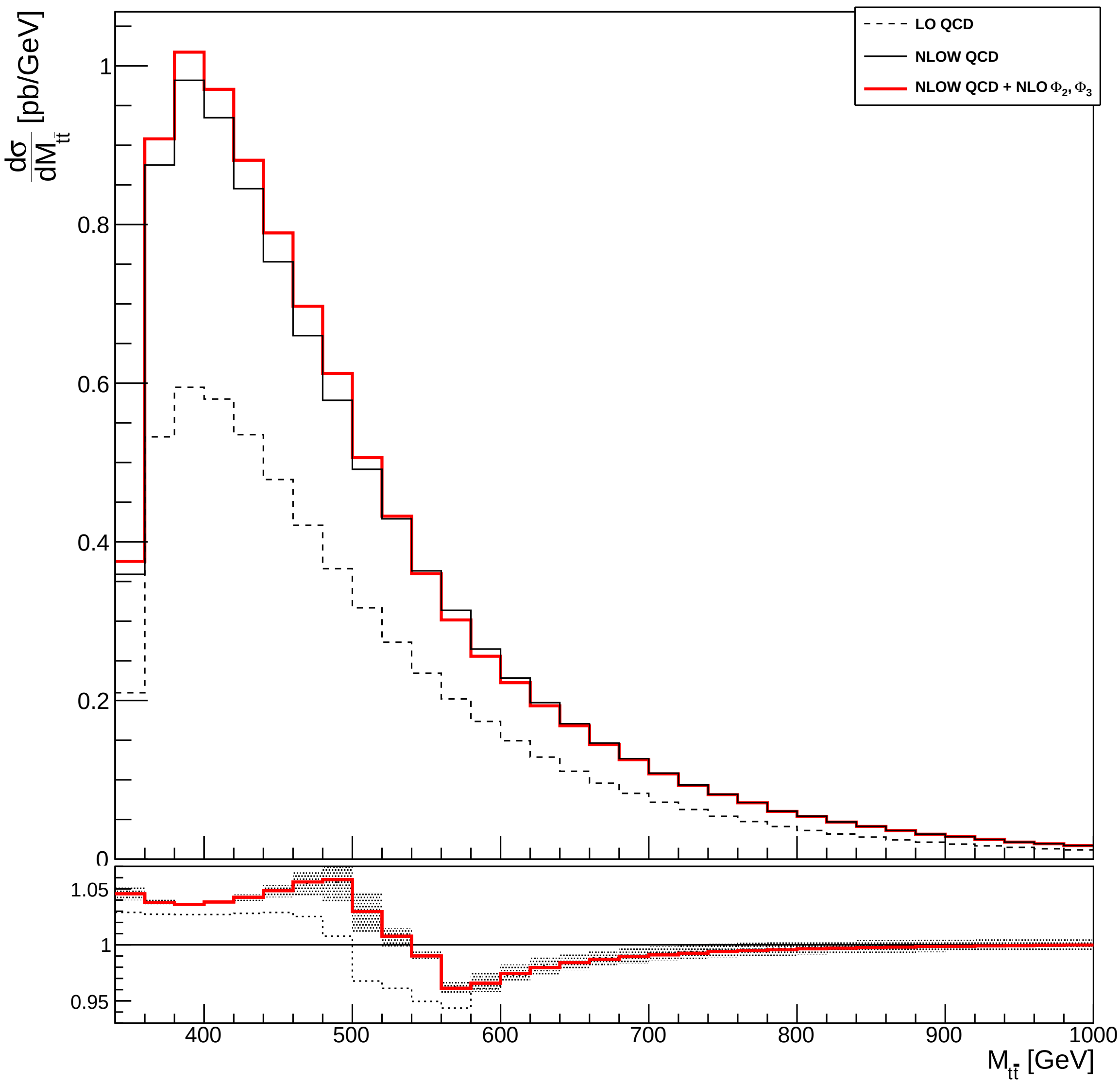

Figure 3.17. – *Top-/Antitop invariant mass distribution for $pp \to t\bar{t}$ including the effects of two neutral Higgs bosons (2HDM **scenario 1**, see 3.7.1) at NLO QCD. The hadronic center-of-mass energy is $\sqrt{s_{\rm had}} = 8$ TeV, renormalization and factorization scales are set to $\mu = \mu_0 =$ 265 GeV, c.f. (3.115). The lower pane shows the ratios $d\sigma^{\rm NLO(W)}_{QCD+\phi_2,\phi_3}/d\sigma^{\rm NLOW}_{QCD}$ (thick line) and $d\sigma^{\rm LO}_{QCD+\phi_2,\phi_3}/d\sigma^{\rm LO}_{QCD}$ (dotted line). The effect of scale variation in the interval $[\frac{\mu_0}{2}, 2\mu_0]$ for the NLO(W) ratio is indicated by the shaded rectangles.*

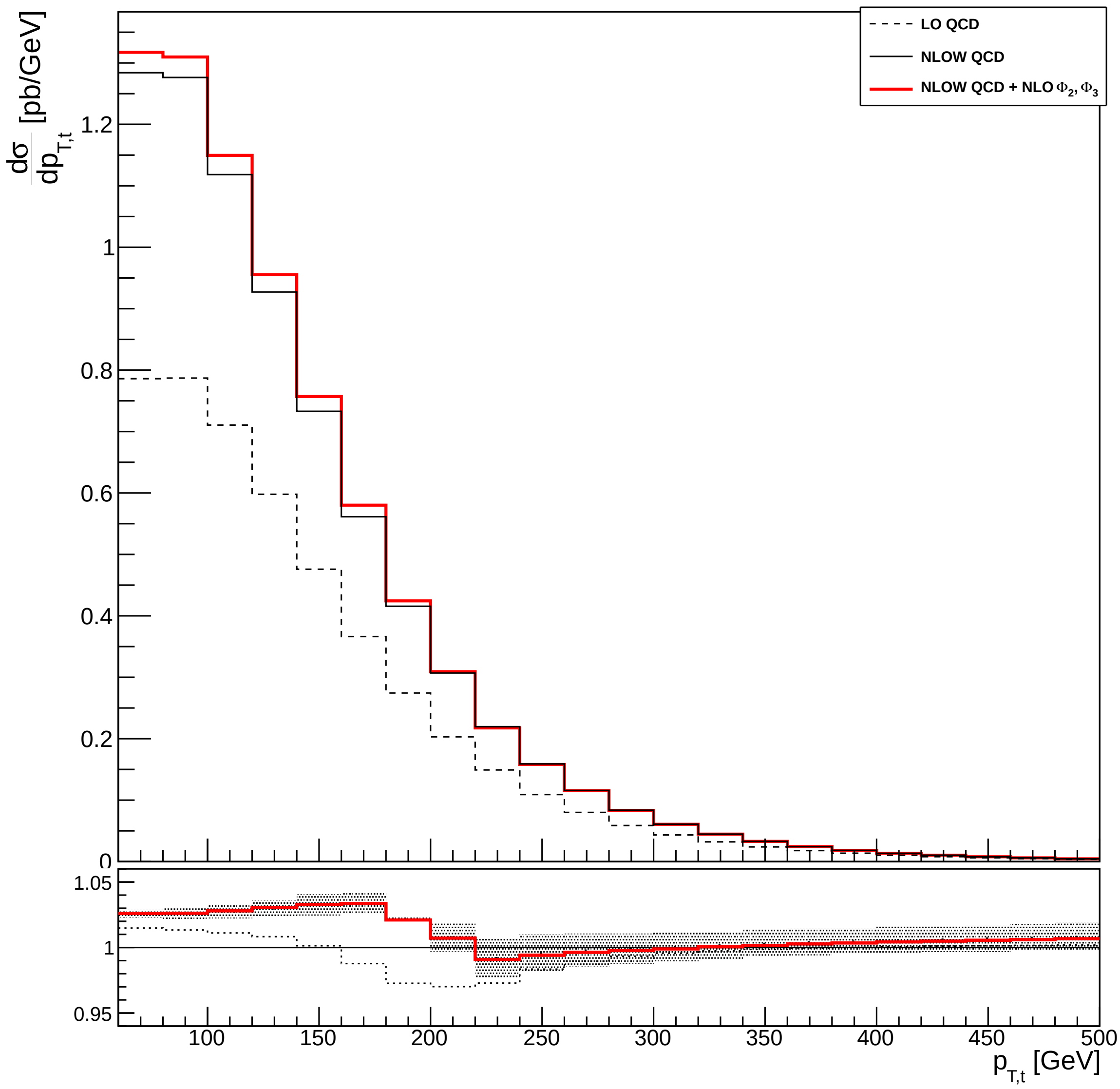

Figure 3.18. – *Top transverse momentum distribution for $pp \to t\bar{t}$ including the effects of two neutral Higgs bosons (2HDM* ***scenario 1****, see 3.7.1) at NLO QCD. The hadronic center-of-mass energy is $\sqrt{s_{\rm had}} = 8$ TeV, renormalization and factorization scales are set to $\mu = \mu_0 =$ 265 GeV, c.f. (3.115). The lower pane shows the ratios $d\sigma^{\rm NLO(W)}_{QCD+\phi_2,\phi_3}/d\sigma^{\rm NLOW}_{QCD}$ (thick line) and $d\sigma^{\rm LO}_{QCD+\phi_2,\phi_3}/d\sigma^{\rm LO}_{QCD}$ (dotted line). The effect of scale variation in the interval $[\frac{\mu_0}{2}, 2\mu_0]$ for the NLO(W) ratio is indicated by the shaded rectangles.*

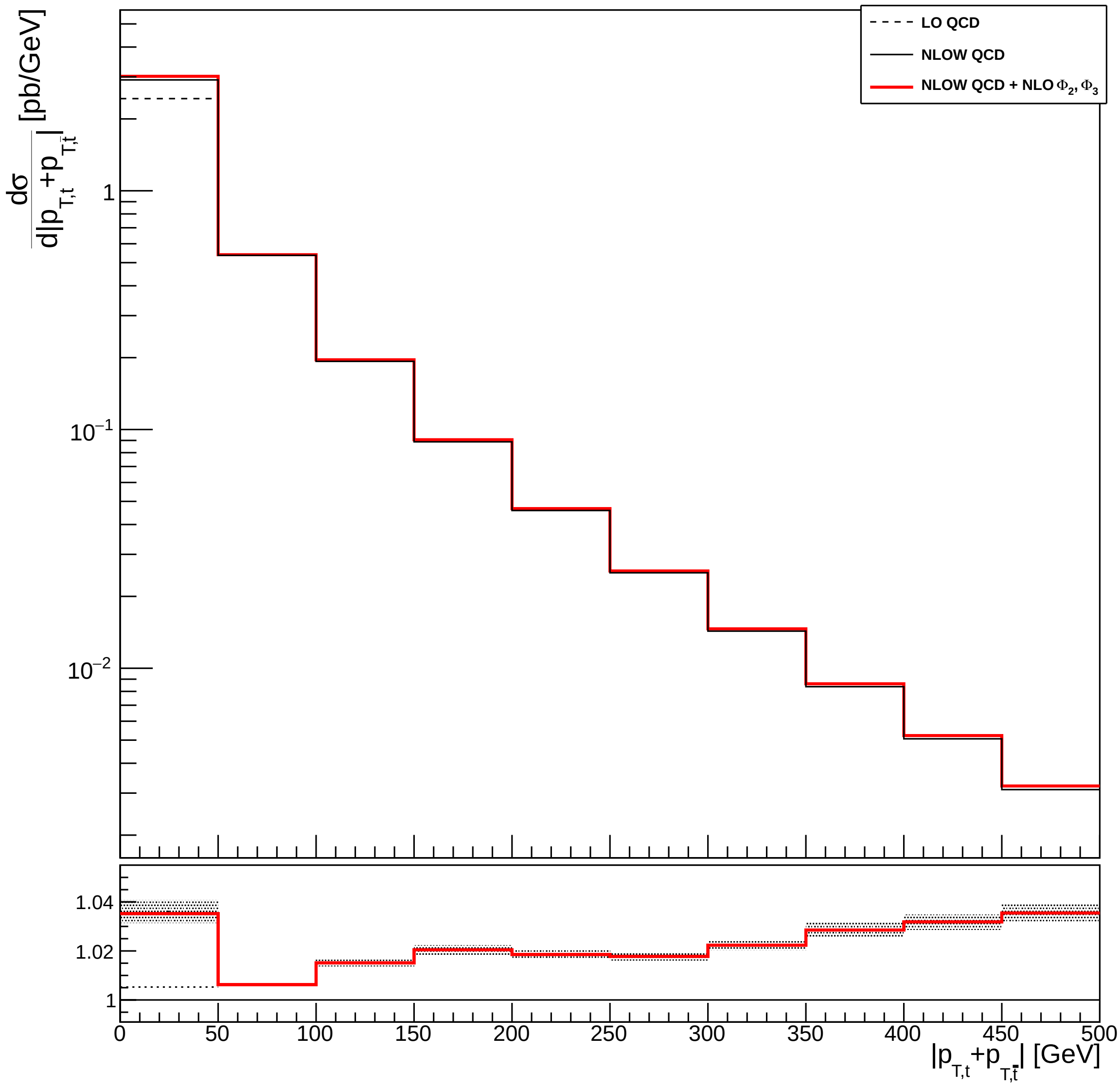

Figure 3.19. – *Transverse momentum distribution of the top + antitop system for $pp \to t\bar{t}$ including the effects of two neutral Higgs bosons (2HDM **scenario 1**, see 3.7.1) at NLO QCD. The hadronic center-of-mass energy is $\sqrt{s_{\rm had}} = 8$ TeV, renormalization and factorization scales are set to $\mu = \mu_0 = 265$ GeV, c.f. (3.115). The lower pane shows the ratios $d\sigma^{\rm NLO(W)}_{QCD+\phi_2,\phi_3}/d\sigma^{\rm NLOW}_{QCD}$ (thick line) and $d\sigma^{\rm LO}_{QCD+\phi_2,\phi_3}/d\sigma^{\rm LO}_{QCD}$ (dotted line). The effect of scale variation in the interval $[\frac{\mu_0}{2}, 2\mu_0]$ for the NLO(W) ratio is indicated by the shaded rectangles.*

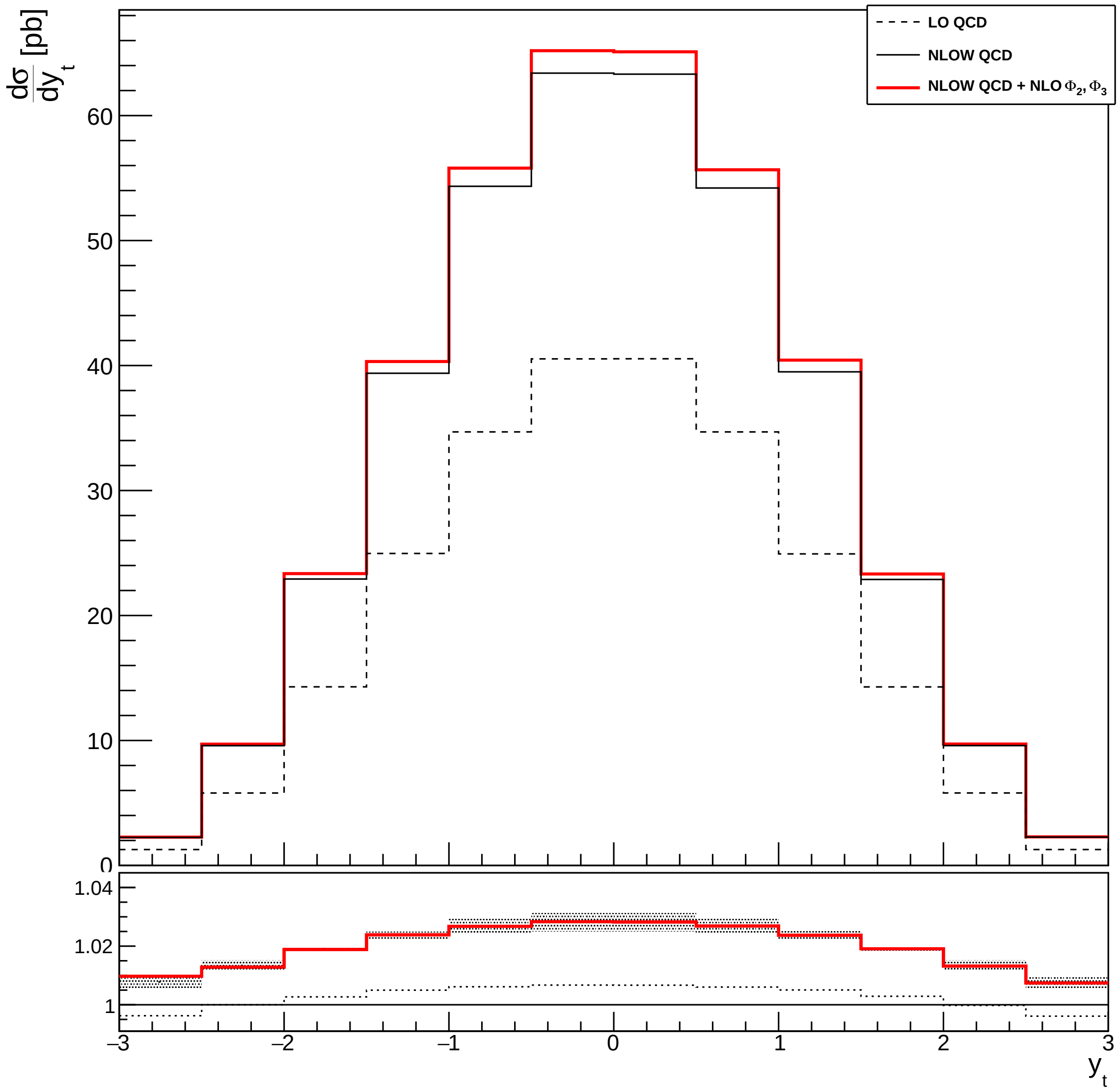

Figure 3.20. – *Top rapidity distribution for $pp \to t\bar{t}$ including the effects of two neutral Higgs bosons (2HDM* ***scenario 1****, see 3.7.1) at NLO QCD. The hadronic center-of-mass energy is $\sqrt{s_{\rm had}} = 8$ TeV, renormalization and factorization scales are set to $\mu = \mu_0 = 265$ GeV, c.f. (3.115). The lower pane shows the ratios $d\sigma^{\rm NLO(W)}_{QCD+\phi_2,\phi_3}/d\sigma^{\rm NLOW}_{QCD}$ (thick line) and $d\sigma^{\rm LO}_{QCD+\phi_2,\phi_3}/d\sigma^{\rm LO}_{QCD}$ (dotted line). The effect of scale variation in the interval $[\frac{\mu_0}{2}, 2\mu_0]$ for the NLO(W) ratio is indicated by the shaded rectangles.*

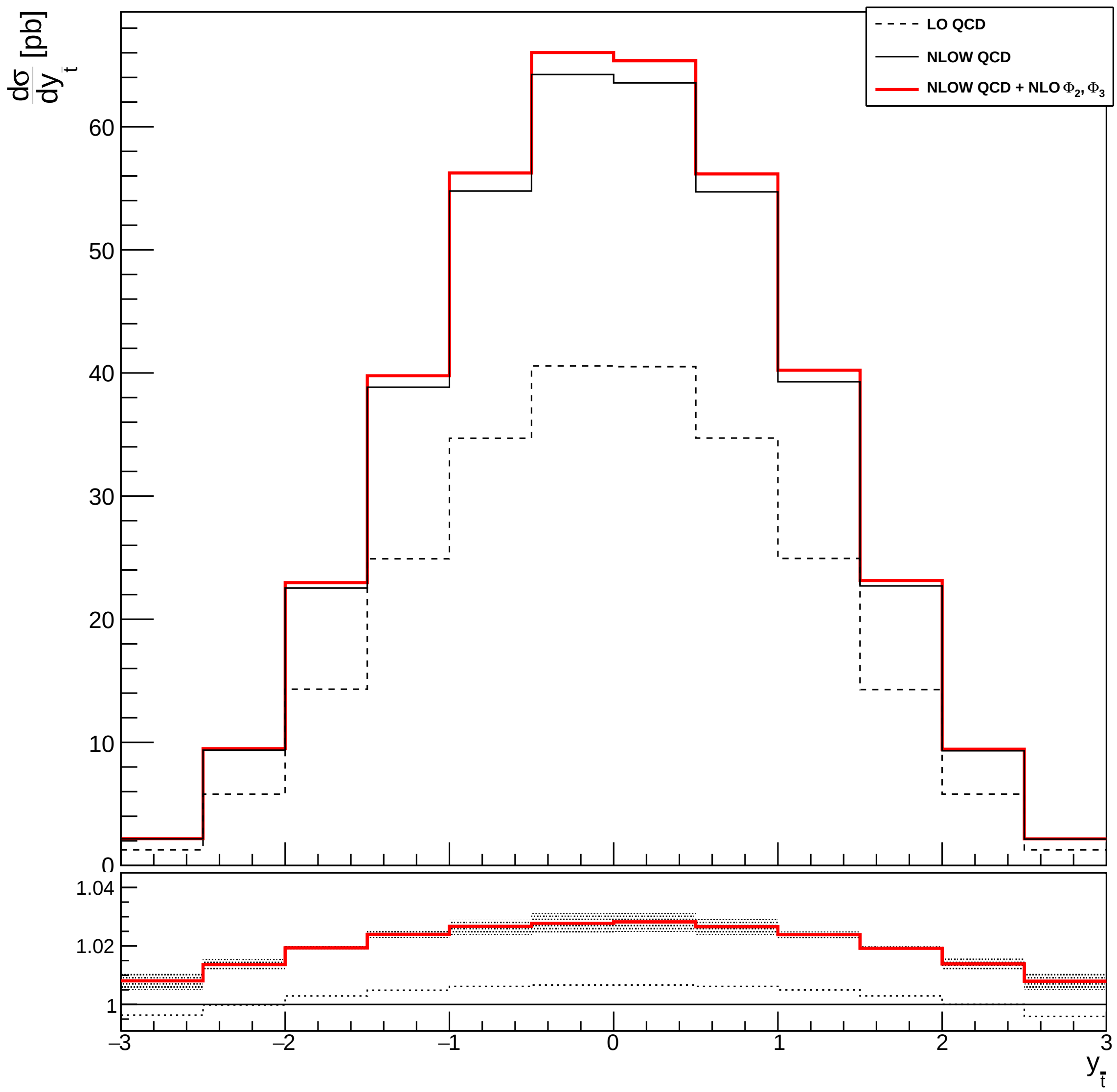

Figure 3.21. – *Antitop rapidity distribution for pp $\to t\bar{t}$ including the effects of two neutral Higgs bosons (2HDM* ***scenario 1****, see 3.7.1) at NLO QCD. The hadronic center-of-mass energy is $\sqrt{s_{\mathrm{had}}} = 8$ TeV, renormalization and factorization scales are set to $\mu = \mu_0 = 265$ GeV, c.f. (3.115). The lower pane shows the ratios $d\sigma^{\mathrm{NLO(W)}}_{QCD+\phi_2,\phi_3}/d\sigma^{\mathrm{NLOW}}_{QCD}$ (thick line) and $d\sigma^{\mathrm{LO}}_{QCD+\phi_2,\phi_3}/d\sigma^{\mathrm{LO}}_{QCD}$ (dotted line). The effect of scale variation in the interval $\left[\frac{\mu_0}{2}, 2\mu_0\right]$ for the NLO(W) ratio is indicated by the shaded rectangles.*

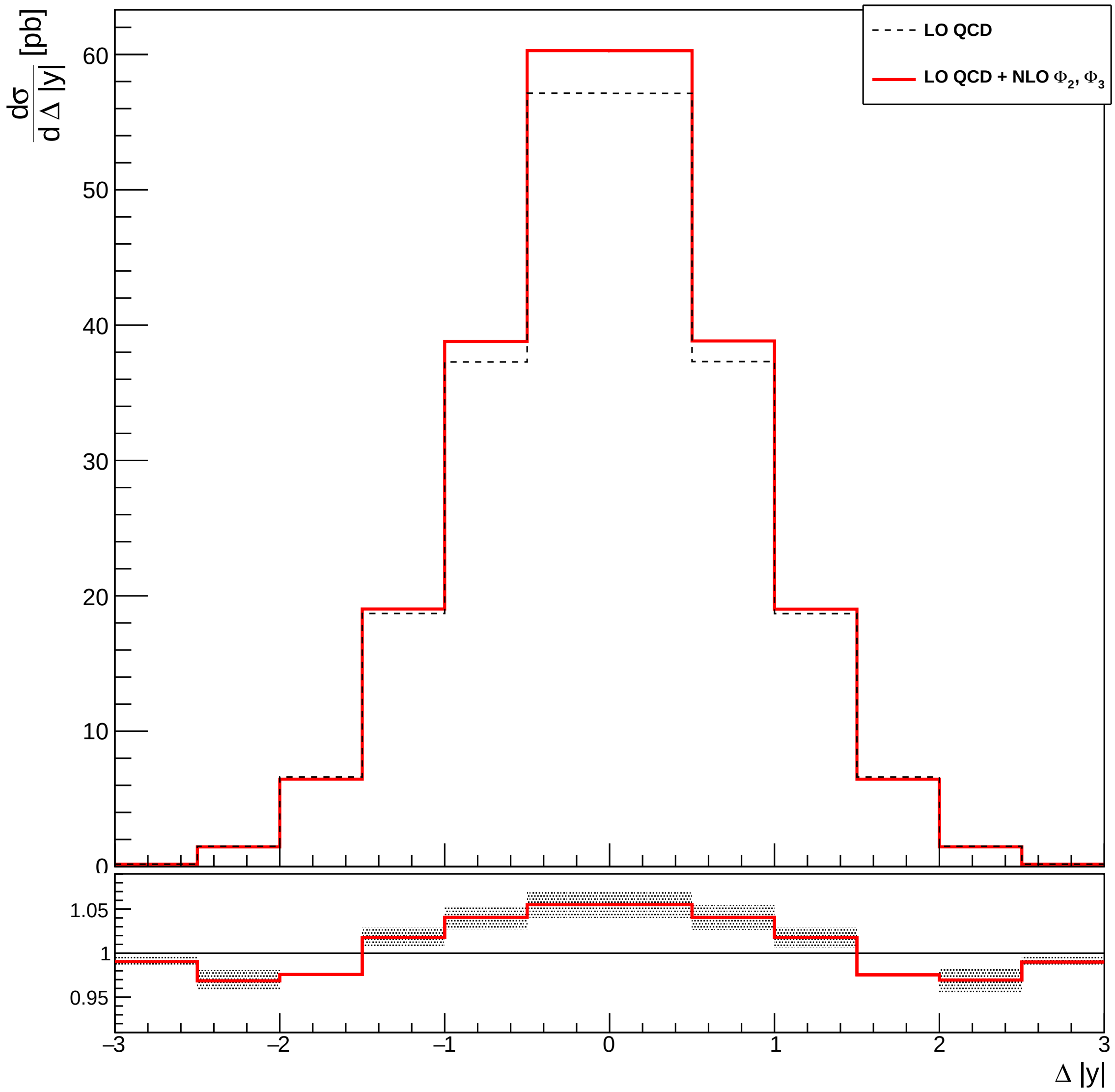

Figure 3.22. – *Distribution of top and antitop rapidity difference for $pp \to t\bar{t}$ including the effects of two neutral Higgs bosons (2HDM* ***scenario 1****, see 3.7.1). The hadronic center-of-mass energy is $\sqrt{s_{\mathrm{had}}} = 8$ TeV, renormalization and factorization scales are set to $\mu = \mu_0 = 265$ GeV, c.f. (3.115). Note that for this distribution the non-resonant QCD processes are computed only at LO, whereas the resonant processes and the interference with the background contain the NLO corrections. The figure shows that there is no significant contribution to the charge asymmetry $A_C^{\Delta|y|}$ at the LHC from the resonant processes.*

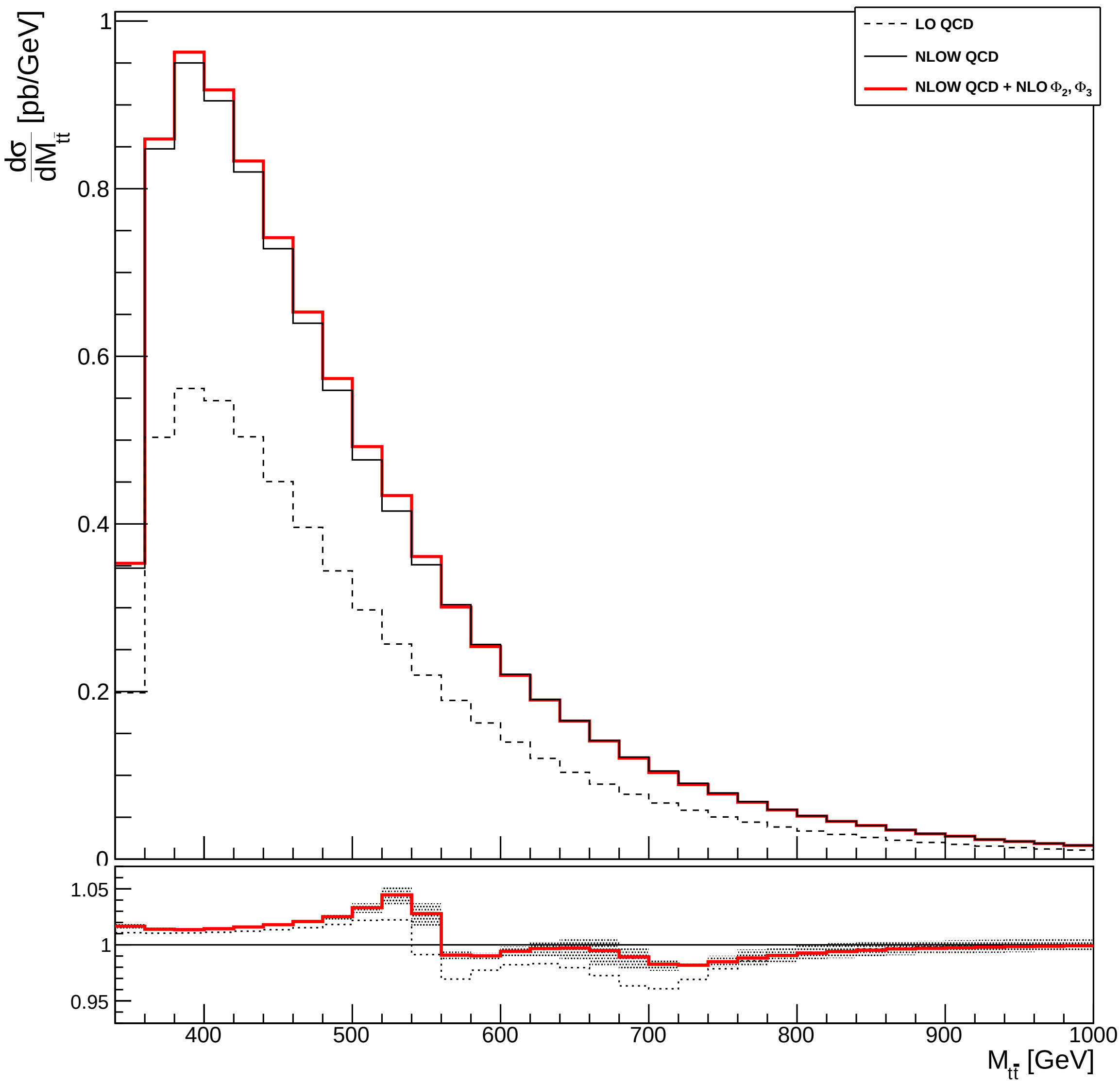

Figure 3.23. – *Top-/Antitop invariant mass distribution for* $pp \to t\bar{t}$ *including the effects of two neutral Higgs bosons (2HDM* ***scenario 2****, see 3.7.1) at NLO QCD. The hadronic center-of-mass energy is* $\sqrt{s_{\text{had}}} = 8$ *TeV, renormalization and factorization scales are set to* $\mu = \mu_0 =$ 312.5 *GeV, c.f. (3.115). The lower pane shows the ratios* $d\sigma^{\text{NLO(W)}}_{QCD+\phi_2,\phi_3}/d\sigma^{\text{NLOW}}_{QCD}$ *(thick line) and* $d\sigma^{\text{LO}}_{QCD+\phi_2,\phi_3}/d\sigma^{\text{LO}}_{QCD}$ *(dotted line). The effect of scale variation in the interval* $[\frac{\mu_0}{2}, 2\mu_0]$ *for the NLO(W) ratio is indicated by the shaded rectangles.*

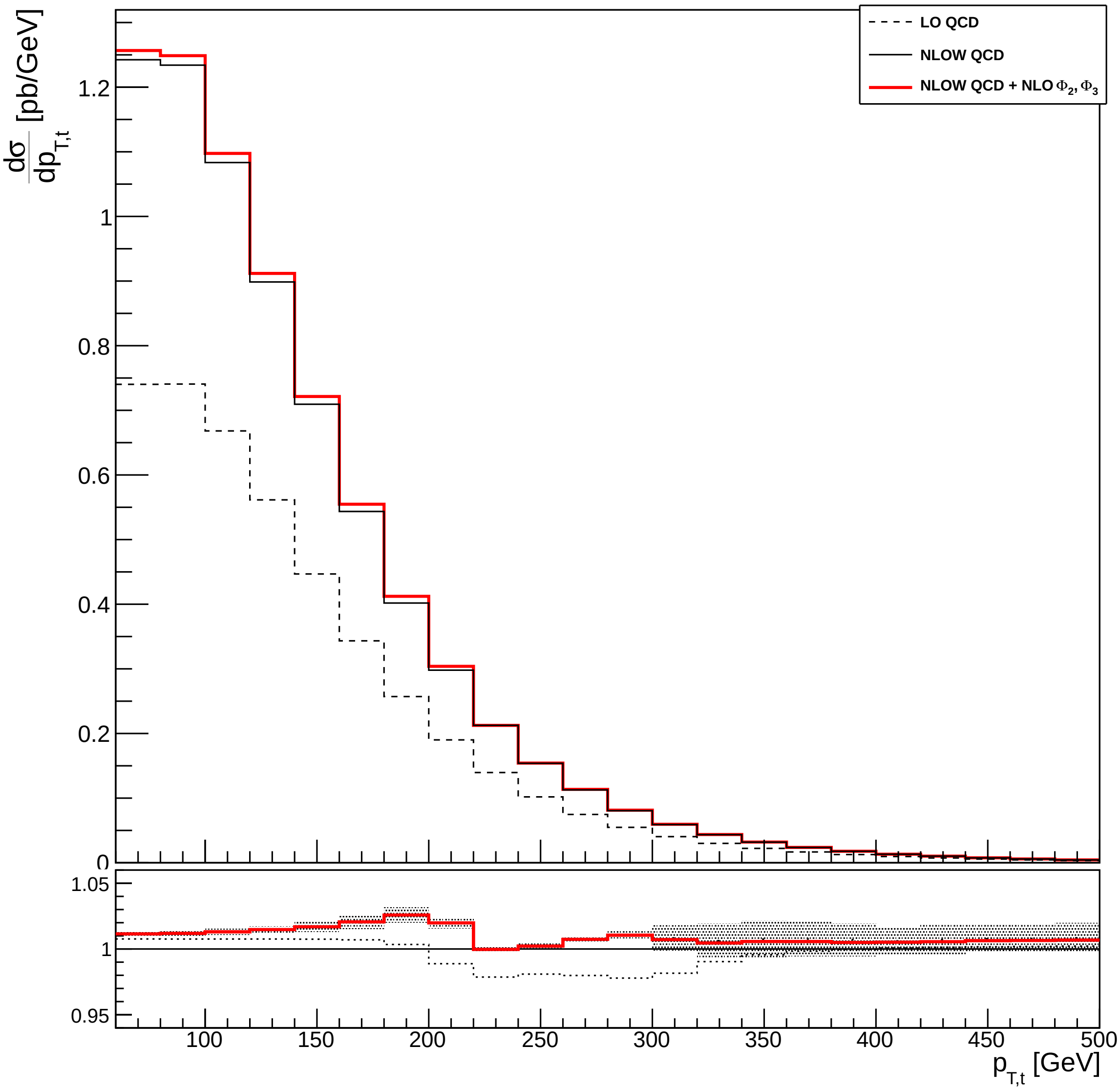

Figure 3.24. – *Top transverse momentum distribution for $pp \to t\bar{t}$ including the effects of two neutral Higgs bosons (2HDM **scenario 2**, see 3.7.1) at NLO QCD. The hadronic center-of-mass energy is $\sqrt{s_{\text{had}}} = 8$ TeV, renormalization and factorization scales are set to $\mu = \mu_0 =$ 312.5 GeV, c.f. (3.115). The lower pane shows the ratios $d\sigma^{\text{NLO(W)}}_{QCD+\phi_2,\phi_3}/d\sigma^{\text{NLOW}}_{QCD}$ (thick line) and $d\sigma^{\text{LO}}_{QCD+\phi_2,\phi_3}/d\sigma^{\text{LO}}_{QCD}$ (dotted line). The effect of scale variation in the interval $[\frac{\mu_0}{2}, 2\mu_0]$ for the NLO(W) ratio is indicated by the shaded rectangles.*

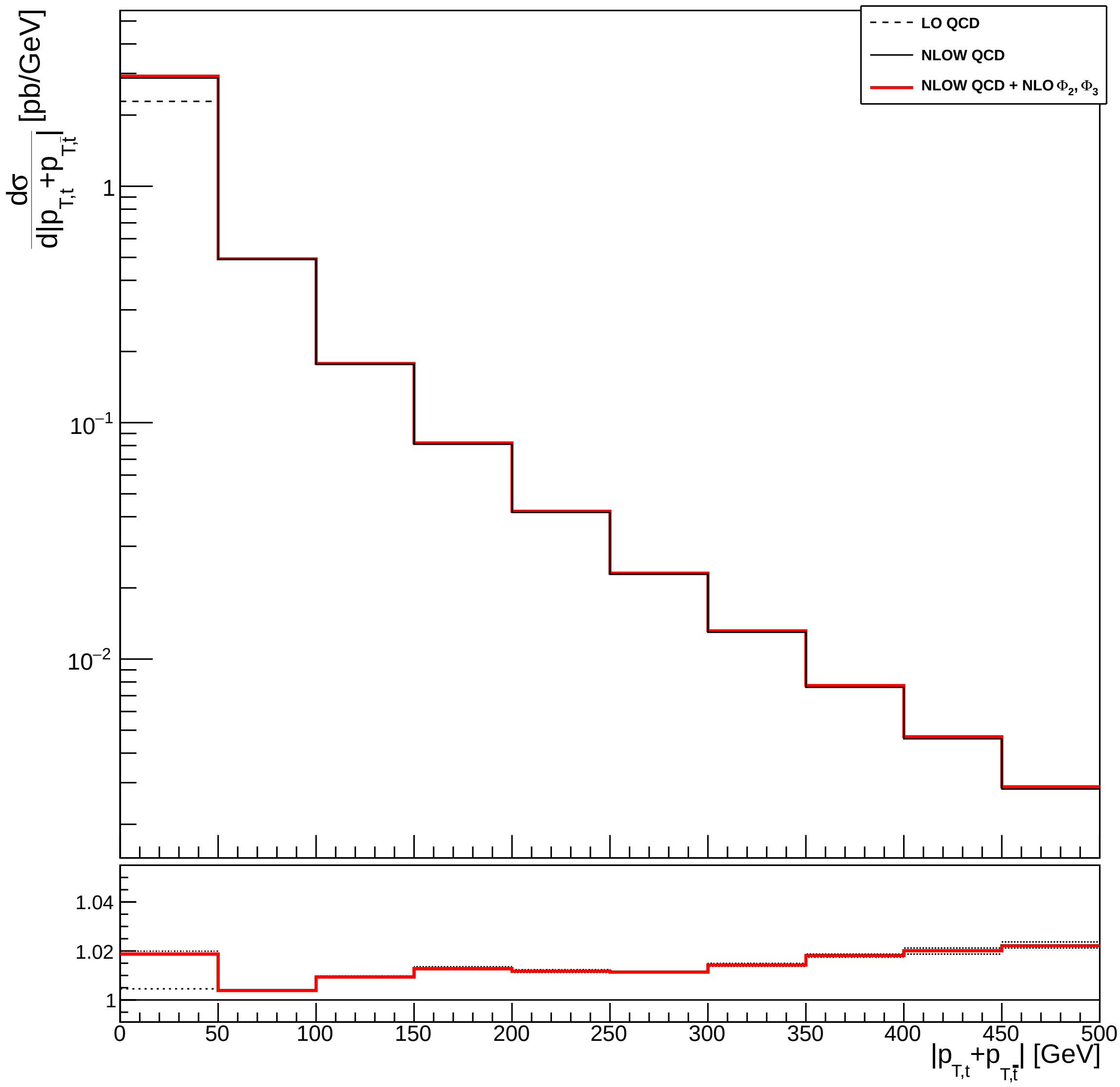

Figure 3.25. – *Transverse momentum distribution of the top + antitop system for $pp \to t\bar{t}$ including the effects of two neutral Higgs bosons (2HDM* ***scenario 2****, see 3.7.1) at NLO QCD. The hadronic center-of-mass energy is $\sqrt{s_{\rm had}} = 8$ TeV, renormalization and factorization scales are set to $\mu = \mu_0 = 312.5$ GeV, c.f. (3.115). The lower pane shows the ratios $d\sigma^{\rm NLO(W)}_{QCD+\phi_2,\phi_3}/d\sigma^{\rm NLOW}_{QCD}$ (thick line) and $d\sigma^{\rm LO}_{QCD+\phi_2,\phi_3}/d\sigma^{\rm LO}_{QCD}$ (dotted line). The effect of scale variation in the interval $[\frac{\mu_0}{2}, 2\mu_0]$ for the NLO(W) ratio is indicated by the shaded rectangles.*

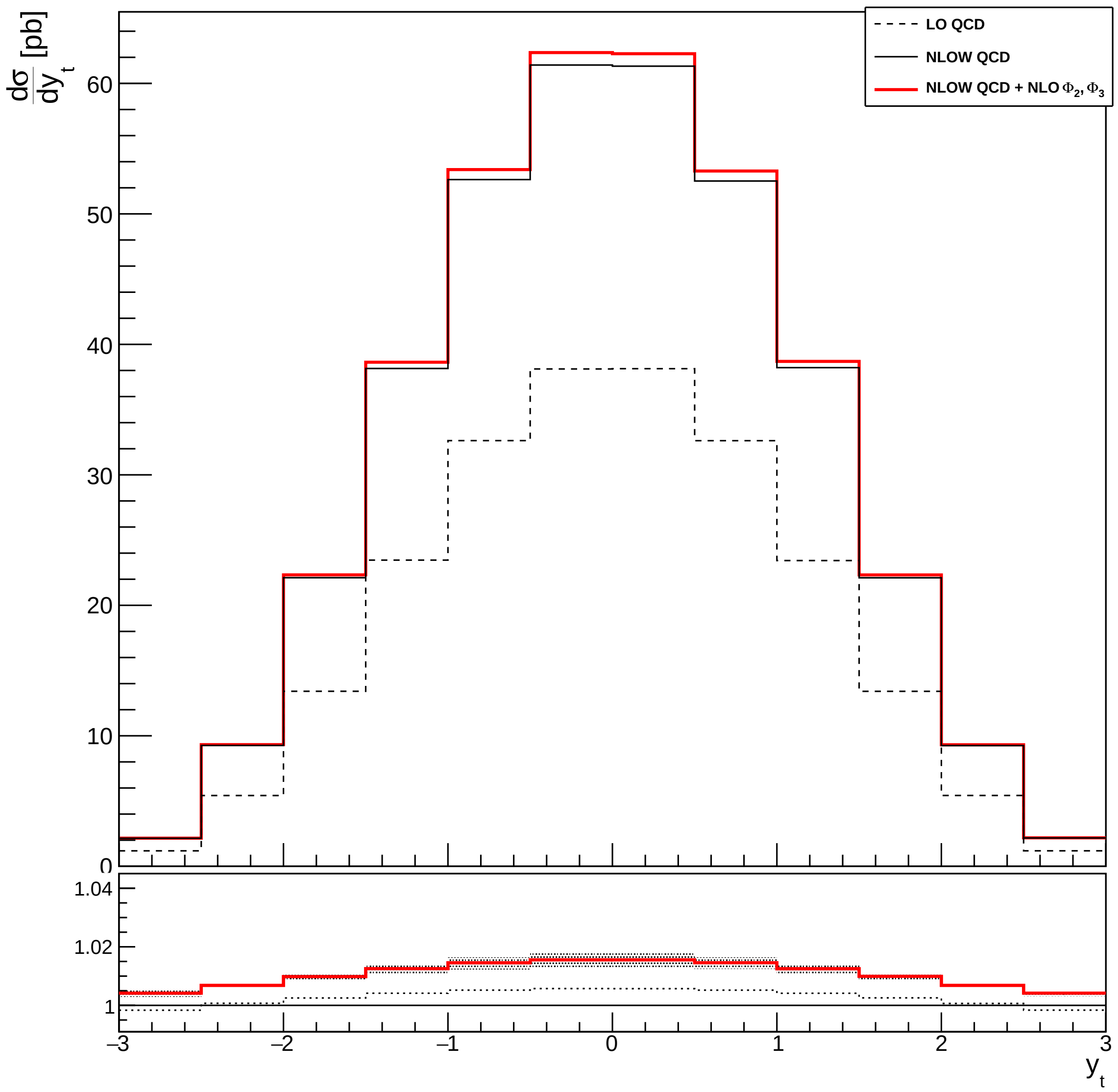

Figure 3.26. – *Top rapidity distribution for $pp \to t\bar{t}$ including the effects of two neutral Higgs bosons (2HDM* ***scenario 2****, see 3.7.1) at NLO QCD. The hadronic center-of-mass energy is $\sqrt{s_{\text{had}}} = 8$ TeV, renormalization and factorizaion scales are set to $\mu = \mu_0 = 312.5$ GeV, c.f. (3.115). The lower pane shows the ratios $d\sigma^{\text{NLO(W)}}_{QCD+\phi_2,\phi_3}/d\sigma^{\text{NLOW}}_{QCD}$ (thick line) and $d\sigma^{\text{LO}}_{QCD+\phi_2,\phi_3}/d\sigma^{\text{LO}}_{QCD}$ (dotted line). The effect of scale variation in the interval $[\frac{\mu_0}{2}, 2\mu_0]$ for the NLO(W) ratio is indicated by the shaded rectangles.*

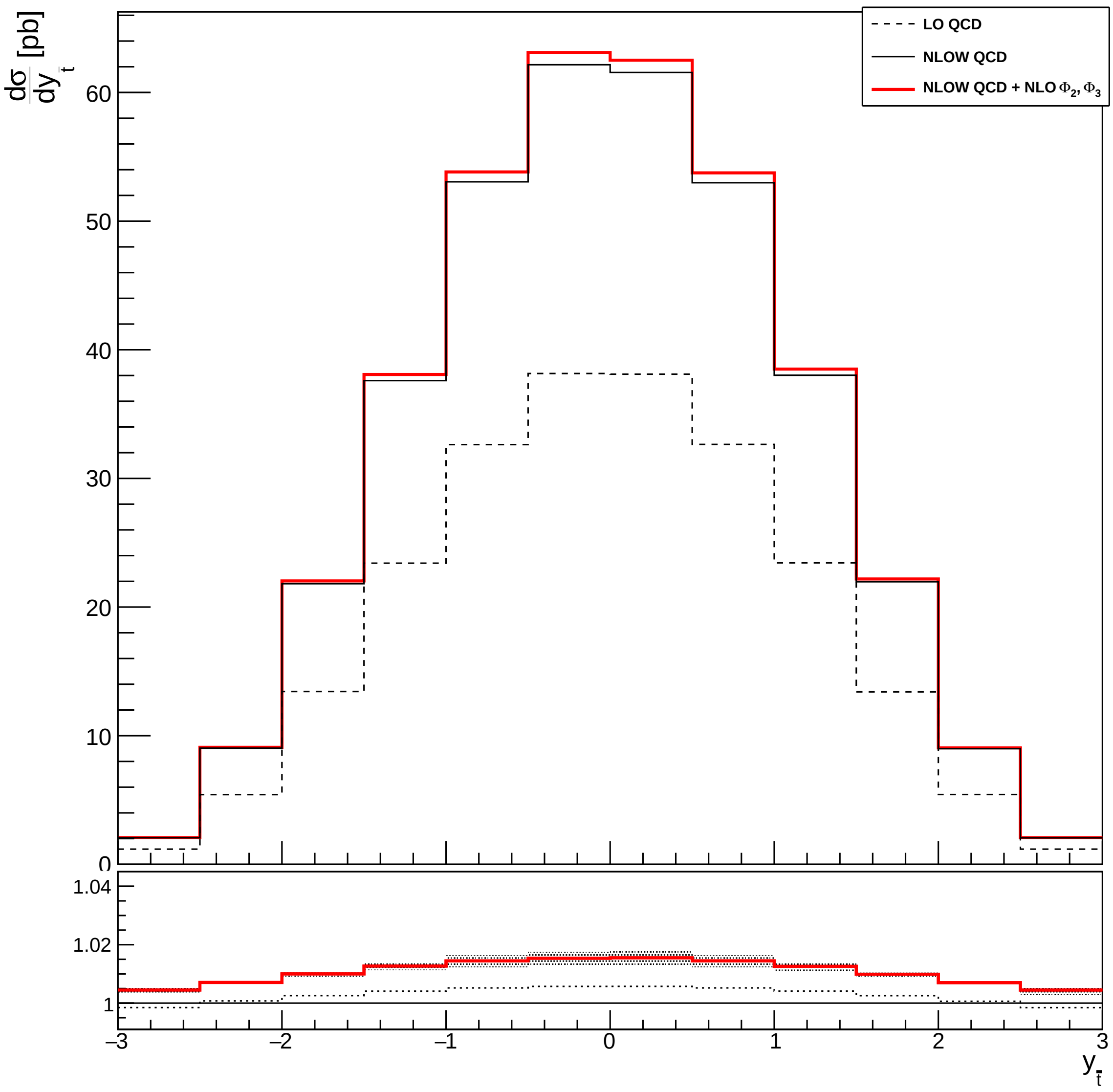

Figure 3.27. – *Antitop rapidity distribution for $pp \to t\bar{t}$ including the effects of two neutral Higgs bosons (2HDM **scenario 2**, see 3.7.1) at NLO QCD. The hadronic center-of-mass energy is $\sqrt{s_{\rm had}} = 8$ TeV, renormalization and factorization scales are set to $\mu = \mu_0 = 312.5$ GeV, c.f. (3.115). The lower pane shows the ratios $d\sigma^{\rm NLO(W)}_{QCD+\phi_2,\phi_3}/d\sigma^{\rm NLOW}_{QCD}$ (thick line) and $d\sigma^{\rm LO}_{QCD+\phi_2,\phi_3}/d\sigma^{\rm LO}_{QCD}$ (dotted line). The effect of scale variation in the interval $[\frac{\mu_0}{2}, 2\mu_0]$ for the NLO(W) ratio is indicated by the shaded rectangles.*

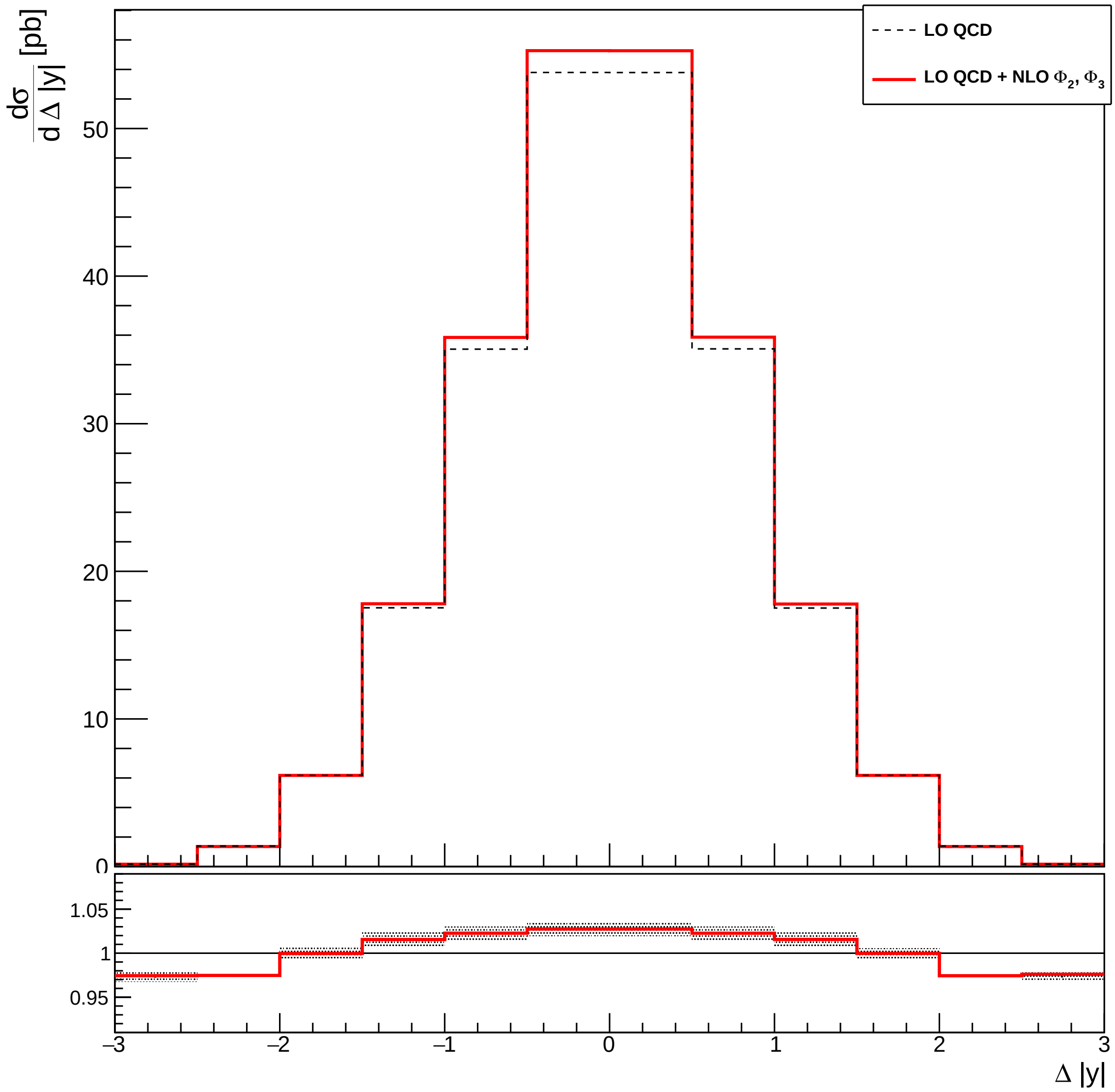

Figure 3.28. – *Distribution of top and antitop rapidity difference for* $pp \to t\bar{t}$ *including the effects of two neutral Higgs bosons (2HDM* ***scenario 2****, see 3.7.1). The hadronic center-of-mass energy is* $\sqrt{s_{\rm had}} = 8$ *TeV, renormalization and factorization scales are set to* $\mu = \mu_0 = 312.5$ *GeV, c.f. (3.115). Note that for this distribution the non-resonant QCD processes are computed only at LO, whereas the resonant processes and the interference with the background contain the NLO corrections. The figure shows that there is no significant contribution to the charge asymmetry* $A_C^{\Delta|y|}$ *at the LHC from the resonant processes.*

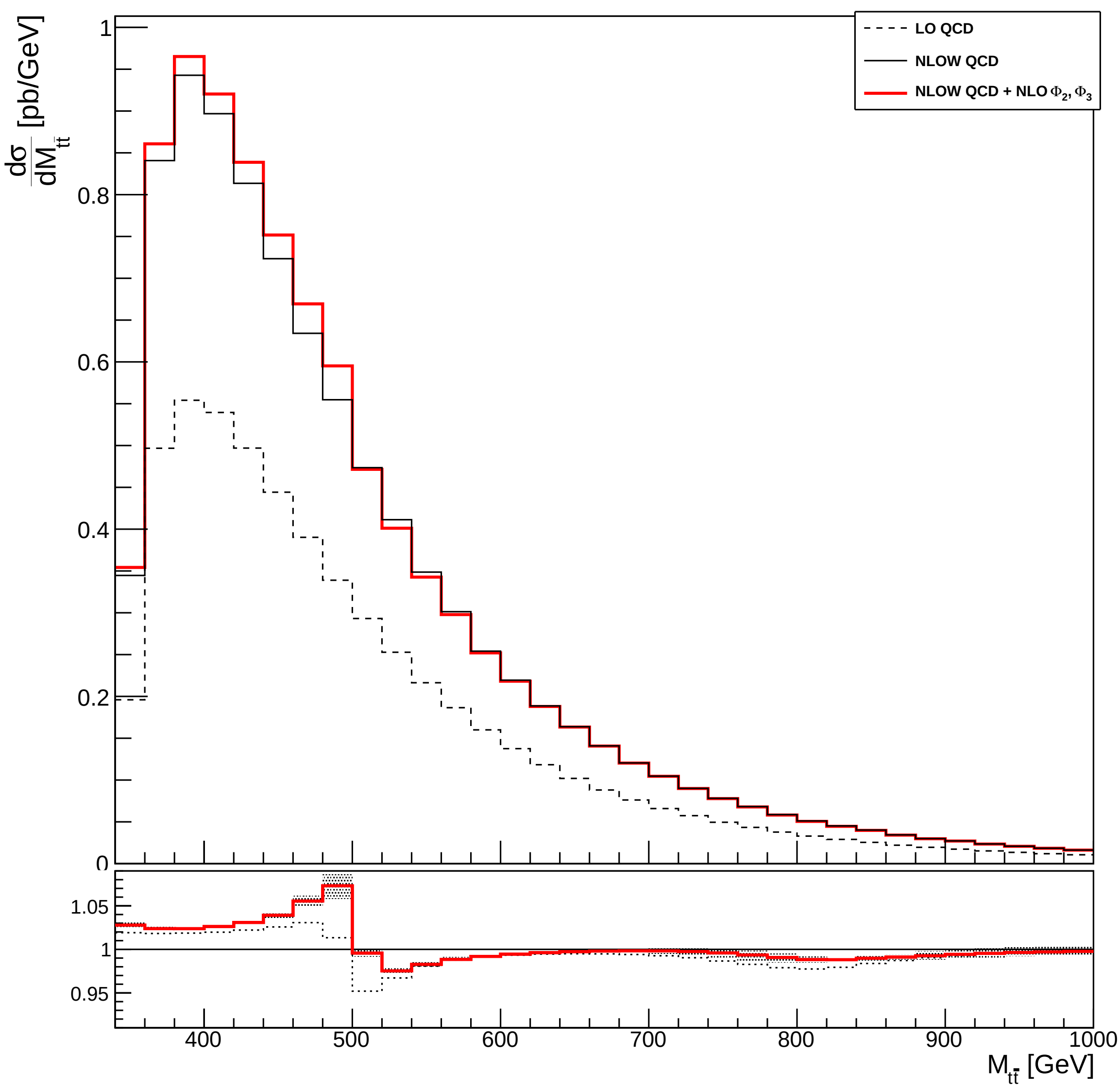

Figure 3.29. – *Top-/Antitop invariant mass distribution for* $pp \to t\bar{t}$ *including the effects of two neutral Higgs bosons (2HDM* ***scenario 3****, see 3.7.1) at NLO QCD. The hadronic center-of-mass energy is* $\sqrt{s_{\text{had}}} = 8$ *TeV, renormalization and factorization scales are set to* $\mu = \mu_0 =$ 325 *GeV, c.f. (3.115). The lower pane shows the ratios* $d\sigma^{\text{NLO(W)}}_{QCD+\phi_2,\phi_3}/d\sigma^{\text{NLOW}}_{QCD}$ *(thick line) and* $d\sigma^{\text{LO}}_{QCD+\phi_2,\phi_3}/d\sigma^{\text{LO}}_{QCD}$ *(dotted line). The effect of scale variation in the interval* $[\frac{\mu_0}{2}, 2\mu_0]$ *for the NLO(W) ratio is indicated by the shaded rectangles.*

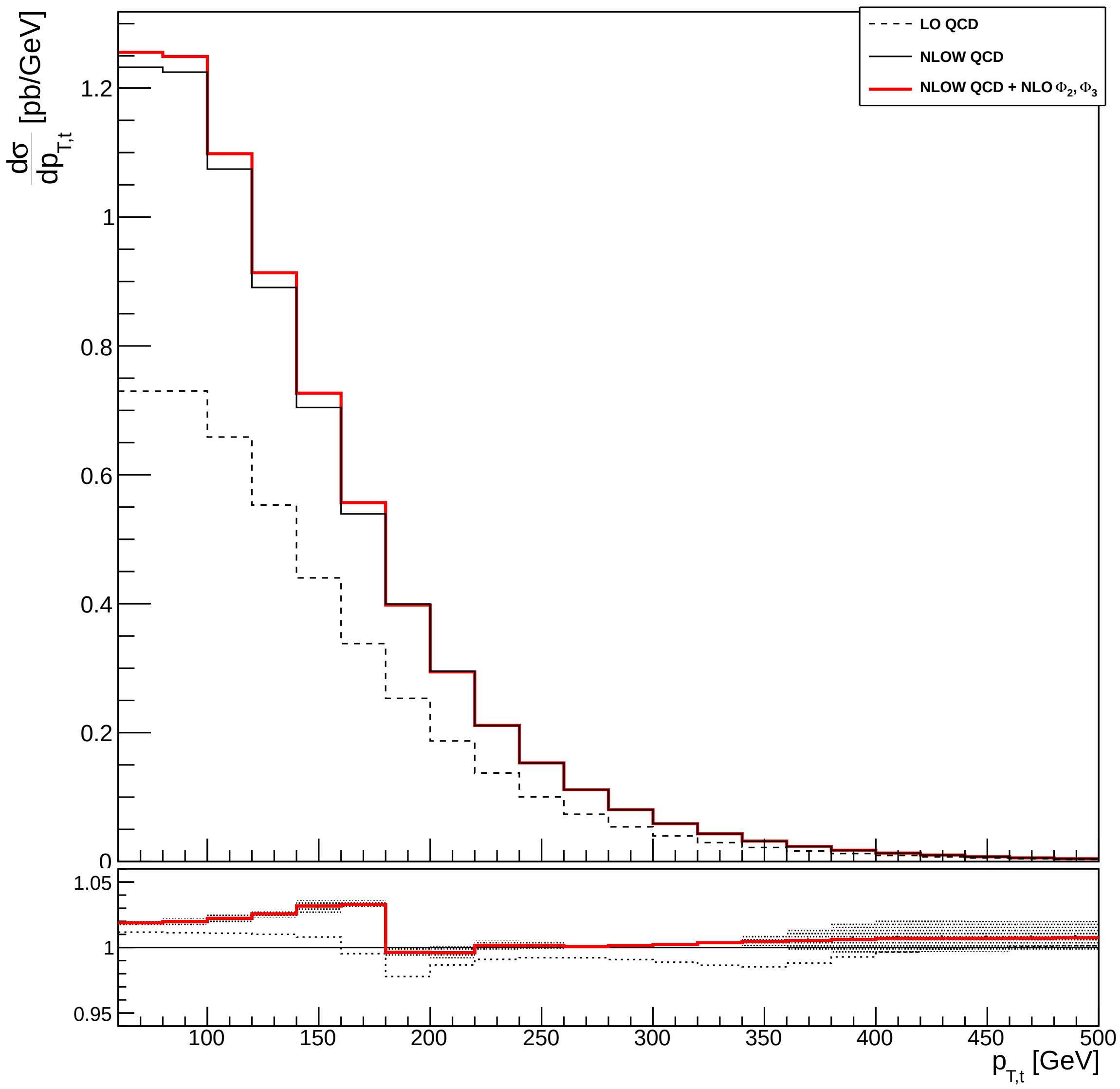

Figure 3.30. – *Top transverse momentum distribution for $pp \to t\bar{t}$ including the effects of two neutral Higgs bosons (2HDM **scenario 3**, see 3.7.1) at NLO QCD. The hadronic center-of-mass energy is $\sqrt{s_{\text{had}}} = 8$ TeV, renormalization and factorization scales are set to $\mu = \mu_0 = 325$ GeV, c.f. (3.115). The lower pane shows the ratios $d\sigma^{\text{NLO(W)}}_{QCD+\phi_2,\phi_3}/d\sigma^{\text{NLOW}}_{QCD}$ (thick line) and $d\sigma^{\text{LO}}_{QCD+\phi_2,\phi_3}/d\sigma^{\text{LO}}_{QCD}$ (dotted line). The effect of scale variation in the interval $[\frac{\mu_0}{2}, 2\mu_0]$ for the NLO(W) ratio is indicated by the shaded rectangles.*

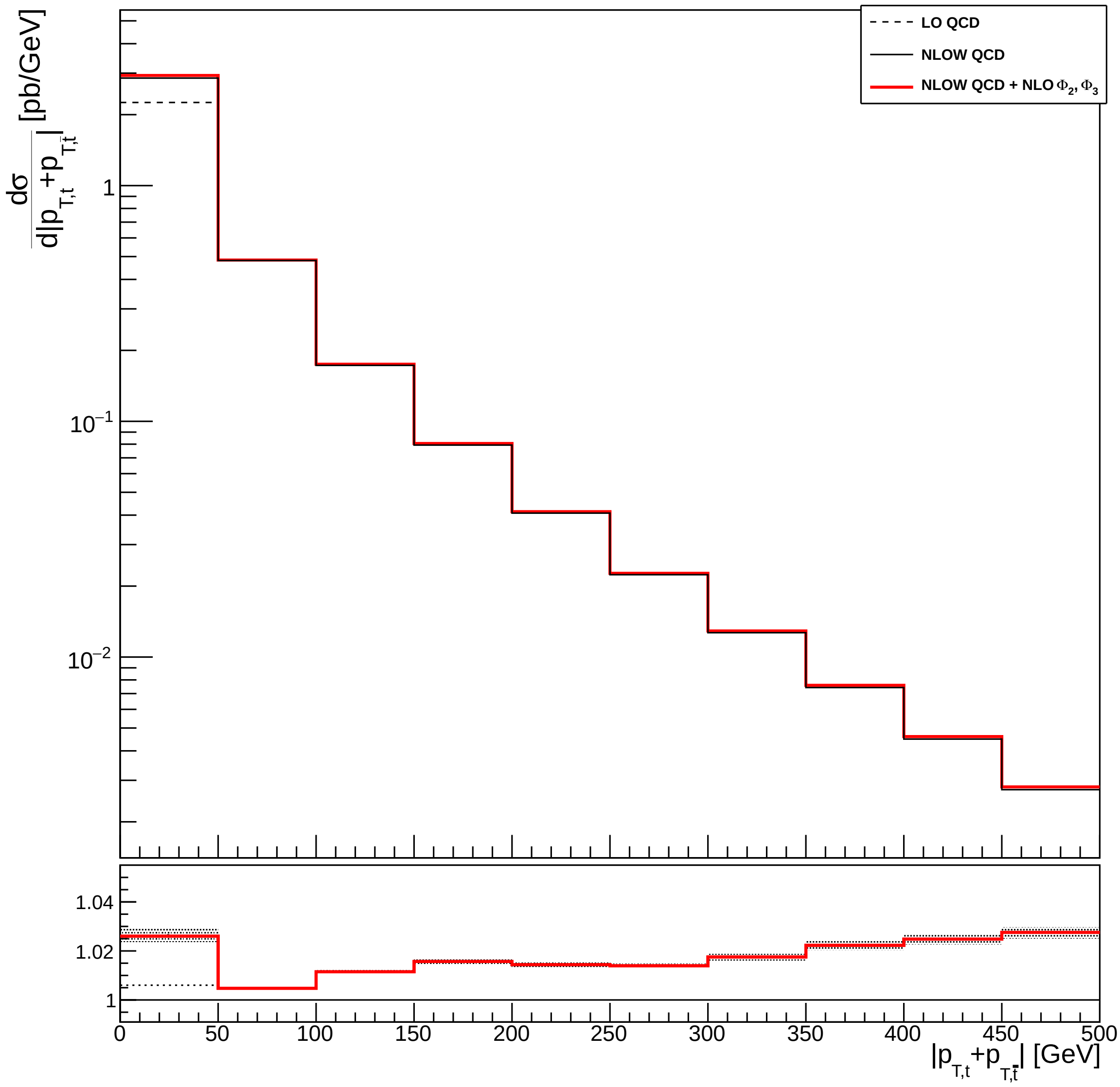

Figure 3.31. – *Transverse momentum distribution of the top + antitop system for $pp \to t\bar{t}$ including the effects of two neutral Higgs bosons (2HDM **scenario 3**, see 3.7.1) at NLO QCD. The hadronic center-of-mass energy is $\sqrt{s_{\text{had}}} = 8$ TeV, renormalization and factorization scales are set to $\mu = \mu_0 = 325$ GeV, c.f. (3.115). The lower pane shows the ratios $d\sigma^{\text{NLO(W)}}_{QCD+\phi_2,\phi_3}/d\sigma^{\text{NLOW}}_{QCD}$ (thick line) and $d\sigma^{\text{LO}}_{QCD+\phi_2,\phi_3}/d\sigma^{\text{LO}}_{QCD}$ (dotted line). The effect of scale variation in the interval $[\frac{\mu_0}{2}, 2\mu_0]$ for the NLO(W) ratio is indicated by the shaded rectangles.*

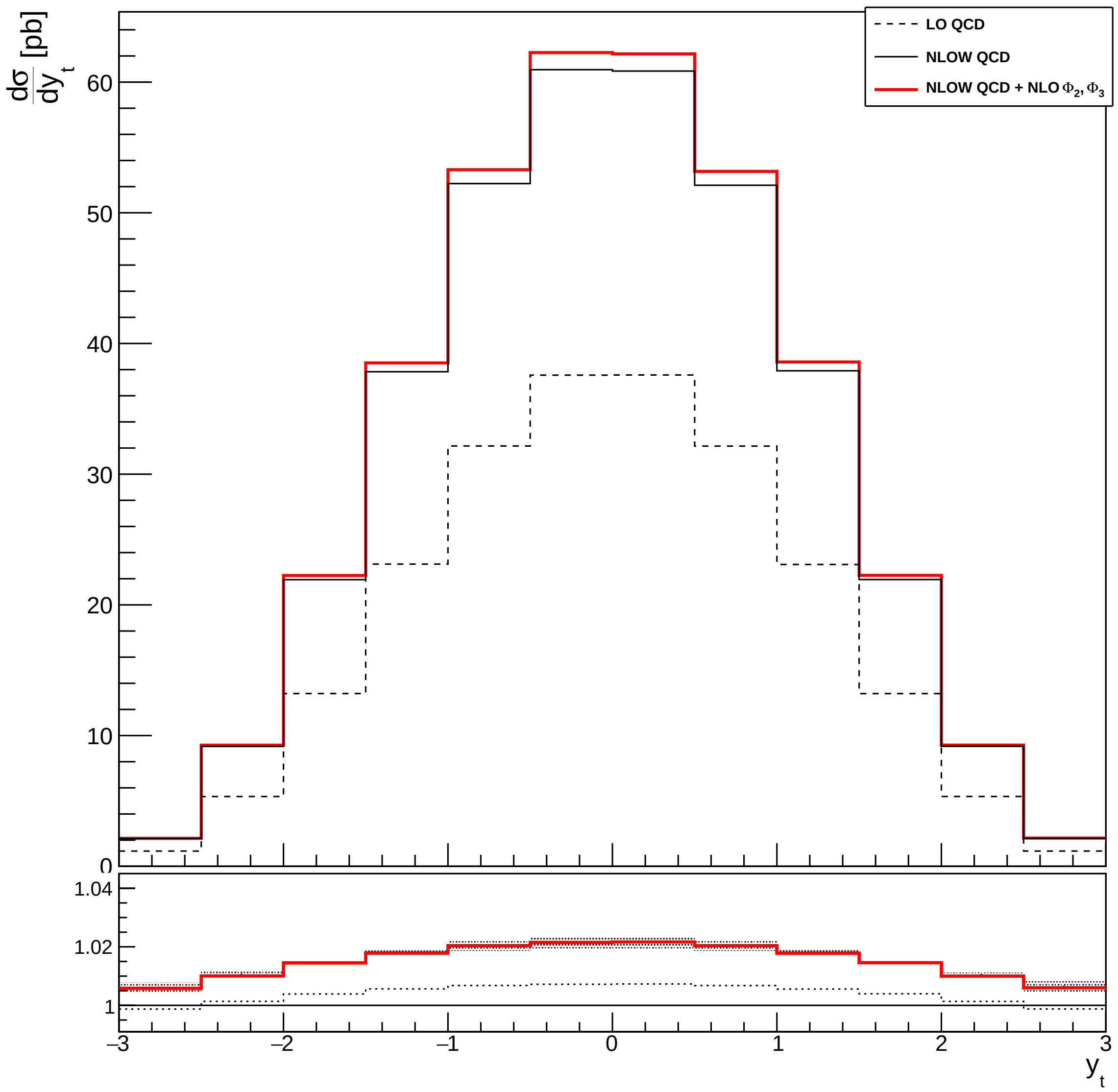

Figure 3.32. – *Top rapidity distribution for* $pp \to t\bar{t}$ *including the effects of two neutral Higgs bosons (2HDM* ***scenario 3****, see 3.7.1) at NLO QCD. The hadronic center-of-mass energy is* $\sqrt{s_{\text{had}}} = 8$ *TeV, renormalization and factorization scales are set to* $\mu = \mu_0 = 325$ *GeV, c.f. (3.115). The lower pane shows the ratios* $d\sigma^{\text{NLO(W)}}_{QCD+\phi_2,\phi_3}/d\sigma^{\text{NLOW}}_{QCD}$ *(thick line) and* $d\sigma^{\text{LO}}_{QCD+\phi_2,\phi_3}/d\sigma^{\text{LO}}_{QCD}$ *(dotted line). The effect of scale variation in the interval* $[\frac{\mu_0}{2}, 2\mu_0]$ *for the NLO(W) ratio is indicated by the shaded rectangles.*

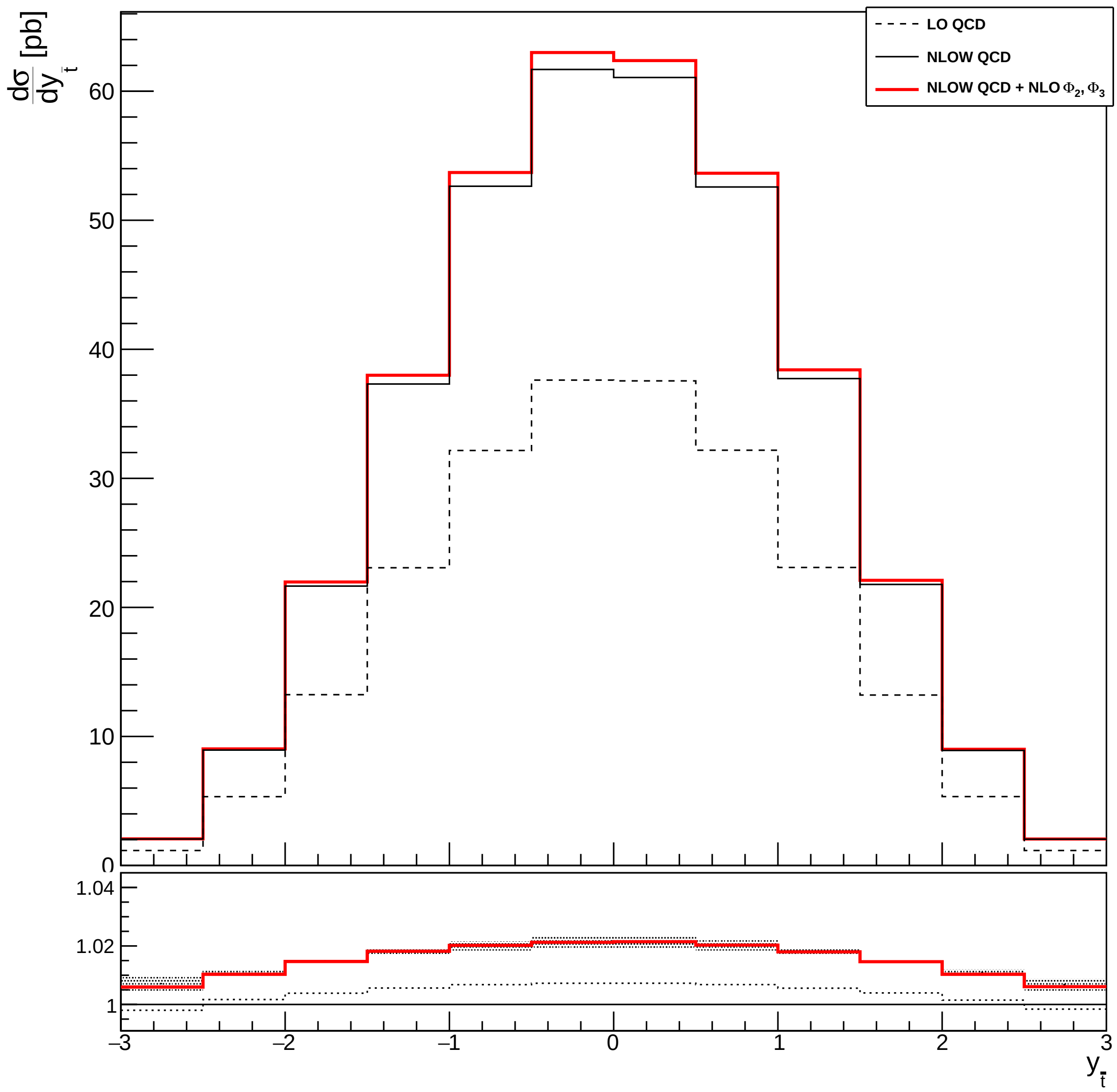

Figure 3.33. – *Antitop rapidity distribution for $pp \to t\bar{t}$ including the effects of two neutral Higgs bosons (2HDM **scenario 3**, see 3.7.1) at NLO QCD. The hadronic center-of-mass energy is $\sqrt{s_{\mathrm{had}}} = 8$ TeV, renormalization and factorization scales are set to $\mu = \mu_0 = 325$ GeV, c.f. (3.115). The lower pane shows the ratios $d\sigma^{\mathrm{NLO(W)}}_{QCD+\phi_2,\phi_3}/d\sigma^{\mathrm{NLOW}}_{QCD}$ (thick line) and $d\sigma^{\mathrm{LO}}_{QCD+\phi_2,\phi_3}/d\sigma^{\mathrm{LO}}_{QCD}$ (dotted line). The effect of scale variation in the interval $[\frac{\mu_0}{2}, 2\mu_0]$ for the NLO(W) ratio is indicated by the shaded rectangles.*

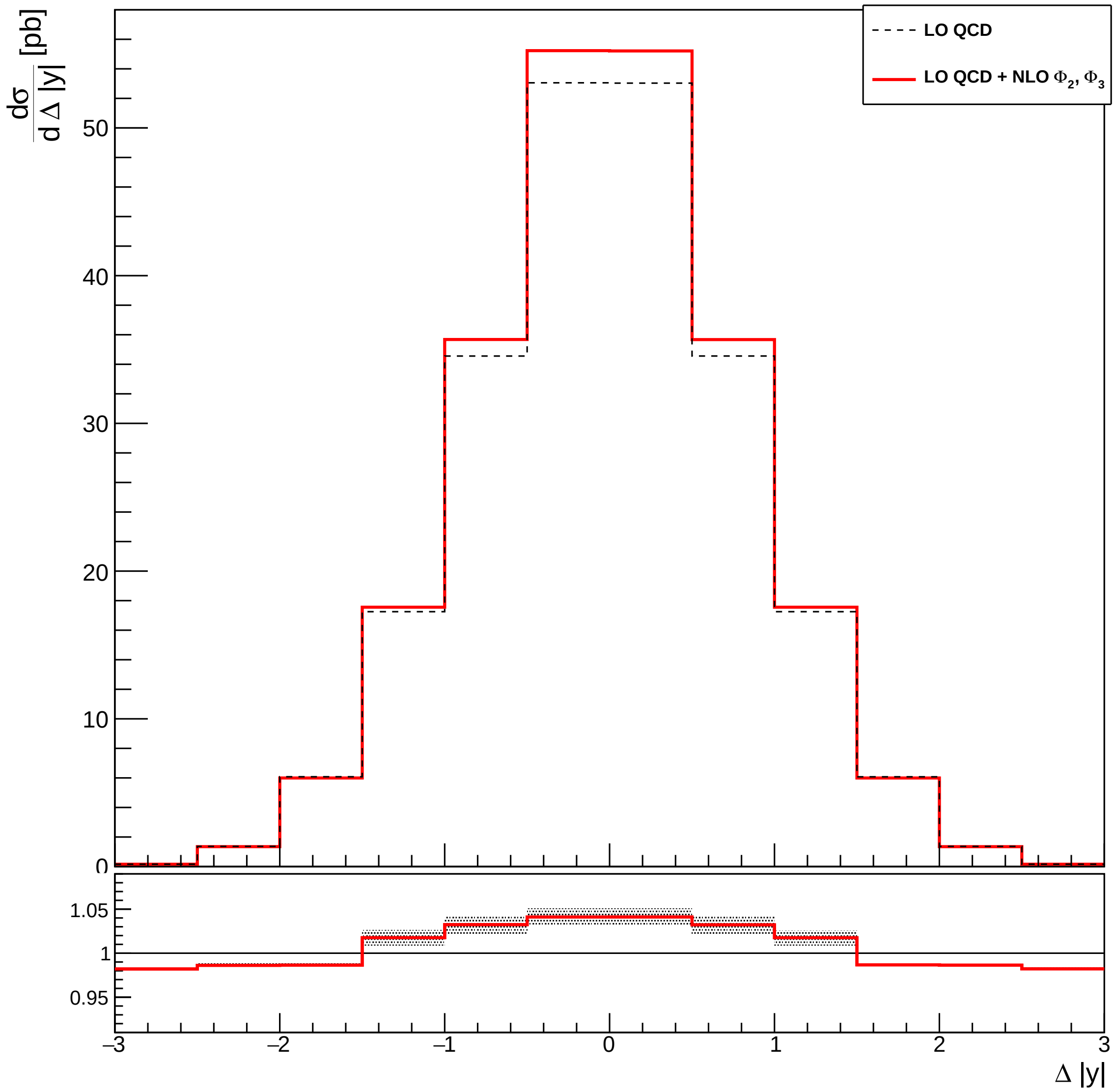

Figure 3.34. – *Distribution of top and antitop rapidity difference for $pp \to t\bar{t}$ including the effects of two neutral Higgs bosons (2HDM **scenario 3**, see 3.7.1). The hadronic center-of-mass energy is $\sqrt{s_{\text{had}}} = 8$ TeV, renormalization and factorization scales are set to $\mu = \mu_0 = 325$ GeV, c.f. (3.115). Note that for this distribution the non-resonant QCD processes are computed only at LO, whereas the resonant processes and the interference with the background contain the NLO corrections. The figure shows that there is no significant contribution to the charge asymmetry $A_C^{\Delta|y|}$ at the LHC from the resonant processes.*

3.7.5. LHC 13 TeV

In this section the results for $\sqrt{s_{\text{had}}} = 13$ TeV proton-proton collisions are summarized. The total cross sections for the three 2HDM scenarios are listed in Tab. 3.9. To obtain the signal event numbers in the dilepton and l+jets channel due to the resonant processes we assumed that in the next few years data corresponding to an integrated luminosity of $100\,\text{fb}^{-1}$ will be collected at the LHC (13 TeV) [78]. We further assume that the combined reconstruction and selection efficiencies for these channels are roughly the same as in the $\sqrt{s_{\text{had}}} = 8$ TeV case given in (3.117):

$$\begin{aligned} L &= 100\,\text{fb}^{-1}, \\ \varepsilon_{2l} &= 0.22, \\ \varepsilon_{lj} &= 0.12. \end{aligned} \tag{3.122}$$

The $M_{t\bar{t}}$ spectra in Figs. 3.35, 3.40 and 3.45 are analyzed in the same way as in the last section to estimate the Higgs effects below and above the resonance region. I.e. the ratios given in Tabs. 3.10 and 3.11 are defined analogously to (3.118). Table 3.10 shows that there is only a slight increase of the Higgs effects relative to the SM background below the resonance region compared to the $\sqrt{s_{\text{had}}} = 8$ TeV results. Due to higher statistics the excesses and deficits given in Tabs. 3.10 and 3.11 have much larger significances than in the $\sqrt{s_{\text{had}}} = 8$ TeV case. Applying (3.119) and (3.120) as in the last section shows that even the deficits in the dilepton channel have significances $S^{(>)} > 3$ in all three scenarios. The distributions of $\Delta|y| = |y_t| - |y_{\bar{t}}|$ will not be considered again at this point. Also at $\sqrt{s_{\text{had}}} = 13$ TeV the distributions generated from the resonant processes are symmetric around $\Delta|y| = 0$ so that there is no significant contribution to the charge asymmetry (3.121).

Table 3.9. – *Total cross-sections for $t\bar{t}$ production in proton-proton collisions at $\sqrt{s_{\text{had}}} = 13$ TeV with and without effects of two heavy neutral Higgs bosons at NLO QCD. In the third and fourth column, the expected number of signal events in the dilepton and l+jets channel ($l = e,\mu$), $\langle \Delta N^{2l}_{\phi_2,\phi_3} \rangle$ and $\langle \Delta N^{lj}_{\phi_2,\phi_3} \rangle$ respectively, due to the resonant processes is given, assuming the parameters given in (3.122). The scale dependence is indicated by a superscript ($\mu = \frac{\mu_0}{2}$) and subscript ($\mu = 2\mu_0$).*

Scenario	$\sigma^{\text{NLOW}}_{QCD}$ [pb]	$\sigma^{\text{NLO(W)}}_{QCD+\phi_2,\phi_3}$ [pb]	$\langle \Delta N^{2l}_{\phi_2,\phi_3} \rangle$	$\langle \Delta N^{lj}_{\phi_2,\phi_3} \rangle$
1	$637.86^{+80.64}_{-77.63}$	$653.06^{+81.98}_{-79.02}$	16523^{+1453}_{-1502}	54074^{+4755}_{-4917}
2	$618.91^{+80.53}_{-76.19}$	$627.09^{+80.92}_{-76.77}$	8885^{+422}_{-635}	29079^{+1382}_{-2078}
3	$614.44^{+80.39}_{-75.81}$	$625.69^{+81.48}_{-76.85}$	12229^{+1175}_{-1128}	40023^{+3845}_{-3691}

Table 3.10. – *Ratio of total cross-sections for $t\bar{t}$ production in proton-proton collisions at $\sqrt{s_{\rm had}} = 13$ TeV with and without effects of two heavy neutral Higgs bosons at NLO QCD. The ratio of the NLO cross sections $R^{(<)}$ below the resonances is defined in Eq.* (3.118). *In the third and fourth column the expected number of signal events, $\langle \Delta N^{2l\,(<)}_{\phi_2,\phi_3} \rangle$ and $\langle \Delta N^{lj\,(<)}_{\phi_2,\phi_3} \rangle$, in the respective $M_{t\bar{t}}$ ranges in the dilepton and l+jets channel ($l = e,\mu$) due to the resonant processes is given, assuming the parameters in* (3.122). *The scale dependence is indicated by a superscript ($\mu = \frac{\mu_0}{2}$) and subscript ($\mu = 2\mu_0$).*

Sc.	$[M^{\rm min}_{t\bar{t}}, M^*_{t\bar{t}}]$ [GeV]	$R^{(<)}$	$\langle \Delta N^{2l\,(<)}_{\phi_2,\phi_3} \rangle$	$S^{2l\,(<)}$	$\langle \Delta N^{lj\,(<)}_{\phi_2,\phi_3} \rangle$	$S^{lj\,(<)}$
1	$[360, 540]$	$1.044^{-0.003}_{+0.002}$	19603^{+1179}_{-1560}	> 16	64156^{+3859}_{-5105}	> 16
2	$[360, 560]$	$1.023^{-0.001}_{+0.001}$	10261^{+834}_{-964}	> 16	33581^{+2728}_{-3153}	> 16
3	$[360, 500]$	$1.040^{-0.001}_{+0.001}$	14473^{+1408}_{-1428}	> 16	47365^{+4608}_{-4673}	> 16

Table 3.11. – *Ratio of total cross-sections for $t\bar{t}$ production in proton-proton collisions at $\sqrt{s_{\rm had}} = 13$ TeV with and without effects of two heavy neutral Higgs bosons at NLO QCD. The ratio of the NLO cross sections $R^{(>)}$ above the resonances is defined in Eq.* (3.118). *In the third and fourth column the expected number of signal events, $\langle \Delta N^{2l\,(>)}_{\phi_2,\phi_3} \rangle$ and $\langle \Delta N^{lj\,(>)}_{\phi_2,\phi_3} \rangle$, in the respective $M_{t\bar{t}}$ ranges in the dilepton and l+jets channel ($l = e,\mu$) due to the resonant processes is given, assuming the parameters in* (3.122). *The scale dependence is indicated by a superscript ($\mu = \frac{\mu_0}{2}$) and subscript ($\mu = 2\mu_0$).*

Sc.	$[M^*_{t\bar{t}}, M^{\rm max}_{t\bar{t}}]$ [GeV]	$R^{(>)}$	$\langle \Delta N^{2l\,(>)}_{\phi_2,\phi_3} \rangle$	$S^{2l\,(>)}$	$\langle \Delta N^{lj\,(>)}_{\phi_2,\phi_3} \rangle$	$S^{lj\,(>)}$
1	$[540, 800]$	$0.980^{+0.003}_{-0.002}$	-3722^{+111}_{-155}	5.5	-12181^{+363}_{-509}	> 16
2	$[560, 800]$	$0.991^{-0.002}_{+0.001}$	-1392^{-520}_{+365}	3.6	-4558^{-1702}_{+1196}	6.8
3	$[500, 800]$	$0.9902^{-0.0001}_{+0.0001}$	-2324^{-334}_{+288}	4.8	-7606^{-1094}_{+942}	> 16

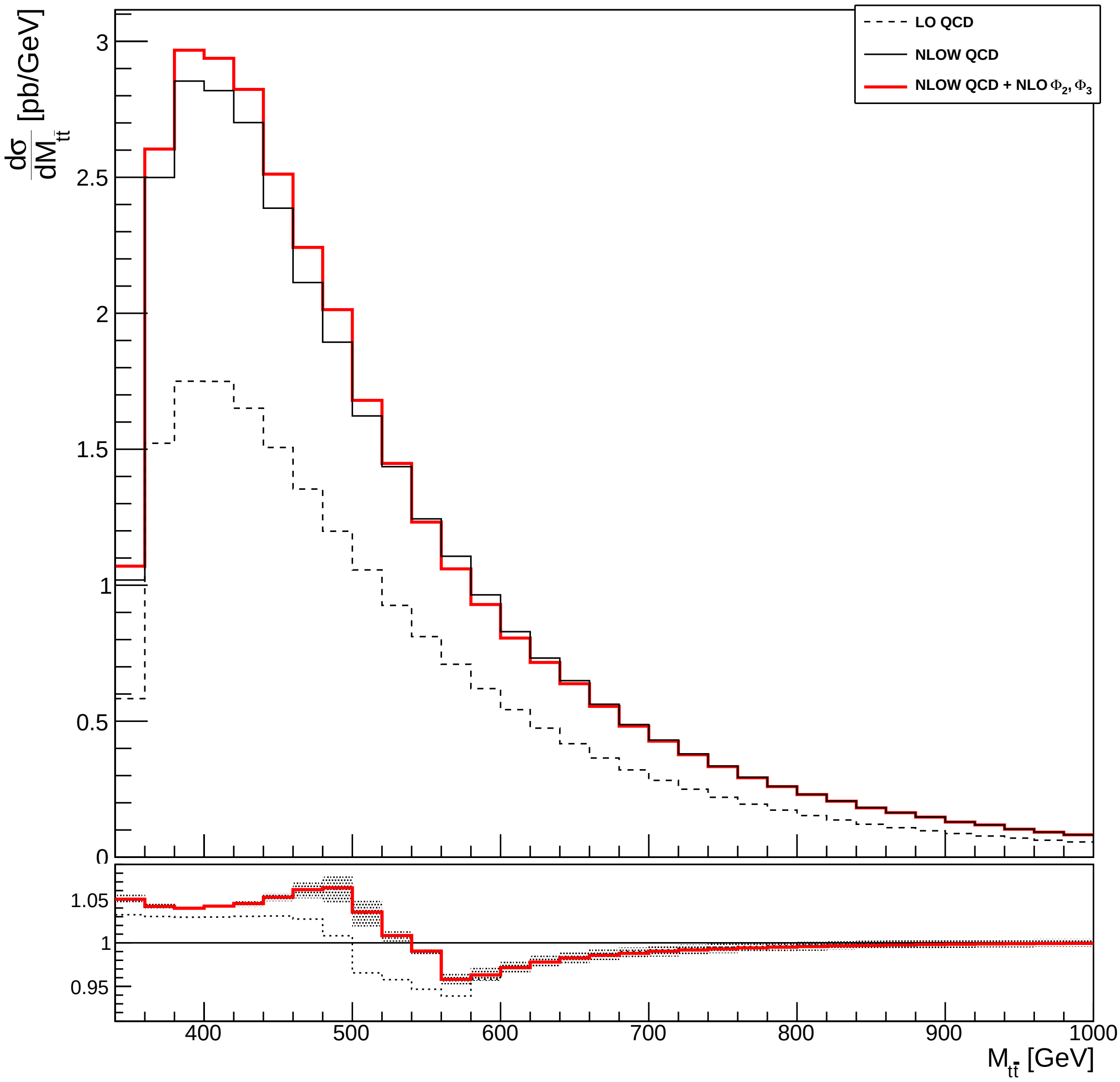

Figure 3.35. – *Top-/Antitop invariant mass distribution for* $pp \to t\bar{t}$ *including the effects of two neutral Higgs bosons (2HDM* ***scenario 1****, see 3.7.1) at NLO QCD. The hadronic center-of-mass energy is* $\sqrt{s_{\text{had}}} = 13$ *TeV, renormalization and factorization scales are set to* $\mu = \mu_0 = 265$ *GeV, c.f. (3.115). The lower pane shows the ratios* $d\sigma^{\text{NLO(W)}}_{QCD+\phi_2,\phi_3}/d\sigma^{\text{NLOW}}_{QCD}$ *(thick line) and* $d\sigma^{\text{LO}}_{QCD+\phi_2,\phi_3}/d\sigma^{\text{LO}}_{QCD}$ *(dotted line). The effect of scale variation in the interval* $[\frac{\mu_0}{2}, 2\mu_0]$ *for the NLO(W) ratio is indicated by the shaded rectangles.*

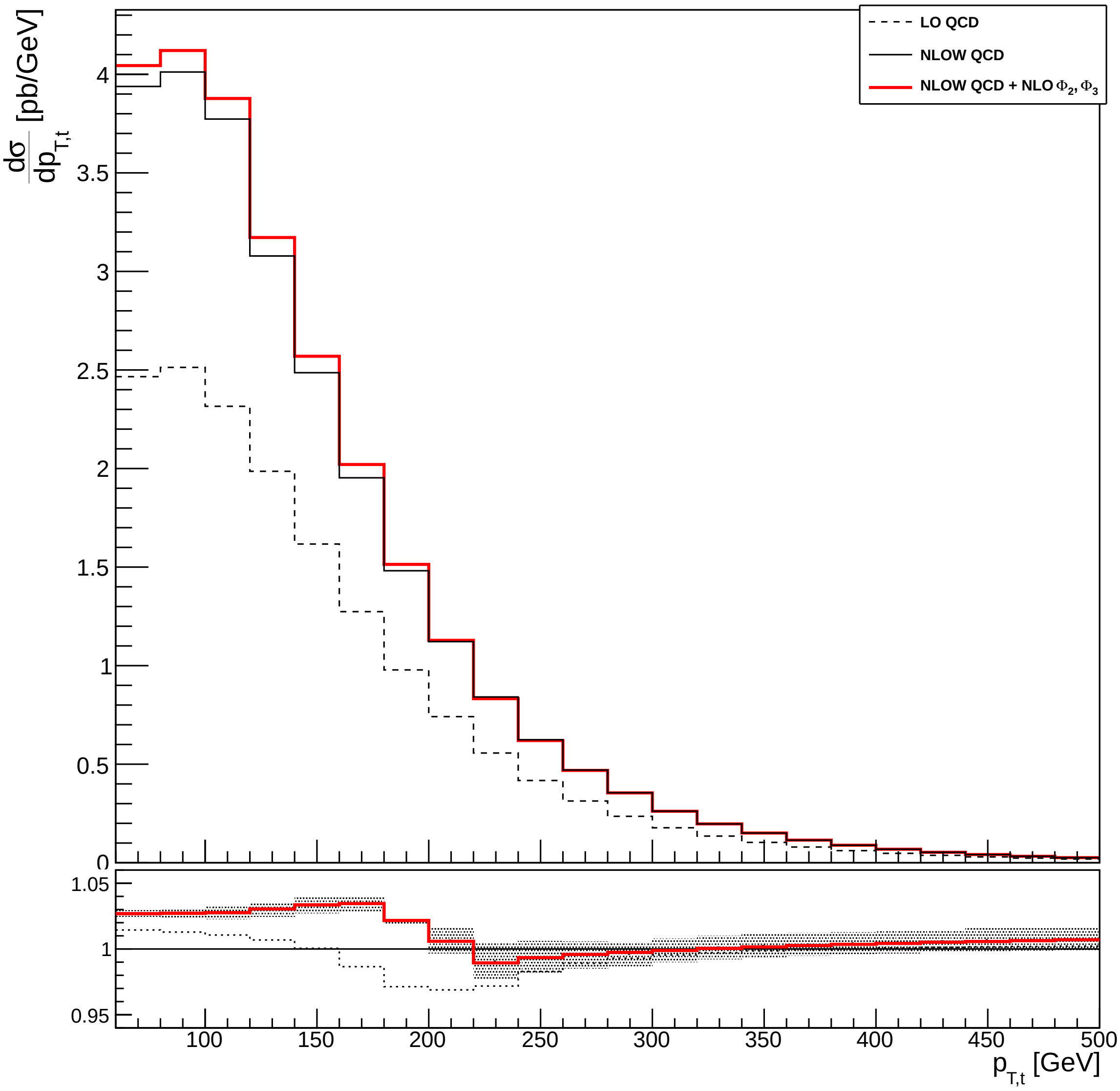

Figure 3.36. – *Top transverse momentum distribution for $pp \to t\bar{t}$ including the effects of two neutral Higgs bosons (2HDM **scenario 1**, see 3.7.1) at NLO QCD. The hadronic center-of-mass energy is $\sqrt{s_{\mathrm{had}}} = 13$ TeV, renormalization and factorization scales are set to $\mu = \mu_0 = 265$ GeV, c.f. (3.115). The lower pane shows the ratios $d\sigma^{\mathrm{NLO(W)}}_{QCD+\phi_2,\phi_3}/d\sigma^{\mathrm{NLOW}}_{QCD}$ (thick line) and $d\sigma^{\mathrm{LO}}_{QCD+\phi_2,\phi_3}/d\sigma^{\mathrm{LO}}_{QCD}$ (dotted line). The effect of scale variation in the interval $[\frac{\mu_0}{2}, 2\mu_0]$ for the NLO(W) ratio is indicated by the shaded rectangles.*

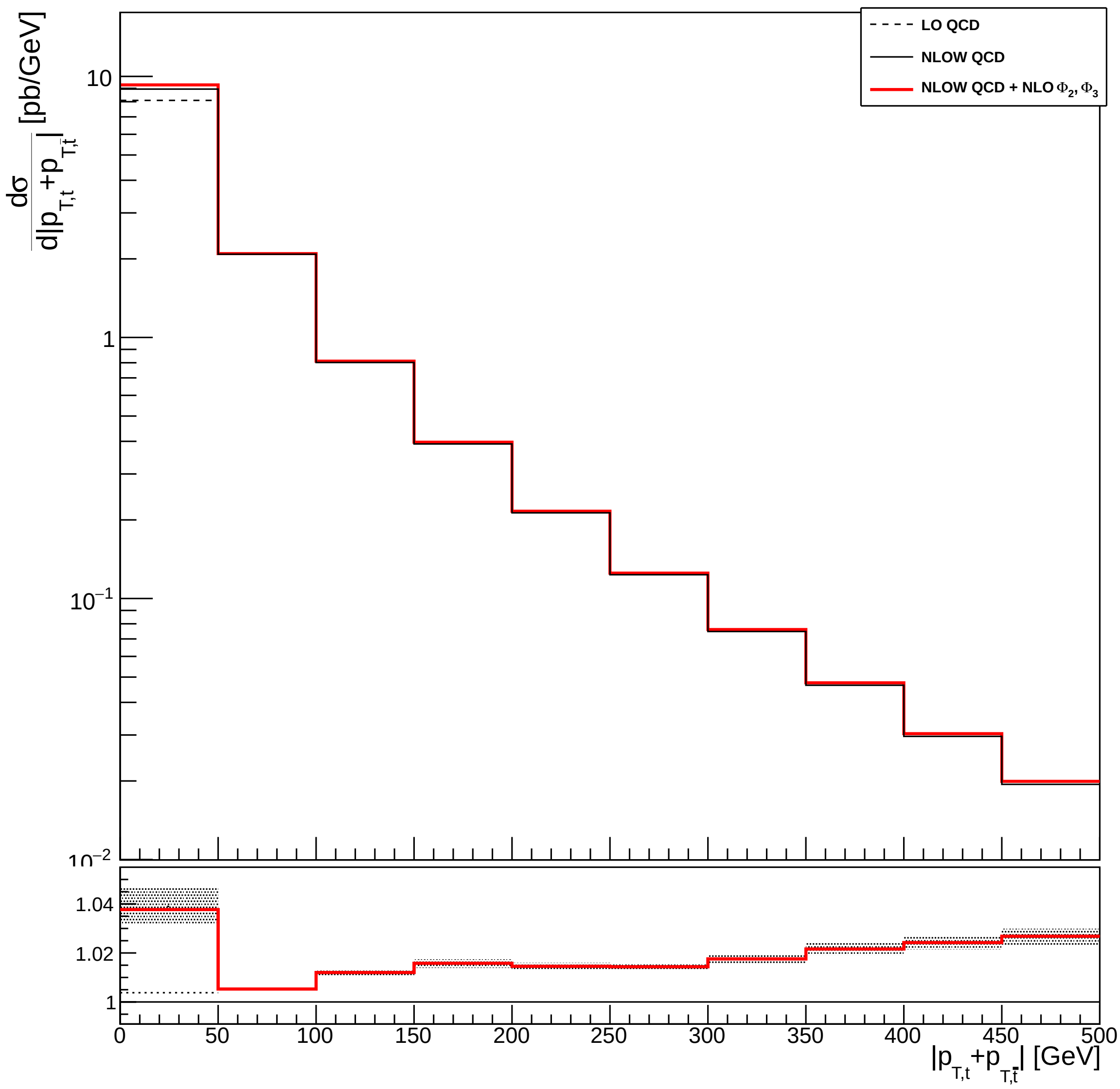

Figure 3.37. – *Transverse momentum distribution of the top + antitop system for $pp \to t\bar{t}$ including the effects of two neutral Higgs bosons (2HDM* ***scenario 1****, see 3.7.1) at NLO QCD. The hadronic center-of-mass energy is $\sqrt{s_{\mathrm{had}}} = 13$ TeV, renormalization and factorization scales are set to $\mu = \mu_0 = 265$ GeV, c.f. (3.115). The lower pane shows the ratios $d\sigma^{\mathrm{NLO(W)}}_{QCD+\phi_2,\phi_3}/d\sigma^{\mathrm{NLOW}}_{QCD}$ (thick line) and $d\sigma^{\mathrm{LO}}_{QCD+\phi_2,\phi_3}/d\sigma^{\mathrm{LO}}_{QCD}$ (dotted line). The effect of scale variation in the interval $[\frac{\mu_0}{2}, 2\mu_0]$ for the NLO(W) ratio is indicated by the shaded rectangles.*

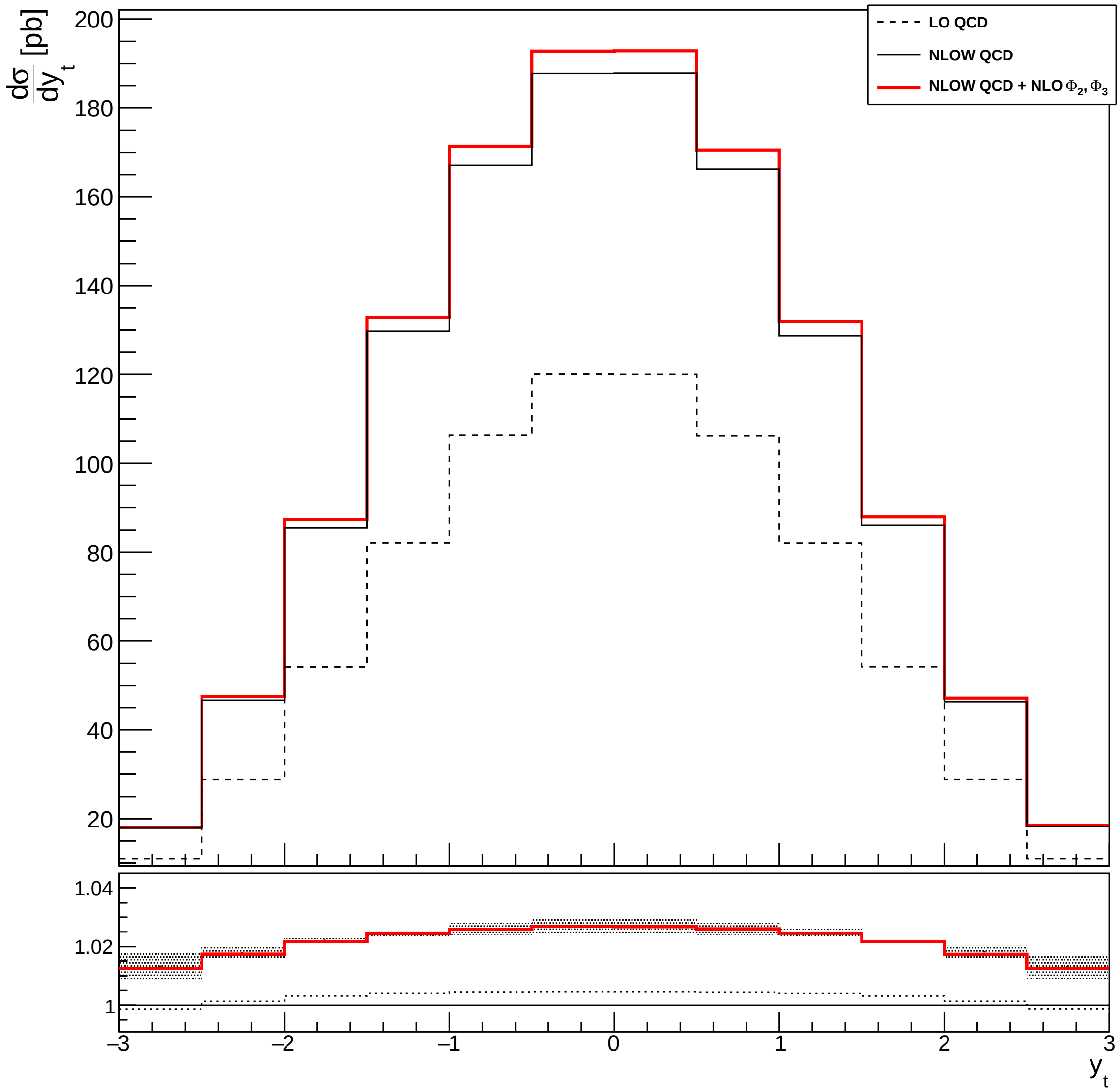

Figure 3.38. – *Top rapidity distribution for* $pp \to t\bar{t}$ *including the effects of two neutral Higgs bosons (2HDM **scenario 1**, see 3.7.1) at NLO QCD. The hadronic center-of-mass energy is* $\sqrt{s_{\rm had}} = 13$ *TeV, renormalization and factorization scales are set to* $\mu = \mu_0 = 265$ *GeV, c.f. (3.115). The lower pane shows the ratios* $d\sigma^{\rm NLO(W)}_{QCD+\phi_2,\phi_3}/d\sigma^{\rm NLOW}_{QCD}$ *(thick line) and* $d\sigma^{\rm LO}_{QCD+\phi_2,\phi_3}/d\sigma^{\rm LO}_{QCD}$ *(dotted line). The effect of scale variation in the interval* $[\frac{\mu_0}{2}, 2\mu_0]$ *for the NLO(W) ratio is indicated by the shaded rectangles.*

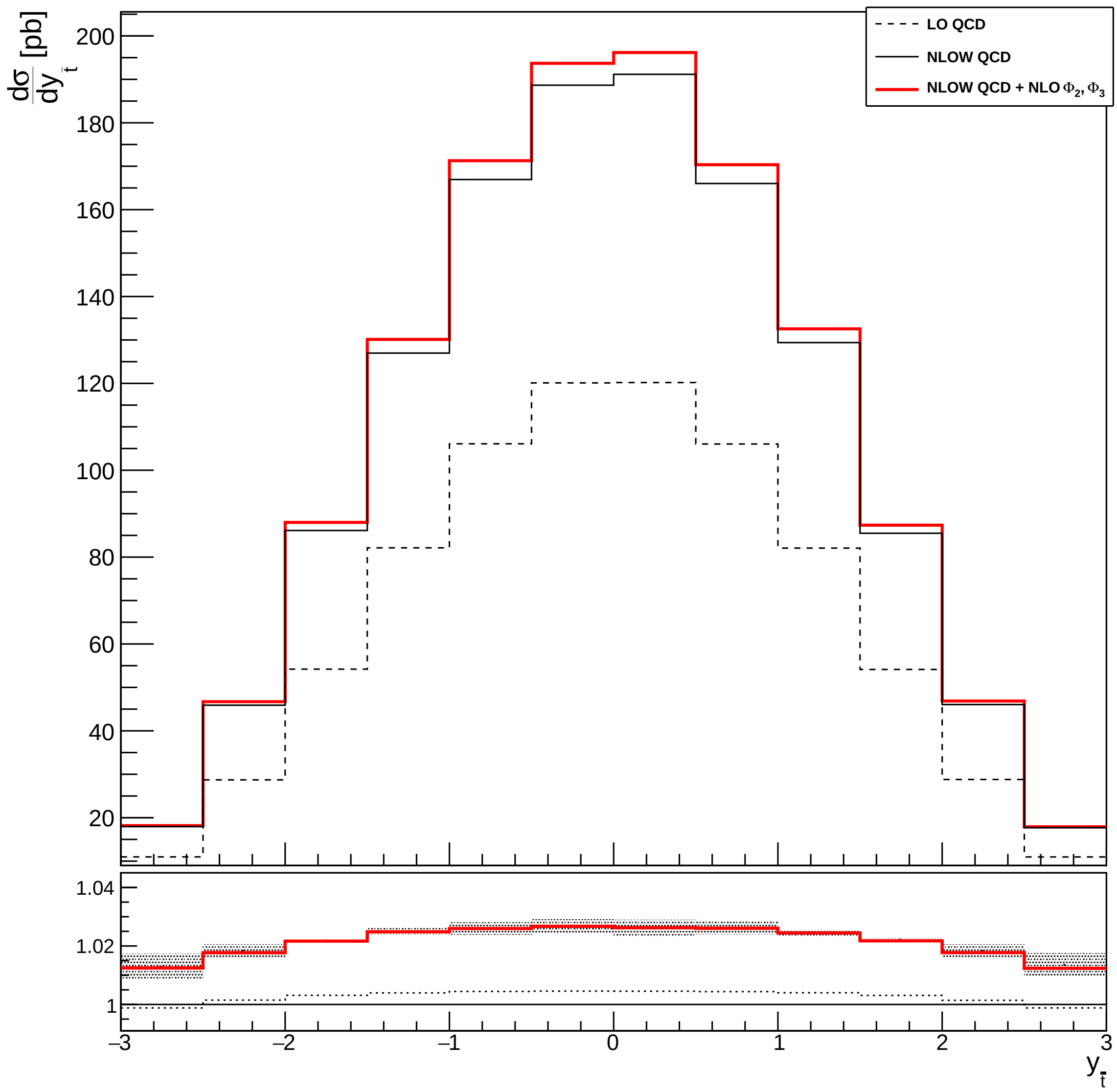

Figure 3.39. – *Antitop rapidity distribution for $pp \to t\bar{t}$ including the effects of two neutral Higgs bosons (2HDM* ***scenario 1****, see 3.7.1) at NLO QCD. The hadronic center-of-mass energy is $\sqrt{s_{\mathrm{had}}} = 13$ TeV, renormalization and factorization scales are set to $\mu = \mu_0 = 265$ GeV, c.f. (3.115). The lower pane shows the ratios $d\sigma^{\mathrm{NLO(W)}}_{QCD+\phi_2,\phi_3}/d\sigma^{\mathrm{NLOW}}_{QCD}$ (thick line) and $d\sigma^{\mathrm{LO}}_{QCD+\phi_2,\phi_3}/d\sigma^{\mathrm{LO}}_{QCD}$ (dotted line). The effect of scale variation in the interval $\left[\frac{\mu_0}{2}, 2\mu_0\right]$ for the NLO(W) ratio is indicated by the shaded rectangles.*

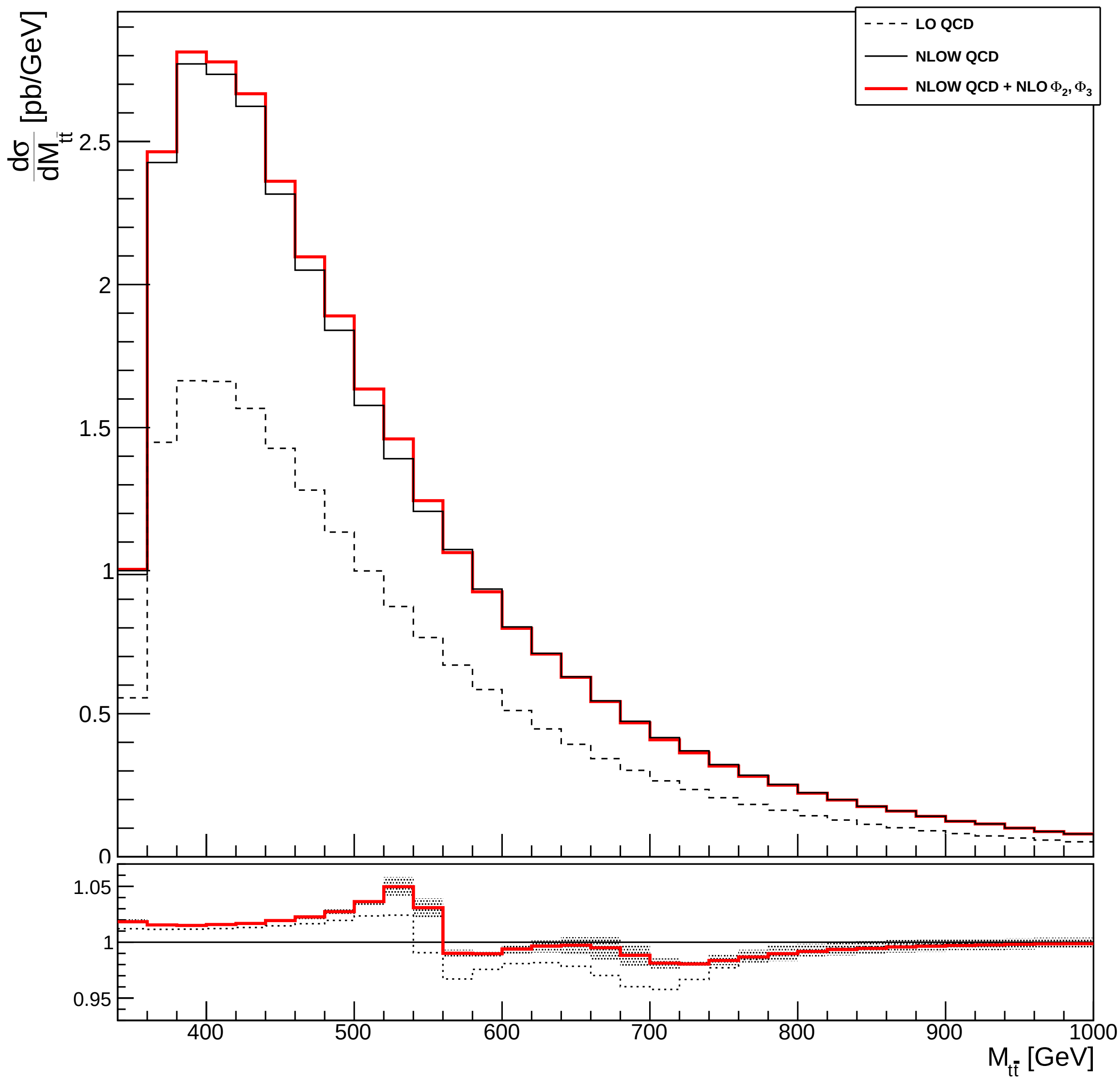

Figure 3.40. – *Top-/Antitop invariant mass distribution for $pp \to t\bar{t}$ including the effects of two neutral Higgs bosons (2HDM **scenario 2**, see 3.7.1) at NLO QCD. The hadronic center-of-mass energy is $\sqrt{s_{\text{had}}} = 13$ TeV, renormalization and factorization scales are set to $\mu = \mu_0 = 312.5$ GeV, c.f. (3.115). The lower pane shows the ratios $d\sigma^{\text{NLO(W)}}_{QCD+\phi_2,\phi_3}/d\sigma^{\text{NLOW}}_{QCD}$ (thick line) and $d\sigma^{\text{LO}}_{QCD+\phi_2,\phi_3}/d\sigma^{\text{LO}}_{QCD}$ (dotted line). The effect of scale variation in the interval $[\frac{\mu_0}{2}, 2\mu_0]$ for the NLO(W) ratio is indicated by the shaded rectangles.*

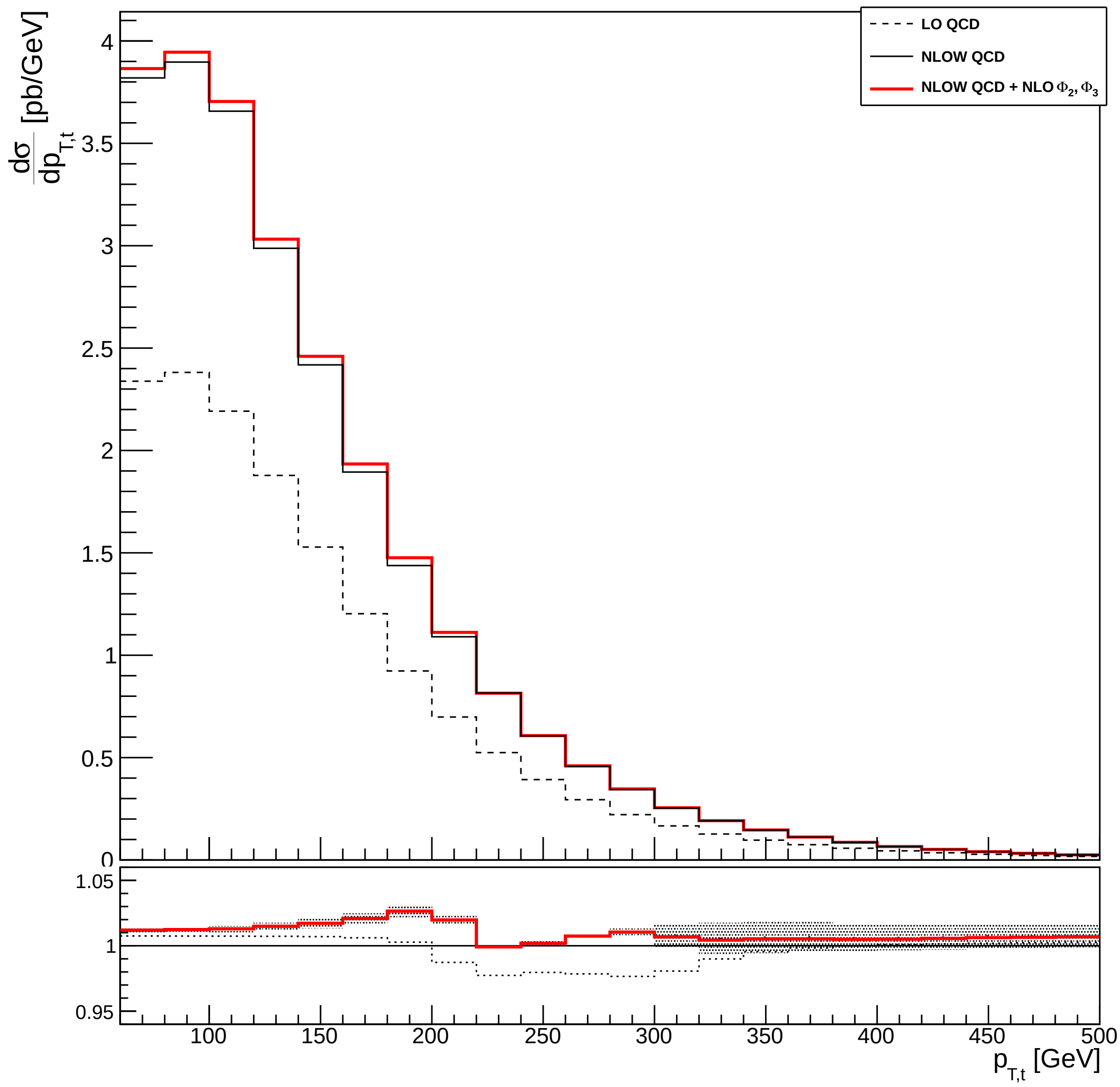

Figure 3.41. – *Top transverse momentum distribution for* $pp \to t\bar{t}$ *including the effects of two neutral Higgs bosons (2HDM* ***scenario 2****, see 3.7.1) at NLO QCD. The hadronic center-of-mass energy is* $\sqrt{s_{\rm had}} = 13$ *TeV, renormalization and factorization scales are set to* $\mu = \mu_0 = 312.5$ *GeV, c.f. (3.115). The lower pane shows the ratios* $d\sigma^{\rm NLO(W)}_{QCD+\phi_2,\phi_3}/d\sigma^{\rm NLOW}_{QCD}$ *(thick line) and* $d\sigma^{\rm LO}_{QCD+\phi_2,\phi_3}/d\sigma^{\rm LO}_{QCD}$ *(dotted line). The effect of scale variation in the interval* $[\frac{\mu_0}{2}, 2\mu_0]$ *for the NLO(W) ratio is indicated by the shaded rectangles.*

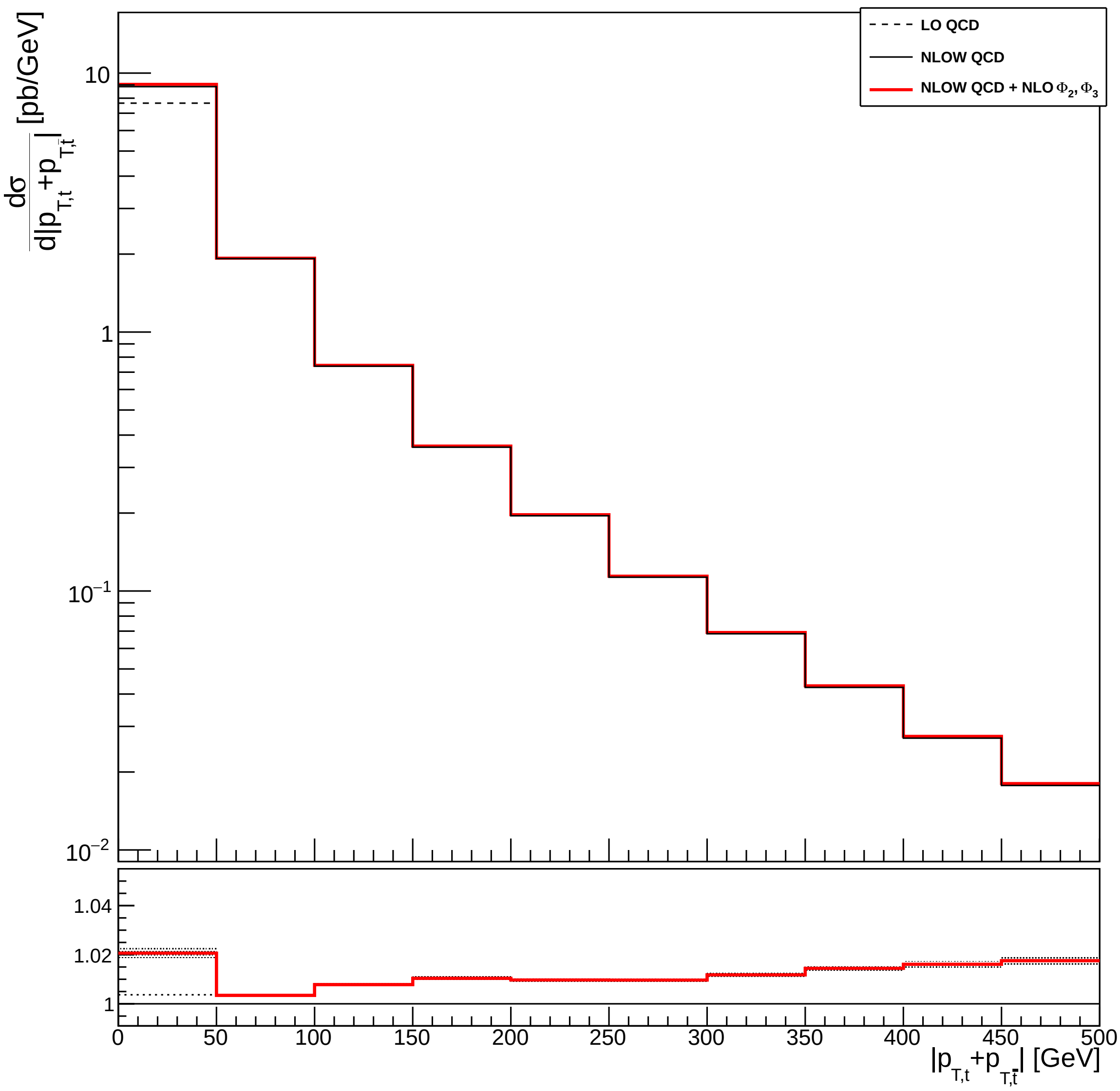

Figure 3.42. – *Transverse momentum distribution of the top + antitop system for $pp \to t\bar{t}$ including the effects of two neutral Higgs bosons (2HDM* ***scenario 2****, see 3.7.1) at NLO QCD. The hadronic center-of-mass energy is $\sqrt{s_{\text{had}}} = 13$ TeV, renormalization and factorization scales are set to $\mu = \mu_0 = 312.5$ GeV, c.f. (3.115). The lower pane shows the ratios $d\sigma^{\text{NLO(W)}}_{QCD+\phi_2,\phi_3}/d\sigma^{\text{NLOW}}_{QCD}$ (thick line) and $d\sigma^{\text{LO}}_{QCD+\phi_2,\phi_3}/d\sigma^{\text{LO}}_{QCD}$ (dotted line). The effect of scale variation in the interval $\left[\frac{\mu_0}{2}, 2\mu_0\right]$ for the NLO(W) ratio is indicated by the shaded rectangles.*

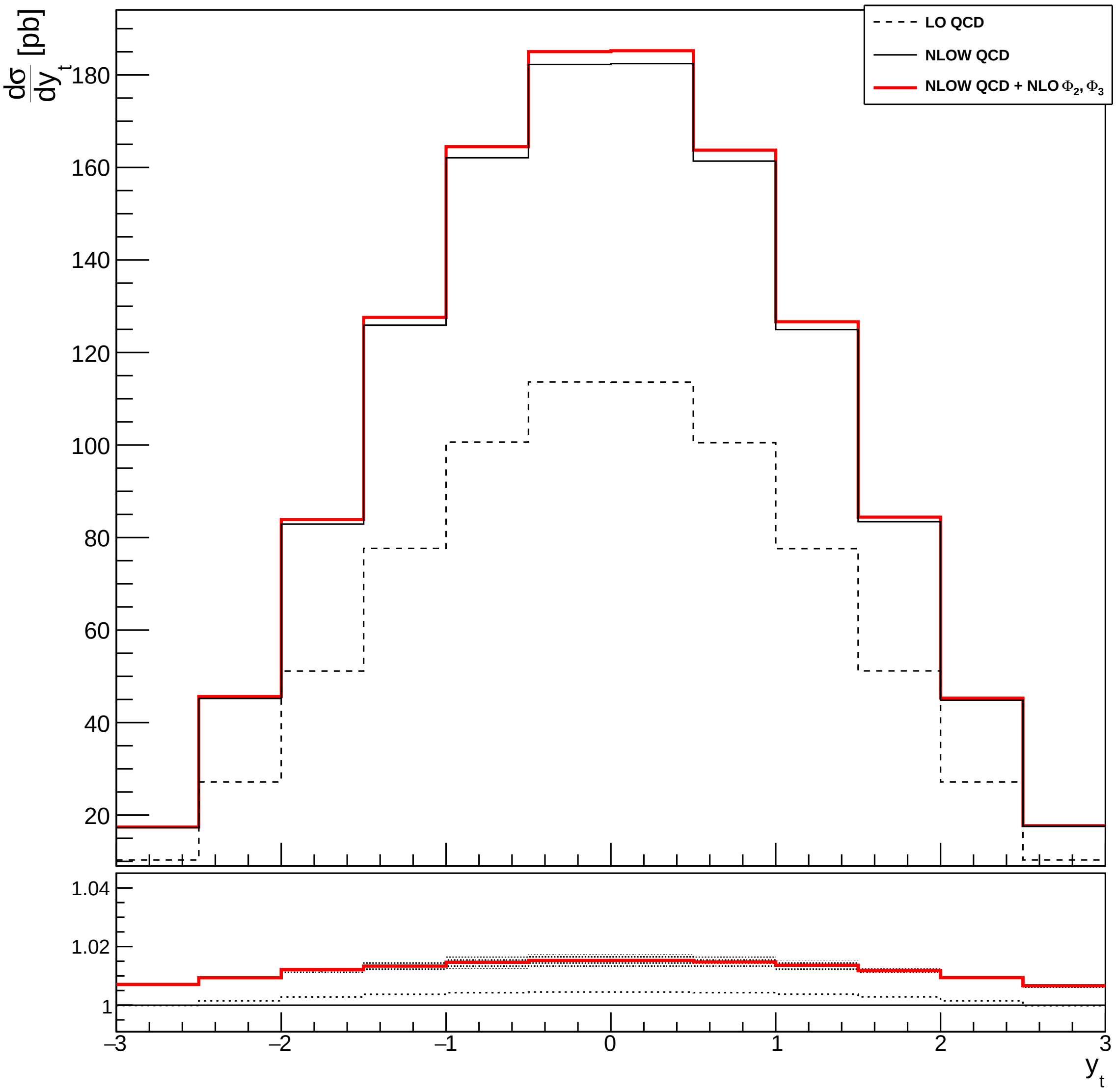

Figure 3.43. – *Top rapidity distribution for $pp \to t\bar{t}$ including the effects of two neutral Higgs bosons (2HDM **scenario 2**, see 3.7.1) at NLO QCD. The hadronic center-of-mass energy is $\sqrt{s_{\text{had}}} = 13$ TeV, renormalization and factorization scales are set to $\mu = \mu_0 = 312.5$ GeV, c.f. (3.115). The lower pane shows the ratios $d\sigma^{\text{NLO(W)}}_{QCD+\phi_2,\phi_3}/d\sigma^{\text{NLOW}}_{QCD}$ (thick line) and $d\sigma^{\text{LO}}_{QCD+\phi_2,\phi_3}/d\sigma^{\text{LO}}_{QCD}$ (dotted line). The effect of scale variation in the interval $\left[\frac{\mu_0}{2}, 2\mu_0\right]$ for the NLO(W) ratio is indicated by the shaded rectangles.*

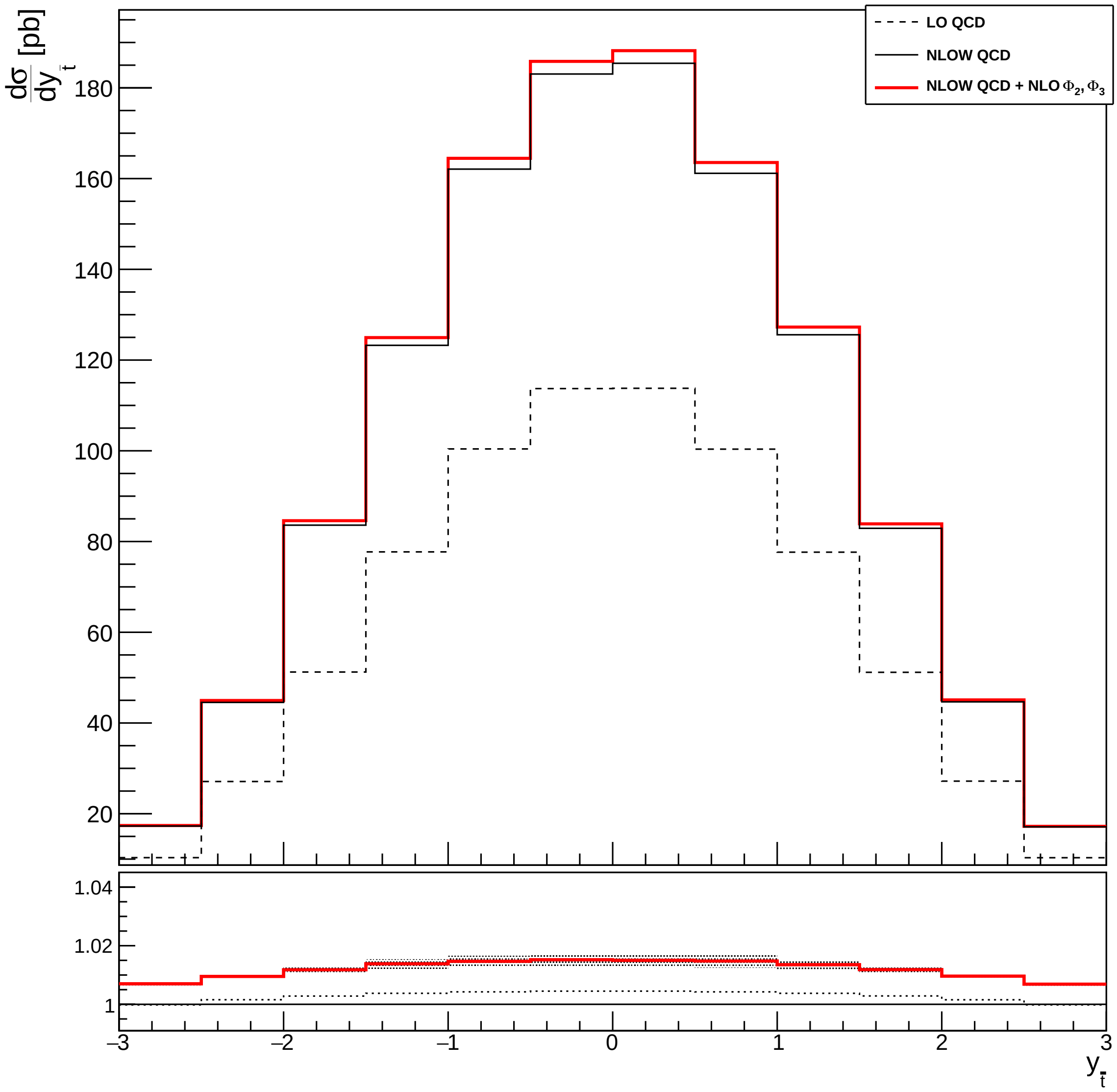

Figure 3.44. – *Antitop rapidity distribution for $pp \to t\bar{t}$ including the effects of two neutral Higgs bosons (2HDM **scenario 2**, see 3.7.1) at NLO QCD. The hadronic center-of-mass energy is $\sqrt{s_{\text{had}}} = 13$ TeV, renormalization and factorization scales are set to $\mu = \mu_0 = 312.5$ GeV, c.f. (3.115). The lower pane shows the ratios $d\sigma^{\text{NLO(W)}}_{QCD+\phi_2,\phi_3}/d\sigma^{\text{NLOW}}_{QCD}$ (thick line) and $d\sigma^{\text{LO}}_{QCD+\phi_2,\phi_3}/d\sigma^{\text{LO}}_{QCD}$ (dotted line). The effect of scale variation in the interval $[\frac{\mu_0}{2}, 2\mu_0]$ for the NLO(W) ratio is indicated by the shaded rectangles.*

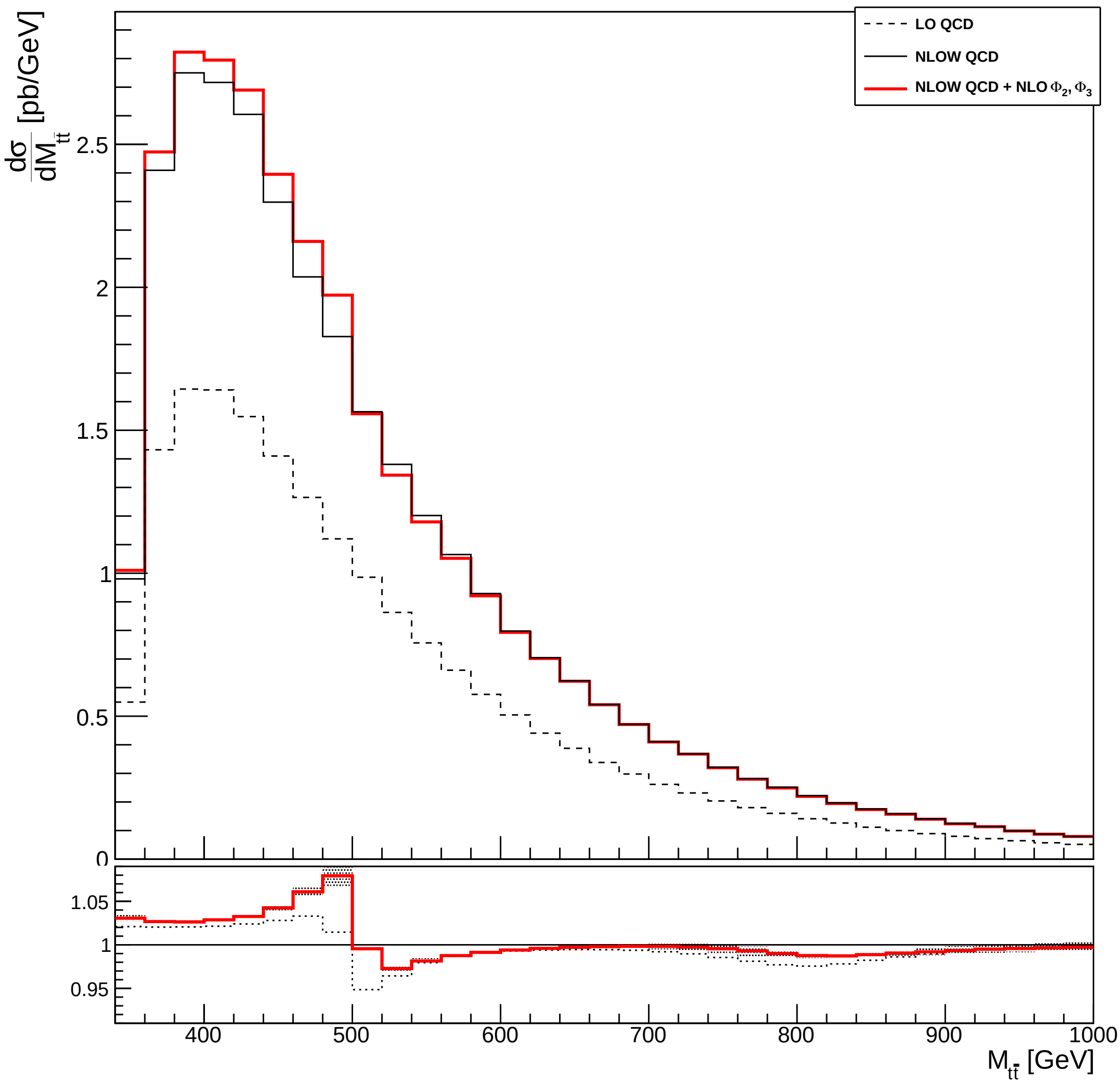

Figure 3.45. – *Top-/Antitop invariant mass distribution for $pp \to t\bar{t}$ including the effects of two neutral Higgs bosons (2HDM **scenario 3**, see 3.7.1) at NLO QCD. The hadronic center-of-mass energy is $\sqrt{s_{\text{had}}} = 13$ TeV, renormalization and factorization scales are set to $\mu = \mu_0 = 325$ GeV, c.f. (3.115). The lower pane shows the ratios $d\sigma^{\text{NLO(W)}}_{QCD+\phi_2,\phi_3}/d\sigma^{\text{NLOW}}_{QCD}$ (thick line) and $d\sigma^{\text{LO}}_{QCD+\phi_2,\phi_3}/d\sigma^{\text{LO}}_{QCD}$ (dotted line). The effect of scale variation in the interval $[\frac{\mu_0}{2}, 2\mu_0]$ for the NLO(W) ratio is indicated by the shaded rectangles.*

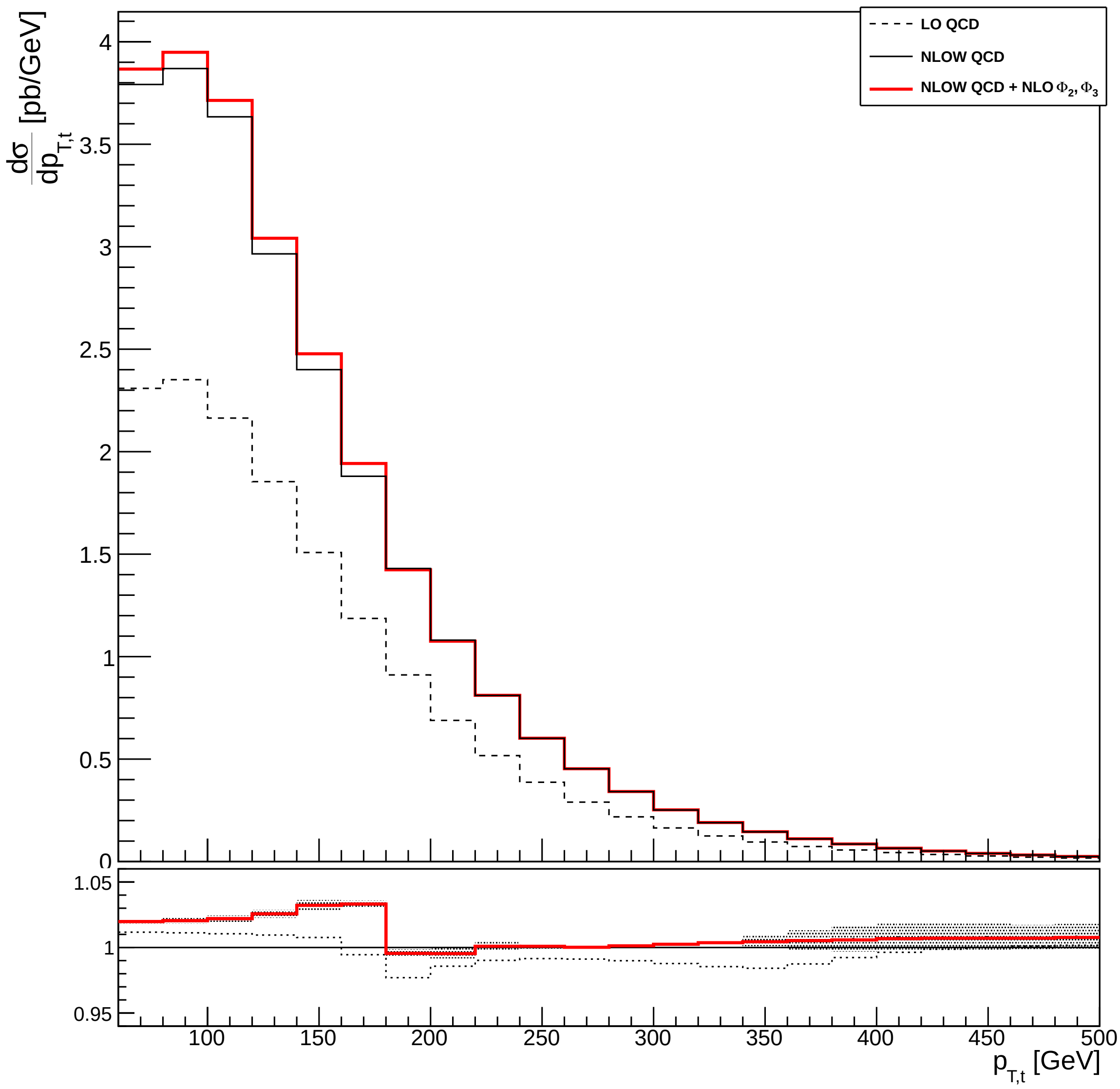

Figure 3.46. – *Top transverse momentum distribution for $pp \to t\bar{t}$ including the effects of two neutral Higgs bosons (2HDM **scenario 3**, see 3.7.1) at NLO QCD. The hadronic center-of-mass energy is $\sqrt{s_{\text{had}}} = 13$ TeV, renormalization and factorization scales are set to $\mu = \mu_0 = 325$ GeV, c.f. (3.115). The lower pane shows the ratios $d\sigma^{\text{NLO(W)}}_{QCD+\phi_2,\phi_3}/d\sigma^{\text{NLOW}}_{QCD}$ (thick line) and $d\sigma^{\text{LO}}_{QCD+\phi_2,\phi_3}/d\sigma^{\text{LO}}_{QCD}$ (dotted line). The effect of scale variation in the interval $[\frac{\mu_0}{2}, 2\mu_0]$ for the NLO(W) ratio is indicated by the shaded rectangles.*

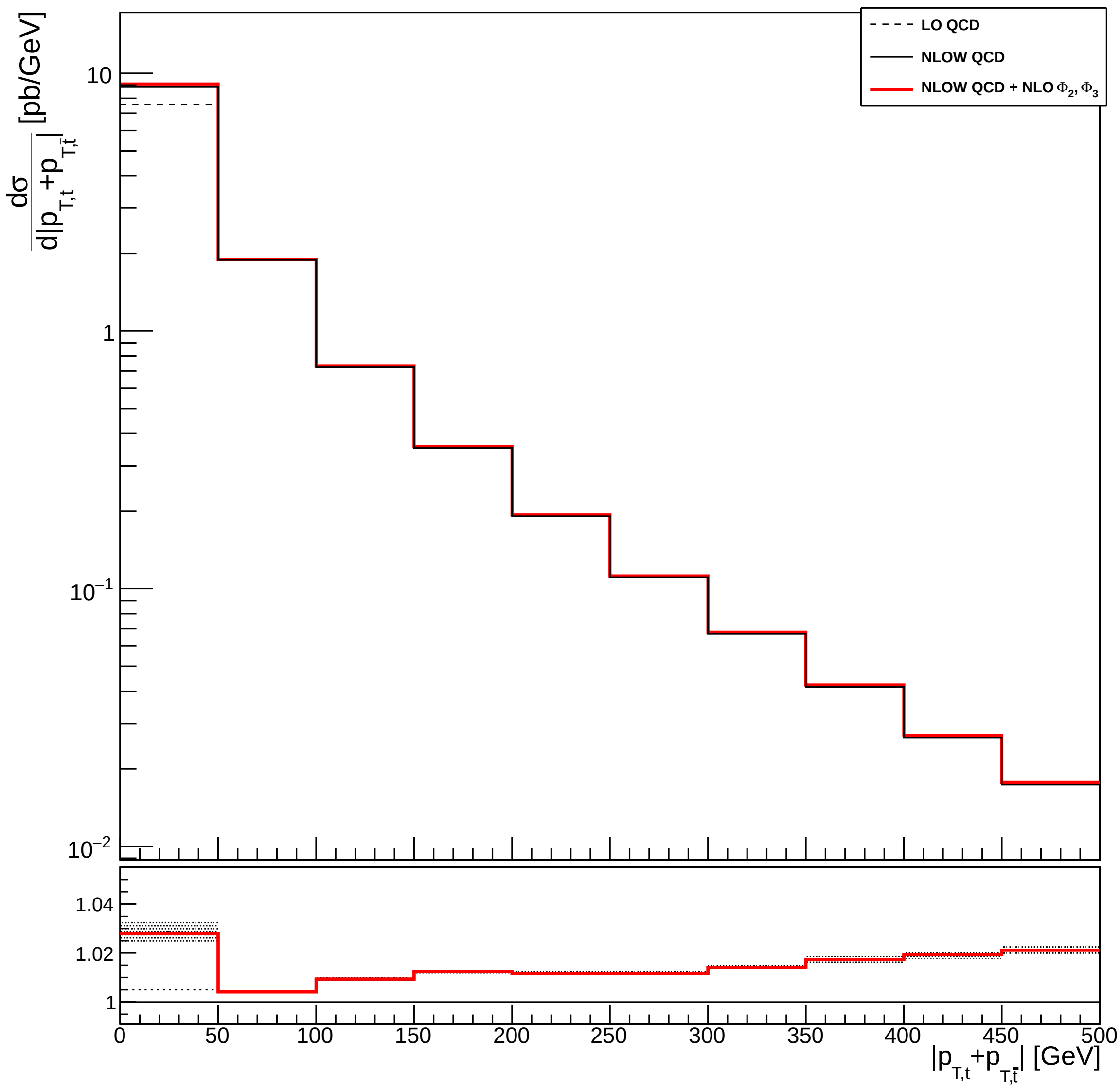

Figure 3.47. – *Transverse momentum distribution of the top + antitop system for* $pp \to t\bar{t}$ *including the effects of two neutral Higgs bosons (2HDM* ***scenario 3****, see 3.7.1) at NLO QCD. The hadronic center-of-mass energy is* $\sqrt{s_{\rm had}} = 13$ *TeV, renormalization and factorization scales are set to* $\mu = \mu_0 = 325$ *GeV, c.f. (3.115). The lower pane shows the ratios* $d\sigma^{\rm NLO(W)}_{QCD+\phi_2,\phi_3}/d\sigma^{\rm NLOW}_{QCD}$ *(thick line) and* $d\sigma^{\rm LO}_{QCD+\phi_2,\phi_3}/d\sigma^{\rm LO}_{QCD}$ *(dotted line). The effect of scale variation in the interval* $[\frac{\mu_0}{2}, 2\mu_0]$ *for the NLO(W) ratio is indicated by the shaded rectangles.*

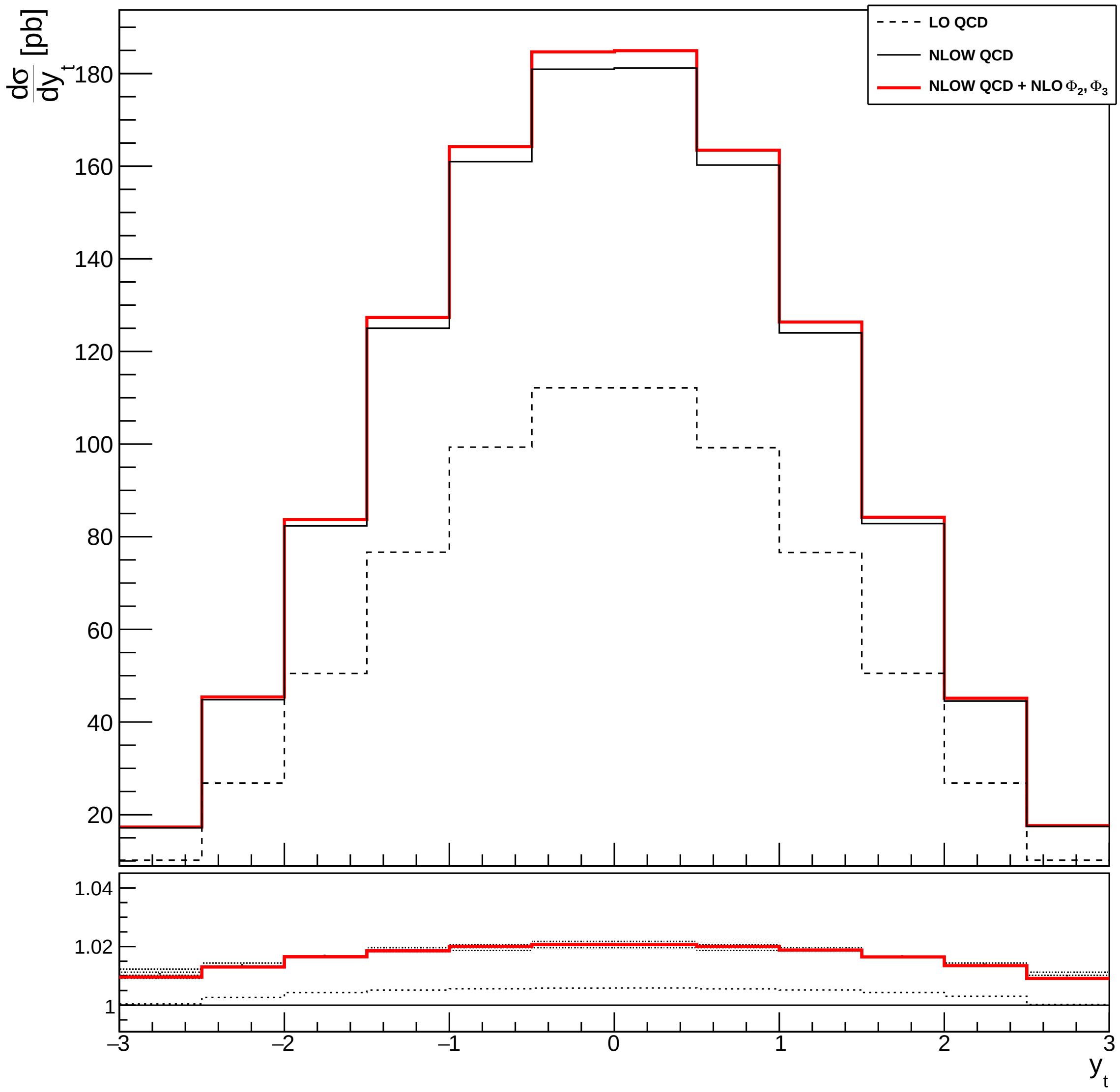

Figure 3.48. – *Top rapidity distribution for $pp \to t\bar{t}$ including the effects of two neutral Higgs bosons (2HDM **scenario 3**, see 3.7.1) at NLO QCD. The hadronic center-of-mass energy is $\sqrt{s_{\mathrm{had}}} = 13$ TeV, renormalization and factorization scales are set to $\mu = \mu_0 = 325$ GeV, c.f. (3.115). The lower pane shows the ratios $d\sigma^{\mathrm{NLO(W)}}_{QCD+\phi_2,\phi_3}/d\sigma^{\mathrm{NLOW}}_{QCD}$ (thick line) and $d\sigma^{\mathrm{LO}}_{QCD+\phi_2,\phi_3}/d\sigma^{\mathrm{LO}}_{QCD}$ (dotted line). The effect of scale variation in the interval $[\frac{\mu_0}{2}, 2\mu_0]$ for the NLO(W) ratio is indicated by the shaded rectangles.*

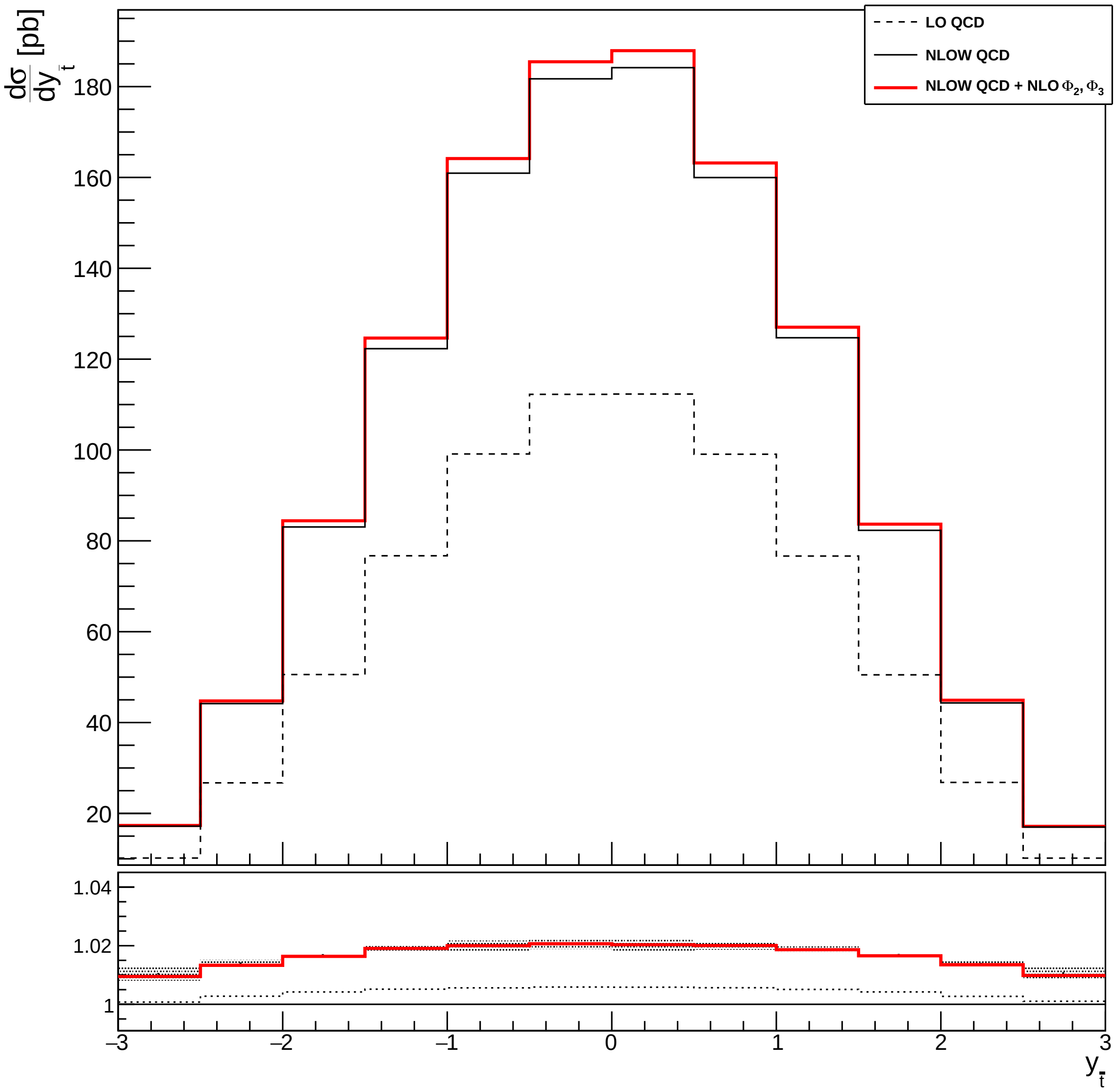

Figure 3.49. – *Antitop rapidity distribution for $pp \to t\bar{t}$ including the effects of two neutral Higgs bosons (2HDM **scenario 3**, see 3.7.1) at NLO QCD. The hadronic center-of-mass energy is $\sqrt{s_{\text{had}}} = 13$ TeV, renormalization and factorization scales are set to $\mu = \mu_0 = 325$ GeV, c.f. (3.115). The lower pane shows the ratios $d\sigma^{\text{NLO(W)}}_{QCD+\phi_2,\phi_3}/d\sigma^{\text{NLOW}}_{QCD}$ (thick line) and $d\sigma^{\text{LO}}_{QCD+\phi_2,\phi_3}/d\sigma^{\text{LO}}_{QCD}$ (dotted line). The effect of scale variation in the interval $\left[\frac{\mu_0}{2}, 2\mu_0\right]$ for the NLO(W) ratio is indicated by the shaded rectangles.*

3.7.6. Spin correlation and polarization observables

For the study of spin correlation and polarization observables in $t\bar{t}$ events at the LHC we will focus on dilepton final states, i.e. on the reaction

$$p\,p \;\; \to \;\; t\,\bar{t} + X \to l^+\, l'^- + \text{jets} + E_T^{\text{miss}}, \quad l, l' \in \{e, \mu\},$$

taking into account the decays of top and antitop quark at leading order QCD. For the sake of brevity we consider here only proton-proton collisions at 13 TeV. We will consider the following observables:

$$\begin{aligned}
\mathcal{O}_{\pm} &= \cos\theta_{\pm}, \\
\mathcal{O}_{\text{hel}} &= \cos\theta_{+}\cos\theta_{-}, \\
\mathcal{O}_{\text{open}} &= \cos\varphi, \\
\mathcal{O}_{\text{CP}} &= \left(\hat{l}_+ \times \hat{l}_-\right)\cdot \hat{k}_t,
\end{aligned} \tag{3.123}$$

where $\theta_+ = \angle\left(\hat{l}_+,\hat{k}_t\right)$, $\theta_- = \angle\left(\hat{l}_-,\hat{k}_{\bar{t}}\right)$ and $\varphi = \angle\left(\hat{l}_+,\hat{l}_-\right)$. The normalized 3-vectors $\hat{l}_+$ and $\hat{l}_-$ indicate the lepton/antilepton direction of flight in the top/antitop rest frames, whereas $\hat{k}_t$ and $\hat{k}_{\bar{t}}$ denote the direction of flight of top/antitop in the $t\bar{t}$ zero-momentum frame. We denote the expectation values as follows:

$$\begin{aligned}
\hat{B}_{\pm} &= 3\,\langle\cos\theta_{\pm}\rangle, \\
\hat{C}_{\text{hel}} &= -9\,\langle\cos\theta_{+}\cos\theta_{-}\rangle, \\
\hat{D}_{\text{open}} &= -3\,\langle\cos\varphi\rangle, \\
\hat{O}_{\text{CP}} &= \langle\left(\hat{l}_+ \times \hat{l}_-\right)\cdot \hat{k}_t\rangle,
\end{aligned} \tag{3.124}$$

where

$$\langle\mathcal{O}\rangle = \frac{\int d\sigma\,\mathcal{O}}{\int d\sigma}.$$

In the plots below we will also show the unnormalized quantities

$$
\begin{aligned}
B_{\pm} &= 3\int d\sigma \cos\theta_{\pm}, \\
C_{\text{hel}} &= -9\int d\sigma \cos\theta_{+}\cos\theta_{-}, \\
D_{\text{open}} &= -3\int d\sigma \cos\varphi, \\
O_{\text{CP}} &= \int d\sigma \left(\hat{l}_{+}\times\hat{l}_{-}\right)\cdot\hat{k}_{t}.
\end{aligned}
\tag{3.125}
$$

The helicity correlation $\hat{C}_{\text{hel}}$ and the lepton opening angle correlation $\hat{D}_{\text{open}}$ are generated in the SM and by the resonant processes in the 2HDM already at tree-level. If no cuts other than $M_{t\bar{t}}$ cuts are applied, the opening angle correlation $\hat{D}_{\text{open}}$ can be extracted from the normalized distribution

$$
\sigma^{-1}\frac{d\sigma}{d\cos\varphi} = \frac{1}{2}\left(1-\hat{D}_{\text{open}}\cos\varphi\right).
$$

Similarly, the polarization observables $\hat{B}_{\pm}$ and the helicity correlation $\hat{C}_{\text{hel}}$ can be extracted from the double distribution

$$
\sigma^{-1}\frac{d^{2}\sigma}{d\cos\theta_{+}d\cos\theta_{-}} = \frac{1}{4}\left(1+\hat{B}_{+}\cos\theta_{+}+\hat{B}_{-}\cos\theta_{-}-\hat{C}_{\text{hel}}\cos\theta_{+}\cos\theta_{-}\right).
$$

In the 2HDM scenarios 1 and 2 the Higgs bosons do not make P-odd and CP-odd contributions to the matrix elements. In this case the t and $\bar{t}$ polarizations B_{+} and B_{-} are generated solely by the SM interactions, that is, by the parity-odd contributions from

$$
q\,\bar{q}\to Z\to t\,\bar{t},
$$

at LO and by the parity-odd terms of the mixed QCD-weak contributions in the matrix elements of $t\bar{t}$ production by the $gg, q\bar{q}$ and gq reactions. Note that (approximate) CP symmetry in the SM then implies $\hat{B}_{+}=\hat{B}_{-}$ and $\hat{O}_{\text{CP}}=0$ to a very high accuracy. In the 2HDM scenario 3 however, contributions to the polarization observables $\hat{B}_{\pm}$ and the CP-odd triple correlation $\hat{O}_{\text{CP}}$ are generated by the resonant processes already at tree-level. In particular the t and $\bar{t}$ polarization difference

$$
\Delta\hat{B} = \hat{B}_{+}-\hat{B}_{-},
$$

is non-zero in this case. Note that the effects of the two heavy Higgs resonances are only included at LO QCD in the following results.

LHC 13 TeV

The inclusive results for the normalized observables (3.124) are given in Tabs. 3.12, 3.13 and 3.14. One can observe that the relative effects of the two heay Higgs bosons on the helicity correlation $\hat{C}_{\mathrm{hel}}$ and on the lepton opening angle correlation $\hat{D}_{\mathrm{open}}$ are around 10%, while the triple correlation $\hat{O}_{\mathrm{CP}}$ and the longitudinal polarization $\hat{B}_{\pm}$, respectively the polarization difference $\Delta\hat{B}$ are very small in scenario 3 and zero in the scenarios 1 and 2. In Figs. 3.50–3.55, the unnormalized opening angle correlation coefficients D_{open} and helicity correlation coefficients C_{hel} are shown within $M_{t\bar{t}}$ bins of 10 GeV in the range from 340 GeV to 1.2 TeV for all three 2HDM scenarios. In case of the CP violating scenario 3 we also consider the observables O_{CP} and ΔB, the results are shown in Figs. 3.56 and 3.57. One can see that the expectation values (3.124) can be enhanced by restricting them to convenient $M_{t\bar{t}}$ intervals, i.e. we will consider

$$\langle\mathcal{O}\rangle^{[M_A,\,M_B]} \quad = \quad \frac{\int d\sigma\, \mathcal{O}|_{M_A<M_{t\bar{t}}<M_B}}{\int d\sigma|_{M_A<M_{t\bar{t}}<M_B}},$$

in the following and compute the ratio of SM NLOW background plus resonant processes and SM processes only:

$$R^{[M_A,\,M_B]}_{\langle\mathcal{O}\rangle} \quad = \quad \frac{\langle\mathcal{O}\rangle^{[M_A,\,M_B]}_{NLOW+LO\,\phi_2,\phi_3}}{\langle\mathcal{O}\rangle^{[M_A,\,M_B]}_{NLOW}}.$$

As in the last section, $R^{[M_A,\,M_B]}$ simply denotes the ratio of the cross sections in the given $M_{t\bar{t}}$ interval. The results for some specific choices of $[M_A, M_B]$ are given in Tabs. 3.15 and 3.16. One can see that in this way the effects of the heavy Higgs bosons can be enhanced up to 30% in the CP-even observables in case of scenario 1 and nearly one order of magnitude in the CP-odd observables in case of scenario 3. Still the absolute value of the normalized CP-odd observables in scenario 3 is very small. We estimate the statistical error on these numbers as

$$\delta^{[M_A,\,M_B]} = \frac{1}{\sqrt{N^{[M_A,\,M_B]}}},$$

where $N^{[M_A,\,M_B]}$ is the number of dileptonic events in the specific $M_{t\bar{t}}$ interval. This shows that – assuming (3.122) – the results of the CP-odd observables given in Tab. 3.16 are not statistically significant.

Table 3.12. – *LHC* $\sqrt{s_{\text{had}}} = 13$ *TeV, dileptonic* $t\bar{t}$ *events, 2HDM* ***scenario 1****, c.f. 3.7.1. Inclusive results of helicity and lepton opening angle correlation coefficients, evaluated at the scale* $\mu_0 = 265$ *GeV.*

	$\hat{C}_{\text{hel}}$	$\hat{D}_{\text{open}}$	$\hat{O}_{\text{CP}}$	$\Delta\hat{B}$
NLOW	0.3279	-0.2390	0	0
NLOW + ϕ_2, ϕ_3	0.3377	-0.2478	0	0

Table 3.13. – *LHC* $\sqrt{s_{\text{had}}} = 13$ *TeV, dileptonic* $t\bar{t}$ *events, 2HDM* ***scenario 2****, c.f. 3.7.1. Inclusive results of helicity and lepton opening angle correlation coefficients, evaluated at the scale* $\mu_0 = 312.5$ *GeV.*

	$\hat{C}_{\text{hel}}$	$\hat{D}_{\text{open}}$	$\hat{O}_{\text{CP}}$	$\Delta\hat{B}$
NLOW	0.3283	-0.2387	0	0
NLOW + ϕ_2, ϕ_3	0.3210	-0.2350	0	0

Table 3.14. – *LHC* $\sqrt{s_{\text{had}}} = 13$ *TeV, dileptonic* $t\bar{t}$ *events, 2HDM* ***scenario 3****, c.f. 3.7.1. Inclusive results of helicity and lepton opening angle correlation coefficients, evaluated at the scale* $\mu_0 = 325$ *GeV.*

	$\hat{C}_{\text{hel}}$	$\hat{D}_{\text{open}}$	$\hat{O}_{\text{CP}}$ $[\times 10^{-4}]$	$\Delta\hat{B}$ $[\times 10^{-4}]$
NLOW	0.3284	-0.2387	0	0
NLOW + ϕ_2, ϕ_3	0.3707	-0.2614	-5.74	6.74

Table 3.15. – *Ratios of the spin observables C_{hel} and D_{open} in proton-proton collisions at $\sqrt{s_{\mathrm{had}}} = 13$ TeV in $M_{t\bar{t}}$ intervals $[M_A, M_B]$ with and without effects of two heavy neutral Higgs bosons at LO QCD. The statistical fluctuation $\delta^{[M_A,\,M_B]}$ is calculated assuming the parameters (3.122). The scale dependence is indicated by a superscript ($\mu = \frac{\mu_0}{2}$) and subscript ($\mu = 2\mu_0$).*

Sc.	$[M_A, M_B]$ [GeV]	$R^{[M_A,\,M_B]}_{C_{\mathrm{hel}}}$	$R^{[M_A,\,M_B]}_{D_{\mathrm{open}}}$	$\delta^{[M_A,\,M_B]}[10^{-3}]$
1	$[500, 580]$	$0.686^{-0.044}_{+0.030}$	$0.719^{-0.031}_{+0.022}$	2.9
2	$[480, 560]$	$0.823^{-0.024}_{+0.017}$	$0.841^{-0.017}_{+0.012}$	2.8
3	$[420, 520]$	$1.084^{+0.011}_{-0.008}$	$1.079^{+0.009}_{-0.006}$	2.1

Table 3.16. – *Scenario 3: triple correlation $\hat{O}_{\mathrm{CP}}$ and polarization difference $\Delta\hat{B}$ in proton-proton collisions at $\sqrt{s_{\mathrm{had}}} = 13$ TeV in the $M_{t\bar{t}}$ interval $[M_A, M_B]$. The statistical fluctuation $\delta^{[M_A,\,M_B]}$ is calculated assuming the parameters (3.122). The scale dependence is indicated by a superscript ($\mu = \frac{\mu_0}{2}$) and subscript ($\mu = 2\mu_0$).*

Sc.	$[M_A, M_B]$ [GeV]	$\hat{O}^{[M_A,\,M_B]}_{\mathrm{CP}}[10^{-3}]$	$\Delta\hat{B}^{[M_A,\,M_B]}[10^{-3}]$	$\delta^{[M_A,\,M_B]}[10^{-3}]$
3	$[400, 490]$	$-2.73^{-0.34}_{+0.25}$	$5.06^{+0.63}_{-0.47}$	2.2

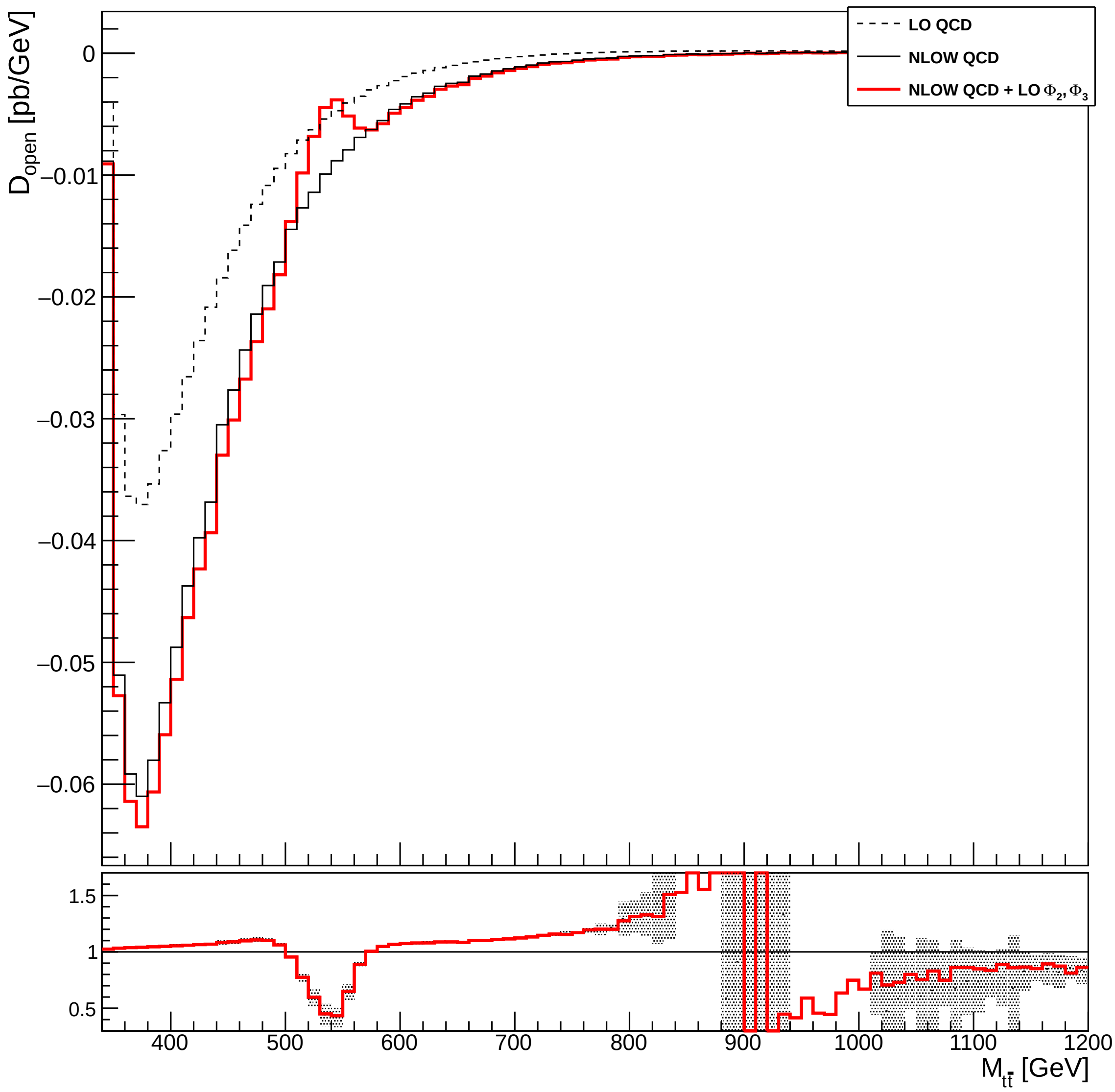

Figure 3.50. – *Unnormalized spin observable* D_{open} *defined in* (3.125) *for* $\sqrt{s_{\text{had}}} = 13$ *TeV proton-proton collisions including the effects of two neutral Higgs bosons (2HDM* ***scenario 1****) at LO QCD. Renormalization and factorization scales are set to* $\mu = \mu_0 = 265$ *GeV. The structures above* 800 *GeV in the ratio* $(NLOW + LO\,\phi_2, \phi_3)/NLOW$*, indicated by the thick line in the lower plot, are due to the zero-crossing of the two distributions and do not reflect physical effects. The effect of scale variation in the interval* $[\frac{\mu_0}{2}, 2\mu_0]$ *is indicated by the shaded rectangles.*

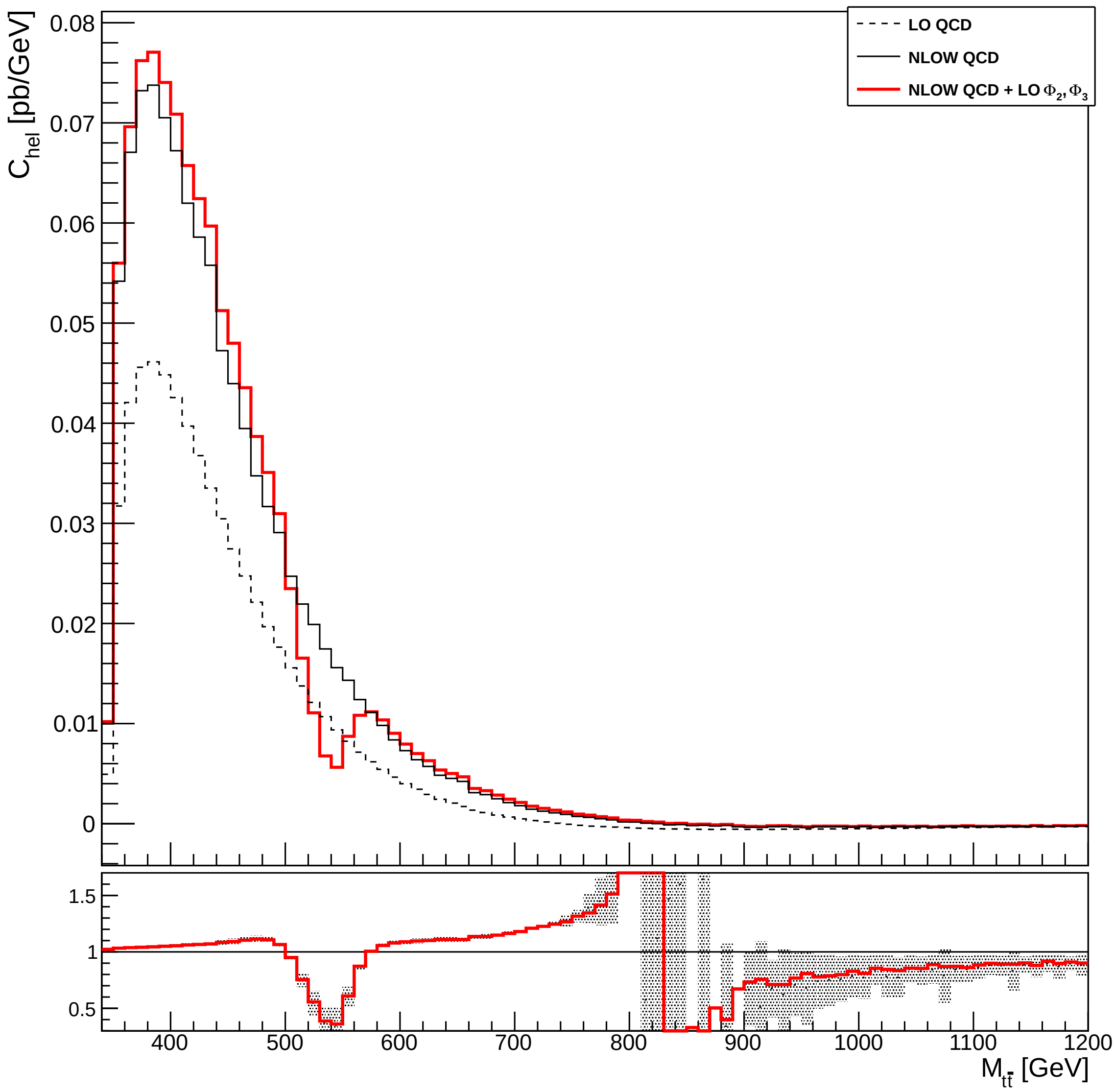

Figure 3.51. – *Unnormalized spin observable* $C_{\rm hel}$ *defined in* (3.125) *for* $\sqrt{s_{\rm had}} = 13$ *TeV proton-proton collisions including the effects of two neutral Higgs bosons (2HDM* ***scenario 1****) at LO QCD. Renormalization and factorization scales are set to* $\mu = \mu_0 = 265$ *GeV. The structures above* 800 *GeV in the ratio* $(NLOW + LO\,\phi_2, \phi_3)/NLOW$*, indicated by the thick line in the lower plot, are due to the zero-crossing of the two distributions and do not reflect physical effects. The effect of scale variation in the interval* $[\frac{\mu_0}{2}, 2\mu_0]$ *is indicated by the shaded rectangles.*

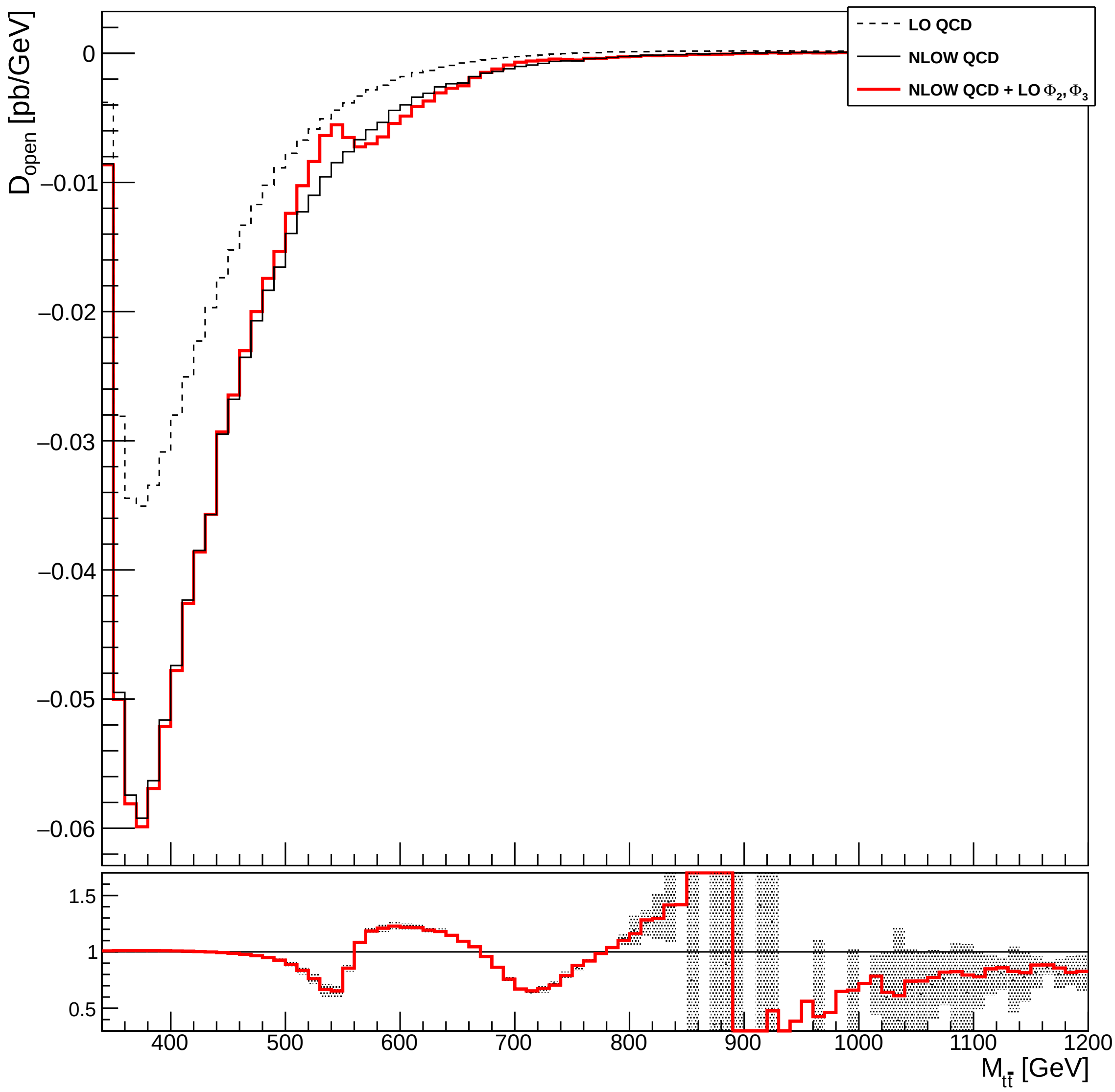

Figure 3.52. – *Unnormalized spin observable* D_{open} *defined in* (3.125) *for* $\sqrt{s_{\text{had}}} = 13$ *TeV proton-proton collisions including the effects of two neutral Higgs bosons (2HDM* ***scenario 2****) at LO QCD. Renormalization and factorization scales are set to* $\mu = \mu_0 = 312.5$ *GeV. The structures above* 800 *GeV in the ratio* $(NLOW + LO\,\phi_2, \phi_3)/NLOW$*, indicated by the thick line in the lower plot, are due to the zero-crossing of the two distributions and do not reflect physical effects. The effect of scale variation in the interval* $[\frac{\mu_0}{2}, 2\mu_0]$ *is indicated by the shaded rectangles.*

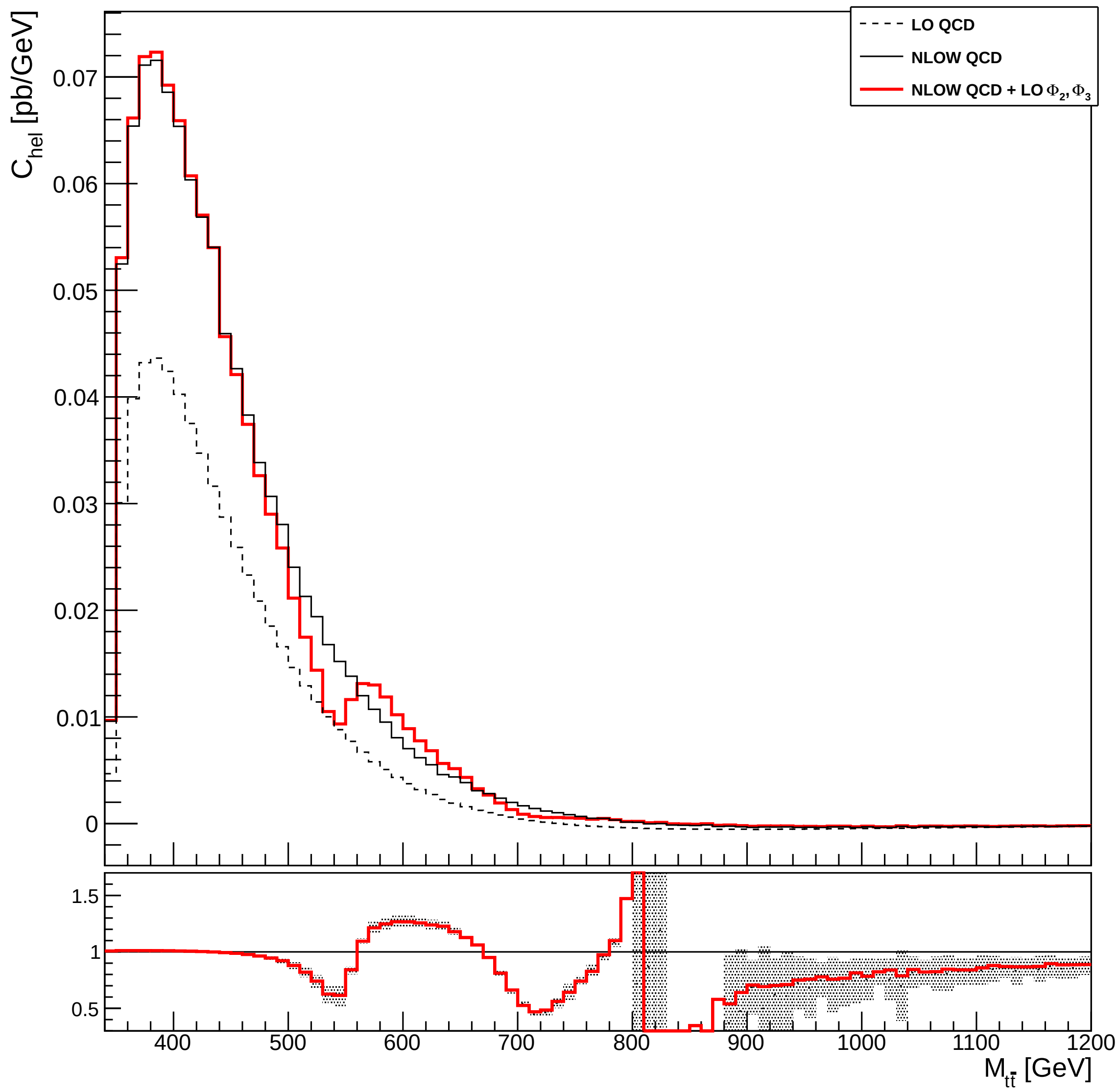

Figure 3.53. – *Unnormalized spin observable* $C_{\rm hel}$ *defined in* (3.125) *for* $\sqrt{s_{\rm had}} = 13$ *TeV proton-proton collisions including the effects of two neutral Higgs bosons (2HDM* ***scenario 2****) at LO QCD. Renormalization and factorization scales are set to* $\mu = \mu_0 = 312.5$ *GeV. The structures above* 800 *GeV in the ratio* $(NLOW + LO\,\phi_2, \phi_3)/NLOW$*, indicated by the thick line in the lower plot, are due to the zero-crossing of the two distributions and do not reflect physical effects. The effect of scale variation in the interval* $[\frac{\mu_0}{2}, 2\mu_0]$ *is indicated by the shaded rectangles.*

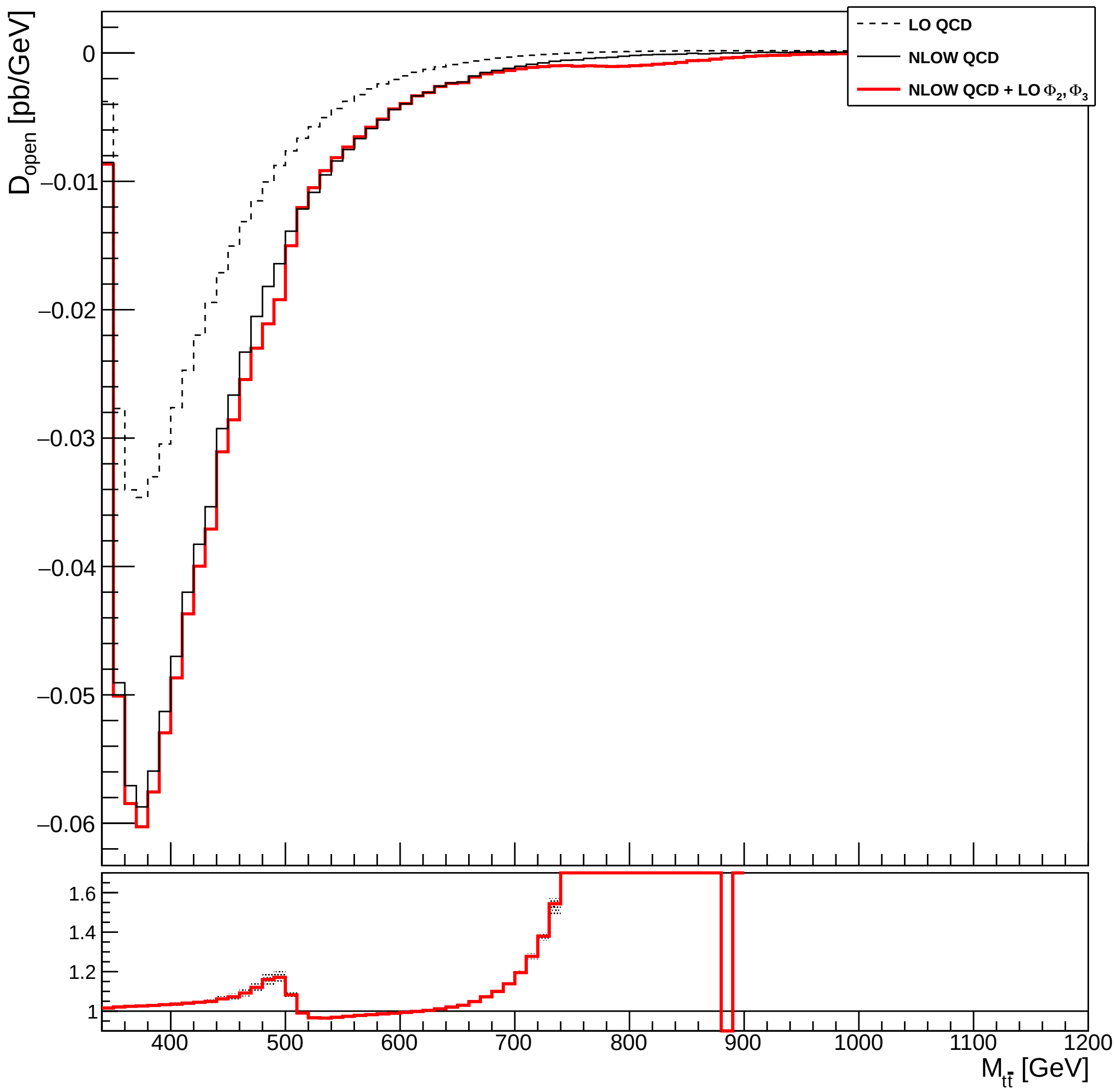

Figure 3.54. – *Unnormalized spin observable D_{open} defined in* (3.125) *for* $\sqrt{s_{\mathrm{had}}} = 13$ *TeV proton-proton collisions including the effects of two neutral Higgs bosons (2HDM **scenario 3**) at LO QCD. Renormalization and factorization scales are set to $\mu = \mu_0 = 325$ GeV. Above* 750 *GeV, the ratio $(NLOW + LO\,\phi_2, \phi_3)/NLOW$, indicated by the thick line in the lower plot, becomes larger than* 2 *due to the effects of the resonance ϕ_3. However, one should notice that the absolute value of the spin observable is small in this $M_{t\bar{t}}$ range. The effect of scale variation in the interval $\left[\frac{\mu_0}{2}, 2\mu_0\right]$ is indicated by the shaded rectangles.*

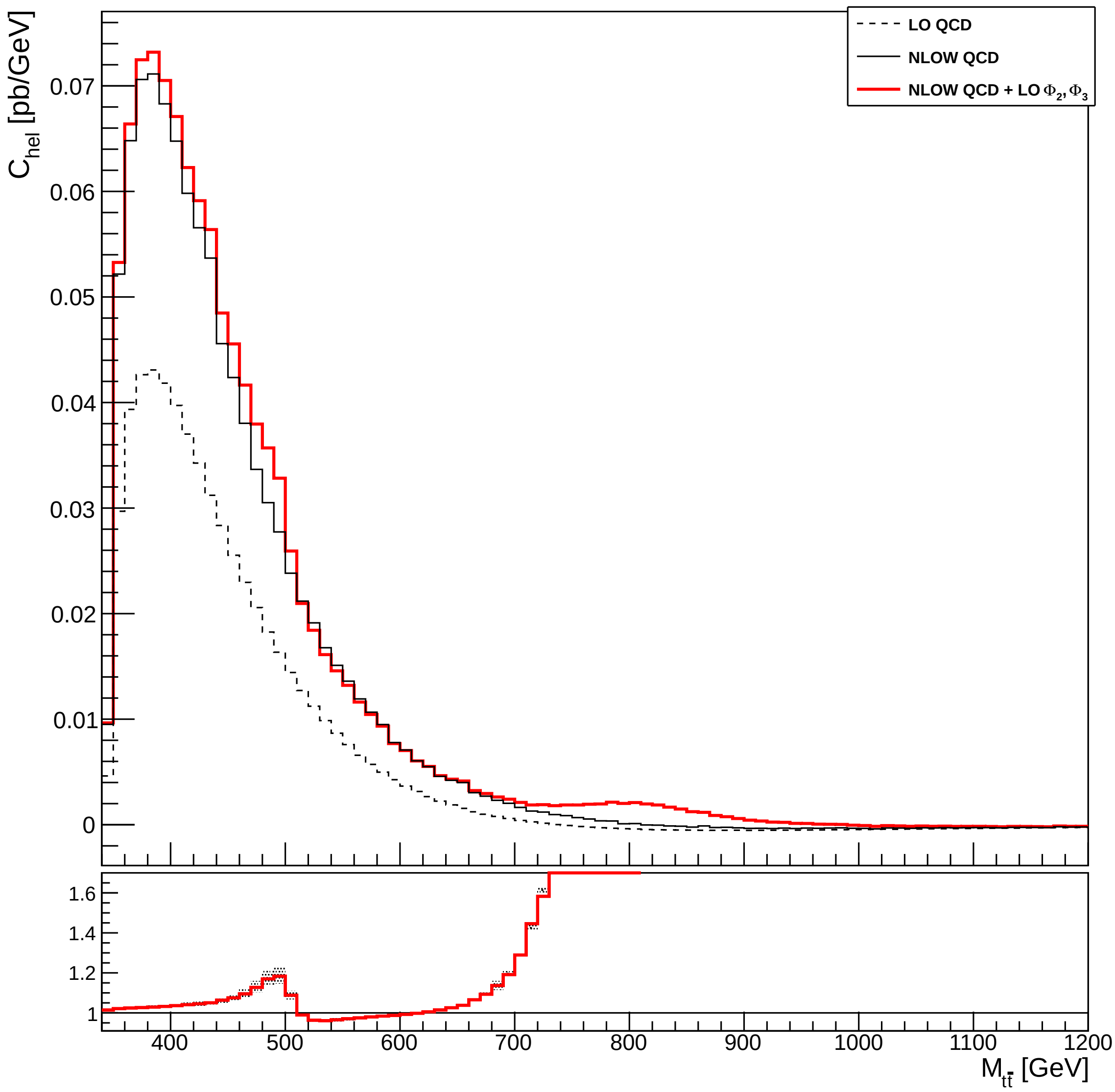

Figure 3.55. – *Unnormalized spin observable C_{hel} defined in* (3.125) *for* $\sqrt{s_{\mathrm{had}}} = 13$ *TeV proton-proton collisions including the effects of two neutral Higgs bosons (2HDM **scenario 3**) at LO QCD. Renormalization and factorization scales are set to $\mu = \mu_0 = 325$ GeV. Above* 750 *GeV, the ratio* $(NLOW + LO\,\phi_2, \phi_3)/NLOW$*, indicated by the thick line in the lower plot, becomes larger than* 2 *due to the effects of the resonance* ϕ_3*. However, one should notice that the absolute value of the spin observable is small in this* $M_{t\bar{t}}$ *range. The effect of scale variation in the interval* $\left[\frac{\mu_0}{2}, 2\mu_0\right]$ *is indicated by the shaded rectangles.*

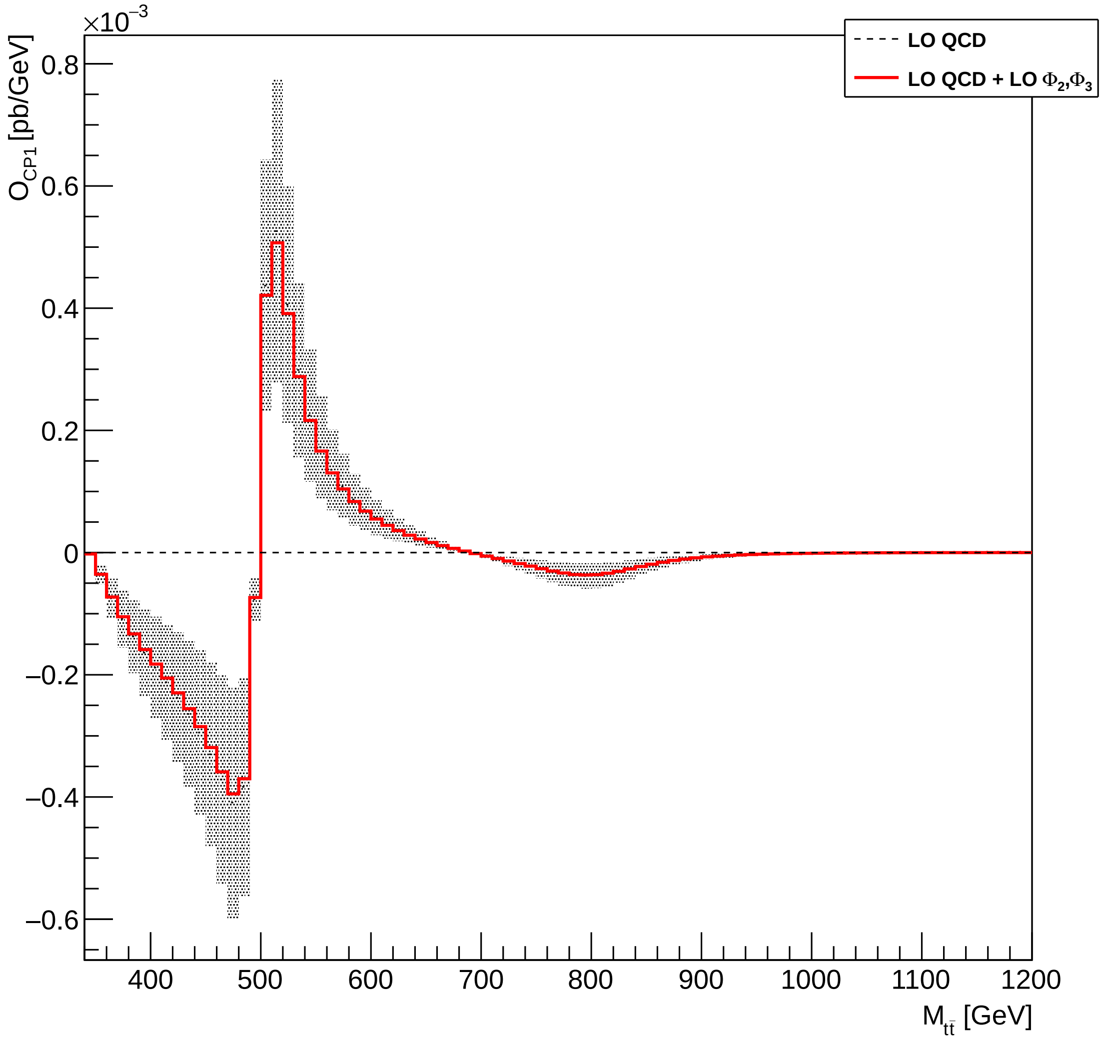

Figure 3.56. – *Unnormalized triple correlation observable* $O_{\rm CP}$ *defined in* (3.125) *for* $\sqrt{s_{\rm had}} =$ 13 *TeV proton-proton collisions including the effects of two neutral Higgs bosons (2HDM* ***scenario 3****) at LO QCD. Renormalization and factorization scales are set to* $\mu = \mu_0 =$ 325 *GeV. The effect of scale variation in the interval* $[\frac{\mu_0}{2}, 2\mu_0]$ *is indicated by the shaded rectangles.*

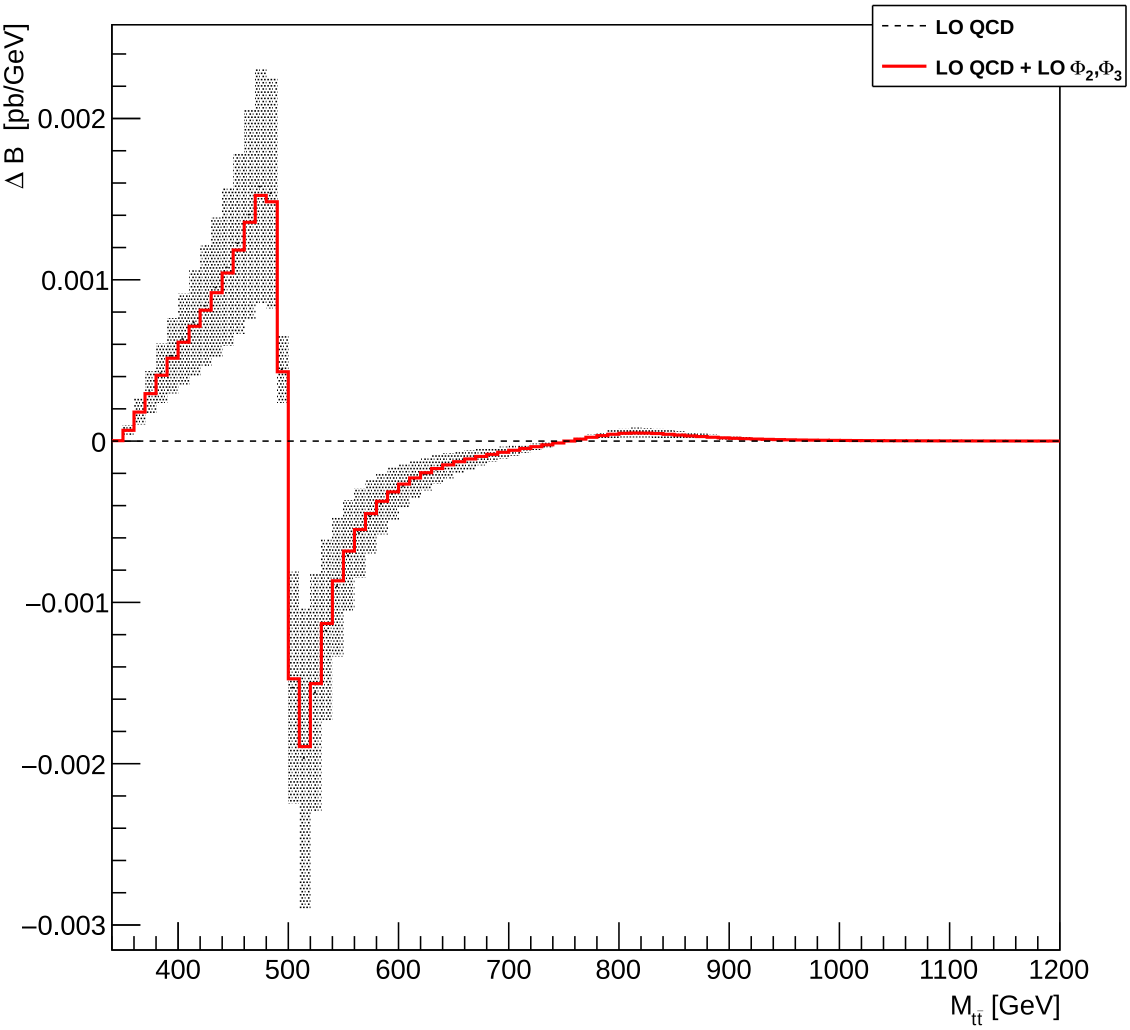

Figure 3.57. – *Unnormalized polarization difference* $\Delta B = B_+ - B_-$ *defined in* (3.125) *for* $\sqrt{s_{\mathrm{had}}} = 13$ *TeV proton-proton collisions including the effects of two neutral Higgs bosons (2HDM* ***scenario 3****) at LO QCD. Renormalization and factorization scales are set to* $\mu = \mu_0 = 325$ *GeV. The effect of scale variation in the interval* $\left[\frac{\mu_0}{2}, 2\mu_0\right]$ *is indicated by the shaded rectangles.*

4. Summary and conclusions

The working hypothesis of this thesis is that, in addition to the 125 GeV Higgs boson, additional heavy neutral Higgs bosons may exist, which have strong couplings to top quarks but suppressed couplings to W and Z bosons. Top-quark pair production at the LHC is the obvious reaction to search for such particles. The analysis of $t\bar{t}$ data at the LHC, which so far has been very rudimentary with regard to this possibility, requires precise theoretical predictions. In this thesis the effects of heavy, neutral Higgs boson resonances in $t\bar{t}$ production at the LHC have been investigated at next-to-leading order in the strong coupling. An essential new ingredient of our analysis, which has not been done before in the literature, is the incorporation of the interferences of the heavy Higgs production amplitudes with the respective non-resonant QCD $t\bar{t}$ amplitudes at NLO QCD. The NLO corrections to heavy Higgs boson production were computed in the large m_t limit with an effective K-factor rescaling. For the case of the inclusive production of a single neutral Higgs boson at the LHC, we could justify this approach by comparing the results obtained with this method to the most precise values available in the literature. We saw that this approximation yields reasonably good results also for heavy Higgs bosons. The effective K-factor rescaling procedure which we applied to obtain the numerical results is of course arbitrary. Other methods should be investigated and compared to this one – and eventually be replaced by the Higgs boson production amplitudes beyond one-loop for finite m_t.

Our NLO QCD computation of heavy Higgs production and decay into $t\bar{t}$ and the interferences with the QCD $t\bar{t}$ amplitudes are in principle rather model-independent. However, an essential ingredient in our analysis are the total decay widths of the Higgs bosons, which must be computed in a concrete model in order to maintain the unitarity of the S matrix. To find viable sets of parameters, we used the type-II two-Higgs doublet models (2HDM) with (and without) softly broken Z_2 symmetry, where three neutral Higgs bosons appear in the physical particle spectrum. We investigated three parameter scenarios in more detail, where one Higgs boson is identified with the 125 GeV neutral spin-0 resonance recently discovered at the LHC. The free parameters of the model are chosen such that this boson has SM-like couplings to the quarks, leptons, and weak gauge bosons. The masses of the other two neutral Higgs bosons were chosen to lie above the $t\bar{t}$ threshold, with top Yukawa couplings that are slightly larger than the SM top-Yukawa coupling. This choice was made to assess – cum grano salis – the maximal size of the effects of the heavy Higgs bosons in the $t\bar{t}$ decay channel.

We computed the (on- and off-shell) production of the heavy Higgs bosons ϕ_2, ϕ_3 and their decay into $t\bar{t}$ and the respective interferences with the QCD amplitudes at NLO QCD for gluon-gluon fusion, $q\bar{q}$ annihilation and qg fusion. For the description of the Higgs resonances we used the complex mass scheme. Moreover we showed, using the soft gluon approximation, that non-factorizable QCD corrections to resonant Higgs production and decay do not contribute. The pure QCD $t\bar{t}$ production at NLO including the weak-interaction corrections and the contribution of the light 125 GeV Higgs boson (NLOW) was computed with an existing computer code. All computations were made for $t\bar{t}$ in an arbitrary spin configuration. Semileptonic and non-leptonic t and $\bar{t}$ decay at LO QCD was incorporated in our computer code in a modular way. This allows to compute distributions, in particular $t\bar{t}$ spin correlations at the level of the final-state leptons/jets.

For the computation on $t\bar{t}$ level we considered proton-proton collisions at $\sqrt{s} = 8$ TeV and $\sqrt{s} = 13$ TeV. We found that in the three 2HDM scenarios the effect of the two heavy Higgs bosons on the inclusive $t\bar{t}$ cross section is at most 5 percent, which is within the present experimental and theoretical (SM) uncertainties. For the three scenarios, we computed several differential distributions at the $t\bar{t}$ level: the $M_{t\bar{t}}$ distribution, transverse momentum, and rapidity distributions. The most important observable for tracing heavy (Higgs) resonances in $t\bar{t}$ events is the $M_{t\bar{t}}$ distribution. Due to the fact that the total widths of the heavy Higgs bosons in our three 2HDM scenarios are rather large, the Higgs-QCD interference effects are important. As a result, the Higgs resonances do not show up as a Breit-Wigner resonance bump in the $M_{t\bar{t}}$ distribution, but produce a peak-dip structure around the respective resonance location. Our results show that the radiative QCD corrections are important for the description of the shape of $M_{t\bar{t}}$ spectrum in the vicinity of the resonances. The heavy Higgs effects on the transverse momentum and rapidity distributions of the t and $\bar{t}$ quarks are less pronounced. We further investigated the distributions of rapidity moduli differences $\Delta|y| = |y_t| - |y_{\bar{t}}|$ concerning asymmetries with respect to $\Delta|y| = 0$. We could not detect such an asymmetry in the NLO distributions originating from the resonant production of the heavy Higgs bosons ϕ_2, ϕ_3 and their interference with the non-resonant background, i.e. the charge asymmetry $A_C^{\Delta|y|}$ is generated solely by the NLOW corrections to the non-resonant $t\bar{t}$ production processes.

An additional tool for tracing these resonances are $t\bar{t}$ spin correlations which lead to characteristic angular correlations among the final-state leptons and/or jets. We considered dileptonic $t\bar{t}$ events in $\sqrt{s} = 13$ TeV proton-proton collisions and computed the so-called helicity correlation and opening angle distribution at NLO QCD including weak-interaction corrections in bins of $M_{t\bar{t}}$, with and without the contribution of the heavy Higgs bosons at LO QCD. Eventually, the NLO QCD corrections to the resonant processes and their interference with the non-resonant background should be taken into account also here. The peak-dip structure in the vicinity of the resonances shows up also in these observables. The Higgs sector of our 2HDM scenario 3 violates the CP symmetry already at tree level, i.e. the heavy Higgs resonances are no longer CP eigenstates. They induce a CP-odd transverse-transverse $t\bar{t}$ spin correlation and lead also to a difference in the longitudinal polarization of the t and $\bar{t}$ quarks. We computed the resulting CP-odd triple correlation and polarization difference at the level of the final-state leptons.

In order to assess the statistical significance of the heavy Higgs effects on the $M_{t\bar{t}}$ distribution and the spin correlation/polarization we computed for the respective observables ratios of the distribution with and without the heavy Higgs contributions within $M_{t\bar{t}}$ intervals of with ~ 100 GeV below and above the lowest resonance. We found that particularly for $\sqrt{s} = 13$ TeV proton-proton collisions at the LHC it is possible to find statistically significant excesses and deficits in the $M_{t\bar{t}}$ distribution in all three scenarios if convenient $M_{t\bar{t}}$ intervals are chosen. Of course, the right $M_{t\bar{t}}$ intervals can not be known beforehand and also the sizes of the reduced Yukawa couplings of the heavy Higgs bosons to top quarks are rather optimistic in the three scenarios. We also found that the CP-odd effects which are induced in scenario 3 are statistically insignificant.

The beyond-the-SM heavy Higgs boson scenarios which we analyzed in this thesis are still viable and lie on one of the several avenues towards answering the question whether the electroweak symmetry breaking mechanism is as described by the SM Higgs mechanism or whether there is more to it. Needless to say, our choice of parameters of the 2HDM, in particular our choice of the masses of the heavy Higgs bosons, are examples and do not exhaust the phenomenologically allowed parameter space of the 2HDM. Our analysis shows that it is not easy to detect heavy Higgs resonances in $t\bar{t}$ events. The only dedicated search so far at the LHC which we are aware of was made by the CMS collaboration in their $t\bar{t}$ data produced at 8 TeV. However, they analyzed their data with an $M_{t\bar{t}}$ distribution computed for Higgs production at LO and took Higgs-QCD interference not into account. This is an unrealistic model, as our analysis shows. A re-analysis of the 8 TeV $t\bar{t}$ data of the ATLAS and CMS experiments and the future analysis of data recorded at 13 TeV with regard to heavy Higgs searches requires a very good experimental resolution of the $M_{t\bar{t}}$ spectrum. As theory can make no prediction where the resonances should be located, one must scan the whole $M_{t\bar{t}}$ spectrum within suitably chosen $M_{t\bar{t}}$ bins. As Higgs physics is one of the central issues of present and future research at the LHC, this is certainly worth the effort. Our computation of the shape of the $M_{t\bar{t}}$ spectrum and of other distributions, in particular spin correlations, in the vicinity of a heavy resonance should become a useful tool in future analysis of $t\bar{t}$ data.

A. Feynman rules

This appendix contains a collection of Feynman rules which were used to obtain the results presented in this dissertation. This list is not intended to be exhaustive. Note that the Feynman rules involving Higgs bosons always refer to the 2HDM with the potential (1.18), where $\lambda_6 = \lambda_7 = 0$. Whenever neccessary, a small arrow above a line indicates the momentum flow direction. The gluon propagator (A.2) is given in the Feynman gauge.

Propagators

p 

$$= i\frac{\not{p} + m}{p^2 - m^2 + i\eta} \tag{A.1}$$

q 

$$= \frac{-ig^{\mu\nu}}{q^2 + i\eta} \tag{A.2}$$

k

$$= \frac{i}{k^2 - m_\phi^2 + i m_\phi \Gamma_\phi} \tag{A.3}$$

QCD vertices

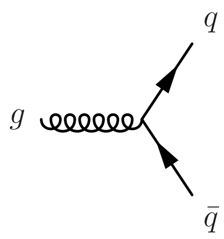

$$= \quad -ig_s T^a \gamma^\mu \tag{A.4}$$

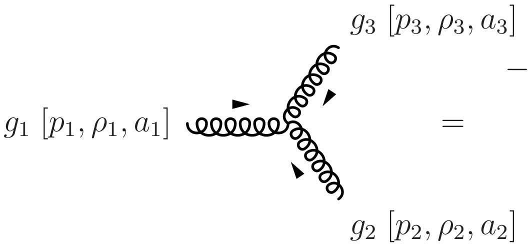

$$= \quad \begin{aligned} -g_s f^{a_1 a_2 a_3} \big[\ & g^{\rho_1 \rho_2} (p_1 - p_2)^{\rho_3} \\ & + g^{\rho_2 \rho_3} (p_2 - p_3)^{\rho_1} \\ & + g^{\rho_3 \rho_1} (p_3 - p_1)^{\rho_2} \big] \end{aligned} \tag{A.5}$$

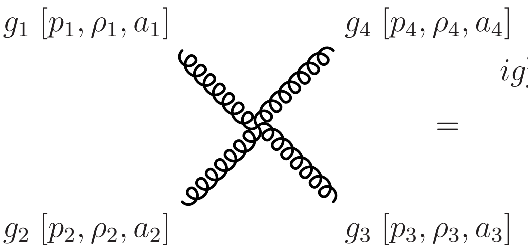

$$= \quad \begin{aligned} ig_s^2 \big[\ & f^{a_1 a_2 c} f^{a_3 a_4 c} \left(g^{\rho_2 \rho_3} g^{\rho_1 \rho_4} - g^{\rho_1 \rho_3} g^{\rho_2 \rho_4}\right) \\ & + f^{a_3 a_1 c} f^{a_2 a_4 c} \left(g^{\rho_1 \rho_2} g^{\rho_3 \rho_4} - g^{\rho_3 \rho_2} g^{\rho_1 \rho_4}\right) \\ & + f^{a_2 a_3 c} f^{a_1 a_4 c} \left(g^{\rho_3 \rho_1} g^{\rho_2 \rho_4} - g^{\rho_2 \rho_1} g^{\rho_3 \rho_4}\right) \big] \end{aligned} \tag{A.6}$$

Higgs-quark and effective Higgs-gluon vertices

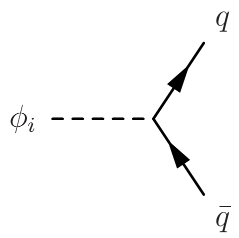

$$= \; i\frac{m_f}{v}\left(-a_{f,i}\mathbb{1} + i b_{f,i}\gamma_5\right) \tag{A.7}$$

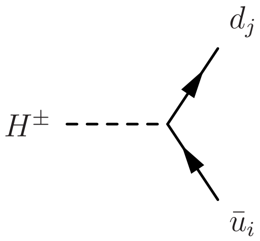

$$= \; -iV_{\mathrm{CKM}}^{ij}\frac{\sqrt{2}}{v}\left[m_i \cot\beta P_{L/R} + m_j \tan\beta P_{R/L}\right] \tag{A.8}$$

with $P_{L/R} = \frac{1}{2}\left(\mathbb{1} \mp \gamma_5\right)$

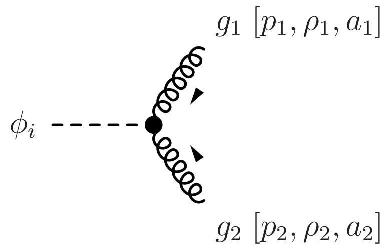

$$= \; 4i\delta^{a_1 a_2}\left[f_{H,i}\left(p_1^{\rho_2} p_2^{\rho_1} - g^{\rho_1,\rho_2}\, p_1.p_2\right) - 2f_{A,i}\,\epsilon^{p_1 p_2 \rho_1 \rho_2}\right] \tag{A.9}$$

with $\epsilon^{0123} = +1$ and

$$f_{H/A,i} = \frac{\alpha_s}{\pi} f_{H/A,i}^{(0)} + \left(\frac{\alpha_s}{\pi}\right)^2 f_{H/A,i}^{(1)} + \cdots$$

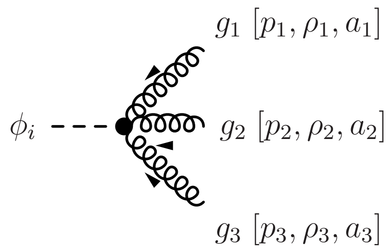

$$\begin{aligned} = \; & 4g_s f^{a_1 a_2 a_3}\Big\{ \\ & f_{H,i}\left[\, g^{\rho_1\rho_2}\left(p_1 - p_2\right)^{\rho_3} + g^{\rho_2\rho_3}\left(p_2 - p_3\right)^{\rho_1} + g^{\rho_3\rho_1}\left(p_3 - p_1\right)^{\rho_2}\right] \\ & +2f_{A,i}\,\left(p_1 + p_2 + p_3\right)_\sigma \epsilon^{\sigma\rho_1\rho_2\rho_3}\Big\} \end{aligned} \tag{A.10}$$

with $\epsilon^{0123} = +1$ and

$$f_{H/A,i} = \frac{\alpha_s}{\pi} f_{H/A,i}^{(0)} + \left(\frac{\alpha_s}{\pi}\right)^2 f_{H/A,i}^{(1)} + \cdots$$

Higgs-gauge boson vertices

The interactions of the physical Higgs bosons with the gauge bosons depend on the entries of the neutral mixing matrix R, c.f. (1.33) for the convention used here.

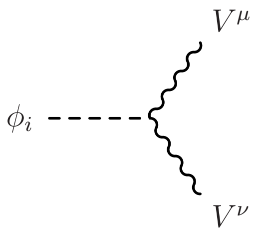

$$= \; 2i\frac{m_V^2}{v}g^{\mu\nu}\underbrace{(\cos\beta R_{i1}+\sin\beta R_{i2})}_{\equiv f_{iVV}} \quad , \quad V=\{W,Z\} \tag{A.11}$$

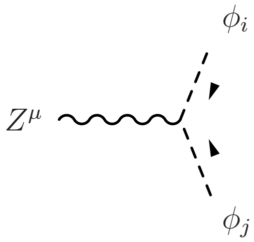

$$= \; \frac{g}{2\cos\theta_W}\underbrace{[(-\sin\beta R_{i1}+\cos\beta R_{i2})\,R_{j3}-(i\leftrightarrow j)]}_{\equiv f_{ijV}}(p_i-p_j)^\mu \tag{A.12}$$

Trilinear neutral Higgs self-interaction

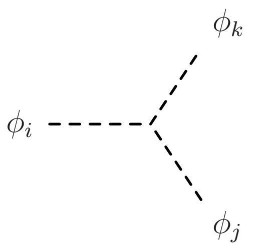

$$= \; if_{ijk} \quad , \quad f_{ijk}=\frac{-i\partial^3 V}{\partial\phi_i\partial\phi_j\partial\phi_k} \tag{A.13}$$

The coupling constants f_{ijk} of the trilinear neutral Higgs interaction are rather complicated expressions. In [35], Eqs. (383f) and (389), the relevant part of the Higgs potential is given in terms of the mass eigenstates ϕ_i:

$$\begin{aligned} V_{3s} \; = \; & \sum_{ijk}\phi_i\phi_j\phi_k \\ & \times\left[\frac{v}{2}C_i\left(\delta_{jk}-T_{1j}T_{1k}\right)+\frac{1}{v}\left(m_\pm^2-\frac{m_i^2}{2}\right)T_{1i}T_{1j}T_{1k}+\frac{m_j^2-m_\pm^2}{v}T_{1i}\delta_{jk}\right], \end{aligned}$$

where

$$C_i = T_{1i}\bar{\lambda}_3 + T_{2i}\,\mathrm{Re}\left(\bar{\lambda}_7\right) - T_{3i}\,\mathrm{Im}\left(\bar{\lambda}_7\right).$$

Note that in the convention of [35], the orthogonal matrix T defines the relation of the mass basis to the Higgs basis as

$$\begin{pmatrix} H_1 \\ H_2 \\ A \end{pmatrix} = T \begin{pmatrix} \phi_1 \\ \phi_2 \\ \phi_3 \end{pmatrix},$$

so that one has to substitute $T = B'^T R^T$ in (A.14). The definitions of R and B' are given in (1.34). The parameters $\bar{\lambda}_3$, $\bar{\lambda}_7$ are the coefficients of the respective quartic interaction terms in the potential (1.18) when the doublets are transformed to the Higgs basis (1.28). One can use Eqs. (124), (128) and (129) in [35] to express these in terms of $\lambda_{1,2,3,4,5}$ and $\tan\beta$[1]. The relevant relations read

$$\begin{aligned}
\bar{\lambda}_3 &= \lambda_3 + \frac{\sin^2 2\beta}{4}\left(\lambda_1 + \lambda_2 - 2\lambda_{345}\right), \\
\bar{\lambda}_7 &= -\frac{\sin 2\beta}{2}\left(\lambda_1 \sin^2\beta - \lambda_2\cos^2\beta + \lambda_{345}\cos 2\beta + i\ \mathrm{Im}\left(\lambda_5\right)\right),
\end{aligned}$$

with

$$\lambda_{345} = \lambda_3 + \lambda_4 + \mathrm{Re}\left(\lambda_5\right).$$

In the appendices of [40] and [79] the relations of the λ_i to the physical parameters (1.36) are given. Setting $\xi = \lambda_6 = \lambda_7 = 0$ in these equations one gets

$$\begin{aligned}
\lambda_1 &= \nu^2\tan^2\beta + \sum_{i=1}^{3}\frac{m_i^2}{v^2\cos^2\beta}R_{i1}^2, \\
\lambda_2 &= \nu^2\cot^2\beta + \sum_{i=1}^{3}\frac{m_i^2}{v^2\sin^2\beta}R_{i2}^2, \\
\lambda_3 &= \frac{2m_\pm^2}{v^2} - \nu^2 + \sum_{i=1}^{3}\frac{m_i^2}{v^2\cos\beta\sin\beta}R_{i1}R_{i2}, \\
\lambda_4 &= \nu^2 - \frac{2m_\pm^2}{v^2} + \sum_{i=1}^{3}\frac{m_i^2}{v^2}R_{i3}, \\
\lambda_5 &= \nu^2 - \frac{1}{v^2}\left(\sum_{i=1}^{3}m_i^2R_{i3}^2 - i\left(\frac{\sum_{i=1}^{3}m_i^2R_{i1}R_{i3}}{\sin\beta} + \frac{\sum_{i=1}^{3}m_i^2R_{i2}R_{i3}}{\cos\beta}\right)\right).
\end{aligned} \tag{A.14}$$

[1] Use $\chi = \xi = 0$ and $\psi = \beta$ in these equations. Note that the case $\lambda_6 = \lambda_7 = 0$ is considered here.

Combining these relation one can express the trilinear Higgs couplings (A.14) in terms of the physical parameters (1.36).

B. The 2HDM mass spectrum

In this appendix I will derive some equations that are useful to understand the mechanism of EWSB and the physical implications within the 2HDM discussed in Sec. 1.2, assuming that the potential has the form (1.18) with $\lambda_6 = \lambda_7 = 0$. In particular, the transition from the parameter set (1.35) to the physical parameters (1.36) should become more comprehensible.

Assuming that the minimum of the potential (1.18) has the form (1.25), i.e. that the VEVs are real and do not break $U(1)_{\mathrm{em}}$, the minimization conditions (1.24) lead to two complex equations. The real parts of these equations are

$$\begin{aligned} \mu_1^2 &= \frac{v_2^2}{2}\lambda_{345} + v_1^2\lambda_1 - \frac{v_2}{v_1}\,\mathrm{Re}\left(\mu_3^2\right), \\ \mu_2^2 &= \frac{v_1^2}{2}\lambda_{345} + v_2^2\lambda_2 - \frac{v_1}{v_2}\,\mathrm{Re}\left(\mu_3^2\right), \end{aligned} \tag{B.1}$$

where we have used the abbreviation $\lambda_{345} = \lambda_3 + \lambda_4 + \mathrm{Re}\,(\lambda_5)$. The imaginary parts yield only one independent equation,

$$2\ \mathrm{Im}\left(\mu_3^2\right) = \mathrm{Im}\,(\lambda_5)\, v_1 v_2. \tag{B.2}$$

Thus the parameters $\mathrm{Im}\,(\mu_3^2)$ and $\mathrm{Im}\,(\lambda_5)$ are related if one demands a purely real expectation value such as (1.25), and in particular none of them can be zero in the CP violating scenario. In the following we will express the VEVs through the angle β as $v_1 = v\cos\beta$ and $v_2 = v\sin\beta$, such that $\tan\beta = \frac{v_2}{v_1}$. We will further make use of the definition of the dimensionless parameter ν given in (1.32).

We defined the charged and neutral mass matrices in (1.27) in terms of the basis states $\left(\varphi_1^+, \varphi_2^+\right)^T$ and $(\varphi_1, \varphi_2, \chi_1, \chi_2)^T$. The explicit expressions derived from the potential (1.18) with $\lambda_6 = \lambda_7 = 0$ are

$$\mathcal{M}_{ij}^{\pm\,2} = \frac{v^2}{2}\begin{pmatrix} \sin^2\beta\,(2\nu - \lambda_{45}) & -\sin\beta\cos\beta\,(2\nu - \lambda_{45}) \\ -\sin\beta\cos\beta\,(2\nu - \lambda_{45}) & \cos^2\beta\,(2\nu - \lambda_{45}) \end{pmatrix}, \tag{B.3}$$

for the charged Higgs mass matrix, and

$$\begin{aligned}
\mathcal{M}^2_{[1,2|1,2]} &= v^2 \begin{pmatrix} \nu \sin^2\beta + 2\lambda_1 \cos^2\beta & \cos\beta \sin\beta\,(\lambda_{345} - \nu) \\ \cos\beta \sin\beta\,(\lambda_{345} - \nu) & \nu \cos^2\beta + 2\lambda_2 \sin^2\beta \end{pmatrix}, \\
\mathcal{M}^2_{[3,4|3,4]} &= v^2 \begin{pmatrix} \sin^2\beta\,(\nu - \mathrm{Re}\,(\lambda_5)) & \cos\beta \sin\beta\,(\mathrm{Re}\,(\lambda_5) - \nu) \\ \cos\beta \sin\beta\,(\mathrm{Re}\,(\lambda_5) - \nu) & \cos^2\beta\,(\nu - \mathrm{Re}\,(\lambda_5)) \end{pmatrix}, \\
\mathcal{M}^2_{[1,2|3,4]} &= \frac{v^2}{2} \begin{pmatrix} \sin^2\beta\,\mathrm{Im}\,(\lambda_5) & \sin\beta\cos\beta\,\mathrm{Im}\,(\lambda_5) \\ -\sin\beta\cos\beta\,\mathrm{Im}\,(\lambda_5) & -\cos^2\beta\,\mathrm{Im}\,(\lambda_5) \end{pmatrix}.
\end{aligned} \tag{B.4}$$

for the neutral Higgs mass matrix. The latter is a 4×4 matrix which, for readability, is split here into 2×2 blocks, the numbers in square brackets indicating the respective submatrices.

Now me make the transition to the Higgs basis. Arranging the component fields of the Higgs doublets appropriately into column vectors, the basis transformation (1.28) takes the form

$$\begin{pmatrix} G^+ \\ H^+ \end{pmatrix} = B \begin{pmatrix} \varphi_1^+ \\ \varphi_2^+ \end{pmatrix} \quad , \quad \begin{pmatrix} H_1 \\ H_2 \\ A \\ G_0 \end{pmatrix} = \begin{pmatrix} B & 0 \\ 0 & B \end{pmatrix} \begin{pmatrix} \varphi_1 \\ \varphi_2 \\ \chi_1 \\ \chi_2 \end{pmatrix}, \tag{B.5}$$

with

$$B = \begin{pmatrix} \cos\beta & \sin\beta \\ -\sin\beta & \cos\beta \end{pmatrix},$$

which we already used in (1.28). In the Higgs basis, the charged mass matrix (B.3) is diagonal:

$$B\mathcal{M}^{\pm\,2}B^T = \begin{pmatrix} 0 & 0 \\ 0 & m_\pm^2 \end{pmatrix},$$

with eigenvalues 0 and $m_\pm$. The latter is the mass of the physical charged Higgs boson H^+, expressed in (1.31) in terms of the parameters (1.35).

As to the neutral Higgs mass matrix, we will convert only the two CP-odd fields χ_1 and χ_2 to their Higgs basis counterparts, i.e. we will apply the following basis transformation:

$$\begin{pmatrix} \varphi_1 \\ \varphi_2 \\ A \\ G_0 \end{pmatrix} = \underbrace{\begin{pmatrix} \mathbb{1} & 0 \\ 0 & \sigma_1 B \end{pmatrix}}_{=\hat{B}} \begin{pmatrix} \varphi_1 \\ \varphi_2 \\ \chi_1 \\ \chi_2 \end{pmatrix}. \tag{B.6}$$

In the new basis, the neutral mass matrix (B.4) has the form

$$\hat{B}\mathcal{M}^2\hat{B}^T = \begin{pmatrix} \hat{\mathcal{M}}^2 & 0 \\ 0 & 0 \end{pmatrix},$$

with

$$\hat{\mathcal{M}}^2 = v^2 \begin{pmatrix} \nu\sin^2\beta + 2\lambda_1\cos^2\beta & \sin\beta\cos\beta\,(\lambda_{345}-\nu) & -\frac{1}{2}\sin\beta\,\mathrm{Im}\,(\lambda_5) \\ \sin\beta\cos\beta\,(\lambda_{345}-\nu) & \nu\cos^2\beta + 2\lambda_2\sin^2\beta & -\frac{1}{2}\cos\beta\,\mathrm{Im}\,(\lambda_5) \\ -\frac{1}{2}\sin\beta\,\mathrm{Im}\,(\lambda_5) & -\frac{1}{2}\cos\beta\,\mathrm{Im}\,(\lambda_5) & \nu - \mathrm{Re}\,(\lambda_5) \end{pmatrix}. \tag{B.7}$$

Note the permutation introduced with the Pauli matrix σ_1 in (B.6) to move the eigenvalue 0, corresponding to the neutral pseudo-Goldstone boson G_0, to the lower right corner. We can now focus on the part of the mass matrix (B.7) which corresponds to the fields $(\varphi_1, \varphi_2, A)^T$. The transformation to the mass eigenstates $(\phi_1, \phi_2, \phi_3)^T$ is defined in (1.33). In our convention the orthogonal matrix R is defined such that it diagonalizes the remaining 3×3 block $\hat{\mathcal{M}}^2$ of the neutral mass matrix, i.e.

$$\begin{pmatrix} m_1^2 & 0 & 0 \\ 0 & m_2^2 & 0 \\ 0 & 0 & m_3^2 \end{pmatrix} = R\hat{\mathcal{M}}^2R^T, \tag{B.8}$$

where the eigenvalues $m_{1,2,3}^2$ correspond to the masses of the neutral physical Higgs bosons, i.e. in all physical scenarios the eigenvalues of $\hat{\mathcal{M}}^2$ have to be real and positive. The inverse of this relation,

$$R^T \begin{pmatrix} m_1^2 & 0 & 0 \\ 0 & m_2^2 & 0 \\ 0 & 0 & m_3^2 \end{pmatrix} R = \hat{\mathcal{M}}^2, \tag{B.9}$$

provides 6 equations, which relate the physical parameters $m^2_{1,2,3}$ and $\alpha_{1,2,3}$ to the original set (1.35). Focusing on the entries (1,3) and (2,3) of the matrix equation (B.9) and using the explicit expression (B.7) of $\hat{\mathcal{M}}^2$ we find

$$\begin{aligned} m_1^2 R_{11} R_{13} + m_2^2 R_{21} R_{23} + m_3^2 R_{31} R_{33} &= -\frac{1}{2} \sin\beta \, \mathrm{Im}\,(\lambda_5)\,, \\ m_1^2 R_{12} R_{13} + m_2^2 R_{22} R_{23} + m_3^2 R_{32} R_{33} &= -\frac{1}{2} \cos\beta \, \mathrm{Im}\,(\lambda_5)\,. \end{aligned} \tag{B.10}$$

Note that the two entries of the neutral mass matrix are related via $\hat{\mathcal{M}}^2_{13} = \tan\beta \hat{\mathcal{M}}^2_{23}$[1]. For $\mathrm{Im}\,(\lambda_5) \neq 0$ we can divide the two equations (B.10) and express for example m_3^2 in terms of $m^2_{1,2}$, the components of the mixing matrix R, and $\tan\beta$:

$$m_3^2 = \frac{m_1^2 R_{13} \left(R_{12} \tan\beta - R_{11}\right) + m_2^2 R_{23} \left(R_{22} \tan\beta - R_{21}\right)}{R_{33} \left(R_{31} - \tan\beta R_{32}\right)}. \tag{B.11}$$

Note that the requirement $m_3^2 > 0$ implies boundaries on the values of the mixing angles $\alpha_{1,2,3}$ for given $\tan\beta$ and $m^2_{1,2}$. In models with $\lambda_6, \lambda_7 \neq 0$ the relation (B.11) for m_3 does not hold.

As to the relation of the parameter set (1.35) to the physical parameters (1.36): The conditions (B.1) and (B.2) allow us to express μ_1^2, μ_2^2 and $\mathrm{Im}\,(\mu_3^2)$ in terms of v, $\tan\beta$ and $\mathrm{Im}\,(\lambda_5)$. We further use the definition of ν, given in (1.32), to eliminate $\mathrm{Re}\,(\mu_3^2)$. The 6 equations (B.9) are then used to relate $m^2_{1,2,3}$ and $\alpha_{1,2,3}$ to the remaining parameters $\lambda_{1,2,3,4}$, $\mathrm{Re}\,(\lambda_5)$ and $\mathrm{Im}\,(\lambda_5)$, see [42] for the explicit expressions. Finally, in the case $\mathrm{Im}\,(\lambda_5) \neq 0$ we see from (B.11) that m_3^2 is determined by $m^2_{1,2}$, $\alpha_{1,2,3}$ and $\tan\beta$. Thus, there are in total 8 parameters that can be chosen independently, for example the physical set (1.36). Alternatively one could solve (B.11) for $\tan\beta$.

In the case $\mathrm{Im}\,(\lambda_5) = 0$, which corresponds to the CP conserving scenarios within the type-II 2HDM, the mass matrix of the neutral Higgs fields (B.7) in the Higgs basis reduces to a 2×2 block and one non-zero diagonal element. The latter is the mass $m_A^2 = v^2 \left(\nu - \mathrm{Re}\,(\lambda_5)\right)$ of the CP-odd field A, which consitutes a physical Higgs boson in this case. The matrix that diagonalizes the remaining 2×2 block can be parametrized by means of a single angle α, describing the mixing of the two CP-even fields φ_1 and φ_2. Thus all physical Higgs fields are also CP eigenstates in this case. Equation (B.10) poses no additional constraint in the case of $\mathrm{Im}\,(\lambda_5) = 0$, so that the 7 parameters $m^2_{1,2,3}$, α, $m^2_{\pm}$, $\tan\beta$ and ν can be chosen independently.

[1] This is not the case anymore if $\lambda_7 \neq 0$.

Bibliography

[1] F. Englert and R. Brout, "Broken Symmetry and the Mass of Gauge Vector Mesons", *Phys. Rev. Lett.* **13** (1964) 321–323.

[2] P. W. Higgs, "Broken Symmetries and the Masses of Gauge Bosons", *Phys. Rev. Lett.* **13** (1964) 508–509.

[3] **ATLAS Collaboration**, G. Aad *et al.*, "Observation of a new particle in the search for the Standard Model Higgs boson with the ATLAS detector at the LHC", *Phys. Lett. B* **716** .

[4] **CMS Collaboration**, S. Chatrchyan *et al.*, "Observation of a new boson at a mass of 125 GeV with the CMS experiment at the LHC", *Phys. Lett. B* **716** .

[5] **ATLAS Collaboration**, G. Aad *et al.*, "Measurements of Higgs boson production and couplings in diboson final states with the ATLAS detector at the LHC", *Phys. Lett. B* **726** (2013) 88–119, `arXiv:1307.1427 [hep-ex]`.

[6] **CMS Collaboration**, V. Khachatryan *et al.*, "Precise determination of the mass of the Higgs boson and tests of compatibility of its couplings with the standard model predictions using proton collisions at 7 and 8 TeV", `arXiv:1412.8662 [hep-ex]`.

[7] T. D. Lee, "A Theory of Spontaneous T Violation", *Phys. Rev. D* **8** (1973) 1226–1239.

[8] S. P. Martin, "A Supersymmetry primer", *Adv. Ser. Direct High Energy Phys.* **21** (2010) 1–153, `arXiv:hep-ph/9709356 [hep-ph]`.

[9] A. Djouadi, "The Anatomy of electro-weak symmetry breaking. II. The Higgs bosons in the minimal supersymmetric model", *Phys. Rept.* **459** (2008) 1–241, `arXiv:hep-ph/0503173 [hep-ph]`.

[10] **ATLAS, CDF, CMS, D0**, "First combination of Tevatron and LHC measurements of the top-quark mass", `arXiv:1403.4427 [hep-ex]`.

[11] A. Czarnecki and K. Melnikov, "Two loop QCD corrections to top quark width", *Nucl. Phys. B* **544** (1999) 520–531, `arXiv:hep-ph/9806244 [hep-ph]`.

[12] **Particle Data Group**, K. Olive *et al.*, "Review of Particle Physics", *Chin. Phys. C* **38** (2014) 090001.

[13] D. Dicus, A. Stange, and S. Willenbrock, "Higgs decay to top quarks at hadron colliders", *Phys.Lett.* **B333** (1994) 126–131, `arXiv:hep-ph/9404359 [hep-ph]`.

[14] W. Bernreuther, M. Flesch, and P. Haberl, "Signatures of Higgs bosons in the top quark decay channel at hadron colliders", *Phys. Rev. D* **58** (1998) 114031,

arXiv:hep-ph/9709284 [hep-ph].

[15] **CMS**, S. Chatrchyan *et al.*, "Searches for new physics using the $t\bar{t}$ invariant mass distribution in pp collisions at $\sqrt{s} = 8$ TeV", *Phys.Rev.Lett.* **111** (2013) no. 21, 211804, arXiv:1309.2030 [hep-ex].

[16] **CMS Collaboration**, "A search for resonant ttbar production in all final states in pp collisions at $\sqrt{s} = 8$ TeV", Tech. Rep. CMS-PAS-B2G-13-008, CERN, Geneva, 2015. http://cds.cern.ch/record/2000999.

[17] **CMS Collaboration**, "Search for top-Higgs resonances in all-hadronic final states using jet substructure methods", Tech. Rep. CMS-PAS-B2G-14-002, CERN, Geneva, 2014. http://cds.cern.ch/record/1706121.

[18] **ATLAS Collaboration**, "A search for $t\bar{t}$ resonances using lepton plus jets events in proton-proton collisions at $\sqrt{s} = 8$ TeV with the ATLAS detector", Tech. Rep. ATLAS-CONF-2015-009, CERN, Geneva, Mar, 2015. http://cds.cern.ch/record/2002440.

[19] M. Czakon, P. Fiedler, and A. Mitov, "Total Top-Quark Pair-Production Cross Section at Hadron Colliders Through $\mathcal{O}(\alpha_S^4)$", *Phys. Rev. Lett.* **110** (2013) 252004.

[20] S. Dawson, "Radiative corrections to Higgs boson production", *Nucl. Phys. B* **359** (1991) 283.

[21] A. Djouadi, M. Spira, and P. Zerwas, "Production of Higgs bosons in proton colliders. QCD corrections", *Phys. Lett. B* **264** (1991) 440–446.

[22] D. Graudenz, M. Spira, and P. M. Zerwas, "QCD corrections to Higgs-boson production at proton-proton colliders", *Phys. Rev. Lett.* **70** (1993) 1372–1375.

[23] R. V. Harlander and W. B. Kilgore, "Soft and virtual corrections to proton proton $\to H + X$ at NNLO", *Phys. Rev. D* **64** (2001) 013015, arXiv:hep-ph/0102241 [hep-ph].

[24] C. Anastasiou and K. Melnikov, "Higgs boson production at hadron colliders in NNLO QCD", *Nucl. Phys. B* **646** (2002) 220–256, arXiv:hep-ph/0207004 [hep-ph].

[25] S. Catani, D. de Florian, M. Grazzini, and P. Nason, "Soft gluon resummation for Higgs boson production at hadron colliders", *JHEP* **0307** (2003) 028, arXiv:hep-ph/0306211 [hep-ph].

[26] D. de Florian and M. Grazzini, "Higgs production through gluon fusion: Updated cross sections at the Tevatron and the LHC", *Phys. Lett. B* **674** (2009) 291–294, arXiv:0901.2427 [hep-ph].

[27] **LHC Higgs Cross Section Working Group**, S. Dittmaier *et al.*, "Handbook of LHC Higgs Cross Sections: 1. Inclusive Observables", arXiv:1101.0593 [hep-ph].

[28] V. Borodulin, R. Rogalev, and S. Slabospitsky, "CORE: COmpendium of RElations: Version 2.1", arXiv:hep-ph/9507456 [hep-ph].

[29] A. Djouadi, "The Anatomy of electro-weak symmetry breaking. I: The Higgs

boson in the standard model", *Phys. Rept.* **457** (2008) 1–216,
`arXiv:hep-ph/0503172 [hep-ph]`.

[30] G. C. Branco, L. Lavoura, and J. P. Silva, *CP violation.* The International Series of Monographs on Physics. Oxford University Press, 1999.

[31] W. Bernreuther, T. Schroeder, and T. N. Pham, "CP-violating dipole form factors in $e^+e^- \to \bar{t}t$", *Phys. Lett. B* **279** .

[32] W. Bernreuther and A. Brandenburg, "Signatures of Higgs sector CP violation in top quark pair production at proton-proton supercolliders", *Phys. Lett. B* **314** .

[33] W. Bernreuther and A. Brandenburg, "Tracing CP violation in the production of top quark pairs by multiple TeV proton-proton collisions", *Phys. Rev. D* **49** (1994) 4481–4492.

[34] J. Gunion, H. E. Haber, G. Kane, and S. Dawson, *The Higgs hunter's guide.* Frontiers in physics. Addison-Wesley, 1990.

[35] G. Branco, P. Ferreira, L. Lavoura, M. Rebelo, M. Sher, *et al.*, "Theory and phenomenology of two-Higgs-doublet models", *Phys. Rept.* **516** (2012) 1–102, `arXiv:1106.0034 [hep-ph]`.

[36] S. Davidson and H. E. Haber, "Basis-independent methods for the two-Higgs-doublet model", *Phys. Rev. D* **72** (2005) 035004, `arXiv:hep-ph/0504050 [hep-ph]`.

[37] A. W. El Kaffas, W. Khater, O. M. Ogreid, and P. Osland, "Consistency of the two Higgs doublet model and CP violation in top production at the LHC", *Nucl. Phys. B* **775** (2007) 45–77, `arXiv:hep-ph/0605142 [hep-ph]`.

[38] W. Grimus, L. Lavoura, O. Ogreid, and P. Osland, "A Precision constraint on multi-Higgs-doublet models", *J. Phys.* **G35** (2008) 075001, `arXiv:0711.4022 [hep-ph]`.

[39] J. Gunion, H. Haber, and J. Wudka, "Sum rules for Higgs bosons", *Phys. Rev. D* **43** (1991) 904–912.

[40] B. Grzadkowski, O. Ogreid, and P. Osland, "Measuring CP violation in Two-Higgs-Doublet models in light of the LHC Higgs data", *JHEP* **1411** (2014) 084, `arXiv:1409.7265 [hep-ph]`.

[41] **ATLAS Collaboration**, "Combined coupling measurements of the Higgs-like boson with the ATLAS detector using up to 25 fb^{-1} of proton-proton collision data", Tech. Rep. ATLAS-CONF-2013-034, CERN, Geneva, 2013.

[42] A. W. El Kaffas, P. Osland, and O. M. Ogreid, "CP violation, stability and unitarity of the two Higgs doublet model", *Nonlin. Phenom. Complex Syst.* **10** (2007) 347–357, `arXiv:hep-ph/0702097 [HEP-PH]`.

[43] **CMS Collaboration**, "Combination of standard model Higgs boson searches and measurements of the properties of the new boson with a mass near 125 GeV", Tech. Rep. CMS-PAS-HIG-13-005, CERN, Geneva, 2013.

[44] T. Hermann, M. Misiak, and M. Steinhauser, "$\bar{B} \to X_s\gamma$ in the Two Higgs Doublet

Model up to Next-to-Next-to-Leading Order in QCD", *JHEP* **1211** (2012) 036, arXiv:1208.2788 [hep-ph].

[45] J. Brod, U. Haisch, and J. Zupan, "Constraints on CP-violating Higgs couplings to the third generation", *JHEP* **1311** (2013) 180, arXiv:1310.1385 [hep-ph].

[46] D. Eriksson, J. Rathsman, and O. Stal, "2HDMC: Two-Higgs-Doublet Model Calculator Physics and Manual", *Comput. Phys. Commun.* **181** (2010) 189–205, arXiv:0902.0851 [hep-ph].

[47] P. Bechtle, K. Desch, H. K. Dreiner, M. Hamer, M. Kraemer, *et al.*, "Constrained Supersymmetry after the Higgs Boson Discovery: A global analysis with Fittino", *PoS* **EPS-HEP2013** (2013) 313, arXiv:1310.3045 [hep-ph].

[48] A. Pilaftsis, "Higgs scalar-pseudoscalar mixing in the minimal supersymmetric Standard Model", *Phys. Lett. B* **435** .

[49] M. Carena, J. Ellis, A. Pilaftsis, and C. E. M. Wagner, "Renormalization-group-improved effective potential for the MSSM Higgs sector with explicit CP violation", *Nucl. Phys. B* **586** .

[50] H. M. Georgi, S. L. Glashow, M. E. Machacek, and D. V. Nanopoulos, "Higgs Bosons from Two-Gluon Annihilation in Proton-Proton Collisions", *Phys. Rev. Lett.* **40** (1978) 692–694.

[51] J. Collins, *Foundations of perturbative QCD.* Cambridge monographs on particle physics, nuclear physics and cosmology. 2011.

[52] R. Harlander, M. Muhlleitner, J. Rathsman, M. Spira, and O. Stal, "Interim recommendations for the evaluation of Higgs production cross sections and branching ratios at the LHC in the Two-Higgs-Doublet Model", arXiv:1312.5571 [hep-ph].

[53] C. Anastasiou, R. Boughezal, and F. Petriello, "Mixed QCD-electroweak corrections to Higgs boson production in gluon fusion", *JHEP* **0904** (2009) 003, arXiv:0811.3458 [hep-ph].

[54] R. V. Harlander and W. B. Kilgore, "Production of a pseudoscalar Higgs boson at hadron colliders at next-to-next-to leading order", *JHEP* **0210** (2002) 017, arXiv:hep-ph/0208096 [hep-ph].

[55] M. Kramer, E. Laenen, and M. Spira, "Soft gluon radiation in Higgs boson production at the LHC", *Nucl. Phys. B* **511** (1998) 523–549, arXiv:hep-ph/9611272 [hep-ph].

[56] H.-L. Lai, M. Guzzi, J. Huston, Z. Li, P. M. Nadolsky, *et al.*, "New parton distributions for collider physics", *Phys. Rev. D* **82** (2010) 074024, arXiv:1007.2241 [hep-ph].

[57] A. Martin, W. Stirling, R. Thorne, and G. Watt, "Parton distributions for the LHC", *Eur. Phys. J.* **C63** (2009) 189–285, arXiv:0901.0002 [hep-ph].

[58] F. Campanario and M. Kubocz, "Higgs boson CP-properties of the gluonic contributions in Higgs plus three jet production via gluon fusion at the LHC",

JHEP **1410** (2014) 173, arXiv:1402.1154 [hep-ph].

[59] W. Beenakker, F. Berends, and A. Chapovsky, "One-loop QCD interconnection effects in pair production of top quarks", *Phys. Lett. B* **454** (1999) no. 1-2, 129 – 136.

[60] S. Catani and M. H. Seymour, "A General Algorithm for Calculating Jet Cross Sections in NLO QCD", *Nucl. Phys. B* **485** (1997) 291, arXiv:hep-ph/9605323v3.

[61] S. Catani, S. Dittmaier, M. H. Seymour, and Z. Trocsanyi, "The Dipole Formalism for Next-to-Leading Order QCD Calculations with Massive Partons", *Nucl. Phys. B* **627** (2002) 189, arXiv:hep-ph/0201036v1.

[62] A. Brandenburg, Z. Si, and P. Uwer, "QCD corrected spin analyzing power of jets in decays of polarized top quarks", *Phys. Lett. B* **539** (2002) 235–241, arXiv:hep-ph/0205023 [hep-ph].

[63] W. Bernreuther, P. González, and C. Mellein, "Decays of polarized top quarks to lepton, neutrino and jets at NLO QCD", *Eur. Phys. J.* **C74** (2014) no. 3, 2815, arXiv:1401.5930 [hep-ph].

[64] A. Denner, S. Dittmaier, M. Roth, and D. Wackeroth, "Predictions for all processes $e + e- \to 4$ fermions $+ \gamma$", *Nucl. Phys. B* **560** (1999) 33–65, arXiv:hep-ph/9904472 [hep-ph].

[65] A. Denner, S. Dittmaier, M. Roth, and L. Wieders, "Electroweak corrections to charged-current $e + e- \to 4$ fermion processes: Technical details and further results", *Nucl. Phys. B* **724** (2005) 247–294, arXiv:hep-ph/0505042 [hep-ph].

[66] S. Dittmaier, S. Dittmaier, C. Mariotti, G. Passarino, R. Tanaka, *et al.*, "Handbook of LHC Higgs Cross Sections: 2. Differential Distributions", arXiv:1201.3084 [hep-ph].

[67] W. Bernreuther, A. Brandenburg, Z. Si, and P. Uwer, "Top quark pair production and decay at hadron colliders", *Nucl. Phys. B* **690** (2004) 81–137, arXiv:hep-ph/0403035 [hep-ph].

[68] W. Bernreuther and Z. G. Si, "Distributions and correlations for top quark pair production and decay at the Tevatron and LHC", *Nucl. Phys. B* **837** .

[69] G. 't Hooft and M. Veltman, "Regularization and Renormalization of Gauge Fields", *Nucl. Phys. B* **44** (1972) 189–213.

[70] W. Beenakker, A. Chapovsky, and F. A. Berends, "Nonfactorizable corrections to W pair production: Methods and analytic results", *Nucl. Phys. B* **508** (1997) 17–63, arXiv:hep-ph/9707326 [hep-ph].

[71] G. Passarino and M. Veltman, "One-loop corrections for e^+e^- annihilation into $\mu^+\mu^-$ in the Weinberg model", *Nucl. Phys. B* **160** (1979) 151–207.

[72] R. K. Ellis and G. Zanderighi, "Scalar one-loop integrals for QCD", *JHEP* **0802** (2008) 002, arXiv:0712.1851v2.

[73] A. Dabelstein and W. Hollik, "Electroweak corrections to the fermionic decay width of the standard Higgs boson", *Z. Phys. C* **53** (1992) no. 3, 507–515.

http://dx.doi.org/10.1007/BF01625912.

[74] J. Fleischer and F. Jegerlehner, "Radiative corrections to Higgs-boson decays in the Weinberg-Salam model", *Phys. Rev. D* **23** (1981) 2001–2026. http://link.aps.org/doi/10.1103/PhysRevD.23.2001.

[75] **CMS**, S. Chatrchyan *et al.*, "Measurement of the $t\bar{t}$ production cross section in the dilepton channel in pp collisions at $\sqrt{s} = 8$ TeV", *JHEP* **1402** (2014) 024, arXiv:1312.7582 [hep-ex].

[76] **CMS**, V. Khachatryan *et al.*, "Measurement of the differential cross section for top quark pair production in pp collisions at sqrt(s) = 8 TeV", arXiv:1505.04480 [hep-ex].

[77] W. Bernreuther and Z.-G. Si, "Top quark and leptonic charge asymmetries for the Tevatron and LHC", *Phys. Rev. D* **86** (2012) 034026, arXiv:1205.6580 [hep-ph].

[78] W. Barletta, M. Battaglia, M. Klute, M. Mangano, S. Prestemon, *et al.*, "Working Group Report: Hadron Colliders", arXiv:1310.0290 [physics.acc-ph].

[79] P. Osland, P. Pandita, and L. Selbuz, "Trilinear Higgs couplings in the two Higgs doublet model with CP violation", *Phys.Rev.* **D78** (2008) 015003, arXiv:0802.0060 [hep-ph].

Acknowledgments

First I wish to thank my supervisor Werner Bernreuther for all his efforts during the last years. Further I thank Peter Galler, who supported me with many helpful discussions and the comparison of numerical results. I also want to thank the other collaborators, Peter Uwer and Zongguo Si, who contributed to this project and are still engaged in the continuation. Finally I want to thank all the other colleagues in Aachen for the pleasant time.

This work was supported by the DFG through graduate research school GRK 1675.